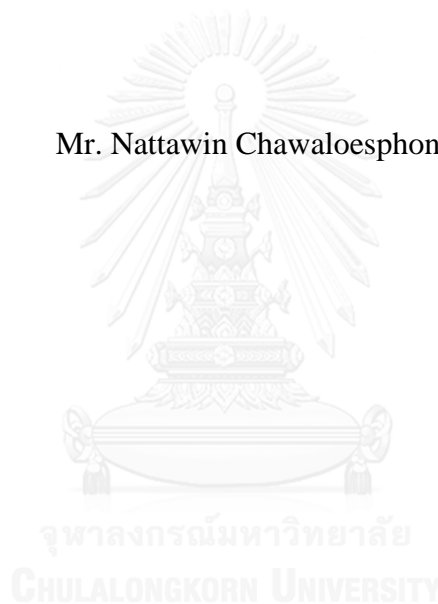


SEPARATION OF OILY EMULSION BY FLOTATION AND
COALESCER PROCESSES FOR WASTEWATER TREATMENT

Mr. Nattawin Chawaloeshonsiya



บทคัดย่อและแฟ้มข้อมูลฉบับเต็มของวิทยานิพนธ์ตั้งแต่ปีการศึกษา 2554 ที่ให้บริการในคลังปัญญาจุฬาฯ (CUIR)
เป็นแฟ้มข้อมูลของนิสิตเจ้าของวิทยานิพนธ์ ที่ส่งผ่านทางบัณฑิตวิทยาลัย

The abstract and full text of theses from the academic year 2011 in Chulalongkorn University Intellectual Repository (CUIR)
are the thesis authors' files submitted through the University Graduate School.

A Dissertation Submitted in Partial Fulfillment of the Requirements
for the Degree of Doctor of Philosophy Program in Environmental Management

(Interdisciplinary Program)

Graduate School

Chulalongkorn University

Academic Year 2014

Copyright of Chulalongkorn University

การแยกอีมีลชันน้ำมันด้วยกระบวนการทำให้ลอยและกระบวนการโคอะเลสเซนส์
ในการบำบัดน้ำเสีย



วิทยานิพนธ์นี้เป็นส่วนหนึ่งของการศึกษาตามหลักสูตรปริญญาวิทยาศาสตรดุษฎีบัณฑิต
สาขาวิชาการจัดการสิ่งแวดล้อม (สหสาขาวิชา)
บัณฑิตวิทยาลัย จุฬาลงกรณ์มหาวิทยาลัย
ปีการศึกษา 2557
ลิขสิทธิ์ของจุฬาลงกรณ์มหาวิทยาลัย

Thesis Title	SEPARATION OF OILY EMULSION BY FLOTATION AND COALESCER PROCESSES FOR WASTEWATER TREATMENT
By	Mr. Nattawin Chawaloeshonsiya
Field of Study	Environmental Management
Thesis Advisor	Associate ProfessorPisut Painmanakul, Ph.D.
Thesis Co-Advisor	ProfessorPascal Guiraud, Ph.D.

Accepted by the Graduate School, Chulalongkorn University in Partial Fulfillment of the Requirements for the Doctoral Degree

..... Dean of the Graduate School
(Associate ProfessorSunait Chutintaranond, Ph.D.)

THESIS COMMITTEE

..... Chairman
(ProfessorPatrice Bacchin, Ph.D.)

..... Thesis Advisor
(Associate ProfessorPisut Painmanakul, Ph.D.)

..... Thesis Co-Advisor
(ProfessorPascal Guiraud, Ph.D.)

..... Examiner
(Assistant ProfessorChantra Tongcumpou, Ph.D.)

..... Examiner
(Associate ProfessorSuraphong Wattanachira, Ph.D.)

..... External Examiner
(ProfessorSeok-Oh Ko, Ph.D.)

..... External Examiner
(ProfessorTsuyoshi IMAI, Ph.D.)

ณัฐวิญญู ชวลิตพรศิยา : การแยกอิมัลชันน้ำมันด้วยกระบวนการทำให้ลอยและกระบวนการโคอะเลสเซนส์ในการบำบัดน้ำเสีย (SEPARATION OF OILY EMULSION BY FLOTATION AND COALESCER PROCESSES FOR WASTEWATER TREATMENT) อ.ที่ปรึกษาวิทยานิพนธ์หลัก: พิศุทธิ์ เพ็ชรมนกุล, อ.ที่ปรึกษาวิทยานิพนธ์ร่วม: Pascal Guiraud, 201 หน้า.

งานวิจัยนี้มีวัตถุประสงค์เพื่อศึกษาการแยกอิมัลชันน้ำมันคงตัวด้วยกระบวนการโคอะเลสเซนส์และกระบวนการทำให้ลอย โดยทำการทดลองกับน้ำเสียสังเคราะห์ด้วยน้ำมันตัด Castrol Cooledge BI ในการทดลองการแยกอิมัลชันด้วยกระบวนการโคอะเลสเซอร์จะศึกษาผลกระทบของความเร็วการไหลของน้ำมันรูปแบบการวางตัวในชั้นตัวกลาง และรูปร่างของตัวกลางพอลิพรอฟีลีนที่ใช้เป็นตัวกลางโคอะเลสเซอร์ทั้ง 3 รูปแบบ ได้แก่ แบบเม็ดกลม แบบเส้นใย และแบบท่อกลวง ในส่วนของกระบวนการทำให้ลอยจะพิจารณาผลกระทบของสภาวะการเดินระบบที่มีต่อประสิทธิภาพในการแยกของน้ำมัน ทั้งในกระบวนการทำให้ลอยด้วยอากาศละลาย (DAF) และกระบวนการทำให้ลอยด้วยอากาศ (IAF) ร่วมกับกระบวนการโคแอกกูเลชันด้วยสารส้ม

จากผลการทดลองพบว่า อิมัลชันน้ำมันตัดที่สังเคราะห์ขึ้นมานั้นมีเสถียรภาพสูง อนุภาคน้ำมันมีขนาดอยู่ในช่วงนาโนเมตรและมีประจุลบบนพื้นผิว การแยกอิมัลชันด้วยกระบวนการโคอะเลสเซอร์มีประสิทธิภาพสูงสุดเพียงร้อยละ 44 เมื่อใช้ชั้นตัวกลางชนิดท่อกลวงความหนา 10 เซนติเมตร และความเร็วการไหลของน้ำเสีย 2 เซนติเมตรต่อวินาที โดยพบว่าคุณสมบัติทางด้านพื้นผิวและรูปแบบการเรียงตัวของชั้นตัวกลางเป็นตัวแปรสำคัญในการเลือกตัวกลางโคอะเลสเซอร์ที่มีประสิทธิภาพ ในส่วนของกระบวนการทำให้ลอย พบว่ากระบวนการทำให้ลอยทั้ง 2 ประเภทมีประสิทธิภาพแยกสูงร้อยละ 85 แต่การแยกจะเกิดขึ้นเมื่อมีการใส่สารส้มเท่านั้น โดยเมื่อพิจารณาการทำลายเสถียรภาพของสารส้ม พบว่า กลไกที่เกิดขึ้นคือการสร้างผลึกหรือฟล็อกเพื่อให้อนุภาคน้ำมันมาจับ (Sweep flocculation) ซึ่งเกิดขึ้นในช่วงพีเอช 6.5 – 7.5 และปริมาณอลูมิเนียม 1 มิลลิโมลต่อลิตร โดยฟล็อกที่เกิดขึ้นเป็นนั่น คือ ผลึกอลูมิเนียมไฮดรอกไซด์ จึงช่วยยืนยันได้ว่ากลไกการทำลายเสถียรภาพดังกล่าวเกิดขึ้นจริง นอกจากนี้ ผลการแยกอิมัลชันน้ำมันด้วยการทดสอบกระบวนการทำให้ลอยขนาดเล็กก็สอดคล้องกับผลที่ได้จากระบบขนาดใหญ่ และเมื่อทำการสังเกตปฏิสัมพันธ์ระหว่างฟองอากาศกับอนุภาคน้ำมันและฟล็อกน้ำมัน พบว่า ฟองอากาศจะไม่สามารถจับกับอนุภาคน้ำมันได้ แต่สามารถจับฟล็อกน้ำมันไว้บนพื้นผิวบริเวณด้านหลังฟองได้ จึงเป็นสาเหตุให้เกิดความแตกต่างระหว่างการแยกด้วยกระบวนการทำให้ลอยที่ไม่มีและมีการทำลายเสถียรภาพก่อน

สาขาวิชา การจัดการสิ่งแวดล้อม

ลายมือชื่อนิสิต

ปีการศึกษา 2557

ลายมือชื่อ อ.ที่ปรึกษาหลัก

ลายมือชื่อ อ.ที่ปรึกษาร่วม

5387870720 : MAJOR ENVIRONMENTAL MANAGEMENT

KEYWORDS: OIL EMULSION / SEPARATION / COALESCER / FLOTATION / DESTABILIZATION

NATTAWIN CHAWALOESPHONSIYA: SEPARATION OF OILY EMULSION BY FLOTATION AND COALESCER PROCESSES FOR WASTEWATER TREATMENT.
 ADVISOR: ASSOC. PROF.PISUT PAINMANAKUL, Ph.D., CO-ADVISOR: PROF.PASCAL GUIRAUD, Ph.D., 201 pp.

The objective of this work was to study the separation of the stable oily emulsion by coalescer and flotation processes. The commercial Castrol Cooledge BI cutting oil was applied for synthesizing the oily wastewater since it can easily form a stabilized emulsion with water. The coalescer experiments were conducted by using polypropylene media with different shapes including granule, fiber, and tube. Effects of emulsion flow velocity and bed height as well as the bed packing were considered. For the flotation, both the dissolved air flotation (DAF) and the induced air flotation (IAF) processes in the pilot scale were employed for the emulsion separation with the addition of aluminium sulfate ($\text{Al}_2(\text{SO}_4)_3$) as a coagulant. Influences of operating conditions on the separation efficiency were investigated.

The results indicated that the prepared emulsion was highly stable suggested by its small droplet sizes and high negative zeta potential. The emulsion was partly separated by the coalescer with the highest efficiency of 44% from the 10 cm bed of tubular polypropylene with 2 cm/s flow velocity. In the case of the separation by flotation, the highest efficiency of 85% can be achieved from both DAF and IAF. However, the separation by flotation was ineffective without the coagulation. Therefore, the destabilization of the cutting oil emulsion by aluminium sulfate was further investigated. The main destabilization mechanism was the sweep flocculation occurred at the Al^{3+} concentration of 1.0 mM and pH of 6.5 – 7.5, where solid flocs can be observed. At lower Al^{3+} dosage, the destabilization was inefficient suggesting that only droplet coalescence was insufficient for the separation. The flocs were analyzed for their chemical composition and crystalline structure to confirm the formation of aluminium hydroxide ($\text{Al}(\text{OH})_3$) that plays a role in the sweep flocculation. Furthermore, the results from the bench scale flotation carried out by the Flottatest were correspondent to those obtained from the pilot scale experiments. The addition of coagulant was needed for the effective separation. However, it was also found that the increase of Al^{3+} dosages further the 1.0 mM was unable to enhance the separation efficiency. Finally, the interactions of droplet-bubble and floc-bubble were observed in the special made observation cell. No interaction between oil droplets and a bubble can be seen contrasting with the case of oil flocs, which can attach on the bubble surface. This affirmed the difference between the separation of cutting oil emulsion by flotation with and without the formation of flocs.

Field of Study: Environmental Management Student's Signature

Academic Year: 2014 Advisor's Signature

Co-Advisor's Signature

ACKNOWLEDGEMENTS

I would like to express my special appreciation to my advisors, Associate Professor Dr. Pisut Painmanakul, Professor Pascal Guiraud, and Assistant Professor Dr. Chaiyaporn Puprasert, for the supervision on my thesis. Their helpful and supportive suggestions encouraging me throughout my work and allowing me to progress as a researcher have been invaluable.

I am also grateful to my committee members Professor Patrice Bacchin, Professor Tsuyoshi Imai, Professor Seok-Oh Ko, Assistant Professor Dr. Chantra Tongcumpou, and Associate Professor Dr. Suraphong Wattanachira.

A good support during the thesis conducting is very important. Fortunately, I have got it abundantly from the technical staffs and colleagues in Laboratoire d'Ingénierie des Systèmes Biologiques et des Procédés (LISBP), INSA Toulouse, the Center of Excellence on Hazardous Substance Management (HSM) laboratory, and Department of Environmental Engineering, Faculty of Engineering, Chulalongkorn University

My cordial thanks should be given to all the staffs of University Paul Sabatier – Toulouse III, INSA Toulouse, HSM, and Department of Environmental Engineering, Faculty of Engineering, Chulalongkorn University for their kind cooperation and help.

I would like to express my gratitude for the Erasmus Mundus Program TECHNO Project I for the support on the 18 months mobility in Toulouse and the Center of Excellence on Hazardous Substance Management (HSM) for providing my tuition and research grants in Thailand.

Finally, I would like to express my sincere gratitude to my beloved family and friends for their love, understanding, and heartfelt support and encouragement.

CONTENTS

	Page
THAI ABSTRACT	iv
ENGLISH ABSTRACT.....	v
ACKNOWLEDGEMENTS	vi
LIST OF FIGURES	xi
LIST OF TABLES	xv
LIST OF ABBREVIATIONS	xvii
INTRODUCTION	1
CHAPTER 1 OVERVIEW ON OILY WASTEWATER AND SEPARATION	5
1.1 Introduction to oily wastewater	5
1.1.1 Types of oily wastewater.....	6
1.1.2 Classification of oily wastewater	9
1.1.3 Treatment of oily wastewater	11
1.2 Cutting oil.....	12
1.2.1 Types of cutting oil.....	12
1.2.2 Lifecycle of cutting oil	13
1.2.3 Hazards of cutting oil	14
1.3 Chemical destabilization	15
1.3.1 Properties of stable emulsion	15
1.4 Coalescer process	22
1.4.1 Mechanisms in coalescer process.....	22
1.4.2 Transport of oil droplets to contact with collector	24
1.4.3 Coalescer efficiency equation	26
1.4.4 Treatment of oily emulsion by coalescer	28
1.5 Flotation process.....	31
1.5.1 Dissolved air flotation (DAF).....	31
1.5.2 Induced air flotation (IAF)	32
1.5.3 Mechanisms of flotation process	32

	Page
1.5.4 Treatment of oily emulsion by flotation.....	40
1.6 Dynamic of particles and bubbles	43
1.6.1 Movement of particles.....	44
1.6.2 Movement of bubbles.....	46
1.7 Conclusion.....	51
CHAPTER 2 CHARACTERIZATION OF CUTTING OIL EMULSION.....	52
2.1 Characteristics of cutting oil.....	52
2.2 Observation of droplets under microscope.....	55
2.3 Overview of emulsion characterization.....	56
2.4 Characterization of droplet size.....	59
2.4.1 Measurement apparatus.....	60
2.4.2 Sizes distribution of cutting oil droplets.....	62
2.5 Characterization of zeta potential.....	67
2.5.1 Zetasizer Nano ZS.....	67
2.5.2 Zeta potential of cutting oil emulsion.....	68
2.6 Measurement of pH.....	71
2.7 Measurement of conductivity.....	71
2.8 Measurement of turbidity.....	72
CHAPTER 3 SEPARATION OF CUTTING OIL EMULSION BY COALESCER..	75
3.1 Introduction	75
3.2 Methodology.....	76
3.2.1 Experimental set-up.....	76
3.2.2 Analytical parameters.....	78
3.2.3 Preparation of the synthetic cutting oil emulsion.....	79
3.2.4 Experimental procedure	79
3.3 Results and Discussions	80
3.3.1 Characteristics of coalescer media	80
3.3.2 Effects of operating conditions on treatment efficiencies	82

	Page
3.3.3 Effects of coalescer media characteristics	84
3.4 Conclusions	92
CHAPTER 4 SEPARATION OF CUTTING OIL EMULSION BY FLOTATION ..	94
4.1 Introduction	94
4.2 Methodology.....	95
4.2.1 Jar-test experiment	95
4.2.2 Experimental set-up.....	95
4.2.3 Separation of cutting oil emulsion by flotation processes.....	99
4.2.4 Effects of hydrodynamic parameters.....	102
4.2.3 Overflow rate (<i>OFR</i>)	106
4.2.4 Residence time distribution (RTD) study.....	107
4.3 Results and discussions	109
4.3.1 Jar-test experiments	109
4.3.2 Bubble size and contamination level.....	111
4.3.3 Separation of cutting oil emulsion by flotation	115
4.3.4 Effects of hydrodynamic parameters.....	123
4.3.5 Residence time distribution (RTD)	130
4.6 Conclusions	133
CHAPTER 5 DESTABILIZATION AND AGGREGATION OF CUTTING OIL..	135
5.1 Introduction.....	135
5.2 Hydrolysis of $Al_2(SO_4)_3$	136
5.3 Destabilization experiments	138
5.3.1 Critical coagulation concentration (CCC) and aggregation kinetic	139
5.3.2 Effects of coagulant dose, pH, and oil concentration.....	146
5.3.3 Observation of floc	155
5.4 Conclusions.....	161
CHAPTER 6 FLOTATION TEST	163
6.1 Flotation experiment device and procedure	163

	Page
6.2 Flotation of cutting oil emulsion without coagulant.....	165
6.3 Flotation of cutting oil emulsion with coagulant addition.....	169
6.4 Conclusions.....	174
CHAPTER 7 OBSERVATION OF BUBBLE-AGGREGATE INTERACTION.....	175
7.1 Experimental methods	175
7.2 Experimental methods	175
7.2.1 Materials.....	175
7.2.2 Observation device	176
7.2.3 Experimental procedure	178
7.3 Results and discussions	181
7.3.1 Observation of bubble and glass beads interaction	181
7.3.2 Observation of bubble and oil droplet interaction.....	184
7.3.3 Observation of bubble and oil floc interaction.....	185
7.4 Conclusions	185
CONCLUSIONS AND PERSPECTIVES.....	187
REFERENCES	190
APPENDIX.....	199
VITA.....	209

LIST OF FIGURES

	Page
Figure 1.1 Relations between droplet sizes and rising velocities of primary and secondary emulsions.....	10
Figure 1.2 Summary of oily wastewater classification.....	11
Figure 1.3 Interfacial of oil and water with the presence of surfactants	15
Figure 1.4 Diagram of the electrical double layer	17
Figure 1.5 Force diagrams of oil droplets and relation of repulsive, attractive and resulting force with the distance between oil droplets	18
Figure 1.6 Phenomena in interception, adhesion, and coalescence steps	23
Figure 1.7 Schematic diagram of salting out phenomena of coalesced oil droplets ...	24
Figure 1.8 Schematic diagrams of the transport phenomena (a) sedimentation, (b) direct interception, and (c)	24
Figure 1.9 Schematic diagrams of (a) single collector and (b) entire media bed	27
Figure 1.10 Particle-bubble collision.....	34
Figure 1.11 Schematic of three phases contact among liquid, an air bubble, and a solid particle at the rear of a bubble	39
Figure 2.1 Castrol Cooledge BI cutting oil and the 1 g/L cutting oil emulsion.....	55
Figure 2.2 Microscopic photos of droplet in the 1.0 g/L cutting oil emulsion	57
Figure 2.3 Droplet size distributions from the Mastersizer of the 1.0 g/L cutting oil emulsion	64
Figure 2.4 Droplet size distributions from the Nanotracer of the 1.0 g/L cutting oil emulsion	65
Figure 2.5 Droplet size distributions from the Nano ZS of the 1.0 g/L cutting oil emulsion	66
Figure 2.6 Zeta potential of the 1.0 g/L cutting oil emulsion	69
Figure 2.7 Zeta potentials at varied pH for 1 g/L cutting oil emulsion	70
Figure 2.8 d ₃₂ at varied pH for the cutting oil emulsion.....	70
Figure 2.9 Change of turbidities with concentrations of emulsions	73
Figure 3.1 Schematic diagram of the coalescer process	77

	Page
Figure 3.2 Coalescer media (a) granule, (b) fiber, and (c) tube.....	78
Figure 3.3 Treatment efficiencies in different operating conditions for (a) granular, (b) fibrous, and (c) tubular media.....	83
Figure 3.4 Inclined angles (θ) of (a) fibrous and (b) tubular media.....	86
Figure 3.5 Flow pathways of the emulsion for three medium types in (a) single- phase flow and (b) two-phase flow	91
Figure 4.1 Schematic diagram of DAF process	96
Figure 4.2 Pressure vessel.....	97
Figure 4.3 Flotation tank.....	98
Figure 4.4 (a) Schematic diagram of IAF process (b) Flexible aerator	99
Figure 4.5 Variation of the overflow rate (OFR) with flow rates	107
Figure 4.6 Efficiencies of the coagulation process at varied pH	110
Figure 4.7 Efficiencies of the coagulation with varied alum dosages at different oil concentrations.....	111
Figure 4.8 Bubble velocity and diameter in a function of air flow rate in IAF.....	112
Figure 4.9 Drag coefficient in a function of bubble Reynolds number,	113
Figure 4.10 Efficiency in a function of time in the batch DAF process at varied Q_{pw}	116
Figure 4.11 Effects of pressurized water flow rates at different emulsion flow rates in continuous DAF	117
Figure 4.12 Relation between the A/S ratio and the treatment efficiency in DAF....	118
Figure 4.13 Efficiency of the batch IAF process as a function of time for varied Q_g	119
Figure 4.14 Efficiencies at varied air flow rates in the continuous IAF with different Q_w	120
Figure 4.15 Effects of A/S ratio on the IAF efficiency.....	121
Figure 4.16 Interfacial area of bubbles vs. Q_{pw} in DAF at different Q_w in DAF ..	123
Figure 4.17 Velocity gradients (G) at different Q_{pw} for varied Q_w in DAF	124
Figure 4.18 a/G ratio vs. pressurized water flow rate at varied Q_w in DAF	126
Figure 4.19 Relation between the separation efficiency and the a/G ratio in DAF...	126
Figure 4.20 Comparison of calculated and experimental efficiencies in $\pm 5\%$	127

	Page
Figure 4.21 Interfacial area of bubbles in IAF at different Q_g	128
Figure 4.22 Velocity gradients (G) at varied Q_w in IAF.....	129
Figure 4.23 a/G ratios at varied air flow rates in IAF.....	130
Figure 4.24 Residence time distribution as a function of time in DAF at (—) inlet and (---) contact zone of the flotation tank.....	131
Figure 4.25 Residence time distribution with time of IAF at (—) inlet and (---) contact zone of the flotation tank	132
Figure 5.1 Speciation of hydrolyzed monomeric aluminium in water at equilibrium	137
Figure 5.2 Droplet size distributions with time of the emulsion prepared from DI water for Al^{3+}	140
Figure 5.3 Droplet size distributions with time of the emulsion prepared from tap water for Al^{3+}	142
Figure 5.4 Aggregate growths with fitted curves (coefficients of determination, $R^2 > 0.97$) for Al^{3+}	143
Figure 5.5 (a) stability ratio and (b) zeta potential at varied Al^{3+} concentrations for emulsion in DI water	144
Figure 5.6 (a) stability ratio and (b) zeta potential at varied Al^{3+} concentrations for emulsion in tap water	146
Figure 5.7 (a) turbidity and (b) zeta potential of the emulsion from DI water at different pH for varied Al^{3+} concentration.....	148
Figure 5.8 Evolution of aggregate and droplet size distribution in emulsion with DI water at the optimal pH for different Al^{3+} concentrations.....	150
Figure 5.9 (a) turbidity and (b) zeta potential of the emulsion from tap water at different pH for varied Al^{3+} concentration.....	152
Figure 5.10 Change of aggregate and droplet size distribution in emulsion with tap water at pH 7 for different Al^{3+} concentrations.....	153
Figure 5.11 Effects of oil concentration on the minimum Al^{3+} concentration required.....	155
Figure 5.12 Size distribution of flocs in cutting oil emulsion	156
Figure 5.13 Fractal plots of oil flocs in emulsion with DI water from Mastersizer 2000.....	157

	Page
Figure 5.14 SEM image of aluminium floc in cutting oil emulsion with DI water...	159
Figure 5.15 FTIR spectra of flocs formed in the DI water emulsion at pH 7.....	160
Figure 6.1 Flottatest device.....	163
Figure 6.2 Photographs of the initial emulsion.....	166
Figure 6.3 Emulsions at 5 minutes after flotation for the pressurized water under .	170
Figure 6.4 Emulsions after flotation with coagulation for 5 minutes with the pressurized water.....	171
Figure 6.5 Observation of water surface from the flotation with coagulation at 0.75 mM and 1.0 mM Al^{3+} concentrations.....	173
Figure 7.1 (a) schematic diagram and (b) photograph of the observation device set up.....	177
Figure 7.2 Schematic diagram of the observation cell.....	178
Figure 7.3 Bubble blocked by the capture system ($d_b \approx 1.3$ mm).....	179
Figure 7.4 Diagram of circular turbulent jet profile	180
Figure 7.5 Flow of the cutting-oil emulsion in the observation cell at the flow rate of 95 mL/min.....	181
Figure 7.6 Images of a glass bead moving around a captured bubble ($d_b = 2.4$ mm, $Re_b \approx 744$) at every 22 milliseconds.....	182
Figure 7.7 Flow streamlines around a bubble different Re_b regime (a) $Re_b \rightarrow 0$ (Stokes flow), (b) $Re_b \rightarrow \infty$ (potential flow), and (c) intermediate Re_b (Nguyen, 2011).....	183
Figure 7.8 Colliding area of a bubble at intermediate Reynolds number with asymmetric flow streamline	183
Figure 7.9 Images of the emulsion flow around a bubble ($d_b = 2.1$ mm, $Re_b \approx 651$) every second.....	184
Figure 7.10 Images of oil flocs flow around a bubble ($d_b = 2.1$ mm, $Re_b \approx 651$).....	185

LIST OF TABLES

	Page
Table 1.1 Correlations of Cd for a spherical solid particle at $Re_p < 800$	45
Table 1.2 Correlations for drag coefficient of clean bubble	48
Table 2.1 Composition/information on ingredients of Castrol Cooledge BI.....	53
Table 2.2 Characteristics of Castrol Cooledge BI	53
Table 2.3 Characteristics of DI and tap water used for preparing emulsion.....	54
Table 2.4 Methods and apparatus for size measurements in this work	59
Table 2.5 pH values of the cutting oil emulsion at varied concentration	71
Table 2.6 Conductivities ($\mu\text{S}/\text{cm}$) of the cutting oil emulsion at varied concentration	72
Table 2.7 Turbidities (NTU) of the cutting oil emulsion at varied concentration	73
Table 3.1 Coalescer media characteristics	81
Table 3.2 Oil-droplet sizes (dSV) at 2.0 cm/s flow velocity and 10 cm bed height (in m)	84
Table 3.3 Calculated diameters obtained from Ergun's and filtration efficiency equations.....	87
Table 3.4 Saturated porosity (ε_t) and average saturation factor ($\overline{S_d}$) of packed beds.....	88
Table 3.5 Carman-Kozeny constants for single- and two-phase flow with bed permeability.....	90
Table 4.1 Properties of air at 20°C	101
Table 4.2 Measured values and calculated parameters of bubbles in IAF.....	113
Table 4.3 Bubble parameters for DAF process.....	114
Table 4.4 Parameters in linear relation between the efficiency and a/G ratio	127
Table 5.1 EDX results of aluminium floc in the cutting oil emulsion with DI water at pH 7	159
Table 5.2 Assignment of IR bands in FTIR results	161
Table 6.1 Turbidities and concentrations at different heights for flotation without destabilization.....	167

	Page
Table 6.2 Turbidities and concentrations of the emulsion at the bottom of the cells after flotation without coagulant addition	167
Table 6.3 Turbidities (NTU) at different heights after flotation with coagulant addition with the control experiment.....	171
Table 6.4 Turbidities of the emulsion (NTU) at different time for various volume of pressurized water.....	172
Table 6.5 Photographs and turbidities of emulsion after 5 minutes for the flotation with addition of coagulant at different concentration (300 mL of pressurized water).....	174



LIST OF ABBREVIATIONS

Latin letters

a	Bubble interfacial area (m^{-1})
A	Cross-sectional area of flotation column (m^2)
A/S	Air-to-solid (oil) ratio (g air/g solid)
A_0	Surface area of the equivalent sphere with the same volume as the particle (m^2)
A_{ow}	Interfacial area between oil and water (m^2)
A_p	Surface area of the particle (m^2)
B_0^*	Ratio between the detachment and the attachment forces (-)
$B_{0,1}$	Specific permeability coefficient of single-phase flow (-)
$B_{0,2}$	Specific permeability coefficient of two-phase flow (-)
Bo_b	Bond number or Eötvös number (-)
C_d^m	Drag coefficient of clean bubble (-)
C_d^{im}	Drag coefficient of fully contaminated bubble (-)
C	Oil concentration after passing through coalescer bed (mg/L)
C_0	Initial oil concentration (mg/L)
C_1	Oil concentration after passing coalescer bed (mg/L)
C_2	Oil concentration after decantation (mg/L)
Ca	Capillary number (-)
C_{air}	Dissolved air concentration (g/L)
C_c	Emulsion concentration subjected to the dilution effect (mg/L)
C_d	Drag coefficient (-)
C_f	Final oil concentration in flotation experiments (mg/L)
C_{in}	Oil concentration in the influent of DAF experiment (mg/L)
C_{out}	Oil concentration in the effluent of DAF experiment (mg/L)
D	Diffusion coefficient (m^2/s)
D_0	Diameter of the source of the turbulent jet (m)
ΔD	Distance of the rising bubble between two frames (m)

d_b	Diameter of bubble ($r_b = d_b/2$) (m)
d_c	Diameter of collector (m)
D_f	Fractal dimension of flocs (-)
d_i	Inner diameter of tubular media (m)
d_o	Outer diameter of tubular media (m)
d_p	Diameter of oil droplet ($r_p = d_p/2$) (m)
d_{SV}	Surface-volume (sauter) diameter (m)
$E(t)$	Residence time distribution function (-)
E_{att}	Attachment efficiency of the bubble-particle aggregate (-)
E_{coll}	Collision efficiency of the bubble-particle aggregate (-)
E_{det}	Efficiency of detachment (-)
E_{sta}	Stability efficiency of the bubble-particle aggregate (-)
Fr	Froude number (-)
g	Gravitational acceleration (9.81 m/s^2)
G_{bubble}	Gradient velocity caused by bubbles (s^{-1})
H	Bed height (or length) of the coalescer bed (m)
H_{Darcy}	Pressure loss from Darcy's equation (m)
H_L	Height of liquid in flotation column (m)
K	Boltzmann's constant ($1.38 \times 10^{-23} \text{ kg}\cdot\text{m}^2/\text{K}\cdot\text{s}$)
k	Initial rate of aggregation (-)
k_1	Carman-Kozeny constant of single-phase flow (-)
k_2	Carman-Kozeny constant of two-phase flow (-)
K_H	Henry's constant ($\text{atm}\cdot\text{L}/\text{mol}$)
L	Length of fibrous media (m)
MW	Molecular weight of gas (g/mol)
N	Number of CSTR tank in the tank-in-series model
n_b	Number of bubbles
$n_{p/b}$	Number ratio of particle to bubble
OFR	Overflow rate ($\text{m}^3/(\text{m}^2\cdot\text{min})$)
\bar{P}	Partial pressure of gas (atm)
P	Power input or dissipate to the liquid phase ($\text{N}\cdot\text{m}/\text{s}$)

PS	Applied pressure level in the pressure vessel (bar or atm)
Δp	Pressure loss of flow pass through media bed (Pa or $\text{kg/m}\cdot\text{s}^2$)
Δp_1	Pressure loss of single-phase flow (Pa)
Δp_2	Pressure loss of two-phase flow (Pa)
Q_g	Gas flow rater (L/min)
Q_{pw}	Flow rate of the pressurized water (L/min)
Q_w	Flow rate of the oily emulsion (L/min)
Re_b	Reynolds number of bubble (-)
Re_p	Reynolds number of particle (-)
$\overline{S_d}$	Saturation factor of coalescer media (-)
S_0	Spreading coefficient (-)
S_b	Surface area of a bubble (m^2)
St	Stokes number (-)
T	Absolute temperature of liquid phase (K)
t_d	Time for liquid film drainage (s)
t_e	Time for three phase line contact (TPLC) expansion (s)
t_{frame}	Acquisition time frame (s)
t_{ind} (or t_{att})	Induction or attachment time (s)
t_r	Time for liquid film rupture (s)
u_0	Jet velocity of emulsion at the source (m/s)
U_b	Terminal rising velocity of bubble (m/s)
U_E	Electrophoretic mobility ($\text{m}^2/\text{s}\cdot\text{V}$)
u_{max}	Maximum jet velocity of emulsion at a certain distance (m/s)
U_s	Terminal rising velocity of droplet (m/s)
v_0	Superficial velocity of emulsion (m/s)
V_{air}	Total air volume (m^3)
V_{bubble}	Total volume of bubble (m^3)
V_c	Emulsion volume after the dilution (mg/L)
v_f	Flow velocity of liquid phase (m/s)
V_{min}	Minimum bubble volume required (m^3)
V_p	Total volume of oil (m^3)

V_{total}	Total volume of the flotation cell (m^3)
W	Stability ratio (-)
W_A	Mechanical work for forming the emulsion ($N \cdot m$)
We_b	Weber number (-)
x	Distance from the source in the turbulent jet profile (m)

Greek letters

α	Attachment efficiency of oil droplets on coalescer media (-)
β'	Rate of the reaction-limited aggregation (RLA) regime (-)
β_{fast}	Rate of the diffusion-limited aggregation (RLA) regime (-)
γ_c	Surface energy or critical interfacial tension of material (mN/m)
γ_{oc}	Interfacial tension between oil and coalescer media (mN/m)
γ_{og}	Interfacial tension between oil and air (mN/m)
γ_{ow}	Interfacial tension between oil and water (N/m)
γ_{ow}	Interfacial tension between oil and water (mN/m)
γ_{wc}	Interfacial tension between water and coalescer media (mN/m)
γ_{wg}	Interfacial tension between water and air (mN/m)
ε	Dielectric constant (equals to 80 for normal water)
ε_0	Initial bed porosity (-)
ε_t	Saturated porosity of media bed (-)
η_D	Efficiency of the transportation by diffusion (-)
η_I	Efficiency of the transportation by interception (-)
η_S	Efficiency of the transportation by sedimentation (-)
η_T	Single collector total efficiency of coalescer (-)
θ	Inclined angle of the fibrous and the tubular coalescer media (degree)
θ_c	Contact angle of cutting oil droplet on media (degree)
θ_{cap}	Cap angle in the stagnant cap model (degree)
μ_f	Kinetic viscosity of liquid phase ($Pa \cdot s$ or $kg/m \cdot s$)
ρ_f	Density of liquid phase (kg/m^3)
ρ_o	Oil density (kg/m^3)

ρ_p	Density of oil droplet (kg/m^3)
τ	Mean residence time (minute)
τ_b	Characteristic time of flow (s)
τ_p	Relaxation time (s)
ϕ	Sphericity of object (-)



INTRODUCTION

Nowadays, wastewater is one of the most concerned pollutions, since it causes various severe effects on environment and human being. Wastewater can be generated from many sources, but typically comes from community and industry. The characteristics of wastewater depend on types of contaminant, which result in difference of property and toxicity.

“Oil” is one of the important contaminant in water, which is usually called as oily wastewater. Oily wastewater can be generated from many sources; for example, household (i.e. palm oil), transportation (i.e. gasoline and lubricants), and industry (i.e. cutting oil). Oily wastewater is normally considered as hazardous waste, since it can contain toxic substances such as Poly Aromatic Hydrocarbon (PAHs), which was categorized as mutagenic and carcinogenic substances (Tri, 2002). Furthermore, it should be noted that oily wastewater is rarely degraded by biological process. Oil usually contaminates in water in four forms, including (1) Oil film on water surface; (2) soluble oil in water; (3) oily emulsion with surfactants; and (4) oily emulsion without surfactant (Aurelle, 1985). Among these types, oily emulsion with surfactants generally called as oily emulsion or stabilized emulsion is usually detected, since surfactants are widely used for oil cleaning. This oily wastewater is the most difficult type to be handled as it contains very small droplets that are stable and difficult to be separated (Aurelle, 1985).

In order to treat oily wastewater, physical processes are selected as the primary treatment for separating oil before other treatment techniques e.g. biological treatment. The advantages of physical process are its effectiveness, less time consumption, and economize on investment. Moreover, separated oil from physical process can be either recovered or applied as fuels. Many techniques have been proposed for treating oily wastewater; for example, decantation, coalescence, and flotation. Indeed, physical processes are sometimes coupled with chemical processes, such as coagulation-flocculation or sorption, to enhance their efficiencies.

Cutting oil is widely used in machining industries to improve the process performance. Two effects that benefit the machining process are cooling and lubricating. Typically, cutting fluids can be categorized into 4 types including 1) neat oil, 2) soluble oil, 3) semi-synthetic fluid, and 4) synthetic fluid (Grzesik, 2008). These oil types contain different compositions; however, the exact compositions are rarely provided by manufacturers. Composition of different cutting fluids can be seen in the work of Cheng et al. (2005). Generally, it can be said that cutting fluids have three main components, i.e. base oil, emulsifiers, and additives for specific purposes (Juneja et al., 2003). When using in the process, concentration and composition of cutting fluids are changed due to various effects, e.g. water evaporation and contamination. The fluid also loses its properties and has to be replaced, causing the cutting fluids waste. This waste normally in form of stabilized oily emulsion contains loads of organic components, large amount of surfactants, and high turbidity (Sokovic and Mijanovic, 2001), which posed some problems to environment (Greely and Ragopalan, 2004). Therefore, the cutting fluid waste has to be treated before discharging in an effluent. Numerous processes have been used to handle this wastewater, for example, membrane separation (Hilal et al., 2004), advanced oxidation (Seo et al., 2007), adsorption (Solisio et al., 2002), biological processes (van der Gast and Thompson, 2005; Perez et al., 2006; Rabenstein et al., 2009), and destabilization by electro-coagulation (Kobyas et al., 2006; Bensadok et al., 2008) and chemical coagulation (Rios et al., 1998; Bensadok et al., 2007).

However, the general treatment method of rejected cutting oil is to separate oil by physical or chemical techniques from water and then purified or direct disposal by combustion (Grzesik, 2008). The purified oil can be recovered to be used in manufacturing process again; therefore, an effective separation process is required in order to remove the contaminated oil in water with an efficient cutting oil recovery.

Physical, chemical, and biological processes have been applied for treating rejected cutting oil. Each process contains its pros and cons but can provide a high efficiency. Biological process, for example, could be sensible to changes of oil concentrations and operating conditions. Moreover, presence of biocides in cutting oil

could pose problems to microbial in the system (Cheng et al., 2005). In the case of chemical process, chemical consumption and longtime operation could be a main drawback. In some cases, the treated water could contain high salinity, which requires the successive process to handle (Graff, 2012). These regards can be resolved by physical process due to its adaptability to different oil concentrations and conditions as well as its rapid separation. Though, the main disadvantage of this process can be found on its low efficiency for small particles separation. A study focus on this aspect should be conducted as a result.

The objective of this work was to test two separation techniques including coalescer and flotation on synthetic oily emulsion. These two processes were selected due to its high performance for oil separation and the potential for oil recovery. Factors affecting the separation performance of these two processes were considered. Furthermore, the occurred mechanisms in the separation were also analyzed.

Coalescer is one of the widely used equipment for separating oil from water due to its simplicity and less time required. Numerous researches concerning the oily wastewater separation by coalescer have been conducted mainly focusing on 3 aspects including characteristics of oil phase, properties of media surface (e.g. wettability, surface energy, contact angle, etc.), and geometry of media. Indeed, effects of the first two perspectives have been considerably understood by numerous researches. Impacts of media shape on the efficiency were still unobvious. Moreover, behavior of the media packing, which could affect the separation, was also analyzed.

In the second part, the separation of the cutting oil emulsion by flotation was conducted. Effects of operating conditions were investigated. Afterwards, the mechanisms in the chemical destabilization, which was proved to be vital in the separation by flotation, were examined. Finally, interaction between bubbles and aggregates was analyzed to obtain the in-depth understanding of the emulsion separation by flotation.

The first chapter deals with the theoretical background of oil containing wastewater. Information regarding cutting oil is also provided including its life cycle, hazard, handling, and disposal. Moreover, the separation techniques used in this work,

i.e. coalescer, chemical destabilization, and flotation, are mentioned and the reviews for their application to deal with oily wastewater are also displayed.

In the second chapter, properties of the cutting oil used in this study are shown. The characteristics of the cutting oil emulsion formed in water are presented as well as the principles of the characterization techniques.

Later, the third chapter exhibits the results of the emulsion separation by coalescer. Properties of the coalescer media were analyzed. Moreover, effects of operating conditions, media shape, and bed packing on the efficiency of the coalescer were investigated.

The results regarding the separation of the oily emulsion by the pilot scale flotation, both dissolved air flotation (DAF) and induced air flotation (IAF), are provided in the fourth chapter. Likewise, effects of operating conditions on the separation were determined. In addition, hydrodynamic parameters of these processes were examined and related with the efficiency. The flow behavior in the flotation cell was also investigated by mean of the residence time distribution (RTD) study.

According to the find out from the flotation, the destabilization of the cutting oil emulsion played a key role in the separation. That led to the destabilization study shown in the fifth chapter. Influences of pH, coagulant dosage, and oil concentration were evaluated. The destabilization mechanism was also clarified. Besides, the formed flocs were analyzed to prove the proposed mechanism for the destabilization.

Afterwards, the separation by flotation was tested in the bench scale experiments using the Flottatest. This test was conducted to affirm the finding from the pilot scale experiments in more controlled conditions

Finally, the interactions between a bubble and oil droplets as well as between a bubble and oil flocs were observed. This study was carried out to clarify the difference on the interactions, which can result in the distinct separation performance between these two cases.

CHAPTER 1

OVERVIEW ON OILY WASTEWATER AND SEPARATION

In order to separate the stabilized emulsion effectively, the understanding on its properties and separation techniques are required. This chapter therefore gives the background on oily wastewater and some separation methods applied in this work including coalescer, chemical coagulation, and flotation. Researches conducted by using these processes for treating oily wastewater are also mentioned. Moreover, information regarding cutting oil that was used for forming emulsion in the experiments is presented to offer an overview of this oil type. Finally, dynamics of particles and bubbles, which govern movements of bubbles and particles in flotation, are provided since it can affect the performance of the flotation.

1.1 Introduction to oily wastewater

Oily wastewater is usually binary mixture systems between oil and water. Although, only small amount of oil is generally dispersed in water, a damage can be posed to environment, particularly for aquatic ecology. Oil pollution in water can harm the aquatic flora and fauna by hindering light and natural oxygen transfer. Moreover, oil can deposit in sediment at the bottom or the bank of water body as well as aquatic plants, causing in the accumulation that raising the oil concentration. More and longer damages can be provoked as a result. It should be noted that merely a trace of oil can cause bad odor and taste in water, which could be troublesome in water treatment processes.

In addition, presence of oil can perturb primary and biological units in wastewater treatment plants. The biological process, in particular, can be affected by oil contamination since thin oil film can obstruct the oxygen transfer that is essential for the microorganisms. The treatment efficiency is therefore decreased. Furthermore,

oil and sludge in the process can form “grease balls” that can clog in pumps and pipelines causing a malfunction of the process as well.

From these points, a suitable handling with oily wastewater should be considered. Oil has to be separated or treated before being exposed to natural water. An understanding of oily wastewater properties is therefore necessary.

1.1.1 Types of oily wastewater

Generally, oil in water can present in 4 different forms (Aurelle, 1985), for example,

- 1) dissolved oil,
- 2) oily emulsion without surfactants,
- 3) oily emulsion with surfactants, and
- 4) floating oil film.

These different types can exist independently or simultaneously depending on the characteristics of the contaminated oil. Impacts on water are also dissimilar for each type as follow.

1.1.1.1 Water pollution from dissolved oil

The solubility of oil is dependent on its properties, for instance, polarity of molecule or molecular weight. The solubility is increased with the unsaturation of the molecule, especially for cyclic compounds like benzene. On the other hand, less solubility can be found from oil with high molecular weight. However, the light oil that is mostly soluble in water can be eliminated by stripping process. This form of oily wastewater is clearly distinct to the others as oil cannot be visually detected. The wastewater is usually transparent and clear with merely trace of odor and taste. However, this wastewater form can pose high toxic despite its appearance since the most soluble oil normally contains aromatic molecules, which are carcinogen. The common method used for dealing with this wastewater type is oxidization or mineralization to destruct molecules of oil into carbon and hydrogen.

1.1.1.2 Water pollution by oily emulsion without surfactants

Oily wastewater from industry is typically in form of emulsion induced by the turbulence from centrifugal pump, valve, joint, etc. This emulsion can be formed by agitation or, in some cases, by diphasic condensation phenomena. Forming of the emulsion by agitation can be done by putting the mechanical work (W_A) that equals to the interfacial energy (γ_{ow}) created for dispersing oil in water to form certain interfacial area (A_{ow}), which can be expressed as

$$W_A = \gamma_{ow} \cdot A_{ow} \quad (1.1)$$

It can be seen that lower interfacial tension can facilitate the dispersion of oil droplets to form emulsion. Assuming all droplets in emulsion are spherical with the diameter of d_p , the interfacial area of droplets in the total volume of V_p then equals to $6V/d_p$. Equation 1.1 can be rewritten as

$$d_p = \frac{6V_p \gamma_{ow}}{W_A} \quad (1.2)$$

Equation 1.2 expresses that the droplet diameter is a function of the interfacial tension and the mechanical work. Emulsion with fine droplets can be obtained from oil with lower interfacial tension and higher degree of agitation.

This oily emulsion without surfactants can be categorized into 2 types, which requires different separation techniques, including:

- 1) Primary emulsion which droplet sizes are greater than 100 μm . This type is normally transparent with droplets can be visually observed.
- 2) Secondary emulsion which droplet sizes are smaller than 20 μm . A milky appearance is typically found.

1.1.1.3 Water pollution by oily emulsion with surfactants

Normally, water discharged from industry contains surfactants making the resultant oily wastewater forms a stable emulsion due to the properties of surfactants. The molecule of surfactant has double poles such as hydrophilic and hydrophobic parts, which can migrate to the interface between oil and water. Surfactants can lower the oil/water interfacial tension even with low concentration. The stable can be formed instantaneously when oil is mixed in water. This is the case why cutting oil used in machining industry is called soluble oil since it can emulsify rapidly in water. The emulsion in this case is typically called stabilized emulsion from its high stability and small droplets.

Droplets in this emulsion are usually smaller than 5 μm in diameter. Their rising velocities are very diminutive and can be neglected compared to Brownian movement. Furthermore, the presence of charges on droplet surface also impede the collision between droplets. The coalescence, which could destabilize the emulsion, rarely occurs as a consequence. Occasionally, surfactants in the emulsion are found as co-surfactants. The presence of co-surfactants results in more stable of the emulsion as droplet size much smaller than 1 μm can be found. This type of emulsion also requires specific treatment technique to deal with.

1.1.1.4 Water pollution by oil film

Since oil mostly has lower density than water, it tends to rise to the water surface forming a layer of thin film that can disturb the transfer of light and oxygen into water. Small quantity of oil can form film to cover large area of water surface. This type of oily wastewater can be easily observed by its rainbow reflection on the surface of the contaminated water. Due to the fact that oil already separates from water, this wastewater could be easily handled by skimming oil from the water surface.

Besides, there are other criteria for classifying oily wastewater as follow.

1.1.2 Classification of oily wastewater

1.1.2.1 Classification by characteristics of continuous phase

The mixture between oil and water is usually non-miscible. Particles or droplets suspended in liquid phase is called “disperse phase”, while the other is known as “continuous phase”. For example, the oily emulsion consists of oil as dispersed phase, and the continuous phase is water. Hence, the emulsions can be divided into 2 major groups classifying by their components as

1. *Direct emulsion* (or O/W emulsion) is the emulsion which the continuous phase that of is water.
2. *Inverse emulsion* (or W/O emulsion), on the other hand, is the emulsion, which contain oil as continuous phase.

1.1.2.2 Classification by degree of dispersion

This classified criterion is based on the rising velocity of oil droplets, which relate to the properties of oil and water as well as oil droplet sizes. According to the criterion, oily emulsion can be divided into 5 groups as follows:

- 1) Film or layer of oil on water surface
- 2) Primary emulsion
- 3) Secondary emulsion

Figure 1.1 displays the classification summary of primary and secondary emulsions and relation between oil droplets sizes and their rising velocities.

- 4) Macro-emulsion – This type of oily emulsion usually contains surfactant; thus, the size of oil droplets presented in water is very small, typically in the range of 0.06 to 1.0 μm . The macro-emulsion usually has a milky appearance.

- 5) Micro-emulsion – This type of emulsion contains a large amount of surfactants. The droplet size is between 10 to 60 nanometers. This emulsion is usually transparent or translucent.

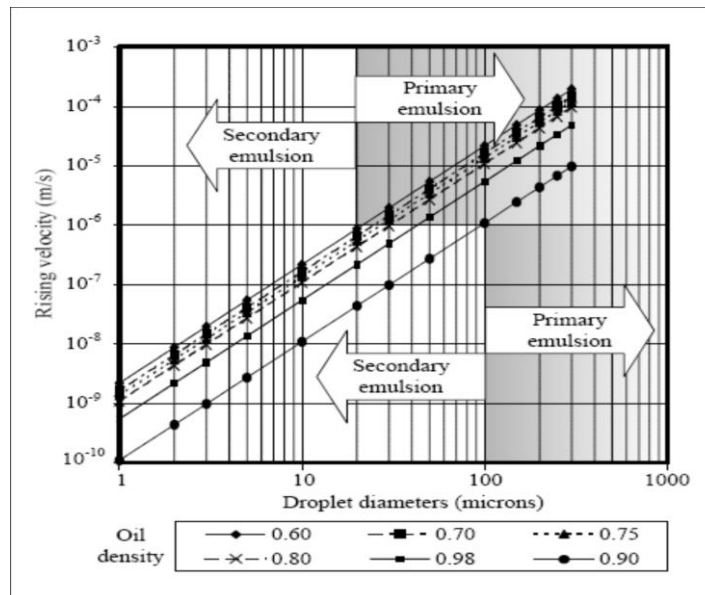


Figure 1.1 Relations between droplet sizes and rising velocities of primary and secondary emulsions (Wanichkul, 2000)

According to these classifications, some overlaps from these criteria can cause a confusion. To avoid that, the summary of the classification of oily wastewater can be illustrated in Figure 1.2.

As aforementioned, it can be concluded that the characteristics of oily emulsion depend on compositions in emulsion and the degree of dispersion also. Therefore, the best method to classify the oily wastewater is to analyze its properties by standard method in order to obtain the necessary data for selecting the appropriate treatment method.

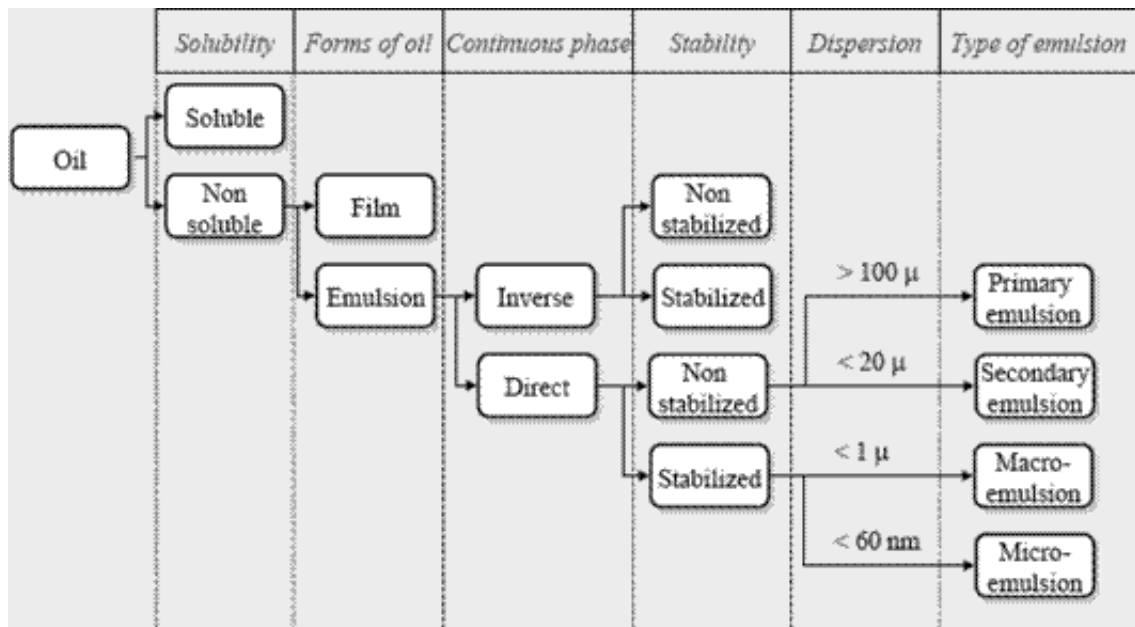


Figure 1.2 Summary of oily wastewater classification (Rachu, 2005)

1.1.3 Treatment of oily wastewater

Treatment methods for each type of oily wastewater is different based on its properties. For example, oil film can be separated by skimming out from the water surface, or dissolved oil can be treated by adsorption or oxidation. In the case of emulsion, the separation is normally used as a primary treatment unit before other process is applied for treatment. The separation of particles or oil droplets is generally based on Stokes's law where the settling or rising velocity of the spherical particles with Reynold's number less than 1 can be defined in Equation 1.3;

$$U_s = \frac{(\rho_p - \rho_f)gd_p^2}{18\mu_f} \quad (1.3)$$

Where U_s is the terminal settling or rising velocity of particles;

g is the gravitational acceleration (9.81 m/s^2);

$\rho_p - \rho_f$ is the density difference between the dispersed and continuous phase;

d_p is the diameter of disperse phase particle;

μ_f is the dynamic viscosity of the continuous phase

For oily emulsion, the dispersed phase is oil droplet, while continuous phase is water. As can be seen in equation, rising velocity of oil particles can be increased by 4 methods including

- 1) reduction of continuous phase viscosity,
- 2) increase of density difference between dispersed and continuous phase,
- 3) increase the gravimetric acceleration, and
- 4) increase the oil droplet size.

In practice, these separation principles are applied to develop variety of techniques for separation of oily emulsion. Furthermore, the destabilization of oily emulsion is sometimes necessary for the separation due to the stability of oil droplets.

1.2 Cutting oil

Cutting fluids or metalworking fluids refer to various types of fluid that are widely used in machining work with different purposes of using and application. Cutting fluids play an important role in every kind of machining e.g. boring, drilling, and grinding (El Baradie, 1996a). Three basic actions of cutting fluid that are beneficial in machinery process are (1) cooling, (2) friction reduction (or lubricating), and (3) shear strength reduction for working materials.

1.2.1 Types of cutting oil

Different types of cutting fluid can be classified according to several criteria; however, the fluids are generally grouped by the constituents that form either solution or emulsion. There are four basic categories of cutting fluids (Boothroyd, 2006); for example,

- 1) Straight or neat oils that are usually undiluted mineral oils, but often include other lubricants. These fluids provide very good lubricity but are relatively poor coolants.
- 2) Mineral-soluble oils (emulsions) that consist of oil with emulsifiers. These oils are used in diluted form, and widely applied in industry.
- 3) Synthetic fluids that are formulated from organic and inorganic compounds. These oil-free solutions are used in water dilution form. They present a very good cooling performance in industrial practice.
- 4) Semi-synthetic fluids (or micro-emulsion) are generally the combination of synthetic and soluble oil fluids; therefore, they offer good corrosion resistance, lubrication and contamination tolerance.

In addition, some additives are added in the cutting oils for increasing its efficiency or for specific intention. For instance, extreme pressure (EP) additives are employed for severe machining operations, which demand high pressure tolerance property and high active temperature regions. Biocides, or bacteria killing agents, must be added when require to clean out of pollutants or contaminants.

1.2.2 Lifecycle of cutting oil

The lifecycle of cutting fluids in a machining facility involves four stages (Grzesik, 2008), such as storage and handling, mixing with water, process using, and disposal. After the using stage, cutting oils, normally in form of oil-in-water emulsion, will consist of different contaminants, for example, particles, heavy metals, and organic matters. These rejected oils are typically handled by two methods. The first one is recycling, which contaminants are separated from rejected oil, and then purified before returning to use in manufacture process. Separation process is operated by variety of physical processes, such as, separation by magnetic or centrifugal force, filtration, and sedimentation. Afterwards, the oils are purified to adjust their properties; for example, oil is heated to reduce viscosity. Sterilization is also the significant process for protecting infection in order to eliminate the bacteria, which

might be in the constituents of emulsion. Another process used with rejected oil is disposal. This method is applied when oil recovering is incapable or difficult, for instance, high water content or inadequate quality recovered oil. The disposal process normally consists of two processes. Firstly, the oil emulsions are destabilized into oil and water, normally by chemical processes. According to Rios et al. (1998), inorganic salts were employed as coagulants to demulsify the emulsion, and then oil droplets in water can be removed by settling. The separated oil then enters the disposal process. The conventional disposal process of oils in industry is combustion where oil is used as an alternative fuel. Besides, biodegradation is another interesting alternative. Cheng et al. (2005) reviewed that the biological degradation, both aerobic and anaerobic, can effectively remove COD and turbidity, which represent the amount of cutting oil in water. Electro-coagulation was another process that applied for treatment of metalworking fluid in water as well (Bensadok et al., 2008; Kobya et al., 2008).

1.2.3 Hazards of cutting oil

The toxicity of cutting fluid commonly occurs from the contaminants in emulsion through skin contact and inhalation exposure pathways. Skin disorders, respiratory diseases, and cancer are the adverse health effects involved in cutting fluids exposure (OSHA, 1999). The severity of effects depends on several factors, such as, type of fluid, concentration and type of contamination, and the level and duration of exposure. The symptoms of skin disorders from cutting fluids are acne and contact dermatitis, which can be divided into two kinds, i.e. irritant and allergic contact dermatitis (El Baradie, 1996b). The exposure through skin contact results from working or accident with inadequate protecting equipment. Whereas, cutting fluid aerosol or mist inhalation can cause the respiratory diseases and also aggravate the effects of existing diseases. The symptoms of the diseases are either acute (e.g. airway irritation, asthma, and lung inflammation) or chronic effects, such as, chronic bronchitis and lung function damage (OSHA, 1999). It should be noted that a number of studies have found relation between cutting fluids exposure and variety of cancers

causing by the fluids composition. Effects of cancer become signified after long period exposure of cutting fluids.

1.3 Chemical destabilization

Chemical treatment for oil/water separation normally refers to chemical destabilization, coagulation, and flocculation processes (Al-Shamrani et al., 2002). The process does not dispose the oil, but intends to transform the oil to the form that facilitates to separate (Rachu, 2005). The chemical treatment is generally required when oils are presented in the form of very stable emulsion, which will not be naturally coalesced. Therefore, it is difficult to separate by merely physical process (Rachu, 2005; Al-Shamrani et al., 2002).

1.3.1 Properties of stable emulsion

1.3.1.1 Thermodynamic stability

The interfacial tension of oil is normally positive. However, the stability of oil droplets is increased when the interfacial tension is lowered, generally by adding surfactants. The surface area of droplets is increased, thus resulting in the decrease of droplets' diameter. Surfactants will try to stretch or increase the droplets' surface area as much as possible in order to locate themselves on the surfaces. Finally, it results in the counter between the virtual force (p), which tries to stretch the surface, and the interfacial tension (γ_{ow}), which attempts to contract the surface, as illustrated in Figure 1.3.

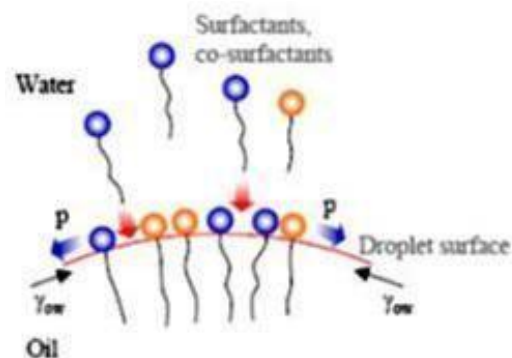


Figure 1.3 Interfacial of oil and water with the presence of surfactants (Rachu, 2005)

When the surfactant concentration is high enough, the interfacial tension is lower until becoming zero, in other words, the thermodynamic equilibrium condition. The droplets' energy is zero. If droplets coalesce, the surface area will be decrease, which disturbing the equilibrium. The energy and tension of droplets will be negative. As a result, droplets will spontaneously redistribute to the small size in order to preserve its equilibrium state.

1.3.1.2 Dynamic stability

This stability is a result of 2 resistances, i.e. electrical and mechanical resistances or barriers.

- *Electrical barrier*

The electrical characteristic of charged particles can be explained by the double layer theory as shown in Figure 1.4. Oil droplets are normally negatively charged due to the adsorption of negative ions. The opposite charges (counter ions), positive charges in this case, are then attracted to surround the bubble. However, the positive ions are usually enclosed with water molecule. Therefore, they can only approach the oil droplet a certain distance called “stern layer thickness” (Ω), which is the inner of the double layer. On the other hands, another layer is called “diffused layer” where other counter ions locate outside the stern layer. The ions are denser near the surface and progressively sparser with distance until equal to that in the bulk liquid. Effects of droplets' charge can be negligible outside the diffused layer.

Electric force from the droplet's charges can be measured by their movement when electrical field is supplied. The movement of the negatively charged (in this case) toward the anode can be converted to the electrical voltage value, which is denoted as “zeta potential” (ζ). The higher the ζ value, the greater the repulsive force between droplets. From that reason, droplets cannot move close to each other.

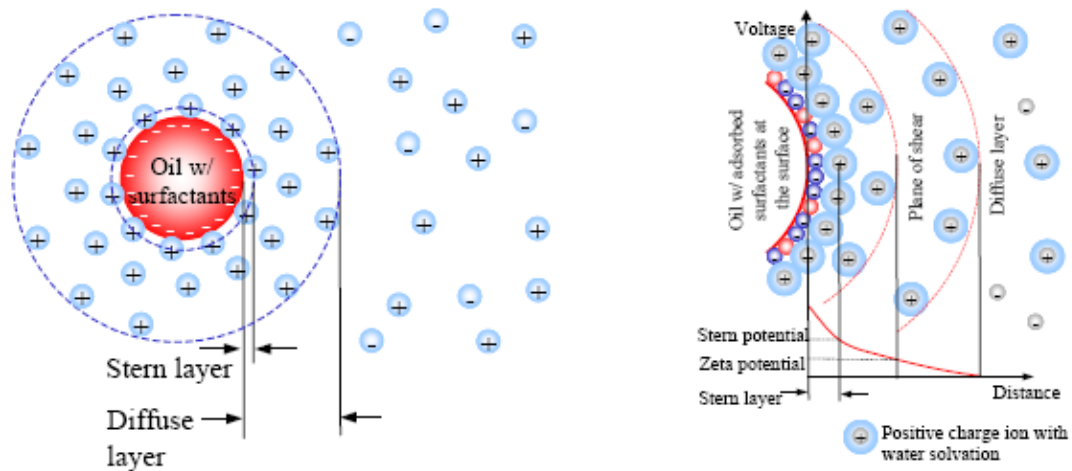


Figure 1.4 Diagram of the electrical double layer (Rachu, 2005).

- *Mechanical (dynamic) barrier*

Some emulsion systems can be very stable even at low zeta potential due to the presence of the mechanical barrier, or so-called dynamic barrier. This barrier causes by a rigid film of surfactants on droplets' surface, which prevent the coalescence of droplets even they collide. In order to increase the emulsion stability by the dynamic barrier, likewise in production of cutting-oil emulsion, co-surfactants or multi-surfactants are added. This added co-surfactant can increase the film rigidity since their molecules can tightly organize on the droplets' surface.

1.3.1.3 Destabilization of stable emulsion

The destabilization of the emulsion is the process to eliminate or minimize the stabilized properties of emulsion by various methods, for instance,

- increase of interfacial tension to eliminate thermodynamic stability,
- minimize or elimination of surfactant films around the droplets, and
- reduction of charge of the droplets to eliminate or minimize electrical barriers.

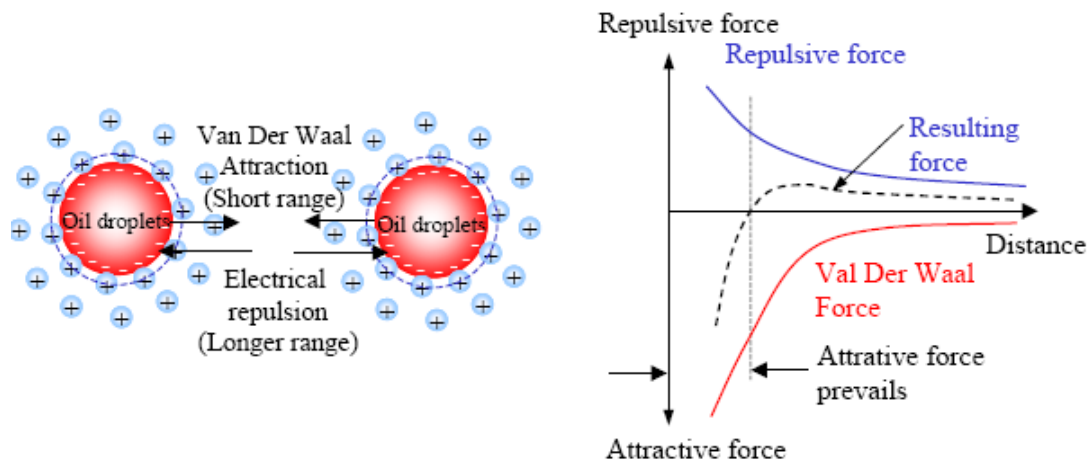


Figure 1.5 Force diagrams of oil droplets and relation of repulsive, attractive and resulting force with the distance between oil droplets (Rachu, 2005).

As droplets approach to each other at some certain distance, the attractive force between molecules can overcome the repulsive force. The net force will then be attractive as displayed in Figure 1.5, and the coalescence probability between droplets is encouraged.

1.3.1.4 Destabilization mechanisms for oily emulsion

In order to destabilize the stable oily emulsion, different types of destabilization methods can be applied as follows:

- *Reduction of diffuse layer thickness*

When counter-ions are added into the wastewater, they will be attracted by charges on droplets' surface. The ions will then surround tightly near the droplets and reduce the diffused layer thickness around the droplets. This effect results in the reduction of zeta potential; thus, droplets can move closer to each other and have higher probability to coalesce. The counter-ions can be added until reaching the iso-electric point (zeta potential = 0). Note that this destabilization method cannot reverse the droplet charges, no matter how many ions are added.

- *Sweep coagulation*

Some metal salts can form complexes with other ions in the water, such as hydroxide ion (OH^-). Normally, these complexes are in solid or precipitated form and can trap the oil-droplets. The droplets are therefore separated from an emulsion. Salts that are typically used are multivalent metal salts, such as alum.

- *Adsorption and charge neutralization*

This method can be done by adding surfactants that contain opposite charges to those present in the emulsion. The added surfactants will be adsorbed on the droplets, thus neutralizing their charge. However, addition of overdose surfactants can cause the charge reversal of droplets and re-stabilization of emulsion.

- *Bridging*

Several commercial chemicals can be applied for destabilizing emulsions by their molecule structure and properties. Oil can be trapped by the bridging properties or adsorbed on the surface.

- *Precipitation of surfactants*

Since emulsion stability is based on presence of surfactants, precipitation of surfactants can certainly destabilize the emulsion. By adding some chemicals, surfactants will be reacted, forming complex with no surfactant property. Bivalent or multivalent salts are used to precipitate the surfactants, for example, CaCl_2 , MgCl_2 , MgSO_4 , $\text{Al}_2(\text{SO}_4)_3$, and FeCl_3 . Generally, the higher the valence of chemical, the better the efficiency to precipitate the surfactants and the smaller dosage required. However, precipitation efficiency also depends on types of salts and surfactants in an emulsion, which should be verified by jar test experiment.

It should be noted that these different methods can act individually or simultaneously with others. Though, all methods require the addition of counter ions or charges to destabilize or coagulate an oily emulsion.

1.3.1.5 Chemicals (coagulant) used for destabilization

Chemicals generally used to achieve the destabilization mechanisms described above include:

- *Monovalent electrolytes*

The mechanism of this chemical type is the reduction of diffuse layer. The required dosage is high in order to provide sufficient concentration of positive ions to destabilize the droplets. Examples of this chemical type are NaCl and H₂SO₄.

- *Bivalent electrolytes*

Examples of this of chemical types are CaCl₂, MgSO₄, and MgCl₂. The main destabilization mechanism is the precipitation of surfactants. The free surfactants in water will react with the added ions (e.g. Ca²⁺ or Mg²⁺) and form complexes. The equilibrium between the free and the adsorbed surfactants on the droplets' surface is therefore shifted. As a result, the adsorbed surfactants will reverse into the free surfactants, thus reducing the stability of emulsion. The effect is practically governed by solubility product of the surfactants. The required dosage is lower than that of monovalent one.

- *Multivalent electrolytes*

For this chemical type, the destabilization mechanisms are combination between precipitation of surfactants and sweep coagulation. The actual dosage is normally lower than that of calculated from the solubility product, and usually lowest among the first three electrolytes. Examples of this type are ferric chloride (FeCl₃) and alum (Al₂(SO₄)₃). Generally, the multivalent electrolytes are more effective than the previous two chemical types. Nonetheless, it might not be capable to use with certain type of surfactants.

- *Surfactants with opposite charge*

Main destabilization mechanism from this type is adsorption and charge neutralization. Overdosed addition must be avoided to prevent charge reversal and re-stabilization. Chemicals in this type are cationic surfactants, for example, N-cetylpyridinium chloride and salts of quaternary ammonium hydroxide.

1.3.1.6 Treatment of oily-emulsion by chemical destabilization

Several researches were conducted for studying the destabilization of emulsion as follows:

Rios et al. (1998) investigated the destabilization of oily emulsion by metal salts. The emulsion was prepared from 3 different types of cutting-oil at 3% volume by volume concentration. CaCl_2 and AlCl_3 were selected as metal salts for destabilization. Effects of type and dose of salts, temperature, and electrolyte concentration were determined.

It was shown that the addition of electrolyte resulted in the reduction of zeta potential; thus, oil-droplets can coalesce to each other and forming the larger size. In addition, increase of temperature can enhance the destabilizing rate due to Brownian diffusion movement. No difference between the used salts was observed. Charge neutralization was suggested as the main destabilization mechanisms. Efficiency of the process was controlled by the droplet-droplet collision, which can be explained by Smoluchowsky's rapid flocculation model

Cañizares et al. (2008) studied the oil-in-water emulsions treatment with chemical coagulation and electrocoagulation processes. Oil mixture, which contained 1:1 lubricating oil to soluble oil ratio, was used as modeled emulsion with concentration of 0.15 – 0.60% volume by volume. Aluminium ions were added to the process by AlCl_3 and $\text{Al}_2(\text{SO}_4)_3$ in chemical coagulation and by aluminium plate in electrocoagulation process.

From the results, key factors governing the process efficiency were dose of aluminium ion (Al^{3+}) and pH of solution. Destabilization of emulsion only occurred at pH 5 – 9. The required dose of Al^{3+} was found to be proportional to oil concentration. Higher oil concentration resulted in lower separation performance. The chemical coagulation provided slightly higher treatment efficiency than that of electrocoagulation and also higher final pH value. It was stated that the destabilization occurred due to coalescence of oil droplets that attached on the precipitation aluminium hydroxide ($\text{Al}(\text{OH})_3$) particles.

1.4 Coalescer process

Coalescer is an equipment suitable for liquid-liquid dispersion or emulsion separation. The process is usually implied as the emulsion upflow through a layer of coalescer media (Wanichkul, 2000). As a result, the tiny oil droplets will attach to the media and each other resulting in the increase of their sizes. An important component of coalescer is the media bed, which is typically hydrophobic since it has higher ability to attach with oil droplets. Oil droplets, therefore, tend to coalesce forming larger droplets. Hence, media selection is an essential point in order to achieve the efficient coalescer performance. The type of coalescer can be divided by different kinds of media into two types, i.e. granular bed coalescer and fibrous bed coalescer.

1.4.1 Mechanisms in coalescer process

The mechanisms in coalescer can be divided into 3 steps as in Figures 1.6 and 1.7 (Rachu, 2005):

- 1) Interception that is similar to the filtration mechanisms, which oil droplets adhere on the collector or coalescer media. This step consist of 3 transport phenomena that will be subsequently defined later.
- 2) Adhesion and coalescence of oil droplets where droplets within the bed will attach to media creating the oil film, which can coalesce with other droplets to form the large oil droplets. This step is important for coalescer process since

the coalescing media should be well chosen in order to encourage the attachment probability between oil and media.

- 3) Salting out or enlargement of coalesced liquid defining as the leaving of coalesced oil droplet from bed to the water surface. The mechanism in this step is critical for oil separating from water. The mechanism is governed by 4 major properties, including (1) the wettability of the salting out surface, (2) the interfacial oil/water tension and the diameter of the drip point, (3) The velocity of emulsion through media bed, and (4) oil in water ratio.

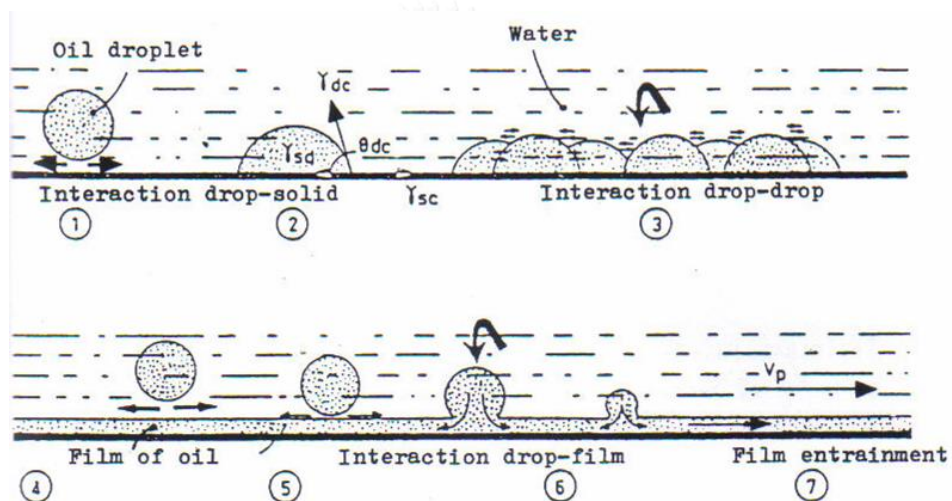


Figure 1.6 Phenomena in interception, adhesion, and coalescence steps (Aurrelle, 1985)

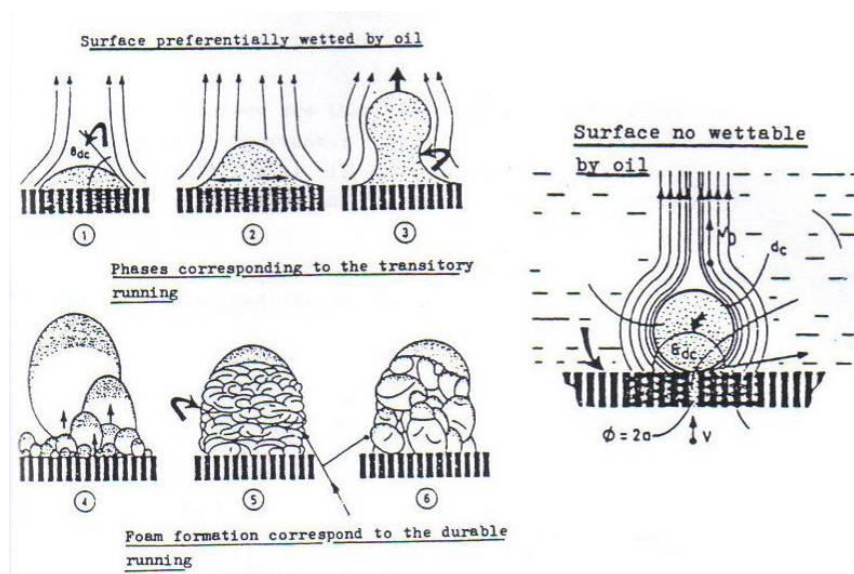


Figure 1.7 Schematic diagram of salting out phenomena of coalesced oil droplets (Aurelle, 1985)

1.4.2 Transport of oil droplets to contact with collector

To understand the treatment mechanisms in the coalescer process, the transport phenomena of oil droplets to contact with media should be considered. Normally, it can be described by 3 mechanisms, including the transportation by 1) sedimentation, 2) direct interception, and 3) diffusion (Aurelle, 1985). These concepts are normally applied from the filtration model, since the interception of oil droplets by collector is relatively close to that of filtration through the media (Rachu, 2005). The schematic diagrams of the transport phenomena are illustrated in Figure 1.8.

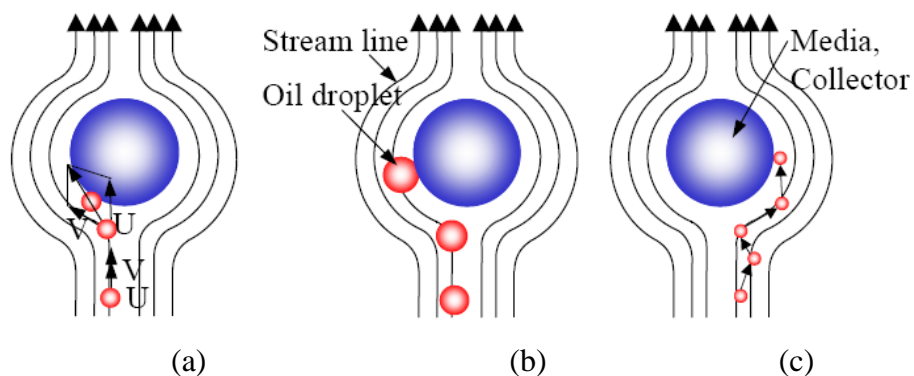


Figure 1.8 Schematic diagrams of the transport phenomena (a) sedimentation, (b) direct interception, and (c) diffusion (Rachu, 2005)

1.4.2.1 Transportation by sedimentation

The oil droplet of diameter “ d ” is subjected to two velocity vectors, including “ U_s ” which is the rising velocity governed by Stokes’s law, and the flow velocity, “ v_f ”, of the water through the collector as displayed in Figure 1.8a. At a far distance from the collector, the two vectors have the same direction, and the oil droplet will follow the streamline. When the oil drop approach to the collector, the rising velocity, “ U_s ” still conserve its direction, but the “ v_f ” flow velocity vector will follow the streamline direction; therefore, the resultant vector causes the oil droplet to leave the streamline. For that reason, the oil drop likely to collide with the collector, thus, sediment on the collector. The efficiency factor of this phenomenon (η_s) can be calculated by Equation 1.4, where d_p is the diameter of oil droplet.

$$\eta_s = \frac{\Delta\rho g d_p^2}{18\mu_f V} \quad (1.4)$$

1.4.2.2 Transportation by direct interception

This phenomenon will occur when the density difference of oil droplet and water is similar. Therefore the $\Delta\rho$ is equal to zero, and transportation by sedimentation cannot occur. However, the oil drop can still contact to the collector by the mechanism of direct interception. Consider oil droplets of diameter “ d ” carried by the streamline, the oil drops that flow within the distance “ $d/2$ ” far from the collector will contact, and will be intercepted by the collector as shown in Figure 1.8b. The direct interception efficiency (η_I) can be calculated from Equation 1.5, where d_c represents the diameter of collector.

$$\eta_I = \frac{3}{2} \left(\frac{d_p}{d_c} \right)^2 \quad (1.5)$$

1.4.2.3 Transportation by diffusion

This transport model is used in order to describe the interception of oil droplet of diameter less than 5 μm . These micro-droplets prone to have Brownian movement, resulting in random direction movements that likely encourage the oil droplets interception in the collector. Figure 1.8c demonstrates the mechanisms of transportation by diffusion. The efficiency factor of this transport phenomenon (η_D) can be calculated from Equation 1.6 where K and T are Boltzmann's constant ($1.38 \times 10^{-23} \text{ kg}\cdot\text{m}^2/\text{K}\cdot\text{s}$) and liquid temperature in Kelvin, respectively.

$$\eta_D = 0.9 \left(\frac{KT}{\mu_f d_p d_c v_f} \right)^{\frac{2}{3}} \quad (1.6)$$

As mentioned above, the efficiency factor of each transport phenomenon can be calculated for single collector. The total efficiency of interception step of coalescer for single collector is the summation of the efficiency factor of those phenomena; hence, the single collector total efficiency (η_T) can be calculated from Equation 1.7.

$$\eta_T = \eta_s + \eta_I + \eta_D \quad (1.7)$$

1.4.3 Coalescer efficiency equation

The equation of coalescer was proposed by Aurelle (1985) based on the filtration efficiency equation due to the fact that emulsion was flowed through medium bed in coalescer process likewise in filtration, despite oil droplets in emulsion in case of coalescer were not supposed to trap in the coalescing bed. Since the efficiency of coalescer mainly depends on the interception, the efficiency equation has to consider in that mechanism. The efficiency equation was proposed by considering the wastewater flow through single spherical collector in laminar flow regime as illustrated in Figure 1.9a, and then adapt for entire volume of medium bed.

First, the fraction of wastewater flowing passes the collector can be defined as the flow through the projected area of the collector (q) as in Equation 1.8. Afterwards, some oil droplets would be transported to the collector (media) due to the single collector total efficiency (η_T), which quantity of dC_1 as in Equation 1.9.

$$q = \frac{\pi}{4} d_c^2 v_0 \quad (1.8)$$

$$dC_1 = \eta_T q C_0 \quad (1.9)$$

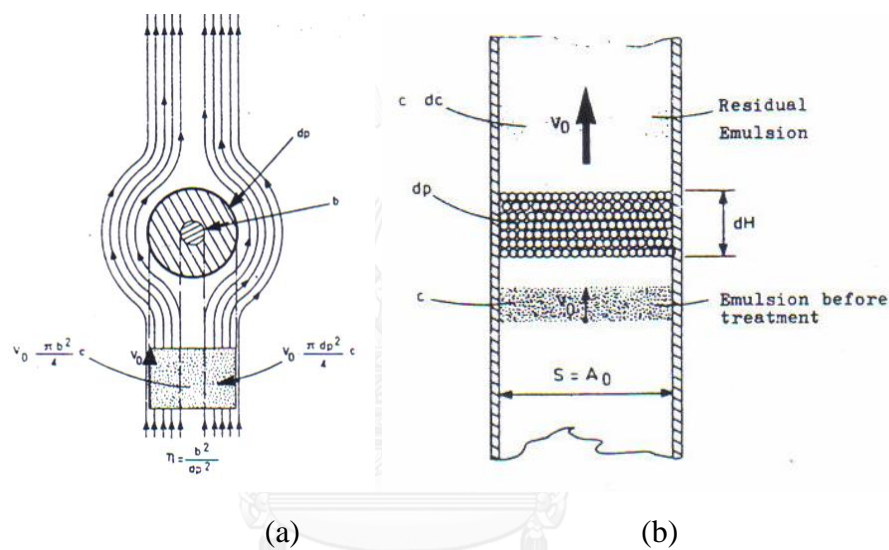


Figure 1.9 Schematic diagrams of (a) single collector and (b) entire media bed (Aurelle, 1985)

Where, v_0 and C_0 are the flow velocity and initial concentration of wastewater, respectively. Then, the equation was accommodated for applying with entire bed volume with slight bed height (dH) as displayed in Figure 1.9b. The number of collector in this bed can be calculated from the cross sectional area of bed (A_0), collector size (d_c), and porosity of the bed (ϵ_0). Total concentration of intercepted oil in this slice bed, dC_2 , equal to the product of concentration intercepted by single collector and number of collector. The attachment efficiency (α) defined as the probability of oil droplets to adhere with collector, has to be considered as the actual quantity of intercepted oil droplet. Hence, the total concentration of intercepted oil in bed can be defined as in Equation 1.10.

The number of collector in slice bed height $dN = \frac{dL(1-\varepsilon_0)A_0}{\pi/6 \cdot d_c^3}$

$$dC_2 = \alpha \frac{dH(1-\varepsilon)A_0}{\pi/6 \cdot d_c^3} dC_1 \quad (1.10)$$

The concentration of oil reduced after passing through the bed dL is equal to $-V_0 A_0 dC$; therefore, the efficiency equation can be defined as in Equation 1.11 and 1.12.

$$-V_0 A_0 dC = \alpha \eta_T \frac{\pi}{4} d_c^2 V_0 C \frac{dH(1-\varepsilon_0)A_0}{\pi/6 \cdot d_c^3} \quad (1.11)$$

$$\frac{dC}{C} = -\frac{3}{2} \alpha \eta_T (1-\varepsilon_0) \frac{dH}{d_c} \quad (1.12)$$

By integrating Equation 1.12, the final equation of filtration (coalescer) efficiency can be obtained as expressed in Equation 1.13.

$$\ln \frac{C}{C_0} = -\frac{3}{2} \alpha \eta_T (1-\varepsilon_0) \frac{H}{d_c} \quad (1.13)$$

This equation could be used to explain the impact of mechanisms occurred in the coalescence process since the effects of medium properties and operating conditions (i.e. flow velocity and bed height) were considered.

1.4.4 Treatment of oily emulsion by coalescer

Li and Gu (2005) have studied the coalescence mechanisms of oil particles in emulsion in fibrous and granular bed coalescer. The apparatus was a 73 mm diameter with 70 cm length stainless steel pipe. Emulsion effluent was horizontally flowed through coalescer media beds, which were polypropylene fiber, nylon fiber, and

granular polypropylene. The studied parameters in this research were the influent flow rate, emulsion concentration, media bed length, and size of fiber media. The results were shown by system efficiencies that evaluated from the coalescer efficiency equation, and oil droplet size distribution.

The study found that the efficiencies of coalescer were influenced by the inlet oil concentration and type of media. An effective coalescence can be achieved by using small fiber media, or low oil inlet concentration. The high efficiency coalescer can be obtained for appropriate flow rate range, which can be investigated in an experiment. However, the effect of media bed length can be neglected for horizontal flow coalescer.

Sokolović et al. (2006) studied the coalescence of oil droplets in diluted emulsion by coalescer process. The impacts on efficiency of various operating conditions, for instance, coalescing media bed height (3 – 15 cm), flow pattern (horizontal, upflow and down flow vertical), media properties, and flow velocity (16 – 50 m/h) as well as oil concentration (500 – 10,000 mg/l with mean diameter 20 μm). The applied medium is Polyurethane (PU) fiber. The results were compared by using critical velocity (defined as the flow velocity that produced the effluent concentration of 15 mg/l) and oil concentration in effluents.

It was found that horizontal flow pattern provided the highest critical velocity in every experiment. The critical velocity is higher when water permeability and length of media bed were increase. Moreover, the influent oil concentration impacted the critical flow velocity as well as the effluent concentration. However, the impacts of oil concentration can be ignored in case of long bed height.

Sokolović et al. (2009) studied treatment of heavily polluted oil wastewater by fiber-bed coalescer. The experimental set-up was carried out in real industrial plant in Serbia. Oily wastewater used in this study was the real one from Oil Company at constant concentration of 500 mg/L with mean droplet diameter as 20 μm . The applied coalescing media were two different types: granular expanded polystyrene

(EPS) and polyurethane fiber (PU) with vertical flow pattern. In all experiments, the steady-state was established from the beginning of the experiment by pre-oiling of the coalescing fiber. Fluid velocity applied in this study was 7 m/h in every experiment with constant temperature of 35°C. Oil concentration in water was investigated by IR spectrometry. It was found that the designed bed coalescer provided effective oil removal from heavily polluted wastewater where effluent oil concentration was less than 15 g/L in whole experiment. The oil separation efficiency was dependent on inlet oil concentration and droplet size. Moreover, higher performance of coalescer was obtained from the special design and application of two medium materials. The design flow orientation provided inertia force, which was one of dominant separation mechanisms. The oil removal mainly occurred by two different mechanisms: coalescence of oil droplets at water surface and capture in the coalescing bed.

Zhou et al. (2009) studied the effects of medium types and also operating parameters on oil separation efficiency of modified resin coalescer. Diesel oil #0 and anionic surfactant (SDBS) were used for preparing synthetic wastewater at 1000 mg/L concentration with 10 µm mean droplet diameter. Coalescing media used in the study were organic medium (i.e. PP and polystyrene resin) and inorganic (granular activated carbon: GAC and ceramic filter: CF), while various considered operating parameters were flow velocity, bed height, influent oil concentration, pH, and temperature. In this study, polystyrene resin was modified by grafting cetyltrimethyl-ammonium bromide for demulsification of oily emulsion purpose. The results indicated that modified resin provided higher efficiency than that of PP, ceramin, can GAC media. Moreover, highest treatment efficiency of resin medium was achieved at more than 80% under optimal operating conditions; for example, flow velocity of 60 – 180 mL/h, bed height of 20 – 40 cm, temperature of 20 – 60°C, and pH value between 2 and 10. This high efficiency might be the integration of both chemical demulsification and coalescence occurred in the process, which was the major disadvantage of this medium.

1.5 Flotation process

Flotation is the physical process applying for separation of disperse phase, i.e. solid or liquid particles, from the continuous phase by increasing the density difference between two phases. In this process, air bubbles are introduced into the system to attach with the dispersed phase (particles), forming the bubble-particle agglomeration. This agglomerate contains higher density difference with continuous phase (water) than that of the initial two phase. Since the difference of density is increased, the rising velocity of the agglomerate is raised according to Stokes's law. Therefore, the particles then rise to the water surface and can be separated by a skimmer.

The separation of particles by flotation process typically consists of 4 steps including, (1) generation of air bubbles, (2) contact between the air bubbles and particles, (3) flotation of particles by the buoyant force, and (4) removal of particle by skimming (Hendricks, 2006). Amongst these steps, the critical one that governs the overall efficiency of the flotation process is the contact between the bubbles and particles.

Normally, flotation processes that have been extensively used for removal of stabilized oily emulsions or suspended particles are the dissolved air flotation (DAF) and induced air flotation (IAF) according to da Rosa and Rubio (2005).

1.5.1 Dissolved air flotation (DAF)

Diffused air flotation (DAF) is the most commonly used flotation process for water treatment. DAF has been widely used due to its versatility and efficiency. Its finest air bubble can be used for several purposes in the environmental applications (Rubio et al., 2002), for example, solid separation, sludge thickening, flocs separation, and dissolved organic chemicals removal.

Bubbles in DAF process are generated by releasing the pressurized water, which is saturated with air in higher pressure than atmosphere. The release of the saturated water into the atmospheric pressure will cause the dissolved air separate

from water in form of micro-bubbles throughout the entire volume of liquid. Generally, the generated bubbles in this DAF process are in the range of 30 – 70 microns (da Rosa and Rubio, 2005).

1.5.2 Induced air flotation (IAF)

In this process, air is introduced and formed bubbles by a mechanical agitator or air injection system in the atmospheric pressure condition. The sizes of the generated bubbles are normally in the range of 700 – 1500 microns. This process provides the advantages due to its high efficiency and little time consuming. Moreover, it requires less maintenance and low construction and operation cost (Rubio et al., 2002).

1.5.3 Mechanisms of flotation process

1.5.3.1 Interaction between bubbles and particles in flotation

Flotation process is based on the capture of particles or droplets by rising bubbles. Capture can occur when bubble and particle approach each other close enough to attach and form a stable aggregate. Derjaguin and Dukhin (1961) explained the bubble-particle interaction by three zones model separating by the distance from bubble's surface, for example,

- Zone 1 is the farthest zone from the surface where the interaction is mainly governed by hydrodynamic.
- Zone 2 that is closer to the bubble's surface. In this zone, the flow around the bubble creates a tangential stream that sweeps the adsorbed surfactants or particles on the front to the rear part of bubble. The particle concentration on the bubble's surface becomes non-uniform, resulting in the occurrence of concentration gradient. The diffusional boundary layer is then generated around the bubble. The interaction in this zone is governed by electrophoretic force.

- Zone 3 is the nearest zone to the bubble's surface. The thickness of the thin film reduces to the range of hundreds nanometers (Derjaguin and Dukhin, 1961). Surface forces are dominant. In this region, an attractive force between particles and bubbles is due to hydrophobic force, while the Van der Waals and electrostatic forces are normally repulsive.

Particle captured in flotation is generally discussed as the series of three sub-processes including collision, attachment, and stability (Ralston and Dukhin, 1999a). Therefore, the capture efficiency (E_{capt}) can be defined as the product of three sub-process efficiencies as Equation 1.14.

$$E_{capt} = E_{coll} \cdot E_{att} \cdot E_{sta} \quad (1.14)$$

Where E_{coll} is the collision efficiency, E_{att} is the attachment efficiency, and E_{sta} is the stability efficiency of the bubble-particle aggregate. Hence, in order to comprehend mechanisms in flotation process as well as its efficiency, the understanding in each sub-step is required. The detail of each sub-process is exhibited as follows:

1.5.3.1.1 Particle-bubble collision in flotation

Collision is the process where particle and bubble approach to each other to the distance close enough for surface forces can act. This process is governed by both hydrodynamics and inertial forces, which affect the movement of both particle and bubble. Particle-bubble collision relates to the flow field around the bubble. Consider a spherical bubble with radius $r_b = d_b/2$ and a spherical particle with $r_p = d_p/2$ as illustrated in Figure 1.10. Particles can collide with the bubble when its trajectory pass the bubble's surface with distance less than r_p , which denoted as limiting stream (i.e. represent by ψ_{crit}).

Generally, collision between particle and bubble is a resultant of several mechanisms (Schulze, 1989) as following.

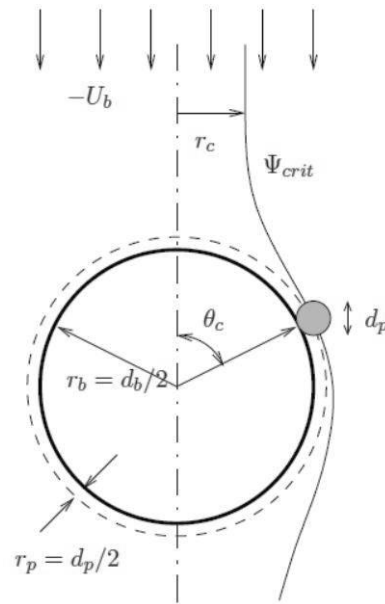


Figure 1.10 Particle-bubble collision (Huang, 2009)

- *Interception*

Interception occurs when the particle with diameter r_p has a trajectory pass the bubble with the distance $d_b/2$ far from the collector. The particle will then collide by the bubble. This mechanism is mainly governed by sizes of particle and bubble.

- *Inertial effect*

Inertia force of particle can affect its trajectory when moving towards a bubble. Normally, effect of inertia is determined by Stokes number (St_p). For sphere particle and bubble, Stokes number can be defined as Equation 1.15.

$$St_p = 2\rho_p r_p^2 U_b / 9\mu_f r_b \quad (1.15)$$

According to Ralston et al. (2002), inertia force can affect the bubble movement in three different way, including

- Change of particle trajectory – Particle with considerable inertia might be unable to follow the changing flow streamline near a bubble; therefore, it breaks the streamline and collides with a bubble.
- Centrifugal force – Inertia can cause the centrifugal force when particle is near the equatorial part of bubble. As a result, the particle is pushed away from the bubble's surface.
- Deformation of bubble's surface during collision – A particle with high inertia (i.e. high St) might bounce off the bubble's surface when colliding due to its high kinetic energy. The particle, therefore, could experience the second collision at other part of bubble.

- *Gravitational sedimentation*

Particles, with their own settling velocity, can separate from the fluid streamline and collide with bubble due to gravitational force. The settling velocity of particle (U_s) with density of ρ_p in the fluid with density and dynamic viscosity of ρ_f and μ_f , respectively, at laminar flow regime can be determined by the terminal velocity from Stokes law as in Equation 1.16.

$$U_s = \frac{2(\rho_p - \rho_f)gr_p^2}{9\mu_f} \quad (1.16)$$

- *Brownian diffusion*

Particles might collide with bubbles by their Brownian motion due to the diffusion phenomenon, particularly for the small particle. This transport mechanism is controlled by the diffusion coefficient (D) of particle, which can be evaluated by Stokes-Einstein equation (Equation 1.17),

$$D = \frac{k_B T}{6\pi\mu_r r_p} \quad (1.17)$$

where k_B is Boltzmann's constant equals to 1.38×10^{-23} J/K, T is temperature of fluid in Kelvin, and μ_f is the dynamic viscosity of fluid.

- *Turbulent diffusion*

Turbulence caused by movement of other bubbles could result in the diffusion of particle, so-called turbulent diffusion, which can increase its collision probability to bubble. This diffusion can be determined by Stokes number in turbulent flow regime, which is defined as ratio between the relaxation time of particle (τ_i) to the characteristic time of fluid (τ_η), i.e. $St^t = \tau_i / \tau_\eta$.

1.5.3.1.2 Particle-bubble attachment in flotation

Nguyen et al. (1997) suggested three elementary steps for a successful particle-bubble attachment, for instance,

- 1) draining or thinning of the liquid film between particle and bubble to a critical thickness where the film will rupture,
- 2) rupture of the liquid film and forming of a three-phase contact line (TPCL),
- 3) expansion of the TPCL to form a stable wetting perimeter.

Each step contains their own characteristic time required for occur. The summation of time for each step is introduced as induction time (t_{ind}), which indicates the time required for bubble-particle attachment. The induction time can be written as in Equation 1.18.

$$t_{ind} = t_{att} = t_d + t_r + t_e \quad (1.18)$$

Where t_{att} is the time required for successful attachment. The t_d , t_r , and t_e represent times for film drainage, film rupture, and TPLC expansion, respectively.

Nevertheless, film rupture is very fast process according to Ralston and Dukhin (1999a), therefore, induction time is only the sum of times for film drainage and TPLC expansion. The successful attachment can occur when the bubble-particle contact time is longer than the induction time, in other words, the attachment can occur before the bubble and particle bounce off. Typically, the contact time is in the range less than 10^{-2} s (Ralston and Dukhin, 1999b). Afterwards, Wang et al. (2006) suggested that the film drainage is the limiting step for attachment. The induction time is then approximately equal to the film drainage time. This induction time is affected by both bubble and particle sizes as increase of either bubble or particle size result in longer induction time due to larger bubble-droplet contact area. Moreover, the t_{ind} was found to be increase for less hydrophobic surfaced particles since the critical film thickness is thinner. The time for film drainage is longer as a result. Several factors were found to impact the induction time. According to Oliveira et al. (1999), the induction time was lengthened by the presence of surfactants, resulting in lower flotation efficiency. On the contrary, the inverse trend was found for the salt concentration. The surface charges of particle and bubble, which are normally positively charged, can be affected by the presented salinity, resulting in shorter induction time and higher flotation efficiency.

For droplet-particle attachment, besides the induction time, spreading coefficient (S_0) was discovered as another important parameter (Oliveira et al., 1999). S_0 was defined as the imbalance between the interfacial tensions acting along a TPLC (Moosai and Dawe, 2003). For oil spreads on water-gas system, the spreading coefficient can be described as in Equation 1.19.

$$S_0 = \gamma_{wg} - (\gamma_{ow} + \gamma_{og}) \quad (1.19)$$

Where γ_{wg} is an interfacial tension between water and gas. γ_{ow} and γ_{og} represent interfacial tensions of oil-water and oil-gas, respectively. The attachment of oil droplet occurs when $S_0 > 0$ when oil layer can spread on the interface. On the other hands, oil will form a drop with a definite contact angle with other two phases when

$S_0 < 0$. However, attachment still happen even $S_0 < 0$, but the adherence of droplet-bubble is weak and tends to break-up when rising.

1.5.3.1.1 Stability of particle-bubble aggregate

The stability of bubble-particle aggregate occurs when the adhesive force is sufficient to hinder the break-up of aggregate under the dynamic condition in flotation (Ralston and Dukhin, 1999a). The adhesive force (F_{ad}) can be determined from the difference between the attachment force (F_{att}) and the detachment force (F_{det}). Particles will return to a liquid phase if F_{ad} is negative. Consider a spherical particle attached on a large bubble in Figure 1.11, forces acting on the bubble-particle interface (Pyke et al., 2003).

- Capillary force (F_c) that tends to draw the particles into the gas phase. As can be seen in Figure 1.7, only the vertical component of this force plays a role to strengthen the attachment.
- Hydrostatic force (F_h) that acts on the three phase contact area
- Buoyancy force (F_b) of the immersed particle
- Force from weight of particles (F_g) that is likely to pull the particle to the liquid phase
- Forced from the capillary pressure (F_t) in the bubble that acts on the particle's surface in the bubble
- In some cases, there is another external force causing the detachment, for example, acceleration force from turbulence caused by the machine (F_d)

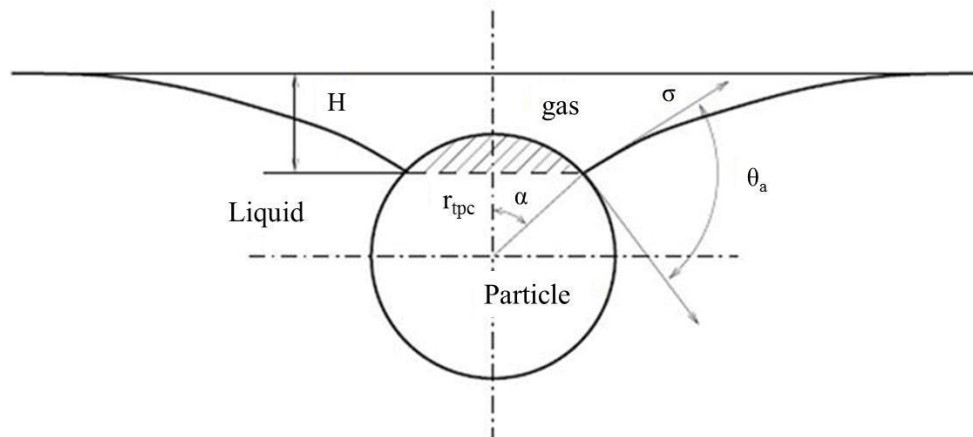


Figure 1.11 Schematic of three phases contact among liquid, an air bubble, and a solid particle at the rear of a bubble (Huang, 2009)

The adhesive force of the bubble-particle aggregate can be described as $F_{ad} = F_{att} - F_{det}$. The F_{att} is the sum of the forces encouraging attachment, which equals to $F_c + F_h$. Whilst the F_{det} equals to $F_g - F_b + F_t + F_d$. The force balance can then be written as $F_c + F_h + F_b - F_g - F_t - F_d = 0$. The aggregate stability can be characterized by a B_0^* , which is the ratio between the detachment force to the attachment force as in Equation 1.20.

$$B_0^* = \frac{F_{det}}{F_{att}} = \frac{F_g - F_b + F_t + F_d}{F_c + F_h} \quad (1.20)$$

B_0^* depends on several factors, including particle properties, fluid properties, and feature of the three phase contact area. The detachment probability can be approximated as in Equation 1.21.

$$E_{det} = \exp\left(1 - \frac{1}{B_0^*}\right) \quad (1.21)$$

Finally, the stability efficiency can be evaluated as $E_{sta} = 1 - E_{det}$.

1.5.4 Treatment of oily emulsion by flotation

Flotation processes have been applied for treating stabilized emulsions in numerous researches. Examples are displayed as following.

Zouboulis and Avranas (2000) conducted the study for effects of numerous parameters on oil-in-water emulsion treatment by coagulation and DAF. The emulsion was prepared n-octane with non-ionic surfactant (Tween 80). A coagulant (i.e. ferric chloride) and flocculants (i.e. cationic and anionic polyelectrolytes) were added in the process to encourage the separation. DAF was operated at 4 bars pressure level with sodium oleate used as collector and controlled ionic strength.

The results showed that the DAF process with coagulant addition can effectively treat the oil-in-water emulsion. The highest efficiency of 95% was found at the optimal operating condition as Fe^{3+} concentration of 100 mg/l and 30% recirculation ratio with controlled pH at 6. Addition of flocculating polymers provided no effects on the treatment. However, the coagulant was required for separating the oily emulsion.

Al-Shamrani et al. (2002) studied the separation of oil from water by DAF with coagulant polymer addition. Paraffinic process oil was applied for preparing the emulsion with non-ionic surfactant. A coagulant used in this study was aluminium sulphate (alum; $\text{Al}_2(\text{SO}_4)_3$). Four types of cationic polymers with different molecular weight and charge density were also employed as flocculants. The DAF process was operated at the pressure level of 50 – 80 psi.

It was found that the separation efficiency of 99% can be achieved by adding 100 mg/l alum and 10% recirculation ratio. At the optimal condition, the A/S ratio, which is generally used for operating the DAF process, was 0.0075 g-air/g-oil. Likewise, no effects of polymer additions were observed. It was stated that destabilization was needed for efficient emulsion separation.

Meysami and Kasaeian (2005) applied the combining IAF with coagulation process for treating oily wastewater. The wastewater was synthesized by olive oil with six different stabilizers, such as, sodium dodecylsulphate (SDS), aniline, butanol, di- and tri-sodium phosphate, and texapon. Coagulants used in this study were chitosan, starch solution, alum, and ferric chloride. The study can be divided into 2 parts, including jar test experiment and flotation process. The IAF was operated at air flow rate of 1 – 6 l/min.

From the results, only chitosan and alum can be used in the coagulation of the emulsion. The 90% highest efficiency was obtained from chitosan and alum in the jar test experiment. Nevertheless, charge reversal was observed when excessive coagulant was added, thus resulting in decrease of efficiency. Application of IAF process can enhance the efficiency to 95% at the condition of 3 l/min air flow rate for 45 seconds with 100 ppm chitosan added at pH 6.

Bensadok et al. (2007) studied the cutting-oil emulsion treatment by coagulation and DAF processes. Two different types of soluble cutting oil were employed for preparing emulsions with different concentrations. The destabilizing agents in this work were calcium chloride (CaCl_2), ferric chloride, and alum. The study was divided into jar test experiment and flotation test. Note that the pressure levels of 4.5 – 6.5 bars were applied for the DAF process.

According to this work, calcium chloride and alum can only be used as destabilizing agents. The efficiency of higher than 90% was obtained from the coagulation process in jar test experiment. It was also found that the efficiency was affected by oil formulation and oil concentration. Increase of oil concentration can reduce the treatment time but provide lower treatment efficiency. Combination of DAF and coagulation process can improve the separation efficiency. Moreover, the performance of DAF process was affected by the operating condition, representing by the A/S ratio.

Painmanakul et al. (2010) investigated effects of bubble hydrodynamic parameters and coagulant dose on treatment efficiency of oily emulsion by IAF process. The emulsion was prepared from lubricating oil with anionic surfactant. Alum was applied as the destabilizing agent. Air flow rates of 0.3 – 16.7 ml/s were used for the operation.

From jar test experiment, the optimal dose of alum was obtained at 800 – 1400 mg/l with pH 8 – 10. IAF process solely can provide the separation efficiency of 60%. The efficiency was improved to more than 90% when combining IAF with coagulation processes, denoted as the modified induced air flotation (MIAF). It was also found that bubbles can provide mixing in the flotation cell. This mixing condition can be represented by the velocity gradient (G). The ratio between bubbles' surface area (a) to the velocity gradient (G), a/G ratio, was stated as the important factor for design the effective IAF process. This ratio could be applied for predicting the efficiency of the process as well.

Tansel and Pascual (2011) examined the emulsified fuel oils removal from brackish and fresh water by DAF both with and without coagulant. The emulsion was synthesized from mixture of fuel oils (i.e. unleaded gasoline, jet fuel, and diesel fuel). Artificial brackish water was prepared from 10000 ppm salt concentration in distilled water, while fresh water obtained from real pond. Commercial cationic coagulant was applied. The pilot-scaled DAF process was operated at 354.6 kPa (3.54 bars) with maximum flow rate of 19 L/s in batch mode, continuous mode with full pressurization, and continuous mode with 50% recirculation.

The results showed that DAF process can efficiently remove oil from emulsion even with or without coagulant. Lighter oil tended to be more removed than the heavy one. The higher oil removal was obtained from the pond water, which might be due to the suspended solid presented in the water assisted the aggregation of oil-droplets. Moreover, the suitable treatment time of this process was found at 10 minutes. However, turbidities of the wastewaters were rarely removed by the process.

According to these works, flotation processes (IAF and DAF) can be used for treating oily-emulsion, mostly with coagulant addition. Destabilization of emulsions also plays a key role in an emulsion separation. Hence, understanding in destabilizing mechanisms apart from flotation mechanisms could be essential. The review regarding destabilization of oily-emulsion is displayed in the latter section.

1.6 Dynamic of particles and bubbles

In the flotation process, the bubble-particle interaction is greatly impacted by hydrodynamic forces from the fluid on the movement of bubbles and particles. Movement of a particle in a liquid phase is governed by numerous forces. Consider a particle with the diameter d_i and the mass m_i moving at the velocity of U_i in a fluid with dynamic viscosity and density of μ_f and ρ_f , respectively, subjected by the gravitational acceleration (g). The force balance of this particle can be described as

$$\begin{aligned} \rho_i \frac{\pi d_i^3}{6} \frac{d\bar{U}_i}{dt} = & (\rho_i - \rho_f) \frac{\pi d_i^3}{6} \bar{g} + C_d \rho_f \frac{\pi d_i^2}{8} \|\bar{U}_f - \bar{U}_i\| (\bar{U}_f - \bar{U}_i) \\ & + C_m \rho_f \frac{\pi d_i^3}{6} \left(\frac{D\bar{U}_f}{Dt} \Big|_i - \frac{d\bar{U}_i}{dt} \right) + \rho_f \frac{\pi d_i^3}{6} \frac{D\bar{U}_f}{Dt} \Big|_i \\ & + C_l \rho_f \frac{\pi d_i^3}{6} (\bar{U}_f \Big|_i - \bar{U}_f) \times \bar{\Omega} + 3\pi\mu_i d_f \int_0^t K_H(t-s) \frac{\partial(\bar{U}_f - \bar{U}_i)}{\partial s} ds \end{aligned} \quad (1.22)$$

where the term in the left-handed side is the force due to particle's inertia force. The right-handed side, respectively, are buoyancy force (F_g), drag force (F_d), added mass force (F_m), pressure force or Tchen force (F_t), lift force (F_l), and history force (F_h). The index i indicate the inclusion. The C_d , C_l , and C_m stand for coefficients of drag, lift, and added mass forces, respectively. U_f exhibits the fluid velocity, and $\bar{\Omega}$ is vorticity. The $K_H(t-s)$ is the core of the history force. The D/Dt and d/dt terms represent the time derivative of a motion along fluid streamline and particle trajectory, respectively. This equation can be simplified depending on the practical condition. For example, a particle moves by the gravitational effect in a stationary fluid ($U_f = 0$)

will reach a steady state when the buoyancy and viscous drag forces are balanced as follows:

$$0 = C_d \rho_f \frac{\pi d_i^2}{8} |\bar{U}_i| \bar{U}_i + (\rho_i - \rho_f) \frac{\pi d_i^3}{6} g \quad (1.23)$$

This equation can be applied to determine the terminal rising velocity of bubble and settling velocity of particles when knowing the drag coefficient. This velocity is affected by the density difference, size, and inertia. Moreover, it will be shown later that the velocity is also impacted by the surface condition.

1.6.1 Movement of particles

The analytical solution of Stokes equation expressed the drag coefficient at the limit $Re_p = \rho_f U_s d_p / \mu_f \rightarrow 0$ (Stokes, 1851). For $Re_p \ll 1$, the relation can be written as

$$C_d = \frac{24}{Re_p} \quad (1.24)$$

Hence, terminal settling velocity can be deduced as

$$U_s = \frac{(\rho_p - \rho_f) g d_p^2}{18 \mu_f} \quad (1.25)$$

At larger Re_p , C_d has to be corrected by a function $f(Re_p)$ to account of inertia, i.e.

$$C_d = \frac{24}{Re_p} f(Re_p) \quad (1.26)$$

Expressions for drag coefficient determination for a spherical solid particle in the range of Re_p applied in this study are displayed in Table 1.1.

Table 1.1 Correlations of C_d for a spherical solid particle at $Re_p < 800$

Re_p	Correlation of C_d	References	Equations
$Re_p \ll 1$	$\frac{24}{Re_p}$	Stokes (1851)	(1.27)
$Re_p \leq 1$	$\frac{24}{Re_p} \left(1 + \frac{3}{16} Re_p + \frac{9}{160} Re_p^2 \ln Re_p + O(Re_p^2) \right)$	Oseen (1910)	(1.28)
$Re_p \leq 800$	$\frac{24}{Re_p} (1 + 0.15 Re_p^{0.687})$	Schiller and Nauman (1935)	(1.29)

If a particle is put in the quiescent fluid with no initial velocity, it will accelerate to balance the drag and the buoyance force. The characteristic time needed to reach the balance condition is called the relaxation time (τ_p):

$$\tau_p = \frac{(\rho_p + C_m \rho_f) d_p^2}{18 \mu_f} \quad (1.30)$$

This relaxation time also indicates the required time of particle for adapting to any change in the flow of the fluid. In the particle-bubble capture, the velocity field that passes a particle is owing to the flow of bubble. For a bubble with diameter d_b moves at a velocity U_b , the characteristic time (τ_b) of flow, which induced by the passage of bubble, experienced by the particle is:

$$\tau_b = \frac{d_b}{2U_b} \quad (1.31)$$

The ratio between the relaxation time of a particle and the characteristic time of fluid provides the dimensionless Stokes number (St_p):

$$\begin{aligned}
St_p &= \frac{\tau_p}{\tau_b} = \frac{1}{9} \frac{(\rho_p + C_m \rho_f) d_p^2 U_b}{\mu_f d_b} \\
&= \frac{1}{9} Re_b \left(\frac{\rho_p}{\rho_f} + C_m \right) \left(\frac{d_p}{d_b} \right)^2
\end{aligned} \tag{1.32}$$

Stokes number expresses the inertia effect in the particle's movement by its own and added mass with the resistance due to the viscosity of fluid. In the case of $St_p \ll 1$, the response time of particles is less than the passing fluid by the bubble. As a result, particles can adapt almost instantaneously to the change of fluid velocity. Particles then follow the flow streamline of the fluid. On a contrary, particles do not have sufficient time for responding to the change of fluid's flow if $St_p \gg 1$. The trajectory of the particle is therefore affected by the displacement of fluid from the passage of bubble. Normally, the effect of the added mass is neglected, and Stokes number is expressed as $St_p = \rho_p U_b d_p^2 / 9 \mu_f d_b$. This Stokes number is used for indicating effects of inertia to the motion of particles, which can impact the particle-bubble interaction in the flotation process.

1.6.2 Movement of bubbles

The movement of a bubble is more complicated than the solid particles due to effects of deformation and interface condition. The terminal velocity of a bubble depends on numerous factors, for instance, the shape of bubble, interface condition, and physical properties of the fluid.

1.6.2.1 Deformation of bubbles

A bubble can deform during the movement in the infinite medium. Three types of bubble shape can be classified as spherical, ellipsoidal, and cap form. The deformation of bubble is often described by the ratio of the minor axis (a) to the major axis (b) when it is ellipsoidal. The equivalent diameter of the ellipsoidal bubble (d_e) can be determined as $d_e = (ab^2)^{1/3}$. The deformation of a bubble is the result of

several impacts, for example, the interfacial tension that tends to maintain the sphere-shaped of bubble, the inertia and gravitational effects that encourage its flatness. The changing in shape of bubbles depends on the fluid characteristics and bubble diameter. According to the dimension analysis, three dimensionless numbers can be applied to indicate the deformation as following (Clift et al., 1978). Note that U_t and σ_{gl} are the terminal rising velocity of a bubble and the interfacial tension between the gas and the liquid phases, respectively.

- Weber number is the ratio of inertial forces and interfacial tension

$$\text{We}_b = \frac{\rho_f U_b^2 d_b}{\gamma_{wg}} \quad (1.33)$$

- Bond number, or also called Eötvös number compares effects of gravitational forces with interfacial tension

$$\text{Bo}_b = \frac{\rho_f g d_b^2}{\gamma_{wg}} \quad (1.34)$$

- Capillary number compares the viscous forces and interfacial tension

$$\text{Ca} = \frac{\mu_f U_b}{\gamma_{wg}} \quad (1.35)$$

Moreover, Froude number is also applied to compare the effects of inertia and gravity effects:

$$\text{Fr} = \frac{\text{We}_b}{\text{Bo}_b} = \frac{U_b^2}{g d_b} \quad (1.36)$$

A bubble maintains its spherical shape when We_b , Bo_b , and $Ca < 1$ as the interfacial tension is dominated. The shape of a bubble could be influenced by the presence of surfactants due to the reduction in the surface tension. It was found that bubbles tend to have spherical shape with higher surfactant concentration (Sam et al., 1996).

1.6.2.2 Interfacial properties

For the gas bubble with clean surface, the liquid can slip on its surface. The liquid velocity at the bubble's surface is therefore non-zero. This surface condition can be called as mobile surface or the slip condition. According to many literatures, correlations of drag coefficient in a function of bubble Reynolds number have been stated as summarized in Table 1.2.

Table 1.2 Correlations for drag coefficient of clean bubble

Re_b	Correlation of C_d	References	Equations
$Re_b \ll 1$	$\frac{16}{Re_b}$	Hadamard (1911); Rybczynski (1911)	(1.37)
$Re_b \leq 1$	$\frac{16}{Re_b} \left(1 + \frac{1}{8} Re_b + \frac{1}{40} Re_b^2 \ln Re_b + O(Re_b^2) \right)$	Taylor and Acrivos (1964)	(1.38)
$Re_b \geq 1$	$\frac{48}{Re_b}$	Levich (1962)	(1.39)
$Re_b > 50$	$\frac{48}{Re_b} \left(1 - \frac{2.211}{Re_b^{0.5}} \right)$	Moore (1963)	(1.40)
Every Re_b	$\frac{16}{Re_p} \left(1 + \frac{Re_b}{8 + 0.5(Re_b + 3.315 Re_b^{0.5})} \right)$	Mei et al. (1994)	(1.41)

However, fluids generally contain impurities, such as surfactants or particles. These impurities can adsorb on the surface of bubble. The surface is then considered as contaminated surface. Cuenot et al. (1997) exhibited contamination effects of the

immobilizing surface of a spherical bubble with direct numerical simulation (DNS). Four situations according to the kinetic of adsorption-desorption of impurities at the interface of bubble were explained as follows:

- Impurities are in the wake of bubbles by convection before reaching the interface. At this point, the interface remains mobile.
- Low concentration of impurities reaches the interface, but the interface is still mobile.
- Impurities at the interface move to the bottom part of the bubble by convection. The bubble then consists of a mobile part (tangential velocity; $u_{\tau} \neq 0$) on the front and an immobile part ($u_{\tau} = 0$) at the rear. This condition of the bubble can be described by the stagnant cap model as illustrated by Figure 1.12.
- The interface of the bubble is completely contaminated. The entire surface is immobile and similar to a spherical solid particle.

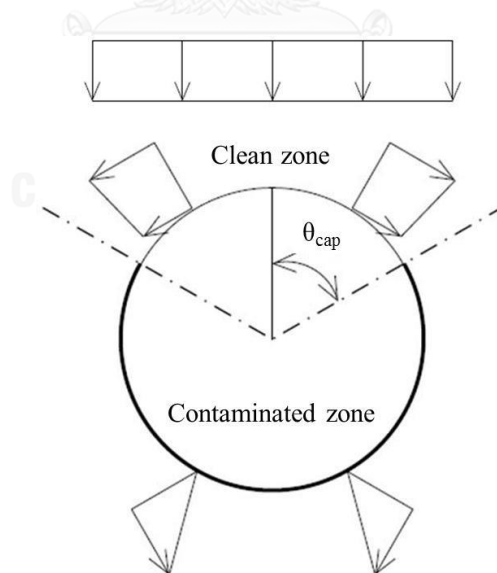


Figure 1.12 Stagnant cap model (Sarrot, 2006)

According to Sadhal and Johnson (1983), the stagnant cap can be explained as in Figure 1.8. The liquid can slide along the bubble's surface to an angle θ_{cap} . Beyond

this θ_{cap} , the bubble's surface is contaminated and the liquid will adhere to the surface. The bubble is completely clean when $\theta_{cap} = 180^\circ$, and the surface is completely contaminated when $\theta_{cap} = 0^\circ$. In the latter case, there is a no-slip condition at the interface where the velocity at the surface equals to zero. The drag force in this case is similar to that of a solid particle.

The drag coefficient in the case of partially contaminated bubble is intermediate between the clean bubble and the spherical solid particle. The first investigation of theoretical hydrodynamic behavior of the cap model was performed by Savic (1953). Afterwards, Sam et al. (1996) conducted the experimental studies to support the idea of partially contaminated bubble by measuring the terminal rising velocities of bubble in distilled and tap waters for a distance of 4 meters. The author concluded that the impurity concentration was not great enough to completely immobilize the bubble.

Sadhil and Johnson (1983) determined the drag coefficient of a partially contaminated bubble ($C_d(\theta_{cap})$) in a relation with cap angle (θ_{cap}) as shown in Equation 1.42.

$$C_d^*(\theta_{cap}) = \frac{C_d(\theta_{cap}) - C_d^m}{C_d^{im} - C_d^m} = \frac{1}{2\pi} \left\{ 2(\pi - \theta_{cap}) + \sin \theta_{cap} + \sin 2\theta_{cap} - \frac{1}{3} \sin 3\theta_{cap} \right\} \quad (1.42)$$

where $C_d^*(\theta_{cap})$ is a normalized $C_d(\theta_{cap})$ in a function of θ_{cap} . C_d^m and C_d^{im} are drag coefficients of clean and completely contaminated bubbles, respectively. This analytical solution was established for Stokes flow condition ($Re_b \ll 1$). However, from the studies of Cuenot et al. (1997) and Dani (2007), this correlation is still applicable until $Re_b \leq 300$.

1.7 Conclusion

From this chapter, it can be seen that the effective separation is necessary to treat the emulsion with high stability. The good separation can reduce the water pollution causing by oil and also promotes the oil recovery, which can be useful in the industrial field. Coalescer and flotation were selected to be used for separating the stabilized emulsion prepared from cutting oil in this work. The separation efficiencies of these processes will be determined as well as their separation mechanisms. The obtained knowledge would be useful for dealing with stabilized emulsion by optimizing these processes to achieve the effective separation performance.



CHAPTER 2

CHARACTERIZATION OF CUTTING OIL EMULSION

A good understanding on the cutting oil emulsion is an important factor for selecting an effective separation. Characteristics of the emulsion should be well identified for selecting an appropriate separation method. Different techniques are applied to obtain sufficient information since several properties are normally required to complement each other. Typically, droplet size and surface charge are two main characteristics needed for considering a treatment condition along with other properties such as pH values. Those two characteristics could affect the separation by flotation and/or destabilization in the further experiments. Moreover, a method to determine the oil concentration for estimating the separation performance is also desired.

This chapter presents the experimental results for properties of the cutting oil emulsion used in this work from several characterization techniques. A brief principle for each instrument was also provided. The characteristics from this part will be used for describing the separation results in the further experiments.

2.1 Characteristics of cutting oil

The commercial Castrol Cooledge BI cutting oil (Castrol Inc.) was used for preparing the stabilized emulsion for the experiments. It is a soluble metalworking fluid designed for several machining e.g. grinding, drilling, and milling. This clear brown oil was used to form the milky emulsion by diluting with water at the concentration of 3 - 10%. Like typical cutting oil, it is composed of the high refined mineral oil, emulsifiers, and additives. The ingredients of this cutting oil revealed in its MSDS are shown in Table 2.1

Table 2.2 presents some characteristics and test method of the Castrol Cooledge BI cutting oil and its emulsion obtained from both the preliminary test and the manufacturer.

Table 2.1 Composition/information on ingredients of Castrol Cooledge BI

Chemical name	CAS no.	%	Classification*
Sulfonic acids, petroleum, sodium salts	68608-26-4	1-5	Xi; R41 N; R50/53
Fatty acids, potassium salts	61790-44-1	1-5	Xi; R36/38
Alcohols, C11-14-iso-, C13-rich	68526-86-3	1-5	N; R50
N,N'-Methylenebismorpholine	5625-90-1	1-5	Xn; R20/21/22 Xi; R36/37/38
Amide, tall oil fatty, N,N-bis(hydroxyethyl)	68155-20-4	1-5	Xi; R38, 41

* Classification defined by European Union in Annex II and Annex III of Directive 67/548/EEC

Xi: Irritant; Xn: Harmful; N: Dangerous for the environment

R38-Irritating to skin; R41-Risk of serious damage to eyes; R50-Very toxic to aquatic organisms

R20/21/22- Harmful by inhalation, in contact with skin and if swallowed;

R36/38-Irritating to eyes and skin; R36/37/38- Irritating to eyes, respiratory system and skin;

R50/53-Very toxic to aquatic organisms, may cause long-term adverse effects in the aquatic environment

Table 2.2 Characteristics of Castrol Cooledge BI

	Test method	Value
Concentrate		
Appearance	Visual	Amber/Brown
Density (at 20°C)	Pycnometer	930 kg/m ³
Surface tension (at 20°C)	Du Noüy ring method	35.2 mN/m
Emulsion		
Appearance	Visual	Milky
pH (at 3% w/w concentration)	DIN 51361	9.7
	ASTM E70-97	
Refractive index		1.0

However, the emulsion in this work was prepared at much lower concentration than in the working condition since it was expected that the effluent oily emulsion in the real scenario could be diluted by other wastewater resulting in lower concentration. Due to the fact that the concentration of cutting fluids is hardly defined (Byers, 2006), the emulsion in this work was prepared to contain a chemical oxygen demand (COD) in the range of 3000 – 4000 mg/L acquired from the closed-reflux method (APHA, AWWA, and WEF 1998). This COD range was found from industrial wastewater those contained metalworking fluids in several works (Kim et al., 1989; Kim et al., 1992; Schreyer and Coughlin, 1999). For this cutting oil, 1.0 g/l concentration was used to obtain the required COD value.

The emulsion was prepared by mixing the cutting oil in deionized water (DI) and tap water at the concentration of 1.0 g/l. The characteristics of these two types of water are different and varied on daily basis as summarized in Table 2.3. The mixture was vigorously mixed by a mechanical stirrer at 500 rpm for 10 minutes forming a homogeneous milky emulsion. Note that effects of the mixing procedure and oil concentrations on the characteristics of the emulsion were also investigated. The appearance of this cutting oil and the emulsion is depicted in Figure 2.1.

Table 2.3 Characteristics of DI and tap water used for preparing emulsion

Characteristics	Deionized water	Tap water
pH	8.02 - 8.31	7.19 - 7.54
Conductivity ($\mu\text{S}/\text{cm}$)	0.8 - 1.1	235 - 240
Turbidity (NTU)	0.119 - 0.184	0.417 - 1.07



Figure 2.1 Castrol Cooledge BI cutting oil (left) and the 1 g/L cutting oil emulsion (right)

2.2 Observation of droplets under microscope

The observation of droplets in the emulsions was conducted under the optical microscope with 40 times magnification (40X). Small volume of emulsions were sampled by a bore-holed dropper to avoid the possibility of droplets breakage and placed on a glass slide. The observation was conducted by the optical microscope (Nikon Eclipse LV100 POL) installed with a camera (Nikon Digital Sight DS-2MBW) for capturing images. Photos of oil droplets in the emulsion prepared from DI water and tap water are exhibited in Figure 2.2a and 2.2b, respectively.

Droplets can be rarely seen in the emulsion with deionized water suggesting that their sizes could be very tiny. The droplets, which were much smaller than the provided scale of 10 μm , could have the size in the nanoscale range. On the other hands, droplets in the emulsion with tap water were easier to be noticed. Therefore, it was expected that droplets in the emulsion prepared from tap water would be larger than that in the deionized water. More information of droplet sizes from the measuring instruments will be further provided in the following section.

2.3 Overview of emulsion characterization

Numerous techniques have been applied for characterizing oily emulsion in many aspects. The result can complement each other and provide a useful information for considering the separation method. The characteristics of emulsion can be classified into two categories including droplet size and physico-chemical properties. The droplet size is an important parameter for selecting the appropriate technique for emulsion separation. It can be determined by the same techniques used with solid particles in suspension. The size can be revealed under various definitions of equivalent sphere (Allen, 1997; Rhodes, 2008); for example,

Volume based particle size: the diameter of the sphere that has the same volume as a given particle,

Weight based particle size: the diameter of the sphere that has the same weight as a given particle,

Area based particle size: the diameter of the sphere that has the same surface area as a given particle,

Hydrodynamic or aerodynamic particle size: the diameter of the sphere that has the same drag coefficient as a given particle

Feret diameter: The mean value of the distance between two parallel tangents on opposite sides of the particle (the reported Feret diameter is usually the maximum value from the measurement),

Sieve diameter: the width of the smallest square of grate that the particle can pass through,

Diffraction diameter: the diameter of the sphere that generates the same deviation as of the real particle irradiated by light wave.

Fortunately, micro-droplets in oily emulsion normally contain sphere shape. The expression of the size is less complicated than that of solid particles. However, particles or droplets practically present in different sizes in a real system.

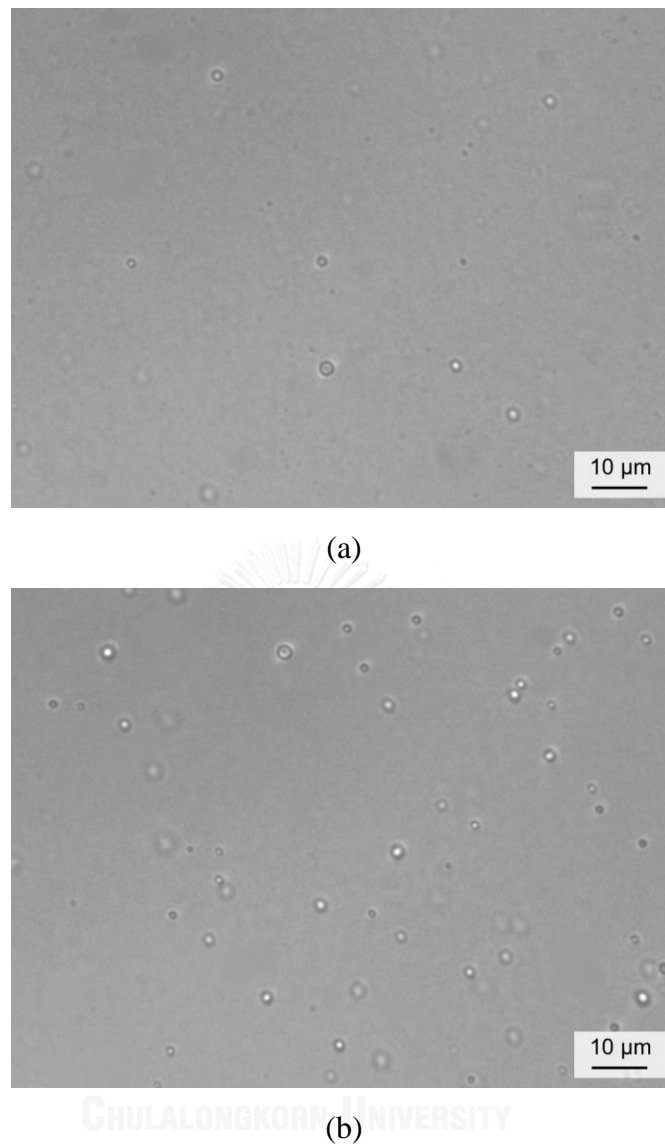


Figure 2.2 Microscopic photos of droplet in the 1.0 g/L cutting oil emulsion from (a) DI water and (b) tap water

The particle size distribution is used to describe the population of particles. The distribution could be expressed as a frequency or cumulative distribution curves. Moreover, particle sizes are mostly presented by a single number as the average size. The definitions of different average sizes are as follows (Allen, 1997; Rawle, 2003; Rhodes, 2008).

Mode is the most frequently occurring in the distribution. Different modes could be found in the same sample for distributions by number, surface, and volume. Moreover, some samples could contain multi-modal size distribution.

Median is the size that divides the frequency distribution into two equal parts including fifty percent of particles with smaller diameter and the rest with larger particles.

Mean is the center of gravity of the distribution. The means represent two characteristics of particles; for example, number, length, surface, volume (or mass), and moment. Different means can be described as:

arithmetic mean: this mean conserves the number and the length of the particle population, known as the number-length mean (x_{NL}). It is sensitive to the particle quantities at the extremely lower and upper ends of the distribution;

$$x_{NL} = \frac{\sum n_i d_i}{\sum n_i} \quad (2.1)$$

quadratic mean: this mean represents the number and the surface area of the particle distribution and is known as the number-surface mean (x_{NS});

$$x_{NS} = \sqrt{\frac{\sum S}{\sum n_i}} = \sqrt{\frac{\sum n_i d_i^2}{\sum n_i}} \quad (2.2)$$

Sauter mean: this mean can be defined as the diameter of a sphere that has the same ratio of volume to surface area. It is also called as the surface-volume mean (x_{SV} or d_{32});

$$x_{SV} = \frac{\sum S_i d_i}{S} = \frac{\sum n_i d_i^3}{\sum n_i d_i^2} \quad (2.3)$$

volume or mass mean: the average diameter based on the unit volume of a particle (x_{VM} or d_{43}).

$$x_{VM} = \frac{\sum V_i d_i}{V} = \frac{\sum n_i d_i^4}{\sum n_i d_i^3} \quad (2.4)$$

It has to be well aware of the size given from different techniques could be dissimilar. Moreover, the mean diameters those measured from the equipment or calculated from the measured results should be distinguished (Rawle, 2003).

After the size characterization of droplets, the surface charge was considered since it could greatly affect the separation process, especially the destabilization. Furthermore, other characteristics (i.e. pH, conductivity, and turbidity) were determined for a good understanding, which could lead to an effective separation.

2.4 Characterization of droplet size

The methods applied to examine droplet size of the cutting oil emulsion are based on two techniques that have been used for measuring particle sizes including the dynamic light scattering (LDS) and the laser diffraction scattering (LDS). Table 2.4 summarizes the methods for the size measurements in this study.

The brief details on the apparatus based on two different techniques used for measuring droplet sizes are provided in the next section.

Table 2.4 Methods and apparatus for size measurements in this work

Sample	Technique	Apparatus
Oil droplets	DLS	Nanotracc
		Zetasizer Nano ZS
Oil droplets and aggregates	LDS	Mastersizer 2000

2.4.1 Measurement apparatus

2.4.1.1 Nanotracs

The Nanotracs NPA250 with an external probe from Microtracs Inc. is used for analyzing sizes of nanoparticles based on the dynamic light scattering (DLS) technique. The light from a laser diode (780 nm) passes through an optical beam splitter in the probe and then encounter the sample. At the probe tip, a sapphire window create an interface between the sample and the probe. The light can be separated into two parts. The first part is reflected by the sapphire window back through the beam splitter to a photo detector as a reference signal for detection. Another part can pass through the window and is scattered by moving suspended particles under Brownian motion. The frequency of this scatter light is Doppler shifted relative to the velocity of the particle it encounters. The light is scattered in all directions including the 180 degrees backwards through the sapphire window to the photo-detector. The signals with various frequencies and the reference are used for generating a wide spectrum of heterodyne difference frequencies. The power spectrum of the interference signal is calculated and inverted to construct the PSD (Vaidyanathan, 2006).

Several parameters can be acquired from the Nanotracs NPA 250 (Vaidyanathan, 2006); for example,

- **Mean intensity diameter (MI)** is calculated from the distribution of intensity (signal). It only indicates the relationship of the detected light signals.
- **Mean volume diameter (MV)** represents the center of gravity of the distribution curve. This diameter is affected by the presence of large particles in the sample and could be considered as a type of average diameter of particles.
- **Mean number diameter (MN)** is determined from the volume distribution of particles and is impacted by the presence of small particles.

- **Mean area diameter (MA)** is the measurement of particle surface. It is also calculated from the volume distribution. This diameter is less affected by the large particle than MV and can express the presence of smaller particles.

2.4.1.2 Zetasizer Nano ZS

The Zetasizer Nano S from Malvern Instrument Ltd. is employed for measuring the droplet size distribution by the dynamic light scattering (DLS) technique. A sample is introduced to the instrument in a small cell, which light provided by a laser can pass through. A laser can mostly penetrate the sample but is partially scattered by particles at every angle. This scattered light is detected and measured for its intensity. Note that the intensity of the light source that can affect the scattered intensity can be automatically adjusted. A sample with very small particles or diluted concentration required high intensity of the laser source since the light cannot be scattered much. Therefore, size information can be analyzed from the changing of scattered light intensity in successive durations by the Zetasizer Nano S software. Moreover, this instrument can be used for examining the zeta potential by measuring the electrophoretic mobility, which will be further mentioned in the following part.

Though, it should be well aware that the size information from the Zetasizer is only accurate for spherical particles with narrow size distribution (Vaidyanathan, 2006). The results from the Nanotracer were mainly used to defining the size information in this work with the comparison from the measurements from the Zetasizer Nano ZS for the accuracy of the data.

2.4.1.3 Mastersizer 2000

The Mastersizer from Malvern Instrument Ltd. can be applied to analyze the particle size distribution based on the laser diffraction scattering (LDS) technique, which is widely used for particle size analysis. Particles are introduced through a laser beam and can scatter light at an angle, which is inversely proportional to their size (i.e. small particles scatter light at high angles). The intensity of the scattered light at

any angle is measured by photosensitive detectors. In addition, the particle size distribution can be provided from the measurements of wavelength and polarization of light and then applied with scattering models. The applicable range of the Mastersizer is 0.02 - 2000 μm ; therefore, it was used in this work for examine size of aggregates that exceeded the applicable range of the instruments based on the DLS techniques.

2.4.2 Sizes distribution of cutting oil droplets

2.4.2.1 Size distribution from LDS

2.4.2.1.1 Mastersizer 2000

The droplet sizes of the cutting oil emulsion were firstly analyzed by the LDS technique via the Mastersizer 2000 as respectively depicted in Figure 2.3a and 2.3b for the size distributions of droplets in the 1 g/L cutting oil emulsion from DI water and tap water. For the emulsion with DI water, droplet sizes were in the range of 0.04 - 0.4 μm , which can be considered as a size in the nanoscale. No aggregate with larger sizes was observed. On the contrary, the second peak can be noticed in the case of tap water suggesting the presence of larger droplets. The aggregation of droplets was expected in this case due ions in tap water, which could partially destabilize the surface charge of oil droplets. Since the droplets contained the nanoscale sizes, the emulsion should be analyzed by the DLS technique via Nanotracs and Nano ZS, which are designed to deal with nanoparticles for more accurate information regarding the sizes and their distribution.

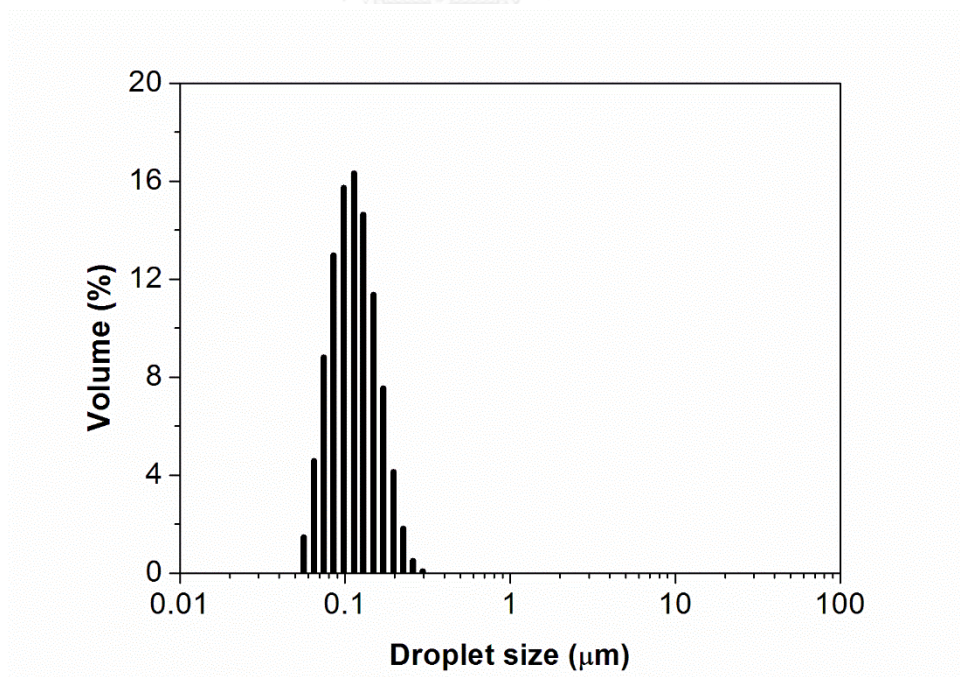
2.4.2.2 Size distribution from DLS

2.4.2.2.1 Nanotracs

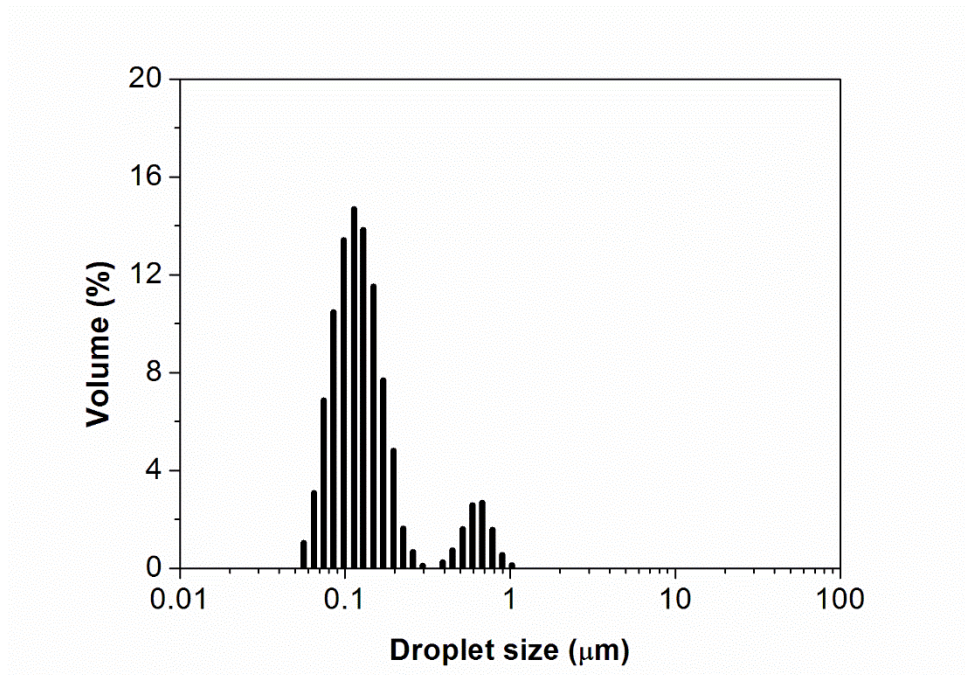
The results from the Nanotracs are displayed in Figure 2.4 for the cutting oil emulsion with DI water and tap water. The size distributions confirmed the results obtained from the Mastersizer that droplets' sizes were in the nanoscale range. The droplet sizes in the range of 30 - 400 nm were found for the DI water emulsion. In addition, the bimodal distribution in the same size range as from the Mastersizer can

be observed for the emulsion with tap water. The presence of aggregates was insisted. From the size distribution results, the average diameter in term of the surface-volume mean diameter (d_{32}) can be calculated as 174 nm for the DI water emulsion.

On the contrary, the d_{32} in tap water emulsion was 444 nm. Note that the d_{32} was selected to represent the average droplet size since it conserves the surface area and volume of droplets. The volume should be used for indicating oil the quantity in the suspension due to the fact that the number of droplets can be changed from shrinkage or coalescence. Furthermore, the surface volume of droplets is one of the factors that could affect the separation performance. It should be noted that no difference of the sizes and their distributions can be found for varied mixing rate beyond 500 rpm and mixing time further 10 minutes. This preparation procedure was valid to be used in this work with good reproducibility on the emulsion characteristics. Effects of oil concentration in the range of 0.5 - 5.0 g/L on droplet sizes were also unable to be observed for both emulsion with DI and tap water.

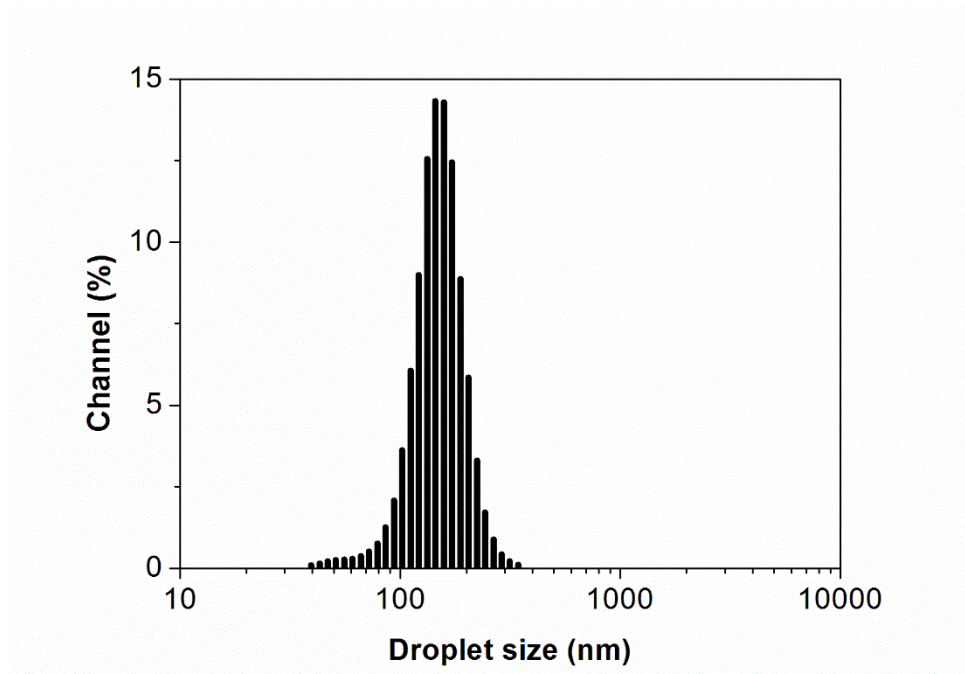


(a)

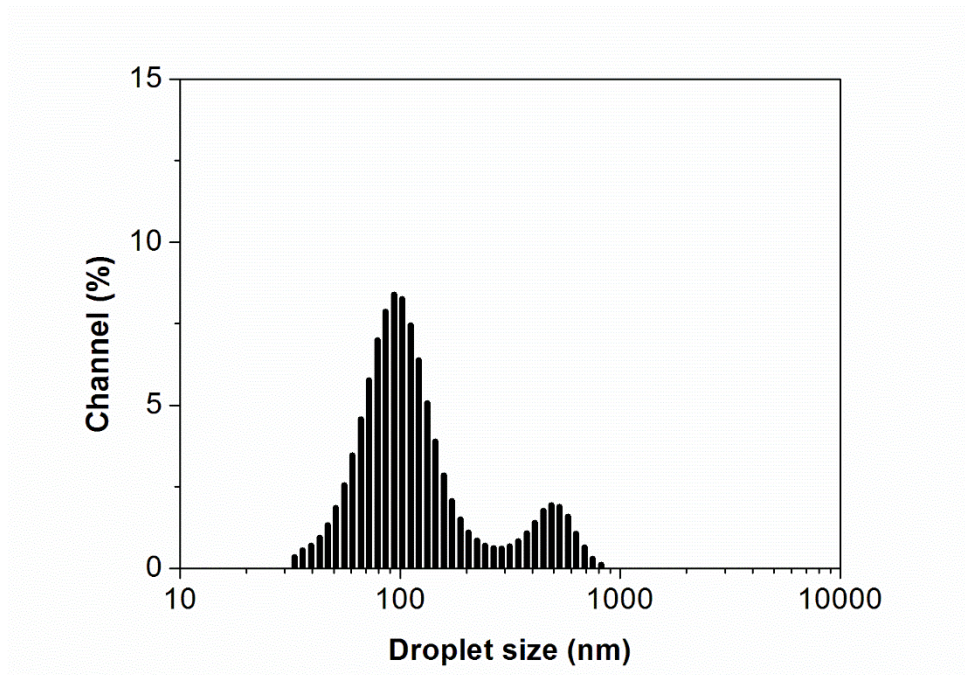


(b)

Figure 2.3 Droplet size distributions from the Mastersizer of the 1.0 g/L cutting oil emulsion in (a) DI water and (b) tap water

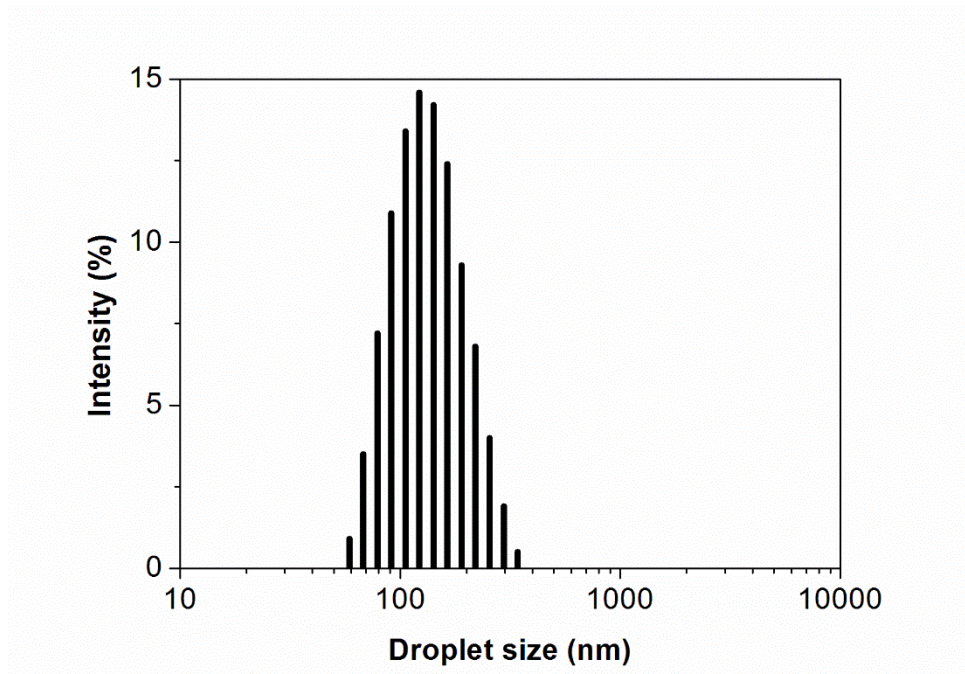


(a)

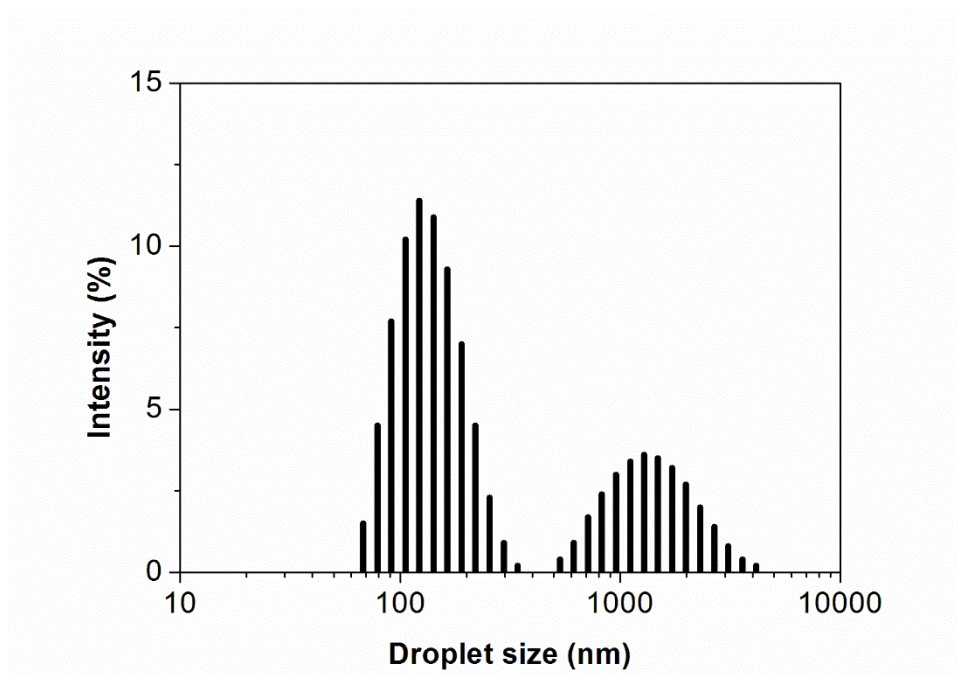


(b)

Figure 2.4 Droplet size distributions from the Nanotracer of the 1.0 g/L cutting oil emulsion in (a) DI water and (b) tap water



(a)



(b)

Figure 2.5 Droplet size distributions from the Nano ZS of the 1.0 g/L cutting oil emulsion in (a) DI water and (b) tap water

2.4.2.2.2 Zetasizer Nano ZS

The size distributions of droplets in the cutting oil emulsions at 1.0 g/L concentration measured by the Zetasizer Nano ZS are illustrated in Figure 2.5. The size distribution of the emulsion with DI water was similar to that from the Nanotracs with the d_{32} of 184 nm. The sizes in tap water emulsion also presented bimodal distribution, which can confirm the existence of larger droplets in this emulsion. However, the right peak of the distribution was in larger size range compared to the results of Nanotracs. Consider the constraint of the Nano ZS on the data accuracy, the broad distribution of droplet sizes in tap water emulsion could produce a discrepancy on the size information. Therefore, the results regarding droplet sizes in the experiments further was obtained from the Nanotracs since it is specifically designed for analyzing sizes of nanoparticles with less limitation on the usage than the Nano ZS, which could provide more accurate size information.

2.5 Characterization of zeta potential

The surface charge is another important parameter for the emulsion separation. As aforementioned, the existence of electrical charges on droplet surface relates to the stability of the emulsion. Typically, the surface charge of particles or droplets is evaluated in term of zeta potential. The measurement is conducted by applying a sample under the electric field. Charged particles suspended in a sample are attracted towards the opposite charged electrode in the electric field while the viscous force acting on the particles are opposed this movement. The particles then move with a constant velocity, which is normally denoted as the electrophoretic mobility, when the force equilibrium is reached. This electrophoretic mobility can be measured and converted to the zeta potential from the theoretical consideration by Henry equation.

$$U_E = \frac{2\varepsilon\zeta f(ka)}{3\mu_f} \quad (2.5)$$

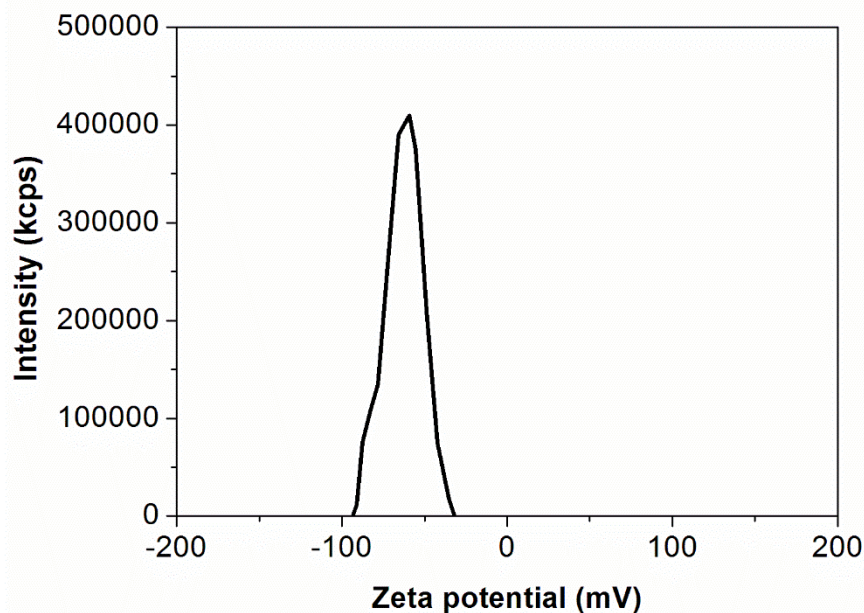
where ζ is the zeta potential and U_E is the electrophoretic mobility. The dielectric constant and the liquid viscosity are respectively represented by ε and η , while $f(ka)$ is Henry's function. Generally, the $f(ka)$ can be approximated in 2 different cases. The $f(ka)$ value of 1.5 is obtained from the Smoluchowski approximation for particles larger than $0.2 \mu\text{m}$ dispersed in 10^{-3} M or higher concentration of electrolytes. For small particles in low dielectric constant media, $f(ka)$ equals to 1.0.

2.5.1 Zetasizer Nano ZS

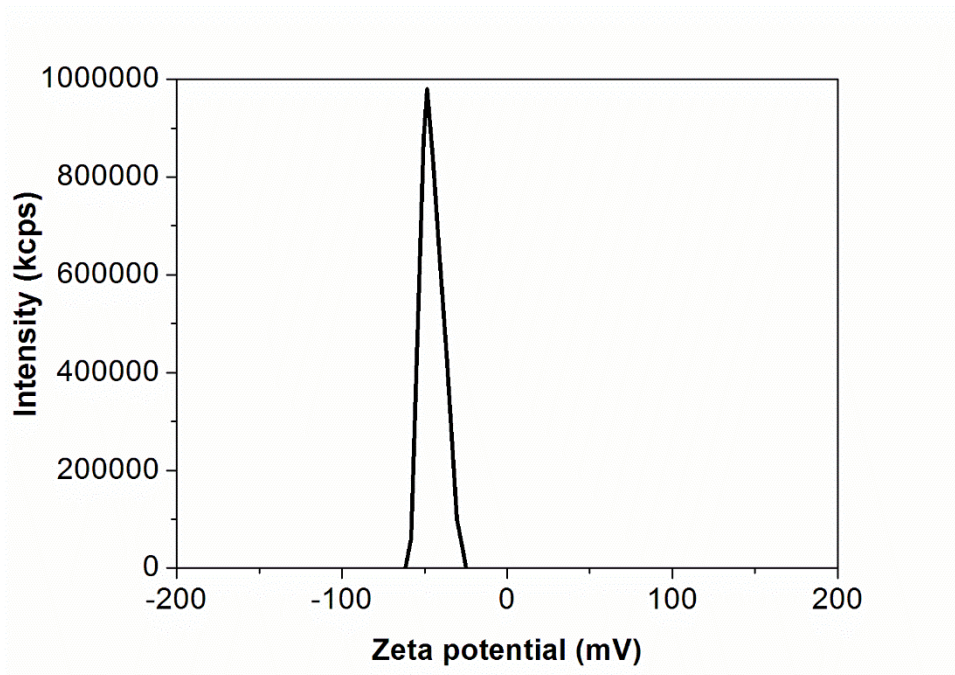
The Zetasizer NanoS from Malvern Instrument was used for analyzing the zeta potential. The principle of this instrument is to detect the fluctuated intensity of light pass through the moving particles under the electric field. The frequency of the fluctuated light is proportional to the particle velocity. The detected signal is processed by the software to produce a frequency spectrum, which can be used for calculating the electrophoretic mobility and the zeta potential.

2.5.2 Zeta potential of cutting oil emulsion

The zeta potential (ζ) value can provide the information of the surface charge of droplets in the emulsion. The magnitude of ζ indicates the stability of the system. Typically, the colloidal system with the absolute value $|\zeta| > 30$ mV is considered as a very stable system with the repulsive interaction. The results for the 1.0 g/L emulsions are exhibited in Figure 2.6. Note that the zeta potentials were measured at the initial pH when the emulsions were formed, i.e. 8.91 and 7.95 for DI water and tap water emulsions, respectively. The emulsion with DI water (-65.8 mV) contained higher ζ than that of the tap water (-48.4 mV). The zeta potential result could describe the presence of larger droplets in the case of tap water and insist effects of ions in the water as mentioned in section 2.3.2.



(a)



(b)

Figure 2.6 Zeta potential of the 1.0 g/L cutting oil emulsion from (a) DI water and (b) tap water

Effects of pH on the zeta potential was also determined. The pH was adjusted by hydrochloric acid (HCl) and the sodium chloride (NaCl) solutions. No obvious change of the zeta potential can be seen in the varied pH range of 3 - 10 as shown in Figure 2.7. The change of zeta potential affected the droplet size as indicated by the change of the mean diameter d_{32} in Figure 2.8.

The largest d_{32} in both cases can be noticed at the pH of 6.5 - 7.5 where the zeta potential was lowest. However, this minor changes of droplet size was insufficient for separating oil from the emulsion. Therefore, only pH adjustment was unable to destabilize and separate the emulsion.

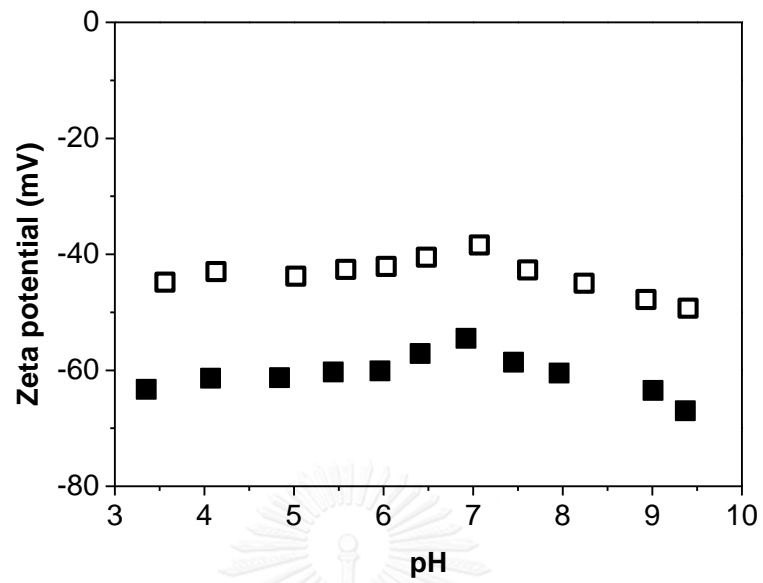


Figure 2.7 Zeta potentials at varied pH for 1 g/L cutting oil emulsion in DI (■) and tap (□) water

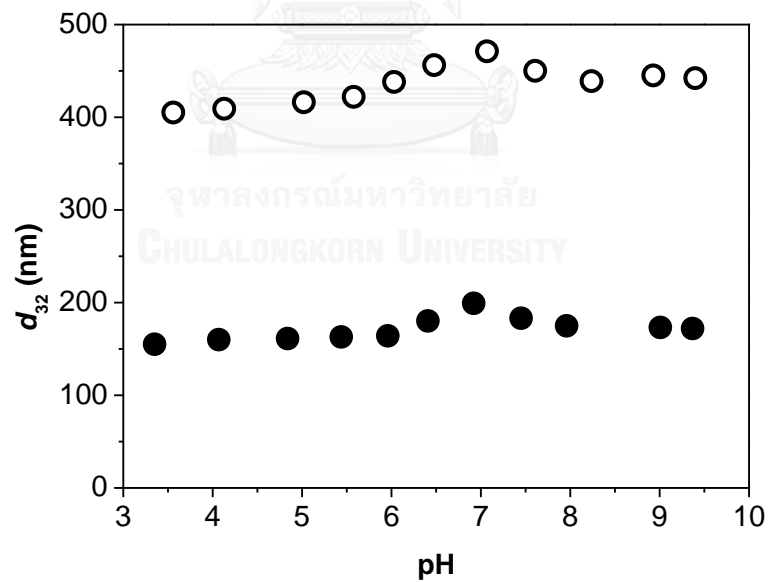


Figure 2.8 d₃₂ at varied pH for the cutting oil emulsion from DI water (●) and tap water (○)

2.6 Measurement of pH

The pHs of the cutting oil emulsion were measured by a pH meter (pH-539, WTW GmbH) as displayed in Table 2.5. Due to its compositions, the cutting oil emulsion contains high pH in the basic range as suggested in the product data from the manufacturer. The pH values were gradually increased along with oil concentrations. Nevertheless, the pH of the emulsion prepared from DI water was higher than that of the tap water one. This could be the result of the difference in the initial pH of the water. Furthermore, the presence of ions in tap water, including some cations, could result in lower pH values in this case.

Table 2.5 pH values of the cutting oil emulsion at varied concentration

Concentration (g/L)	0.25	0.50	0.75	1.0	2.0	3.0	4.0	5.0
DI water emulsion	8.41	8.64	8.79	8.91	9.10	9.22	9.39	9.47
Tap water emulsion	7.54	7.69	7.82	7.95	8.19	8.31	8.45	8.63

pHs of the emulsion might be changed with due to the adsorption of CO₂ from the environment. The decrease of pH can be found after a period of time if the emulsion was not well kept.

2.7 Measurement of conductivity

The conductivity was evaluated to ensure that the increase of ions in the emulsion merely came from the cutting oil. It was measured by a conductivity meter (LF 538, WTW GmbH). According to Table 2.6, the conductivities were increased with raising oil concentrations in a linear trend. The difference between the DI water and the tap water emulsions was only a result of the initial conductivity in each water.

Table 2.6 Conductivities ($\mu\text{S}/\text{cm}$) of the cutting oil emulsion at varied concentration

Concentration (g/L)	0.25	0.50	0.75	1.0	2.0	3.0	4.0	5.0
DI water emulsion	8.8	16.3	22.7	28.6	56.3	88.7	113	142
Tap water emulsion	243	248	250	252	268	280	293	302

At this point, the characteristics of the cutting oil emulsion were revealed providing a better understanding for the separation. Another property that should be considered was a parameter to represent the oil concentration, in other words, to indicate the separation performance.

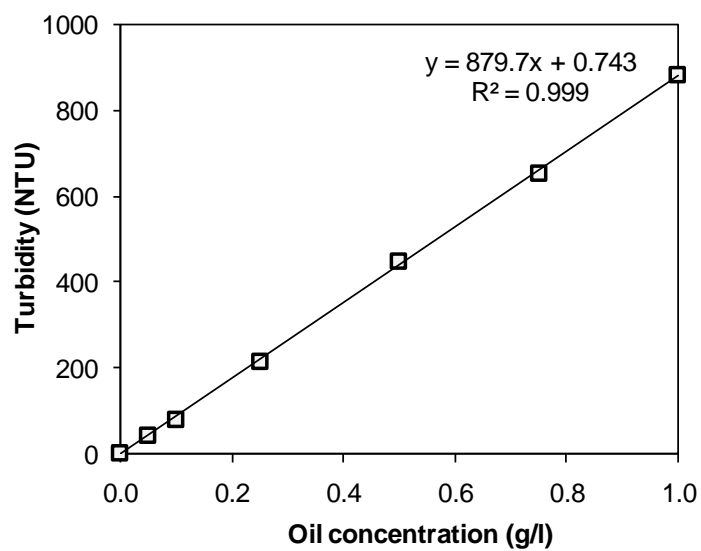
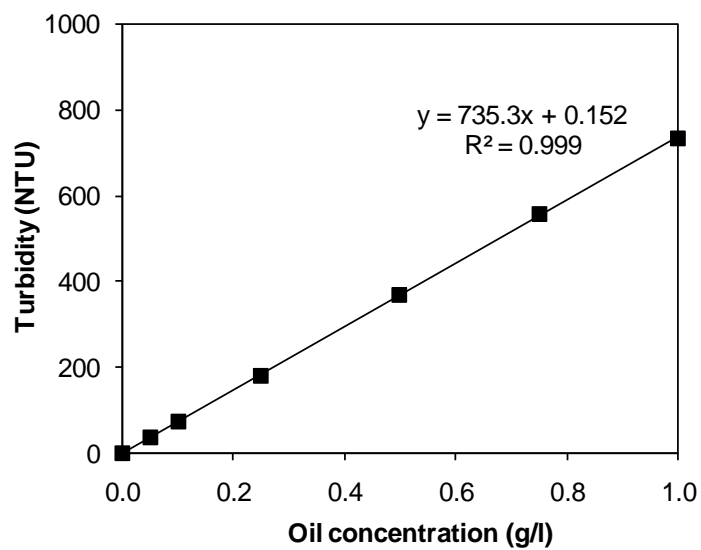
2.8 Measurement of turbidity

Turbidity is a parameter indicate the water quality in term of clarity. The value can be affected by the sizes and the numbers of particles. The nephelometric method is normally used for measuring the turbidity by providing a concentrated beam light to a sample. The amount of the scattered light at a 90° angle from the light source is measured. More light can be detected when lots of particles presented in the sample. The detected light is then reported in the unit of NTU (Nephelometric Turbidity Unit).

Turbidities of the cutting oil emulsion were measured by a turbidimeter (2100N-IS, Hach). The optical system includes an 870 ± 30 nm light diode (LED) and a detector to monitor scattered light at the 90° angle. This instrument can measure turbidity up to the maximum of 1000 NTU. The results are displayed in Table 2.7. It can be noticed that the turbidity of emulsion in tap water was higher than the DI water emulsion. The presence of larger droplets in the tap emulsion could be responsible for this result. Turbidities of the emulsion were increased with the concentration of the cutting oil. However, the turbidity at higher concentration than 1.0 g/L was unable to be measured since it exceeded the applicable range of the turbidimeter.

Table 2.7 Turbidities (NTU) of the cutting oil emulsion at varied concentration

Concentration (g/L)	0.05	0.10	0.25	0.50	0.75	1.0
DI water emulsion	35.7	71.3	178	368	556	734
Tap water emulsion	42.7	81.4	217	448	656	882



(b)

Figure 2.9 Change of turbidities with concentrations of emulsions in (a) DI water and (b) tap water

The change of emulsion turbidities with oil concentrations emulated the linear trend with high coefficient of determination (R^2) as in Figure 2.9. The correlation between turbidities (ordinate y) and oil concentrations (abscissa x) of the emulsion with DI water and tap water can be respectively expressed in Eq. 2.6 and 2.7.

$$y = 735.3x + 0.152 \quad (2.6)$$

$$y = 879.7x + 0.743 \quad (2.7)$$

These correlations would be useful for estimating the oil concentration by the measurement of turbidity. However, only oil concentration in this range (0 - 1 g/L) could be applied with the expressions. Furthermore, this relations might be unable to determine the oil concentration if droplet sizes in the emulsion were changed; for example, when aggregation occurs. The droplet size should be used to complement with the turbidity result for evaluating the separation performance.

According to these characteristics, the cutting oil emulsions in both deionized water and tap water were very stable. They contained tiny droplets in the nanoscale size with high negative zeta potential. Therefore, they were unlikely to separate from water themselves. A separation technique should be used in order to treat the emulsion. Since this cutting oil has less density than water, it could rise upward when a separation occurs. The method that can separate droplets to water surface should be considered. Hence, flotation will be applied for separating this emulsion, which will be discussed further in the following chapters.

CHAPTER 3

SEPARATION OF CUTTING OIL EMULSION BY COALESCER

This chapter presents the results of the cutting oil emulsion separation by coalescer. Effects of media shape and packing on the coalescer efficiency were investigated since it had been rarely determined in the previous researches. These two factors could play a role in the mechanisms of the coalescer, particularly on the collision of oil droplets with the media. Furthermore, influences of operating condition in terms of flow velocity and bed height were also examined. It was expected that the obtained results could provide the understanding in the coalescer mechanisms and the suggestion on the main factors that have to be considered for selecting a coalescer media, which is the most important part of the process.

3.1 Introduction

Oil is a prevalent contaminant in wastewater normally in form of stabilized emulsion with surfactants, which is difficult to separate. Coalescer is a physical process that aims to enlarge oil-droplets sizes in order to increase the separation of oil from water. The important mechanisms of the coalescer that governed its efficiency are collision and attachment droplets to media and droplets to droplets (Aurelle, 1985). Numerous researches reported effects of several parameters on the coalescer performance. For example, impacts of operating conditions (e.g. flow velocity, bed length, and oil concentration) on the separation efficiency were investigated in several works (Hazlett, 1969; Li and Gu, 2003; Sokolović et al., 2006; Zhou et al., 2009; Maiti et al., 2011). It was also found that the coalescer efficiency was affected by the media characteristics, for instance, material type, size, and wettability (Magiera and Blass, 1997; Speth et al., 2002; Ji et al., 2009; Bansal et al., 2011; Kulkarni et al., 2012). Packing of the coalescer bed, by means of porosity and permeability, was also proved for its influences on the process (Mathavan and Viraraghavan, 1992; Speth et al., 2002; Sokolović et al., 2007; Bansal et al., 2011). In addition, several studies mentioned effects of the dispersed phase characteristics, which were justified as

another important factor (Speth et al., 2002; Sokolović et al., 2010; Maiti et al., 2011). According to these studies, a coalescer process has been analyzed in 3 distinct perspectives, including characteristics of oil phase, properties of media surface (wettability, surface energy, contact angle, etc.), and geometry of media. Indeed, effects of the first two perspectives have been considerably understood by numerous researches. Impacts of media geometry on the coalescer efficiency, however, were still unobvious.

The complexity of this aspect resulted in the lack of universal design criteria of the process. In addition, a better understanding in the relation between media shape and size was required since both of them can affect the bed packing (e.g. bed porosity and permeability), separation mechanisms, and operating conditions (e.g. flow velocity and bed length) of the coalescer process. Hence, the objective of this study was to acquire a better understanding in the relation among media shape, size, and bed packing. Polypropylene (PP) media with dissimilar shapes were applied as a coalescer medium. Cutting oil was selected as the modeled emulsion due to its stability. The bed height and the emulsion flow rate were varied. Afterwards, effects of these media characteristics were investigated.

3.2 Methodology

3.2.1 Experimental set-up

The process configuration is schematically displayed in Figure 3.1. The process can be divided into 3 parts including 1) emulsion generation, 2) coalescer column, and 3) decantation tank.

Cutting oil and water in the storage tank (1) were vigorously mixed by the turbine to generate the oily emulsion. This emulsion was then introduced by the centrifugal pump (2) to the coalescer column (5) with the coalescer media (6) and the salting-out device (7). The flow rate of emulsion was controlled by the globe valve (3) and measured by the flow meter (4). The effluent from coalescer will be separated and then entered to the decantation tank (8). Note that the pressure transducers were

installed at the points before and after the coalescer bed for measuring the head loss of the wastewater that pass through the bed.

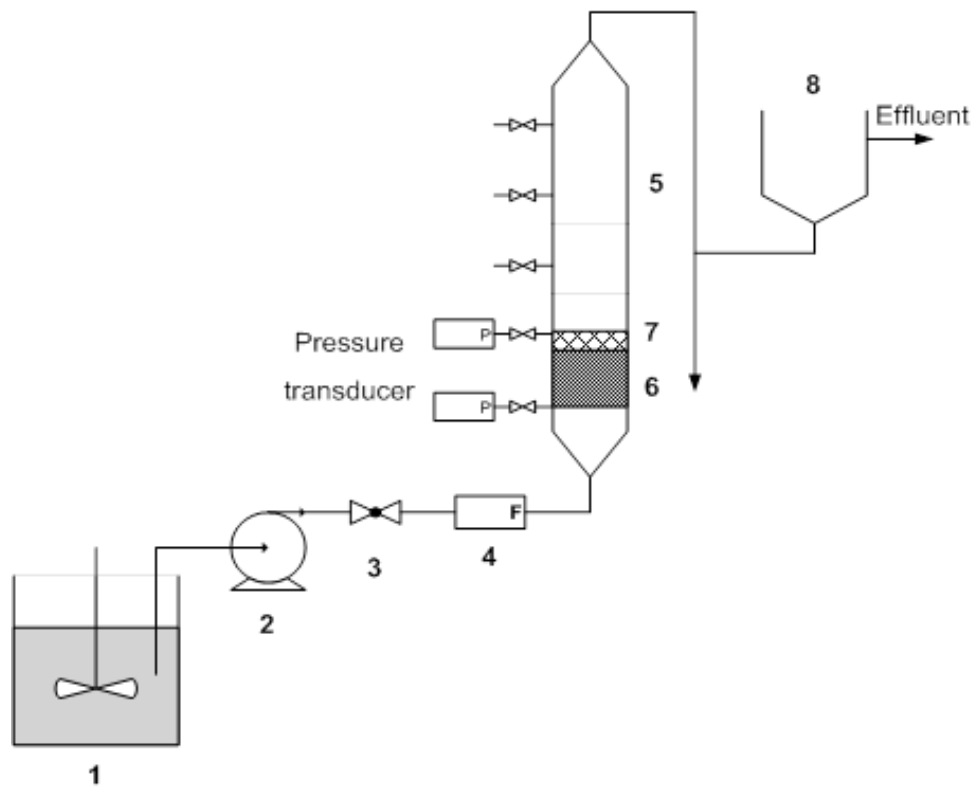


Figure 3.1 Schematic diagram of the coalescer process

The coalescer column was a clear cylindrical acrylic with the diameter and the height of 8 cm and 80 cm, respectively. The polypropylene (PP) materials with different shapes, including granule, fiber, and tube shown in Figure 3.2 were used as the coalescer media. Moreover, the salting out device was the stainless steel mesh-like. The decantation tank was a clear cylinder made of acrylic with 8-cm in diameter and 40-cm in height.

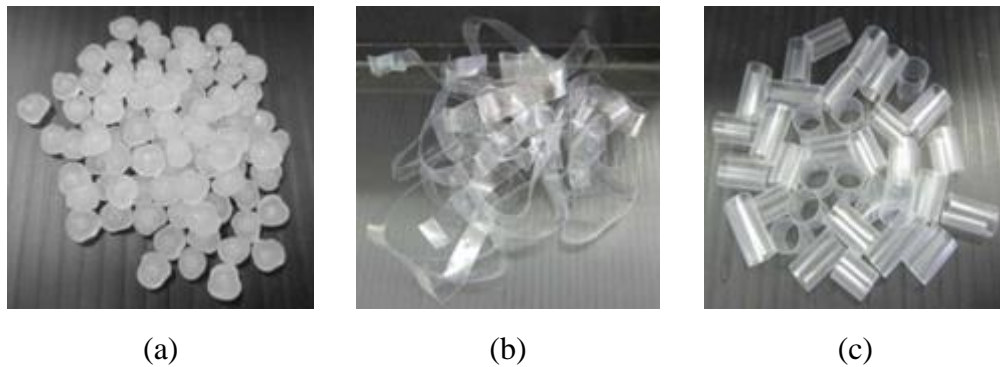


Figure 3.2 Coalescer media (a) granule, (b) fiber, and (c) tube

3.2.2 Analytical parameters

The oil concentrations in this study were analyzed by mean of turbidity in the unit of NTU (Nephelometric Turbidity Unit) by Lovibond PCcheckit turbidimeter. As reported in several researches, turbidity can be used for representing the oil concentration (Gray et al., 1997; Rios et al., 1998; Al-Shamrani et al., 2002; Bensadok et al., 2007). In addition, the oil concentration was also determined in term of COD with the close-reflux standard method (APHA, 1998) as same as other researches (Meysami and Kasaeian, 2005; de Sena et al., 2008; Tir and Moulai-Mostefa, 2008; Painmanakul et al., 2010). The oil concentrations in the unit of mg/L at the influent, coalescer outlet, and decantation tank effluent were denoted as C_0 , C_1 , and C_2 , respectively. The treatment efficiency was determined by the ratio of the difference between the inlet and the outlet oil emulsion concentrations to the initial oil concentration.

In addition, the oil-droplet size distribution of the emulsion was examined by the microscopic technique for investigate the change of droplet sizes. The optical microscope Nikon YS2-H was applied with the ocular scale and the stage microscope. Sizes of approximately 300 oil-droplets were measured and exhibited in terms of the surface-volume mean diameter (d_{sv}) as expressed in Equations 3.1 (Allen, 1997). Note that the surface-volume mean diameter is commonly used in calculation where the active surface area of particles is important (Coulson et al., 2002).

$$d_{sv} = \frac{\sum d_e^3 dN}{\sum d_e^2 dN} \quad (3.1)$$

3.2.3 Preparation of the synthetic cutting oil emulsion

The emulsion was prepared at the concentration of 1 g/L by diluting 1 g of cutting oil in 1 L of tap water at $20\pm 2^\circ\text{C}$. This tap water contained 204 – 221 $\mu\text{S}/\text{cm}$ conductivity with pH and turbidity of 7.2 ± 0.2 and 0.94 – 3.3 NTU, respectively. The mixture was vigorously mixed until the homogeneous milky emulsion was formed.

The synthetic emulsion contained the droplet sizes of 174 nm. Moreover, the zeta potential was measured of -52 mV indicating that the emulsion contained negatively charged droplets. This zeta potential value assured the stability of the emulsion since it was higher than the stability threshold in colloidal systems, i.e. ± 30 mV (Xu, 2001). Due to its small droplet size and high stability, it was found from the preliminary test that the separation efficiency by coalescer was very low. The addition of 1 g/L CaCl_2 as a destabilizing agent was then conducted to destabilize the emulsion. At this concentration, oil droplets were enlarged but did not separate to form a layer at the water surface. The droplet size and the zeta potential of this destabilized emulsion were 4.1 μm and -24 mV, respectively. Note that the prepared emulsion contained COD and turbidity values of 3900 mg/l and 1600 NTU, respectively.

3.2.4 Experimental procedure

The experiment was divided into 3 parts. First, the coalescer media were analyzed for their characteristics, including surface energy (γ_c), contact angle (θ_c), and porosity (ε_0). The contact angles were measured by the sessile-drop method (Mittal, 2009). The drops of cutting oil and water on the media were captured by the digital camera with sufficient magnification. The contact angles were then measured by the image processing software. The contact angle (θ_c) of cutting oil droplet on the media in water was finally calculated by Young's equation as expressed in Equation 3.2 (Mittal, 2009).

$$\gamma_{wc} = \gamma_{oc} + \gamma_{ow} \cos \theta_c \quad (3.2)$$

The Zisman method was applied for analyze the γ_c values of the polypropylene media (Zisman, 1964). Moreover, the porosities of the bed were determined by water saturation method, which defined as the replacement of void volume with water (Gleabey et al., 1991).

After that, the effects of different operating conditions on the treatment efficiency were evaluated. The experiments were conducted at varied bed length of 2 – 10 cm and flow velocity of 2.0 – 6.8 cm/s. After pass through the coalescer bed, the emulsion was retained in the decantation tank with the retention time of 120 minutes. Note that all experiments were operated at the saturated bed condition achieved by recirculation of emulsion through the bed until the constant pressure loss was observed. The samples were collected at 2 different points, for example, after pass through the bed and at the decantation tank, and then analyzed for the oil concentration and the oil-droplet size distribution. Finally, the mathematical models were applied with the experimented results for describe the occurred mechanisms in the process.

3.3 Results and Discussions

3.3.1 Characteristics of coalescer media

Characteristics of coalescer media are presented in Table 3.1. From the experiments, the surface energy of the polypropylene media obtained was 35mN/m. This γ_c value was slightly greater than those reported in the range of 29 – 31 mN/m (Sabreen, 1991) and 31 mN/m (Zhao and Li, 2011). However, the surface energy of PP was lower than other hydrophobic materials, for example, polyester (41 – 44 mN/m) and nylon (33 – 46 mN/m) (Sabreen, 1991), but higher than that of the polyurethane fiber (23 mN/m) in the work of Sokolović et al. (2007). Due to this γ_c value, the PP can be implied as a low surface energy material; thus, indicating its hydrophobicity (Zisman, 1964). This surface energy result of PP corresponded to the contact angle as the angles of the oil-droplets on the media with different shapes in

water were approximately 68° as shown in Table 3.1. Since the contact angle was between 0° to 90° , these media can be categorized as a hydrophobic material. Therefore, they could be applied as a coalescer medium (Aurette, 1985).

Table 3.1 Coalescer media characteristics

Characteristics	Polypropylene		
	Granule	Fiber	Tube
Porosity	0.55	0.90	0.82
Dimension (mm)	4.5 – 5.5 (Diameter)	10 x 280 x 0.5 (Width x Length x Thickness)	5 x 8 (Diameter x Length) 4 mm of inner diameter
θ_c ($^\circ$)	68.01	68.53	68.37

It can be seen that these PP media with different shapes were hydrophobic with similar contact angle. However, the porosities of the media when packing were obviously different due to their sizes and shapes as well as their arrangement in the bed. The highest porosity was found from the fibrous medium following with the tubular and granular media, respectively. The granular medium contained the porosity of 0.55, which was slightly higher than that of a sand filter (0.40 – 0.45) (AWWA, 1990) and the expanded polystyrene bed (0.45) from the work of Sokolović et al. (2010), could result in the filtration mechanisms in the bed. On the contrary, porosities of tubular and fibrous media (0.82 and 0.90, respectively) were in the same range with other researches (Speth et al., 2002; Vasudevan and Chase, 2004). The influences of the different bed porosity on the separation performance of oily emulsion will be further discussed.

3.3.2 Effects of operating conditions on treatment efficiencies

Figure 3.3 displays treatment efficiencies of coalescer process for all media in different operating conditions. As can be seen, the highest efficiency of each medium was achieved at the bed length of 10 cm with flow velocity of 2 cm/s, which was denoted as the optimal condition in this study. The highest treatment efficiency of approximately 40% was obtained from the tubular medium (Figure 3.3c). It can be noticed that the separation efficiency was influenced by the flow velocity. This optimal flow velocity of 2 cm/s in this work corresponded to the works of Wanichkul (2000) and Rachu (2005).

On the contrary, the efficiency was slightly affected by the bed length, which was similar to the work of Li and Gu (2003). The highest efficiencies of nearly 25% were observed in the cases of granular and fibrous media with no obvious influence from different operating conditions (Figure 3.3a and Figure 3.3b, respectively). However, due to the porosity difference between granular (0.55) and fibrous (0.90) media, the occurred mechanisms might be dissimilar.

Table 3.2 displays the oil-droplet sizes and the treatment efficiencies of decantation and coalescer processes with these 3 media at the optimal condition. It can be seen that the emulsion cannot be separated by the conventional decantation process, and the droplet size did not clearly change. In the case of granular medium, the oil-droplet size after passing the bed did not distinctively varied from the inlet emulsion as well as after the decantation. These sizes indicated that the oil-droplets coalescence was rarely occurred. Filtration of droplet by the media might be the dominated mechanism. On the contrary, the droplet sizes were enlarged after pass through the fibrous and tubular bed, implying the occurrence of oil-droplets coalescence. Furthermore, the highest efficiency of 43% from tubular medium would be the result of differential settling. The large droplets with higher rising velocity would collide with the smaller ones resulting in the aggregation. The separation was then faster due to their larger size and higher possibility for further collision and aggregation (Svarovsky, 2000).

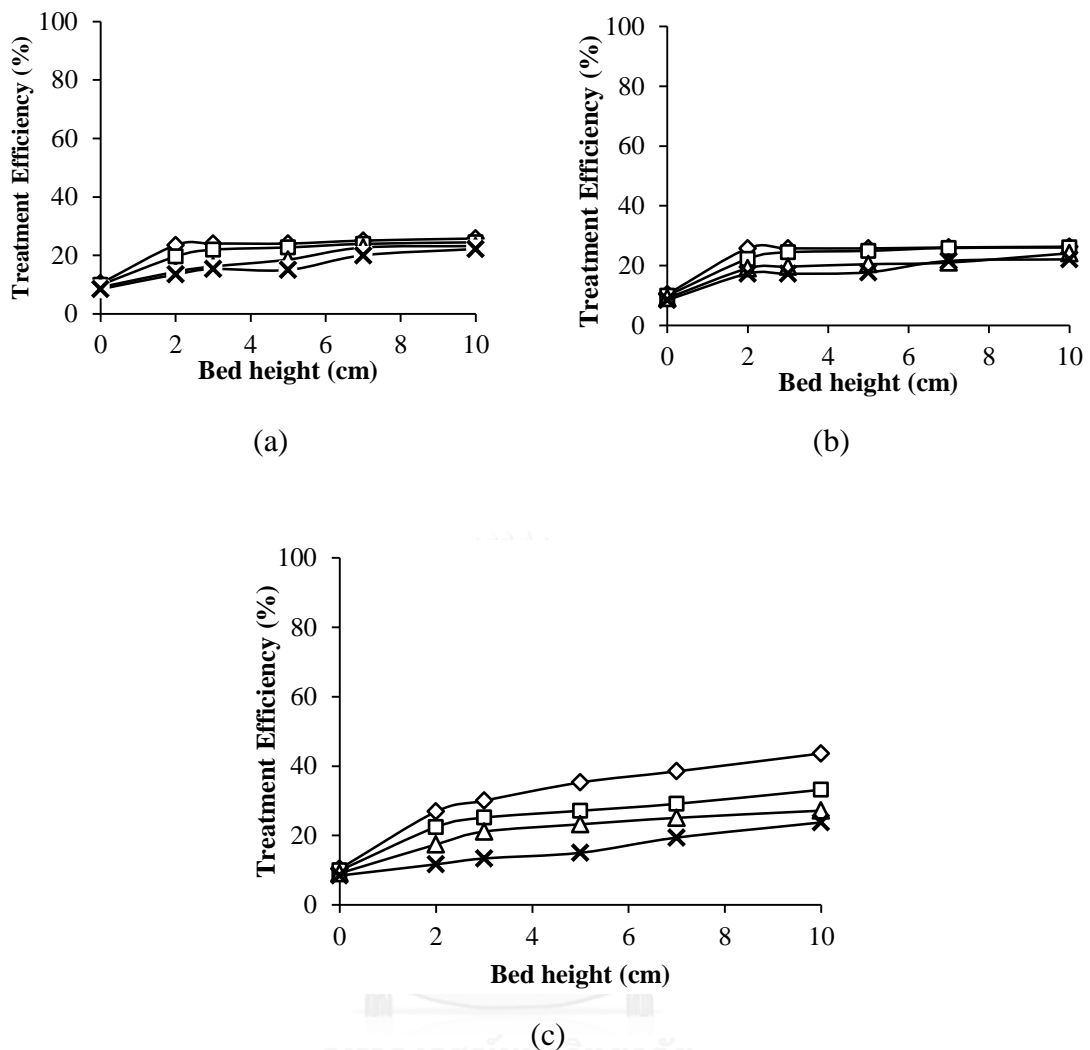


Figure 3.3 Treatment efficiencies in different operating conditions for (a) granular, (b) fibrous, and (c) tubular media (\diamond 2.0 cm/s; \square 3.4 cm/s; \triangle 4.8 cm/s; \times 6.8 cm/s)

At this point, it can be stated that the media shape and the bed porosity could be the key factors affecting the performance of the coalescer process. Moreover, it can be suggested that the larger coalesced droplets can be separated by the decantation, which conformed to the results of discrete settling test. The remaining droplet sizes after decantation of these coalescer processes were relatively close to that of the decantation process.

Table 3.2 Oil-droplet sizes (dSV) at 2.0 cm/s flow velocity and 10 cm bed height (in m)

Coalescer	Inlet emulsion	After bed	After decantation	Efficiency (%)
Decantation		-	6.0	0.0
Granule	4.1	7.9	7.3	25.8
Fiber		17.4	5.8	26.3
Tube		21.9	8.5	43.6

Regarding the media shape, the efficiency difference could be the results of distinctive specific surface area of media. The specific surface area can be defined as a surface area per unit mass of material (Foust et al., 1980). In this work, the tubular media contained the specific surface area of 6708 m^{-1} , which was much higher than those of the granular and fibrous ones (1200 and 2007 m^{-1} , respectively). This difference could impact the collision probability of oil-droplets on the media, which is the relevant phenomenon in the coalescence and the filtration processes (Aurelle, 1985). Besides, the process performance was also influenced by the bed porosity. The denser granular bed ($\varepsilon = 0.55$) might filter oil-droplets out from the emulsion as discussed above. In contrast, the more porous beds, i.e. fiber and tube, could result in higher probability of oil-droplets coalescence as corroborated by the droplet sizes in Table 3.2.

3.3.3 Effects of coalescer media characteristics

In this section, influences of media characteristics on the treatment efficiency of the coalescer were discussed. The impacts were analyzed by means of media size and packing behavior.

3.3.3.1 Size of coalescer media

The media sizes were determined by 2 different approaches. Firstly, Ergun's equation (Equation 3.3), which defined as correlation between the friction factor and

Reynolds number of a packed column with granule collector (McCabe et al., 2000), was applied for determining the media diameter (d_c).

$$\frac{\Delta p}{H} = \frac{150v_0\mu_f(1-\varepsilon_0)^2}{\phi^2 d_c^2 \varepsilon_0^3} + \frac{1.75\rho_f v_0^2(1-\varepsilon_0)}{\phi d_c \varepsilon_0^3} \quad (3.3)$$

Note that ϕ is the sphericity. This ϕ can be defined as the ratio of the surface area of a sphere (with the same volume as the given particle) to the surface area of the particle as expressed in Equation 3.4 (Foust et al., 1980).

$$\phi = \frac{A_0}{A_p} = \frac{\pi d_p^2}{A_p} = \frac{\pi(6V_p/\pi)}{A_p} \quad (3.4)$$

The media size can be calculated from the measured pressure loss of emulsion pass through the bed (Δp) in Ergun's equation. The sizes of 4.8, 7.5, and 8.3 mm were obtained for granular, fibrous, and tubular media, respectively. This calculated diameter of the granular medium was close to its actual size (4.5 – 5.5 mm). Therefore, it can be stated that the media size determination by Ergun's equation can be applied for a sphere-liked media. Though, the calculated sizes of the fibrous and tubular media were larger, which did not correspond to their specific surface area. This approach might restrict to apply with a non-sphere media.

As a result, another approach for determine the media size was proposed by applying the filtration efficiency equation as expressed in Equation 3.5 (i.e. for sphere collectors) (Aurelle, 1985).

$$\ln \frac{C_1}{C_0} = -\frac{3}{2d_p} \alpha \eta_T (1-\varepsilon_0) H \quad (3.5)$$

The α and η_T were the attachment and the collection efficiencies between oil-droplets and collectors, respectively. The collection mechanism of droplets by

collectors features 3 main transport phenomena such as gravitational settling, interception, and diffusion. The η_T is a summation of the sub-efficiency of these three phenomena. The acquired η_T for each medium was then employed for determining the relative sphere-liked diameters of fibrous and tubular media to the diameter of the sphere one. However, the geometric dimension of the media had to be considered since the filtration efficiency equation relied on the projection area of a collector. The areas of these two media were varied due to their shapes and orientations in the packed bed. The filtration efficiency equation was then modified as displayed in Equations 3.6 and 3.7, respectively, for the fibrous and the tubular media. The θ is an inclined angle of medium related to a horizontal plain, which was varied from 0° to 90° in this study, as illustrated in Figure 3.4.

$$\ln \frac{C_1}{C_0} = - \left(\frac{\cos \theta}{t} + \frac{\sin \theta}{L} \right) (1 - \varepsilon) \alpha \eta H \quad (3.6)$$

$$\ln \frac{C_1}{C_0} = - \frac{1}{(d_o^2 - d_i^2)} \left(\frac{4d_o \cos \theta}{\pi} + d_o^2 \sin \theta \right) (1 - \varepsilon) \alpha \eta H \quad (3.7)$$

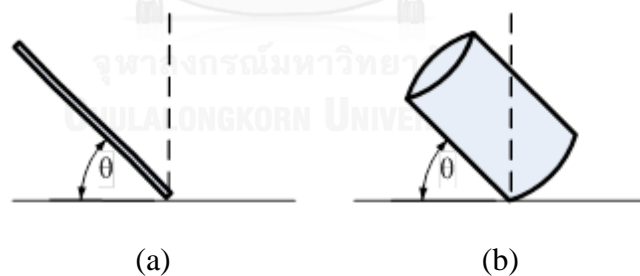


Figure 3.4 Inclined angles (θ) of (a) fibrous and (b) tubular media

Where t and L are thickness and length of the fibrous medium. The d_o is the outer diameter, and d_i is the inner diameter of the tubular medium. The sphere-liked diameters can be therefore determined from the inlet and the outlet concentrations by dividing Equations 3.6 and 3.7 by Equation 3.5. In this work, the attachment efficiency (α) was assumed to be constant in all media as the attachment occurred between the same cutting oil and PP surface. The calculated diameters are

summarized in Table 3.3. As can be seen, sizes of the fibrous and the tubular media calculated from the filtration efficiency equation were smaller than those obtained from Ergun's equation. The diameters from the second approach tended to correspond with the specific surface area as previously discussed.

Table 3.3 Calculated diameters obtained from Ergun's and filtration efficiency equations

Media types	Calculated diameter (mm)	
	Ergun's equation	Filtration efficiency equation
Granule	4.8	-
Fiber	7.5	2.2
Tube	8.3	1.2

In addition, it was found from the calculation that the inclined angle of 90° provided the highest collection efficiency at every operating condition. This 90° orientation of the tubular medium was similar to the stacked raschig ring, which provided the advantages on low pressure drop and good liquid distribution in the bed (Benitez, 2009). Higher contact and attachment probability of oil-droplets to media would be achieved.

At this point, the size determination approach by the filtration efficiency equation provided a more reasonable result. This approach could be applied for a media selection. The efficiency from the small column test could be used for suggesting a media selection in a practical coalescer or filtration process.

3.3.3.2 Packing behavior of coalescer bed

Behavior of a packed bed was a relevant factor affecting the treatment efficiency since it could influence the mechanisms occurred while the emulsion flowed through. Firstly, Ergun's equation (Equation 3.3) and the measured pressure loss was applied to evaluate the bed porosity at the saturated bed condition, denoted as ε_t . Note that the media sizes used for this calculation were obtained from Ergun's

equation for granular medium, and from the filtration efficiency equation for fibrous and tubular media as mentioned in the previous section. This ε_t value was consequently used for estimating the average saturation factor ($\overline{S_d}$) or the fraction of oil amount in the bed at the saturated condition as expressed in Equation 3.8 (Sherony and Kintner, 1971), where ε is an initial porosity of the bed.

$$\overline{S_d} = 1 - \frac{\varepsilon_t}{\varepsilon_0} \quad (3.8)$$

The saturated porosity (ε_t) and the saturation factor ($\overline{S_d}$) of media are exhibited in Table 3.4. As can be seen, the granular medium contained the lowest saturated porosity in this study following with the tubular and the fibrous media, respectively. This result verified the discussion regarding the dominated filtration mechanism in granular bed.

Furthermore, this value can indicate the coalescence possibility in packed bed according to Chieu et al., 1975. It was stated that the complete coalescence can occur with at least the oil volume saturation in bed of 10 – 15%. Therefore, the obtained values in this study exhibited the coalescence probability of oil in every bed.

Table 3.4 Saturated porosity (ε_t) and average saturation factor ($\overline{S_d}$) of packed beds

Media Types	Saturated porosity (ε_t)	Saturation factor ($\overline{S_d}$)
Granule	0.12	0.79
Fiber	0.28	0.68
Tube	0.26	0.68

This accumulated oil indicated by the $\overline{S_d}$ and the ε_t could change the pore structure and affected the emulsion flow in the bed. Furthermore, presence of oil in the bed could alter the single-phase flow (i.e. water) to the two-phase flow (i.e. water

and oil) according to Mathavan and Viraraghavan (1992). To investigate this effect, Carman-Kozeny equation was employed as expressed in Equations 3.9 and 3.10, respectively, for the single-phase and the two phase flows (Sherony and Kintner, 1971).

$$\Delta p_1 = \frac{16Hv_0\mu_f k_1(1-\varepsilon_0)^2}{d_p^2 g \varepsilon_0^3} \quad (3.9)$$

$$\Delta p_2 = \frac{16Hv_0\mu_f k_2(1-\varepsilon_t)^2}{d_p^2 g \varepsilon_t^3} \quad (3.10)$$

The Carman-Kozeny constants (k_1 and k_2) indicate the uniformity of pore structure within the bed. According to Akers and Ward (1977), the Carman-Kozeny constants depend on particle sizes and shapes as well as their packing. Furthermore, it was stated that the low constant value implies to the low pore uniformity (Carman, 1956). Additionally, the specific permeability coefficient of single-phase flow in the bed, denoted as $B_{0,1}$, can be calculated from Equation 3.11 (Carman, 1956). Likewise, the coefficient for two-phase flow ($B_{0,2}$) can be evaluated by substituting the ε and k_1 with ε_t and k_2 , respectively. The specific permeability of bed is a function of only pore structure (Cheremisinoff, 1998), which could impact the ability of emulsion to flow through the bed.

$$B_0 = \frac{d_p^2 \varepsilon_0^3}{16k_1(1-\varepsilon_0)^2} \quad (3.11)$$

Carman-Kozeny constants and specific permeability coefficients in this study are displayed in Table 3.5. As can be noticed, the k_1 and k_2 were distinct, which demonstrated the dissimilar pore uniformity between these two scenarios.

Table 3.5 Carman-Kozeny constants for single- and two-phase flow with bed permeability

Media Types	k_1	k_2	$B_{0,1} (\text{m}^2)$	$B_{0,2} (\text{m}^2)$
Granule	30.3	19.8	6.8×10^{-9}	5.2×10^{-11}
Fiber	19.3	10.7	1.3×10^{-8}	3.8×10^{-11}
Tube	13.6	10.4	3.5×10^{-9}	2.1×10^{-11}

In the case of single-phase flow, the granule contained the highest uniform pore amongst the applied media due to its rigid configuration. The emulsion could flow through the pore structure of the bed as depicted in Figure 3.5(a1). The lower pore uniformity was found in the case of fiber as the emulsion can randomly pass through the porous ($\varepsilon = 0.90$) and disorganized bed as displayed in Figure 3.5(a2). In contrast, the tubular medium possessed the lowest uniformity even with its rigid shape. This can be described as the emulsion can flow through the gap between as well as the hollow of media as shown in Figure 3.5(a3).

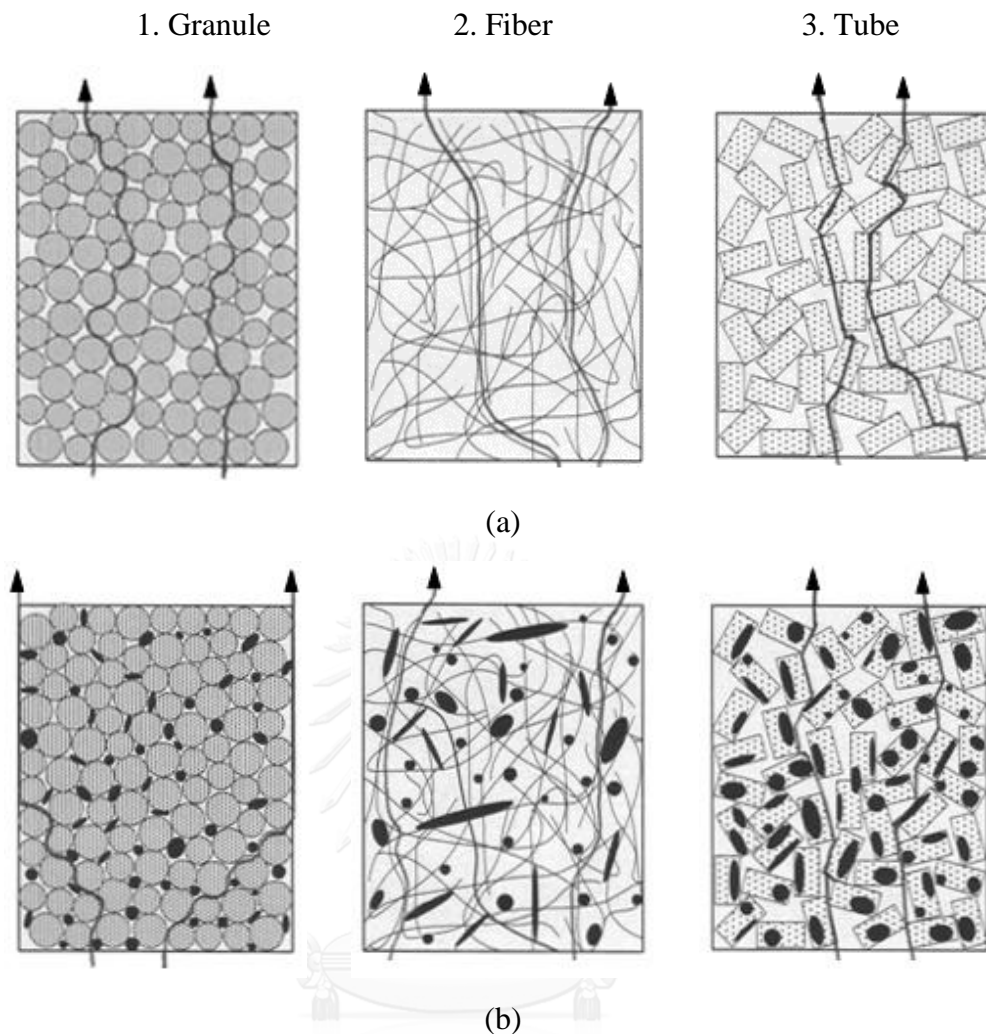


Figure 3.5 Flow pathways of the emulsion for three medium types in (a) single-phase flow and (b) two-phase flow

After the beds were saturated, their porosities were changed as well as the pore uniformity since oil-droplets attached in the bed. The two-phase flow could occur. The oil phase in the emulsion would flow along the attached droplets whilst the water phase passed through the center of pores. The flow streamline of the emulsion was therefore affected as exhibited in Figure 3.5b. The attached oil-droplets in the granular bed could join the media together, resulting in bed clogging. The emulsion flow was obstructed and the pore uniformity was then decreased (Figure 3.5(b1)). This same reason can describe the decrease of pore uniformity in the case of fibrous bed (i.e. 19.3 \rightarrow 10.7) as shown in Figure 5(b2). Nevertheless, the coefficient of the tubular bed was slightly decreased (i.e. 13.6 \rightarrow 10.4). The emulsion can still pass through the

gap between media even the presence of attached oil-droplets in the bed as in Figure 3.5(b3).

The change of bed porosity and pore structure between the single-phase and two-phase flow conditions also resulted in the decrease of the specific permeability coefficient (B_0) as shown in Table 5. The coefficient for the single-phase flow ($B_{0,1}$) in this study was in the range of $10^{-9} - 10^{-8} \text{ m}^2$, which were slightly higher than that of filter bed reported in several studies ($10^{-13} - 10^{-9} \text{ m}^2$) (Mathavan and Viraraghavan, 1992; Sokolović et al., 2007). These higher permeabilities might be the results of the highly porous and disorganized beds. The lowest permeability in this study was found in the case of the tubular bed, which was owing its less pore uniformity and higher surface area. The permeability suggested that the emulsion was able to flow through the bed more than that of the filtration process. On the other hand, the coefficient diminished in the two-phase flow condition ($B_{0,2}$). This result was compatible with the decreased porosity, which expressed that the pore structure was changed as aforementioned. Therefore, the bed permeability could be suggested as a key factor influencing the process performance since it relates to other several parameters such as media size, media shape, and bed porosity.

3.4 Conclusions

The objective of this work was to study the relation among the media shape, size, and packing behavior occurred in the coalescence process. For this purpose, experiments related with different coalescer shapes (granular, fibrous and tubular) and operating conditions (bed height and flow velocity) were performed. According to the result, the conclusion was as follows:

- Polypropylene was partly hydrophobic and can be applied as a coalescer medium. The dissimilar shape of media resulted in the difference of bed porosity

- The highest separation efficiency in this study was 43% obtained from the optimal operating condition of 2 cm/s flow velocity and 10 cm bed of the tubular medium.
- Ergun's equation can only be used for examining size of media with the sphere-liked shape. However, the proposed determination approach by filtration efficiency equation provided more reasonable sizes for non-sphere media
- The difference of media shape affected their equivalent sizes as well as the porosity and saturation factor ($\overline{S_d}$). These latter two parameters can be used for identifying the dominant mechanism whether filtration or coalescence. Besides, the ε and can d_p be applied to determine the bed permeability
- Size and shape of media can impact the porosity and the pore structure of the bed, which affect the flow pathway of the emulsion as well as the separation mechanism

Further study should be conducted in a larger scale process or with other media (in terms of material, size, and shape) to validate the applicable of this media consideration approach. Wetting properties of media and bed permeability were two factors that should be considered.

The results in this chapter suggested that the separation efficiency of the coalescer on the separation of oily emulsion can be affected by several factors, especially media characteristics. However, the efficiency was still low. The separation by other process should be investigated. In the next chapter, flotation will be applied for separating this cutting oil emulsion. The working principle of flotation is also based on the interaction between oil droplets and collectors, which are bubble in this case. The results on the separation performance and the related mechanisms will be exhibited later in the following parts.

CHAPTER 4

SEPARATION OF CUTTING OIL EMULSION BY FLOTATION

As it was found that the separation efficiency of cutting oil emulsion by coalescer was still low, other processes should be applied in order to achieve the effective separation. Flotation was selected since it can successfully treat stabilized emulsions in various study. This chapter presents the results of the emulsion separation by flotation. Two types of flotation that can generate bubbles with different sizes, i.e. dissolved air flotation (DAF) and induced air flotation (IAF) were applied. Effects of operating conditions and hydrodynamic parameters on the separation performance were investigated. Furthermore, the residence time distribution was also studied to analyze the flow pattern occurred in the flotation cell and the difference within the reactor between the DAF and IAF.

4.1 Introduction

The application of flotation was initiated in the mineral processing for the solid-solid or solid-liquid separation (Rubio et al., 2002). With chemical addition, the froth flotation contains high selectivity that can be used for separating different mineral or ore from each other (Kitchener, 1985). Flotation has been later applied in the field of wastewater treatment for removal of numerous particles from water such as solids, plastics, and algae (Kitchener, 1985; Mavros and Matis, 1992; Matis, 1995).

Apart from solid particles, flotation has been studied for its application on the separation of oil from water (Zheng and Zhao, 1993; Al-Shamrani et al., 2002; Meyssami and Kasaeian, 2005; Bensadok et al., 2007; Tansel and Pascual, 2011). It was found to be an effective technique for the separation of oil droplets in microscale range. Therefore, this study was interested to apply flotation for the treatment of the stabilized cutting oil emulsion with nano-droplets. Two types of flotation that usually used in wastewater treatment, i.e. induced air flotation (IAF) and dissolved air flotation (DAF), were applied to determine effects of bubble sizes produced in the system on the separation performance. Moreover, influences of operating conditions

were investigated. Finally, the residence time distribution (RTD) was conducted to examine the flow pattern occur in the flotation cell in both cases.

4.2 Methodology

4.2.1 Jar-test experiment

The cutting oil emulsion was treated by chemical coagulation in the jar-test experiment after it was found that this emulsion cannot be separated by decantation alone. The aim of this experiment was to determine the removal efficiency of cutting oil by the coagulation using alum ($\text{Al}_2(\text{SO}_4)_3 \cdot 14\text{H}_2\text{O}$) as the coagulant. Effects of cutting oil concentration, alum dosages, and pH were determined. The oil concentrations of 0.25 – 1.0 g/L were used in this experiment. The jar test was carried out by the rapid mixing of 100 rpm for 1 minute before 30 minutes of 30 rpm slow mixing and decantation for 30 minutes. The efficiency was determined by the ratio of the difference between the initial and final oil concentrations to the initial one as expressed in Equation 4.1 where C_0 and C_f are initial and final concentrations of the sample.

$$\% \text{ Efficiency} = \frac{C_0 - C_f}{C_0} \times 100 \quad (4.1)$$

4.2.2 Experimental set-up

The experimental set-ups for the dissolve air flotation (DAF) and the induced air flotation (IAF) are presented as follow.

4.2.2.1 Dissolved air flotation (DAF) process

The set-up of the DAF process in this study is schematically shown in Figure 4.1. The process consisted of 3 parts such as 1) pressurized water generation system, 2) emulsion and coagulant feed system, and 3) flotation tank.

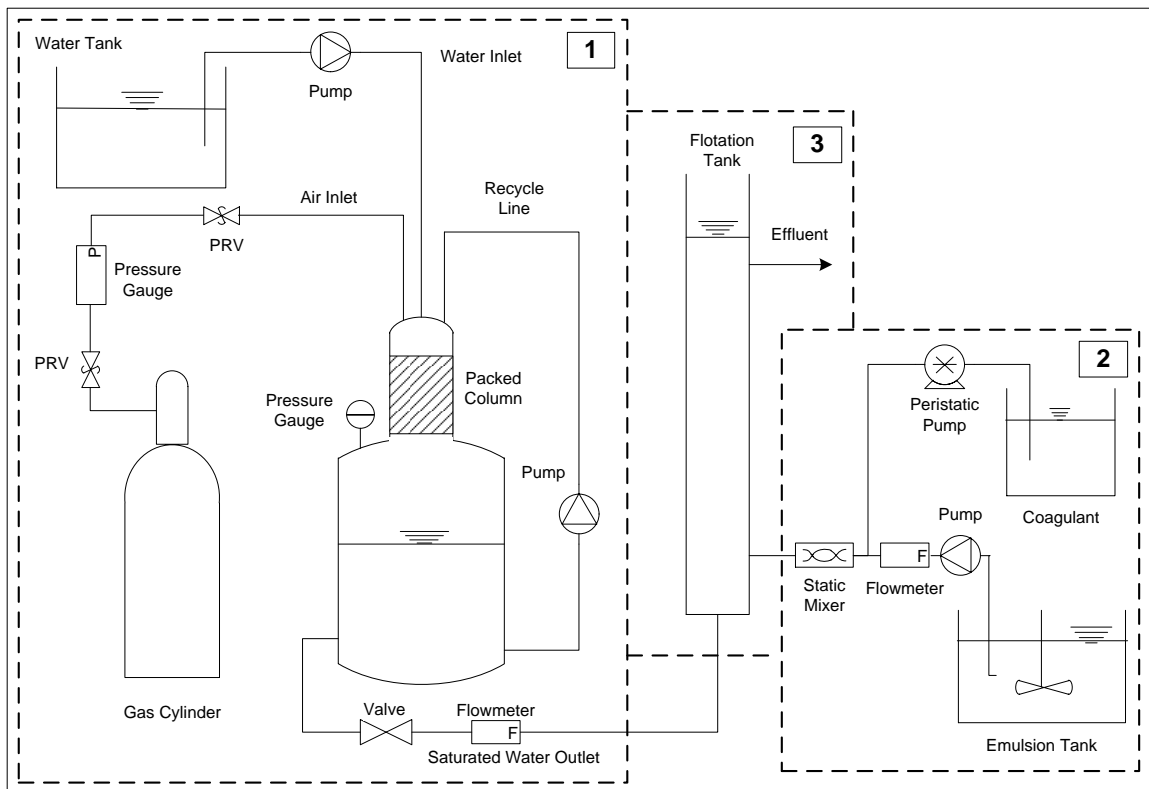


Figure 4.1 Schematic diagram of DAF process

The pressure vessel was a stainless steel tank designed for the maximum operating pressure and flow rate of 8 bars and 50 l/min, respectively. By defining 5 minutes detention time and 1:1 water-to-air ratio, the tank with volume of 500 L was obtained. Details of the pressure vessel are depicted in Figure 4.2. Note that the recycle line was used for promoting more contact between air and water.

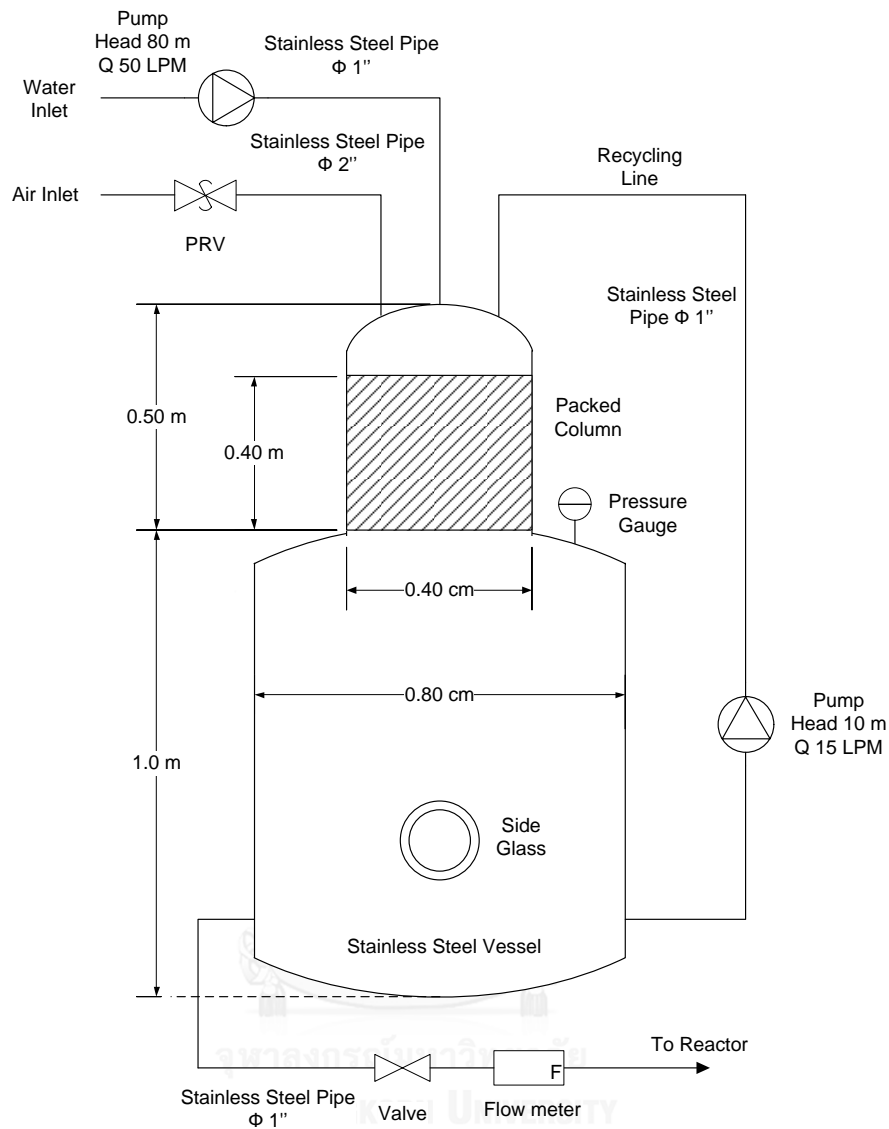


Figure 4.2 Pressure vessel

The flotation tank was an acrylic cylindrical column with the dimensions as displayed in Figure 4.3. The column can be divided into 1) contact zone where oil encountered with bubbles, and 2) separation zone where droplet-bubble aggregates can separate from water. This flotation tank was designed for the hydraulic loading rate (HLR) and contact time of 5 – 15 m/hr and 1.0 – 2.5 minutes, respectively.

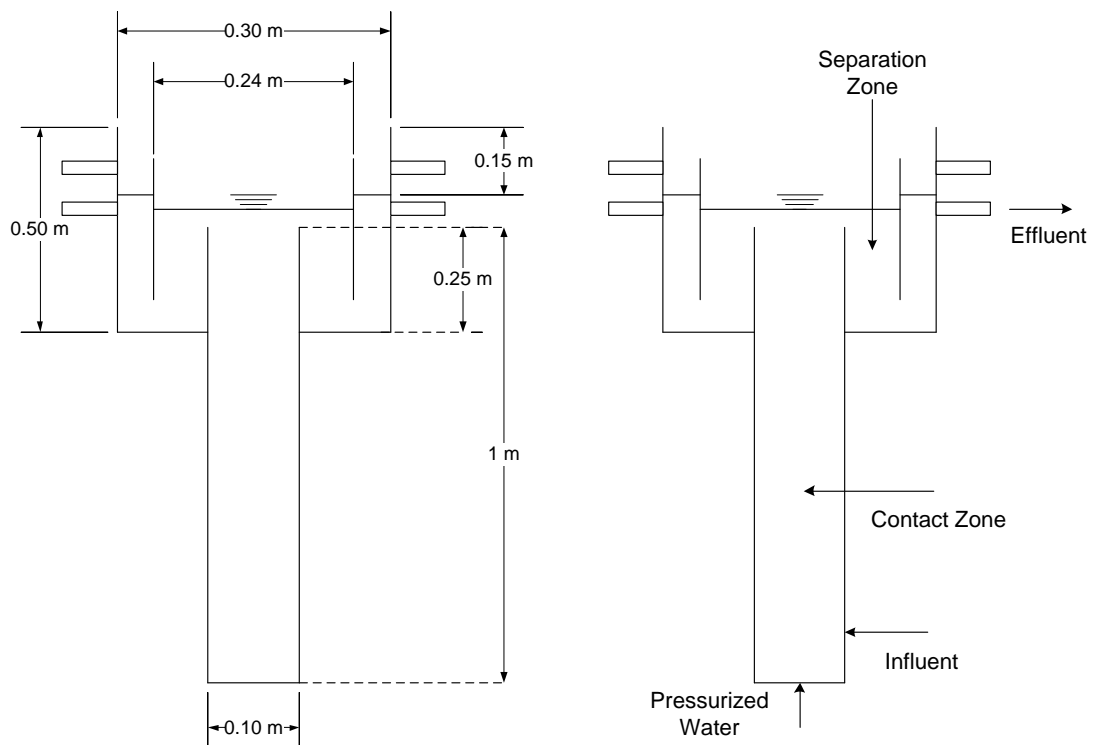


Figure 4.3 Flotation tank

This process was then tested for the sizes of bubbles produced to validate that this process can be classified as DAF.

4.2.2.2 Induced air flotation (IAF) process

The IAF set-up is illustrated in Figure 4.4a. The process included 1) the air injection through the flexible aerator as in Figure 4.4b, 2) emulsion and chemical feed, and 3) the flotation tank, which was similar to the tank used with DAF as depicted in Figure 4.3.

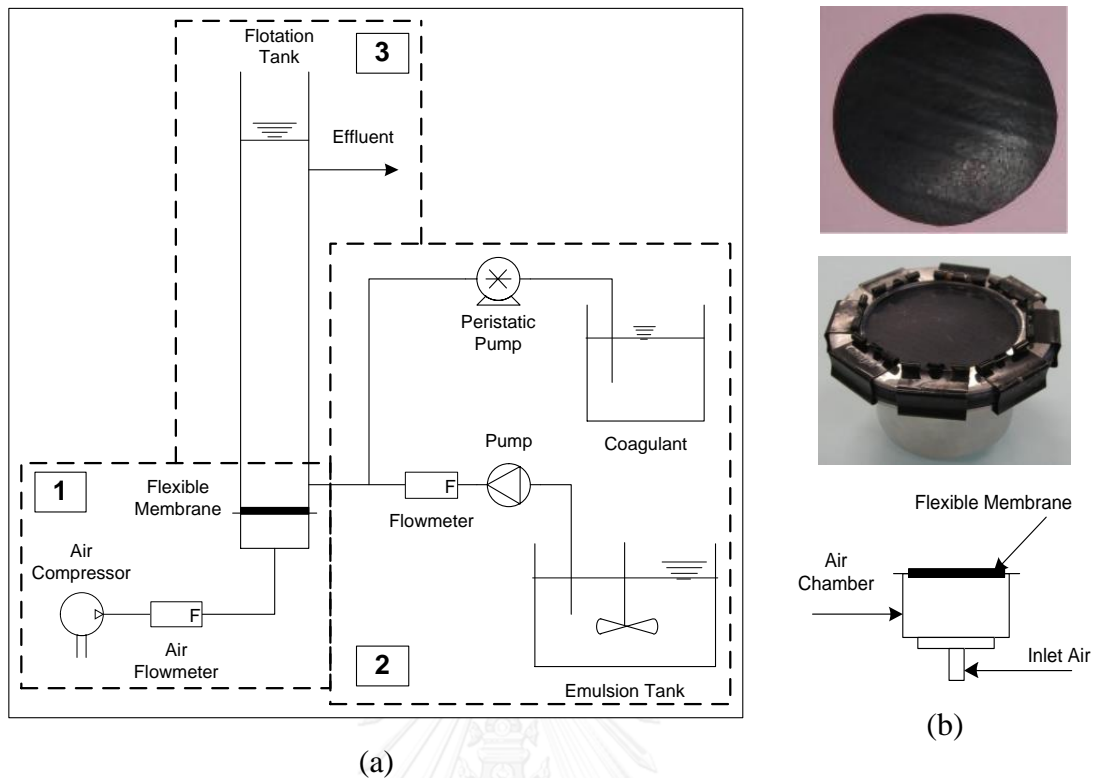


Figure 4.4 (a) Schematic diagram of IAF process (b) Flexible aerator

4.2.3 Separation of cutting oil emulsion by flotation processes

4.2.3.1 Dissolved air flotation (DAF) process

The cutting oil emulsion was separated by the DAF process with and without coagulation. Note that the DAF process with chemical coagulation was called as the modified dissolved air flotation or MDAF. The dosage of alum was acquired from the jar-test experiment. Firstly, the kinetic study was conducted in a batch operation. The flow rates of the pressurized water (Q_{pw}) at the optimal pressure level obtained from the process validation were varied at 0.17, 0.58, 1.30, 2.12, and 3.07 L/min to encounter the emulsion retained in the flotation tank. The effluent was periodically sampled until the efficiency was constant. The sample was analyzed for the concentration and determined for the efficiency by Equation 4.2 as the dilution effect was taken into account.

$$\% \text{ Efficiency} = \frac{[(C_{in} \times Q_w) - C_{out} \cdot (Q_w + Q_{pw})]}{C_{in} \cdot Q_w} \times 100 \quad (4.2)$$

where C_{in} is the concentration of the influent

C_{out} is the concentration of the effluent

This operation time was applied later in the continuous operation. The emulsion with 1 g/l in concentration was introduced into the flotation tank at the flow rates (Q_w) of 0.6, 1.2, 1.8, and 3.0 L/min. The effluent was collected at the operating time from the kinetic study and analyzed for the efficiency.

- Effects of A/S ratio in DAF process

The air-to-solid ratio (A/S ratio), which is the ratio of air volume to mass of solid in a flotation cell, is regarded as the important factor in the operation of DAF for separating solid particles (Metcalf & Eddy, 2004). In this study, influences of this A/S ratio on the process performance were determined. The flow rates of the emulsion and the pressurized water were fixed at 1.2 L/min and 0.17 L/min, respectively. The pressure level was the optimum one obtained from the process validation, and the optimal alum dose from the jar-test experiment. The emulsion concentration was varied at 0.5, 1.0, 1.5, 2.0, 2.5, and 3.0 g/l. Operation and sampling were similar to the MDAF experiments. The A/S ratio for each oil concentration value can be calculated from Equation 4.3.

$$\frac{A}{S} = \frac{Q_{PW} \cdot C_{air}}{Q_w \cdot C_{in}} \quad (4.3)$$

where C_0 is the initial cutting oil concentration (g/L) and C_{air} is the dissolved air concentration in water (g/L) at a certain pressure level determined by Henry's law (Equation 4.4)

$$C_{air} = K_H \cdot \bar{P} \cdot MW \quad (4.4)$$

where K_H is Henry's constant, \bar{P} is partial pressure of gas, and MW is molecular weight of gas.

Since nitrogen (N_2) and oxygen (O_2) are major components in air, its properties that related to solubility are shown in Table 4.1.

Table 4.1 Properties of air at 20°C

Components	Fraction (%)	Henry's constant (atm/(mol/L))	MW (g/mol)	Density (kg/m ³)
N_2	79	1600	28	1.204
O_2	21	756.7	32	

Therefore, Equation 4.4 can be rewritten as

$$C_{air} = PS \cdot [K_{H,N_2} (0.79)(28) + K_{H,O_2} (0.21)(32)] \quad (4.5)$$

where PS is the applied pressure level in the pressure vessel (bar or atm). The dissolved air concentration in fluid phase can then be calculated as well as the A/S ratio. Finally, the ratio was related to the separation efficiency to determine its effects on the performance of the process.

4.2.3.2 Induced air flotation (IAF) process

The procedure of the emulsion separation by IAF was similar to that of DAF. With the addition of coagulant, the process was denoted as the modified induced air flotation (MIAF). The kinetic study was carried out first in a batch operation with the air flow rates (Q_g) of 0.3 – 2.0 L/min. The effluent was sampled and analyzed until the efficiency was stable, which was the optimal operating time.

The continuous experiments were then performed by introducing the 1 g/L cutting oil emulsion in the flotation tank with the flow rates (Q_w) of 0.5 – 1.5 L/min and varied air flow rates. The sample collected at the optimal time and analyzed for the oil concentration. Finally, the efficiency can be determined from Equation 4.1.

- Effects of A/S ratio in IAF process

Effects of the A/S ratio was also investigated in the IAF. In this case, the emulsion concentration was fixed at 1 g/L but the air flow rates were varied resulting in different A/S ratios.

4.2.4 Effects of hydrodynamic parameters

The hydrodynamics parameters considered in this work were the bubble hydrodynamic parameters and mixing as follow.

4.2.4.1 Bubble hydrodynamic parameters

4.2.4.1.1 Bubble rising velocity (U_b)

The bubble rising velocities were examined by using the image analysis technique. The terminal velocity of bubble was calculated from the time that bubbles used to move for the distance between two frames as expressed in Equation 4.6 (Painmanakul et al., 2005).

$$U_b = \frac{\Delta D}{t_{frame}} \quad (4.6)$$

where U_b is the bubble rising velocity

ΔD is the distance between two frames

t_{frame} is the acquisition time frame

4.2.4.1.2 Bubble diameter (d_b)

The methods for determining bubble diameter for the DAF and IAF were different due to the limitation of the camera used for recording. This high speed camera of 120 frames/s (Basler Inc.) was unable to capture bubbles in the case of DAF since their sizes were too small. Bubble sizes in DAF were evaluated from the terminal rising velocity (U_b) in quiescent fluid by recalling Equation 1.23.

$$0 = C_d \rho_f \frac{\pi d_i^2}{8} |\vec{U}_i| \vec{U}_i + (\rho_i - \rho_f) \frac{\pi d_i^3}{6} g \quad (1.23)$$

This equation can be rewritten for determining the bubble diameter (d_b) as in Equation 4.7.

$$d_b = \frac{3}{4} \frac{C_d \rho_f U_b^2}{g(\rho_f - \rho_b)} \quad (4.7)$$

The drag coefficient can be obtained by recalling Equation 1.41 (Mei et al., 1994).

$$C_d = \frac{16}{\text{Re}_p} \left(1 + \frac{\text{Re}_b}{8 + 0.5(\text{Re}_b + 3.315 \text{Re}_b^{0.5})} \right) \quad (1.41)$$

On the contrary, bubble size can be determined directly by recording at 120 frames/s in the case of IAF. The average bubble diameter ($d_{b,avg}$) is measured from 150 – 200 bubbles and calculated by Equation 4.8.

$$d_{b,avg} = \frac{\sum_{i=1}^N d_{b,i}}{N} \quad (4.8)$$

4.2.4.1.3 Bubble interfacial area (a)

The interfacial area (a , m^{-1}) of bubble is defined as the ratio between the total bubble surface area ($S_b = \pi d_b^2$, m^2) and the total volume of fluid in the flotation tank ($V_{Total} = AH_L + V_{air}$, m^3) as expressed in Equation 4.9 (Painmanakul et al., 2004). A and H_L are the cross-sectional of the column (m^2) and the height of fluid in the flotation column (m), respectively.

$$a = n_b \times \frac{S_b}{V_{total}} \quad (4.9)$$

where n_b is the number of bubbles in the system, which can be estimated from the ratio of total air volume (V_{air}) to the volume of a bubble (V_{bubble}) evaluated from the average bubble diameter. n_b can be determined as in Equation 4.10.

$$n_b = \frac{V_{air}}{V_{bubble}} = \frac{V_{air}}{\frac{\pi}{6} d_b^3} \quad (4.10)$$

By substituting Equation 4.10, Equation 4.9 can be rewritten as

$$a = \frac{V_{air}}{d_b} \times \frac{6}{AH_L + V_{air}} \quad (4.11)$$

4.2.4.2 Mixing

Effects of mixing in this work can be represented by mean of gradient velocity (G). This gradient was a result of both the bubble motion and the flow of fluid phase. Generally, the gradient velocity can be calculated as in Equation 4.12 where P and V are the power input and the total volume in the system, respectively.

$$G = \sqrt{\frac{P}{\mu_f V_{total}}} \quad (4.12)$$

4.2.4.2.1 Velocity gradient of bubbles (G_{bubble})

The power P imparted by a bubble can be evaluated from the drag force (F_{drag}) due to the motion of a bubble as expressed in Equation 4.13 where A is the projected area of a bubble ($\pi d_b^2 / 4$).

$$\begin{aligned}
 F_{drag} &= \frac{1}{2} \rho_f U_b^2 C_d A \\
 &= \frac{1}{8} \pi \rho_f d_b^2 U_b^2 C_d
 \end{aligned}
 \tag{4.13}$$

The power imparted due to the motions of n bubbles can be written as Equation 4.14.

$$\begin{aligned}
 P &= n_b (F_{drag} \times U_b) \\
 &= \frac{3}{4} \rho_f C_d V_{air} \frac{U_b^3}{d_b}
 \end{aligned}
 \tag{4.14}$$

Finally, the equation for determining the gradient velocity of bubble (G_{bubble}) can be expressed as

$$G_{bubble} = \sqrt{\frac{3}{4} C_d \frac{U_b^3}{d_b} \frac{\rho_f}{\mu_f} \frac{V_{air}}{V_{total}}}
 \tag{4.15}$$

Note that the drag coefficient (C_d) again can be estimated from Equation 1.41.

4.2.4.2.2 Velocity gradient of fluid (G_{fluid})

The G_{fluid} was assumed as the flow of fluid in a tube (Metcalf & Eddy, 2003).

$$G_{fluid} = \sqrt{\frac{\rho_f g Q H}{V_{total} \mu_f}}
 \tag{4.16}$$

where Q is the flow rate of the fluid phase (m^3/s)

V_{total} is the total volume of fluid (m^3)

H_{Darcy} is the pressure loss from Darcy's equation (m) obtained from Equation 4.17 where f is the friction coefficient of tube (rely on tube's surface and Reynolds number). L and D are the length and diameter of the tube, respectively. U is the fluid velocity.

$$H_{Darcy} = \frac{4fL}{D} \times \frac{U^2}{2g} \quad (4.17)$$

These a and G were stated as important parameters for controlling the IAF process for separation of oily emulsion according to Painmanakul et al. (2010). It was suggested that more bubble surface would be available at greater a resulting in higher contact probability between bubbles and aggregates. Likewise, higher G means greater mixing or turbulence in the system, which could facilitating the bubble-droplet contact. However, excess turbulence could result in the break-up of the bubbles-aggregates agglomerates. These values should be controlled to be in the optimal range to achieve the effective separation performance. Moreover, the a/G ratio was proposed and proclaimed as the key factor for optimizing the process operation. This concept was applied in this work by analyzing effects of a and G on the efficiency. The relation between the efficiency and the a/G ratio was also investigated.

4.2.3 Overflow rate (OFR)

Change of flow rates in the flotation processes resulted in the variation of the overflow rate (OFR). Since the same flotation cell was used in both DAF and IAF, the OFR was varied with the flow rates (Q) as expressed in Equation 4.18.

$$OFR = \frac{Q}{A} \quad (4.18)$$

The change of OFR in a function of Q can be exhibited in Figure 4.5. In this work, the applied flow rates provided the overflow rate in the range of 0.01 – 0.42 $\text{m}^3/(\text{m}^2 \cdot \text{min})$

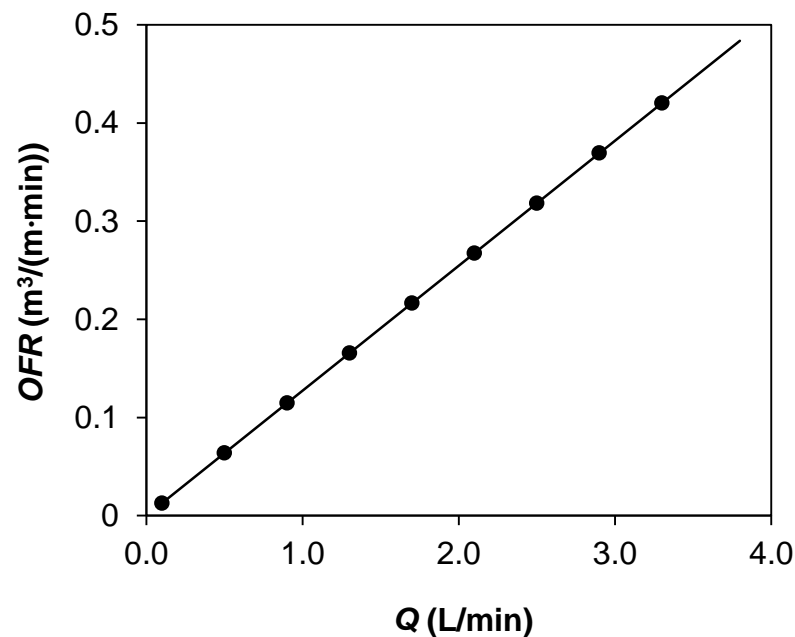


Figure 4.5 Variation of the overflow rate (OFR) with flow rates

4.2.4 Residence time distribution (RTD) study

The residence time distribution (RTD) is a tool that used for 2 major purposes including (1) to diagnose problems of operating reactors and (2) to predict effluent concentrations from reactor if a reaction is occurred in the reactor (Fogler, 2005). Typically, the ideal condition in any reactor can be divided into 2 different types, for example, plug flow reactor (PFR) and completely stirred tank reactor (CSTR). Ideally, all elements in PFR leave the reactor after spending exactly the same amount of time in reactor. The time that atoms have been in reactor is called a “residence time”. For CSTR, atoms partly leave the reactor with time lesser than the residence time, while some stay longer. However, the conditions in a reactor are quite different from the ideal one, such as non-uniform or short-circuit flows. For non-ideal condition, the flow pattern occurred in a reactor is an important information to describe the behavior

of a reactor. The “residence time distribution (RTD)” represents characteristics of mixing occurred in the reactor.

The RTD can be experimentally investigated by injecting an inert chemical, which is called a “tracer”, into the reactor and then measuring the outlet concentration as a function of time. Generally, two injection methods are used including (1) pulse input and (2) step input. The residence time distribution (RTD), denoted as $E(t)$, is the distribution of the exit time of the fluid. The $E(t)$ with a unit of time^{-1} are expressed in Equation 4.19.

$$E(t) = \frac{C(t)}{\int_0^{\infty} C(t) dt} \quad (4.19)$$

$$\text{Then, } \int_0^{\infty} E(t) dt = 1 \quad (4.20)$$

The fraction of the exit fluid with age between t and $t + dt$ is $E(t)dt$. Therefore, the fraction of fluid in the effluent with age less than t_1 is $\int_0^{t_1} E(t) dt$. From this concept, the different flow patterns could provide different $E(t)$, which can be used for determining the mean residence time (τ). The τ can be determined from Equation 4.21.

$$\tau = \frac{\int_0^{\infty} tE(t) dt}{\int_0^{\infty} E(t) dt} = \int_0^{\infty} tE(t) dt \quad (4.21)$$

Besides, $E(t)$ and τ can be used to calculate as a number of CSTR tanks (N) in series by a tank-in-series model (Levenspiel, 1999) as in Equation 4.22 (Essadki et al., 2011). This N can suggest the flow behavior of fluid in the system wheter it is the ideal CSTR ($N \rightarrow 0$) or PFR ($N \rightarrow \infty$).

$$E(t) = \left(\frac{N}{\tau} \right)^N \frac{t^{N-1}}{(N-1)!} \exp\left(-\frac{Nt}{\tau} \right) \quad (4.22)$$

In this work, a sodium chloride (NaCl) solution of 5 M concentration was used as a tracer in a pulse injection experiment. It was carried out only at the optimal condition for both the DAF and IAF. The signal was measured in term of conductivity at the inlet, contact zone, and outlet. The data was processed and fitted in the proposed model by MS Excel.

4.3 Results and discussions

4.3.1 Jar-test experiments

Effects of pH and alum dosage on the separation efficiency of the 1.0 g/L cutting oil emulsion are presented in Figure 4.6. The emulsion pH was adjusted in the range of 4 – 10 by the 0.2 M hydrochloric (HCl) and 0.1 M sodium hydroxide (NaCl) solutions. Note that the pH was decreased to the range of 6 – 7 after the addition of alum at every concentration. The separation can occur at the pH of 5 – 9 with the highest efficiency achieved at pH 7 with the alum dosage of 220 g/L (0.74 mM Al^{3+}). At this concentration, solid flocs can be observed at the water surface in contrast with the dosage of 180 mg/L (0.61 mM Al^{3+}) where only thin oil layer can be seen. The increase of the coagulant dosage did not provide the obvious effect on the separation. This finding was similar to the work of Cañizares et al. (2008) as the lubricant oil and soluble oil emulsions can be separated at the pH between 5 and 9. The sweep flocculation was supposed to be the destabilization mechanism as the solid $\text{Al}(\text{OH})_3$ can precipitate in this pH range (Duan and Gregory, 2003). Further study to clarify the destabilization mechanism was conducted later.

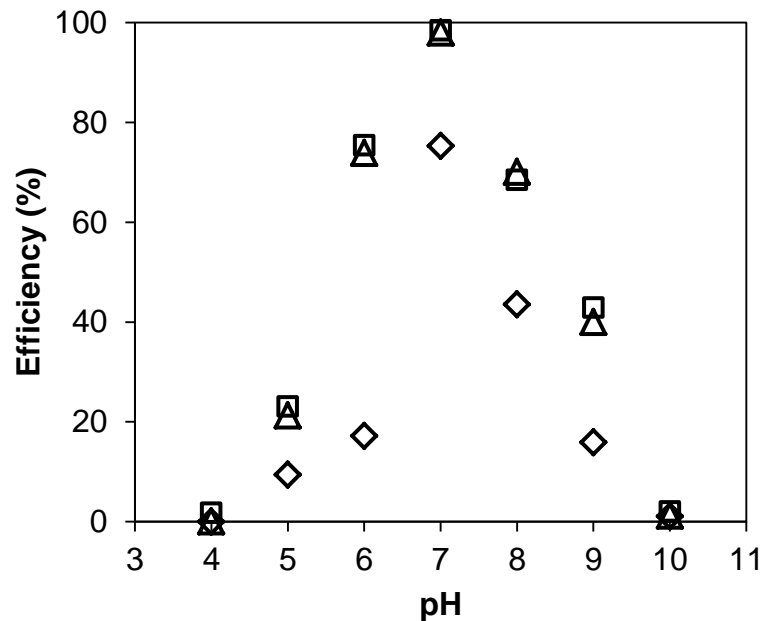


Figure 4.6 Efficiencies of the coagulation process at varied pH for 180 mg/L (◇), 220 mg/L(□), and 260 mg/L (△)

Effects of oil concentration on the required alum dosage at pH of 7 are exhibited in Figure 4.6. It can be seen that the coagulant process can effectively treat the emulsion with the highest efficiencies of more than 98% for every oil concentration with different alum dosages. The optimal dosage, which was defined as the minimum concentration of the coagulant that can provide the highest efficiency, was increased with the oil concentration. This can be explained by the fact that the increase of oil concentration resulted in the increment of oil droplets number; thus, higher Al^{3+} dosage was required for the destabilization. The increases of the coagulant dosage exceed the optimal value had no effects on the efficiency corresponded to the result in Figure 4.7.

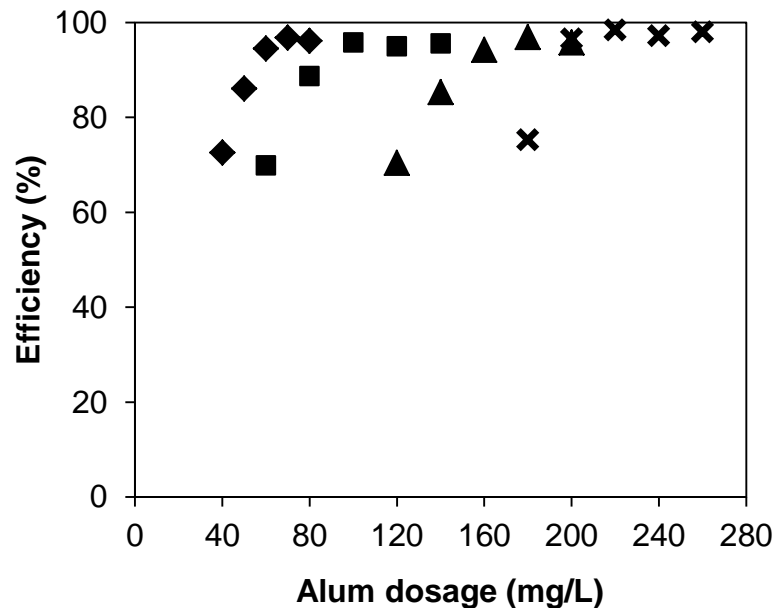


Figure 4.7 Efficiencies of the coagulation with varied alum dosages at different oil concentrations (◆) 0.25 g/L, (■) 0.5 mg/L, (▲) 0.75 mg/L, and (×) 1 mg/L

Therefore, it can be inferred that the alum concentration of 220 mg/L at pH 7 was the optimum condition for treating of the 1 g/L cutting oil emulsion in the coagulation process. This condition was then applied in flotation experiments as presented in the following section.

4.3.2 Bubble size and contamination level

This part dealt with the bubble size, which is an important factor in flotation used for classifying the flotation into DAF and IAF. Moreover, the bubble size can also affirm that the designed process can be categorized as the DAF that can generate bubbles in the sizes of 30 – 70 μm .

4.3.2.1 Bubbles in IAF

Bubble diameters (d_b) and rising velocities (U_b) directly measured at different air flow rates are shown in Figure 4.8. The measured values and the calculated parameters are shown in Table 4.2.

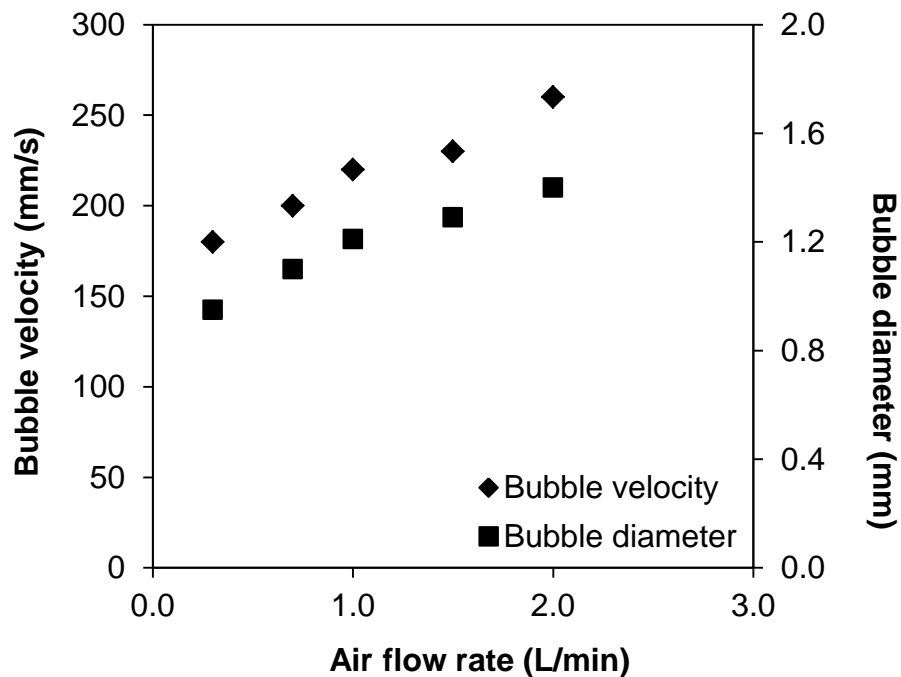


Figure 4.8 Bubble velocity and diameter in a function of air flow rate in IAF

As can be seen, bubble sizes as well as their velocities were increased with air flow rates. This trend was also observed in the works of Loubière and Hébrard (2003) and Painmanakul et al. (2010). By applying Equation 1.33, Weber number (We_b) can be calculated. It indicated that bubbles were spherical except at the air flow rate of 2 L/min where Weber number was higher than 1. The ellipsoidal bubble was expected in this case. The bubble Reynolds number (Re_b) was in the range of 170 – 363, which were in the potential flow condition.

Table 4.2 Measured values and calculated parameters of bubbles in IAF

Air flow rate (L/min)	d_b (mm)	U_b (mm/s)	We_b	Re_b	C_d
0.3	0.95	180	0.42	170	0.38
0.7	1.10	200	0.60	219	0.36
1.0	1.21	220	0.80	265	0.33
1.5	1.29	230	0.94	296	0.32
2.0	1.40	260	1.30	363	0.27

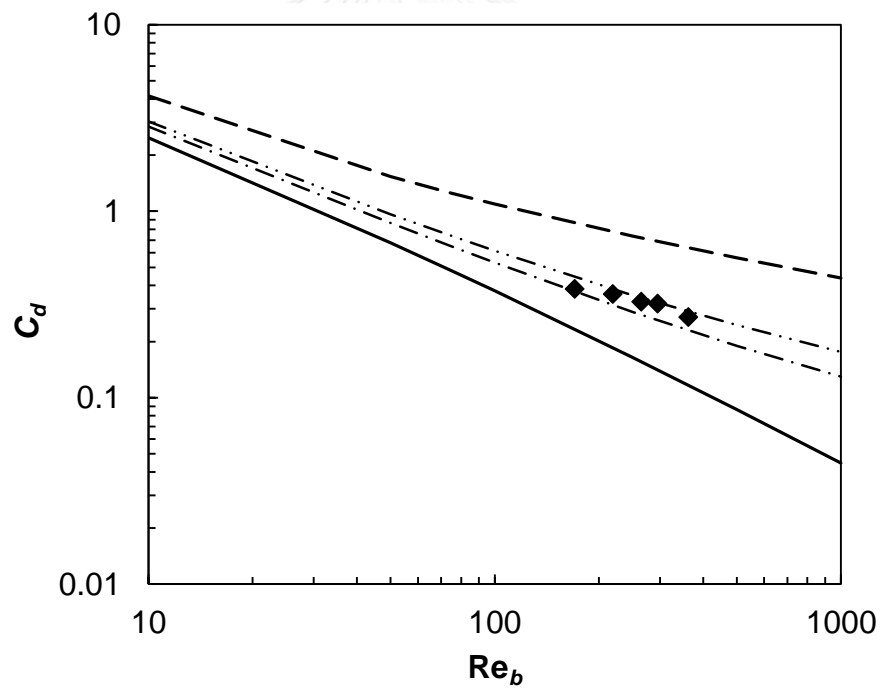


Figure 4.9 Drag coefficient in a function of bubble Reynolds number,
 ◆ : experimental results, -- : fully contaminated bubble, — : clean bubble,
 - · - : $\theta_{\text{cap}} = 130^\circ$, and - · · - : $\theta_{\text{cap}} = 120^\circ$

Moreover, the movement of bubbles can be affected by impurities in water or in the column. The contamination levels of bubbles, therefore, have to be investigated.

One approach to determine the contamination level is to compare the experimental C_d vs Re_b points with the function $C_d = f(Re_b)$ curves at varied cap angle (θ_{cap}) as in Figure 4.9. The experimental C_d was calculated from Equation 1.41 (Mei et al. 1994), whilst the curves can be obtained from Equation 1.42 with the θ_{cap} simulated by Sarrot (2006). It can be seen that the contamination level was between 120° to 130° . This cap angle range can be considered to be similar with the clean bubble according to Sarrot et al. (2007).

4.3.2.2 Bubbles in DAF

In this case, only bubble velocities can be experimentally determined since the cloud of tiny bubbles was generated in the process. The camera encountered the limitation to measure the bubble sizes directly. By assuming the same bubble contamination level with IAF (i.e. $\theta_{cap} = 120^\circ$) due to the fact that these two processes were similarly operated, the drag coefficients of bubbles can be evaluated from Equation 1.38 (Taylor and Acrivos 1964). Therefore, bubble diameters at varied pressure level can be calculated as displayed in Table 4.3.

Table 4.3 Bubble parameters for DAF process

Pressure level (bars)	U_b (mm/s)	C_d	d_b (μm)	Re_b	We_b
2	1.44	312	49.5	0.071	1.41×10^{-6}
3	1.44	312	49.5	0.071	1.41×10^{-6}
4	1.36	340	48.1	0.065	1.22×10^{-6}
5	1.43	316	49.3	0.070	1.38×10^{-6}
6	1.39	328	48.7	0.068	1.30×10^{-6}

From Table 4.3, bubble sizes and velocities in this case were almost identical at different pressure levels. Diminutive We_b suggested that bubbles were spherical in

the Stokes flow condition (small Reynolds number). Furthermore, this indicated that this designed DAF can produce micro bubbles as expected. Since the bubble size at each pressure level was quite similar, the 4 bars pressure was selected for applying in the emulsion separation experiment. This corresponded to the suggested appropriate pressure level for DAF of 4 – 5 bars (Rachu, 2005; Edzwald, 2010). In addition, this pressure level was applied in several studies (Zouboulis and Avranas, 2000; Al-Shamrani et al., 2002).

From this part, it can be seen that bubbles generated by these 2 processes were greatly different in their sizes. These dissimilarities might affect the separation performance, which could be found out in the following section.

4.3.3 Separation of cutting oil emulsion by flotation

The result from the flotation test without addition of the coagulant indicated that only flotation process cannot separate oil from the emulsion. The efficiencies below 3% were obtained from both DAF and IAF processes. As indicated by the zeta potential that oil-droplets contain negative charges as well as bubbles (Edzwald, 2010), the repulsive force between the same charges can hinder the droplet-bubble contact. As a result, the emulsion was unable to be separated in this condition. Therefore, the coagulant was required for effective separation. The optimal dose of alum from the jar-test experiment (220 mg/L) was then applied in the process. The results were as following.

4.3.3.1 DAF with coagulation (MDAF)

4.3.3.1.1 Batch operation

The efficiencies at different flow rates of pressurized water (Q_{pw}) in a function of time are exhibited in Figure 4.10. The final efficiency of nearly 95% was obtained from every flow rate. However, the system can reach the saturation state faster; or higher treatment rate in other words, at the higher Q_{pw} . The presence of more bubble number (n_b) at higher Q_{pw} might be responsible for this. The system was saturated after 30 minutes operation time in all cases.

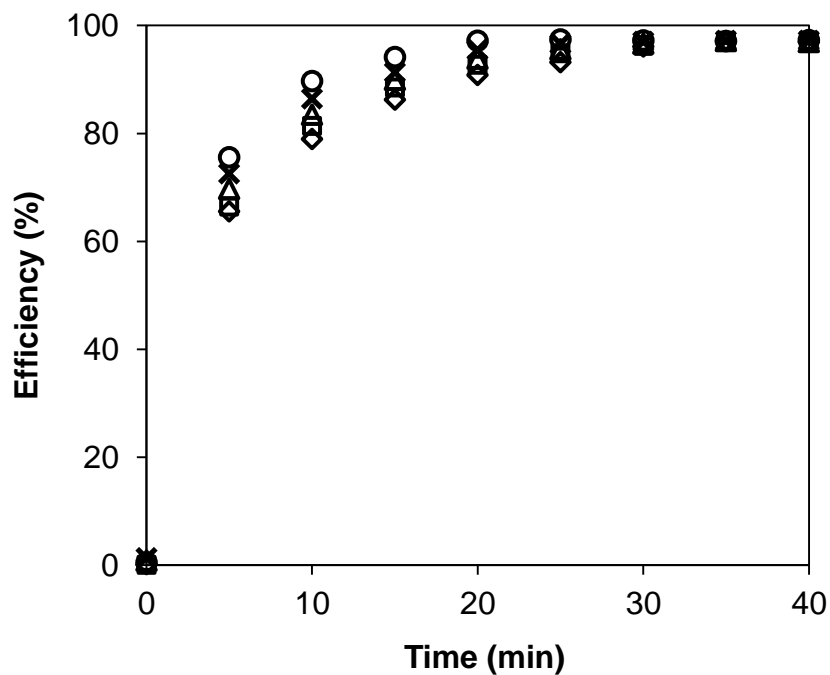


Figure 4.10 Efficiency in a function of time in the batch DAF process at varied Q_{pw} (\diamond) 0.17 L/min, (\square) 0.58 L/min (\triangle) 1.30 L/min, (\times) 2.12 L/min, and (\circ) 3.07 L/min

It can be suggested that the Q_{pw} in this range i.e. $Q_{pw} = 0.1 - 3.0$ L/min or $Q_g = 0.006 - 0.171$ L/min ($OFR = 0.01 - 0.42$ m³/(m²·min)) can be applied for effectively separating the emulsion. The process should be operated for at least 30 minutes. This condition was then applied in the continuous operation shown in the next section.

4.3.3.1.2 Continuous operation

Figure 4.11 exhibits the DAF efficiency in a function of the Q_{pw} at different emulsion flow rate (Q_w). The applied pressure level in the vessel was 4 bars. As can be seen, the efficiency was greatly varied with the flow rate of pressurized water. The increase of the emulsion and the pressurized water flow rates resulted in the reduction of the efficiency due to the shorter contact time. Moreover, the efficiency was decreased at the higher Q_{pw} since less oil-droplet existed in the flotation cell. The droplet-bubble contact probability might be decreased as well as the treatment efficiency. Note that the highest efficiency of 87% in this experiment can be achieved

at pressurized water and emulsion flow rates of 0.17 and 0.6 L/min ($OFR = 0.1 \text{ m}^3/(\text{m}^2 \cdot \text{min})$), respectively.

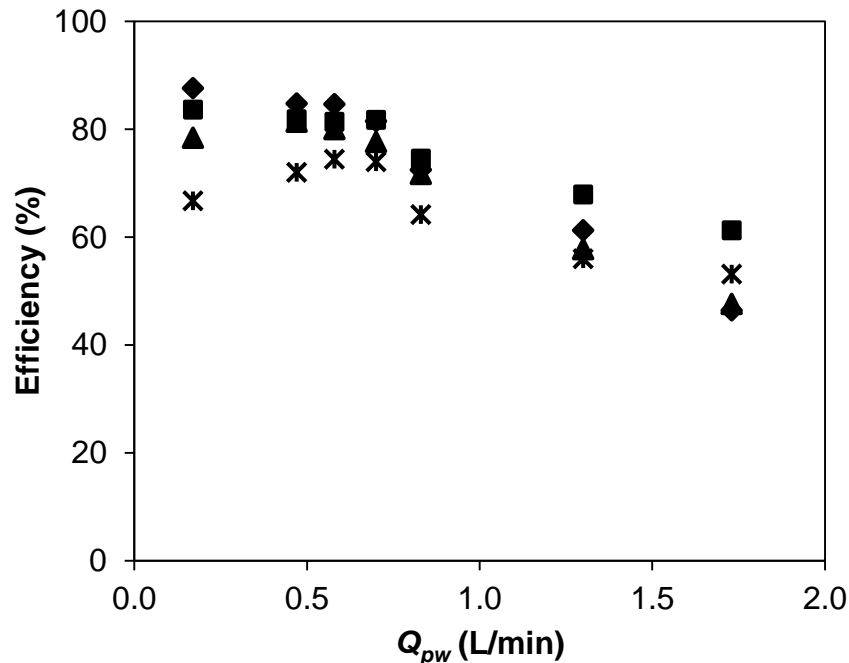


Figure 4.11 Effects of pressurized water flow rates at different emulsion flow rates in continuous DAF for (◆) 0.6 L/min, (■) 1.2 L/min (▲) 1.8 L/min, and (*) 3.0 L/min

However, it can be noticed that the emulsion can be separated even without the pressurized water ($Q_{pw} = 0 \text{ L/min}$). Since the emulsion and the coagulant were mixed in the static mixer before entering the column, bubbles in this case were only used for encouraging the flocculation and separating the aggregates. At the Q_w of 0.6 L/min, the efficiencies with and without the pressurized water were relatively close (i.e. 84% and 87%, respectively). Effects of bubbles were not obvious since flocs could be separated by themselves. On the contrary, presence of bubbles can enhance the efficiency at higher emulsion flow rate. Hence, the condition of 1.2 L/min and 0.17 L/min of emulsion and pressurized water flow rates ($OFR = 0.17 \text{ m}^3/(\text{m}^2 \cdot \text{min})$) was applied in the following study due to the fact that bubbles exhibits clearer effects.

4.3.3.1.3 Effects of the air-to-solid ratio (A/S)

In this case, the air-to-solid ratio was applied as the air-to-droplet ratio, which was the ratio between amounts of air and oil in the flotation column. Effects of the A/S ratio were determined by varying the initial oil concentration between 0.5 – 3.5 g/L. The relation between the A/S ratio and the efficiency is shown in Figure 4.12.

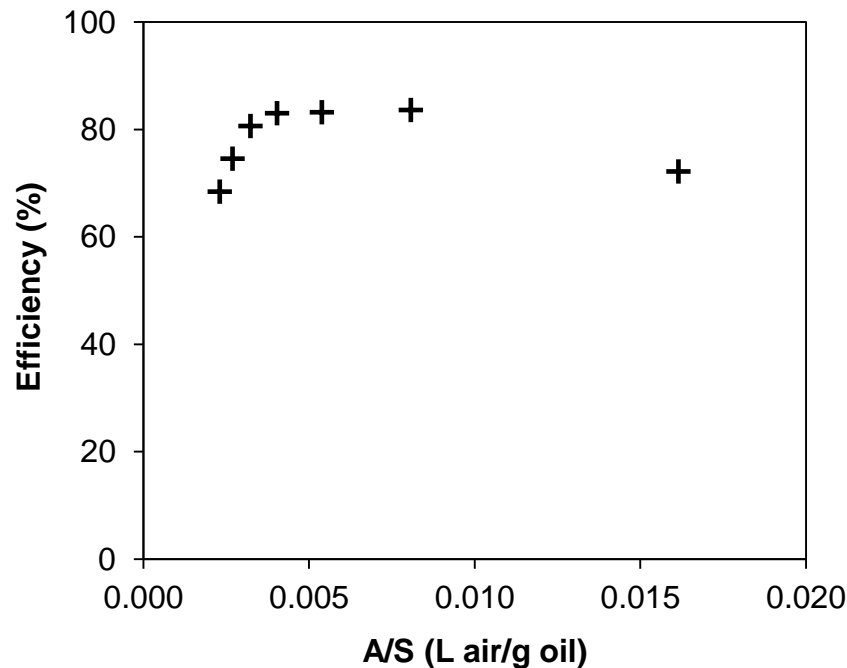


Figure 4.12 Relation between the A/S ratio and the treatment efficiency in DAF

It can be noticed that the high efficiency can be achieved at the certain A/S ratio range. The efficiency of approximately 80% was obtained from the A/S ratio of 0.004 – 0.008 L air/g oil or 0.005 – 0.01 g air/g oil. Apart from this range, the efficiency was lower due to different reasons. For the high A/S ratio (low oil concentration), less oil-droplet in the flotation column resulted in the low droplet-bubble contact and the low efficiency. In contrast, the lower efficiency at the low A/S ratio (high oil concentration) occurred as bubbles in the system were insufficient to separate higher amount of oil-droplets. It can be suggested that the A/S ratio should be considered for the effective DAF design and operation. These optimal A/S ratio was about in the suggested range for solid particles separation i.e. 0.005 – 0.060 g air/g solid (Metcalf & Eddy, 2004). Nevertheless, the ratio in this study was higher

than that obtained in the work of Bensadok et al. (2008) at 3.37×10^{-4} g-air/g-oil for the efficiency of 77%. The A/S ratio might depend on configuration of DAF system and types of oil. Only this A/S ratio cannot explain mechanisms of DAF. Effects of hydrodynamics had to be considered as displayed later.

4.3.3.2 IAF with coagulation (MIAF)

4.3.3.2.1 Batch operation

The separation efficiency nearly 80% can be achieved from every air flow rate (Q_g) as depicted in Figure 4.13. The highest efficiency of 87% was obtained from the Q_g of 2.0 l/min. In all case, the process reached the steady condition after 30 minutes operation. The treatment rate was increased with the Q_g . As these air flow rates can efficient separate the cutting oil emulsion, they were then applied in the continuous study of the IAF process.

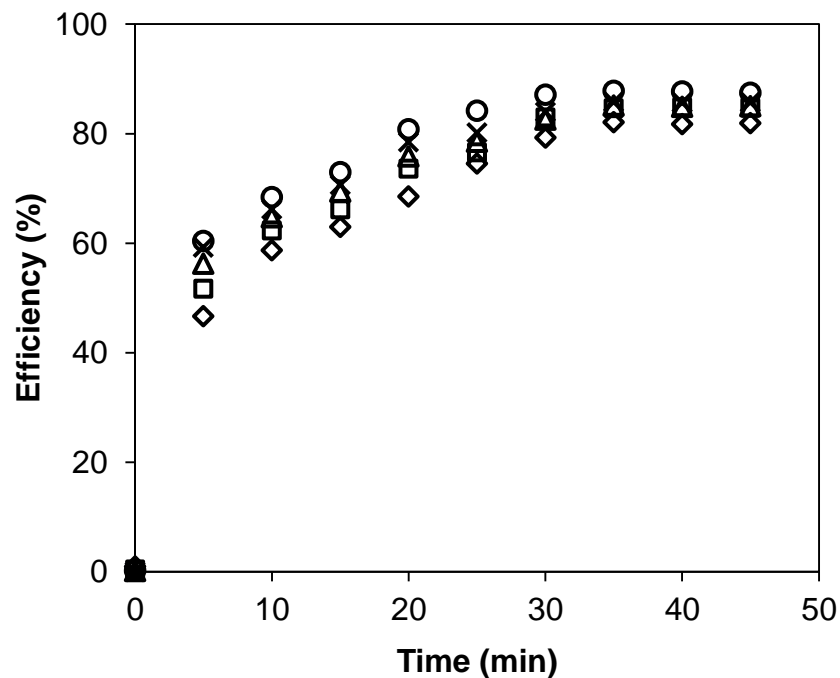


Figure 4.13 Efficiency of the batch IAF process as a function of time for varied Q_g (◇) 0.3 L/min, (□) 0.5 L/min (△) 0.7 L/min, (×) 1.0 L/min, and (○) 2.0 L/min

4.3.3.2.2 Continuous operation

Figure 4.14 shows efficiencies of IAF with effects of Q_g and the emulsion flow rate (Q_w). The increase of Q_w tended to decrease the efficiency due to the shorter contact time. On the contrary, the efficiency was slightly affected by the increase of Q_g in the studied range. The highest efficiency of 87% was obtained at the Q_g and Q_w of 2.0 L/min and 0.75 L/min ($OFR = 0.10 \text{ m}^3/(\text{m}^2 \cdot \text{min})$), respectively.

In addition, without air injection, the emulsion was sparsely removed. This incident was contrast with that of DAF process since bubbles in this case played a role in coagulation, flocculation, and flotation due to the fact that the coagulant was injected to mix with the emulsion in the column without passing through a static mixer. A good mixing between coagulants and oil-droplets cannot be fulfilled without bubbles due to the inadequate turbulence.

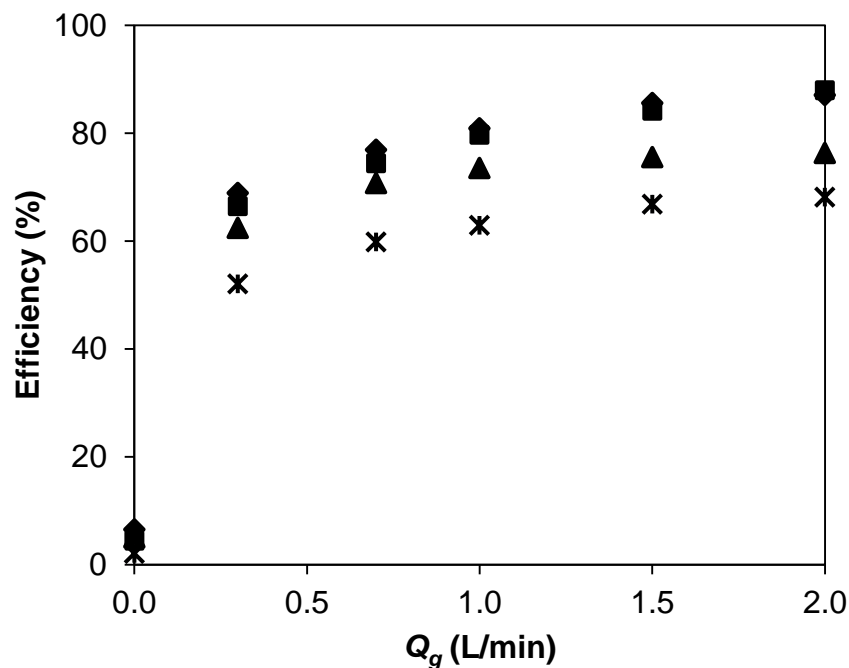


Figure 4.14 Efficiencies at varied air flow rates in the continuous IAF with different Q_w (◆) 0.5 L/min, (■) 0.7 L/min (▲) 1.0 L/min, and (*) 2.0 L/min

4.3.3.2.3 Effects of A/S ratio on IAF

Figure 4.15 exhibits effects of oil concentration via the A/S ratio on the efficiency. It can be seen that the efficiency was increased with the A/S ratio in the

range of 2.5 – 4 L air/g oil, and then became roughly constant at the higher value. This could indicate that the increase of air flow rate beyond this value would not enhance the efficiency. Besides, this was different from the DAF case since bubbles in the IAF were introduced by directly injecting air into the emulsion. The increase in the number of bubbles did not decrease the population density of oil-droplets in the system. The droplet-bubble contact probability was nearly unchanged. In this work, the amount required air was threefold of the oil amount presented in the flotation column.

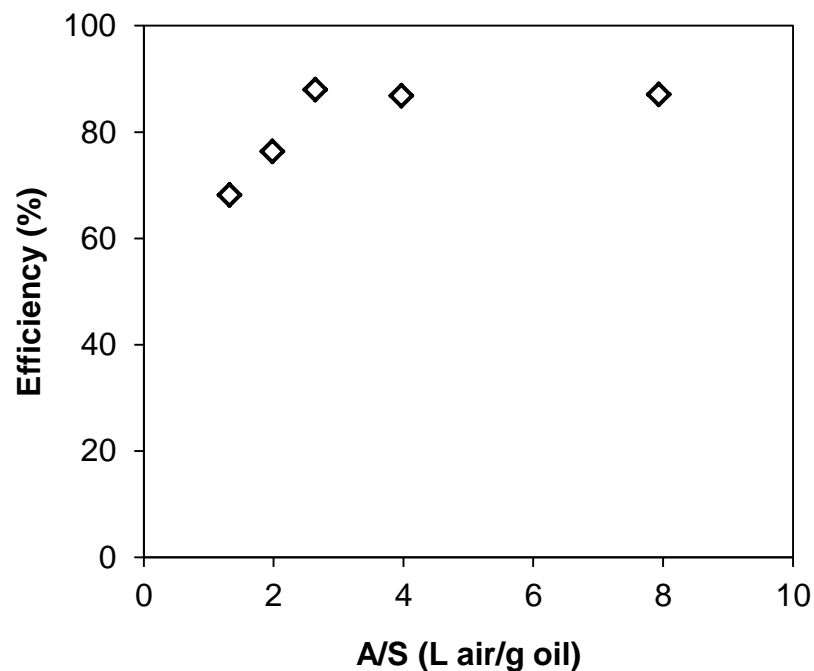


Figure 4.15 Effects of A/S ratio on the IAF efficiency

At this point, the required air amount (or air flow rate) can be roughly estimated. However, only the amount of air cannot describe effects on the efficiency. The impact of hydrodynamic on the IAF process was then examined as mentioned in the following part.

4.3.3.3 Summary

It was found that flotation can separate the cutting oil emulsion when the coagulant ($\text{Al}_2(\text{SO}_4)_3$) was added with the highest efficiency of around 85% for the continuous operation. No difference was noticed from DAF and IAF suggesting that might not be a key factor affecting the separation. This will be further investigated in the following part.

It was worth noting that the efficiency obtained in this work was slightly lower than the application of flotation for separating other types of oil emulsion, for example, 95% for n-octane emulsion by DAF (Zouboulis and Avranas, 2000), 99% for paraffinic process oil by IAF (Al-Shamrani et al., 2002), and 90% for cutting oil emulsion by DAF (Bensadok et al., 2007). This difference could be a result of dissimilar properties of oil used to form emulsion and operating mode.

Several researches on treatment of this cutting oil (Castrol Cooledge BI) by different techniques had been conducted. The highest efficiency of 99% can be achieved by the ultrafiltration membrane (Khiewpuckdee, 2012). However, the drawbacks on membrane clogging and high operating cost have to be taken into account. Electrocoagulation and Electro Fenton were also used for disposing this cutting oil. The efficiency of 99% (Rojvilavan, 2012) was obtained but the chemical consumption and chemical remained in the treated water needed to be considered. It should be noted that these efficiencies were found in the batch operation. On the contrary, the efficiency of 85%, which was similar to the result in this work can be found from the continuous electro-coagulation/flotation (Prommajun, 2012). In this regard, the application of flotation of separating was still interesting since it can be operated continuously with the possibility for oil recovering.

In the following section, effects of parameters that can affect the separation performance of the cutting oil emulsion by flotation were investigated and discussed.

4.3.4 Effects of hydrodynamic parameters

4.3.4.1 Dissolved air flotation

4.3.4.1.1 Bubble interfacial area (a)

The surface area of bubble was estimated by assuming that bubbles contained the uniform size equaled to the average bubble diameter of 0.036 mm. As expected, the a was increased with the flow rate of pressurized water (Q_{pw}) as illustrated in Figure 4.16.

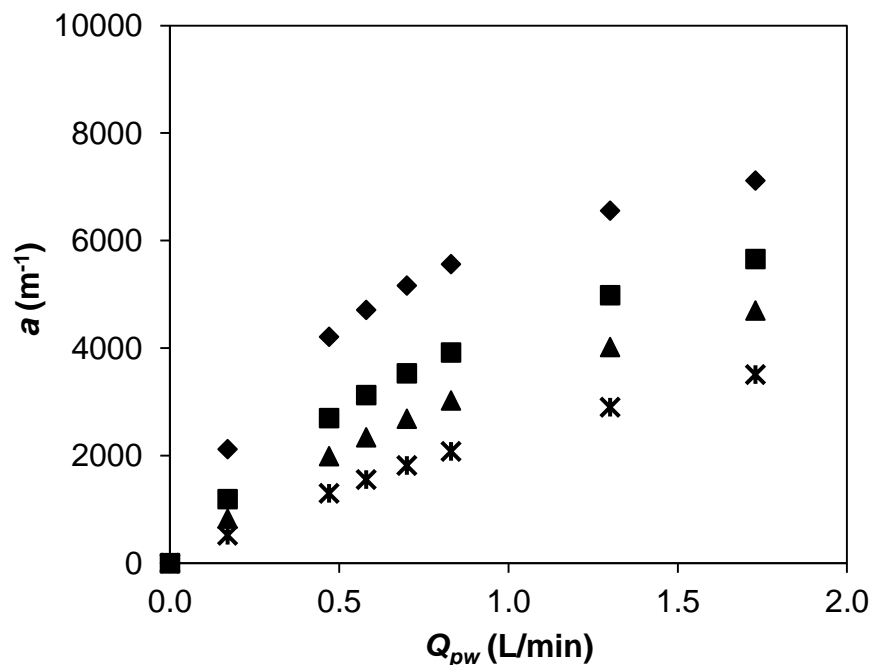


Figure 4.16 Interfacial area of bubbles vs. Q_{pw} in DAF at different Q_w in DAF (◆) 0.6 L/min, (■) 1.2 L/min (▲) 1.8 L/min, and (✱) 3.0 L/min

However, it can be seen that the increase of a at higher Q_{pw} resulted in lower efficiency contrasting to expectancy that presence of more bubble surface should provide higher separation efficiency. Other effects could be contributed to this emulsion separation such as mixing. It should be noted that the highest efficiency was obtained at the a of approximately $2000\ m^{-1}$.

4.3.4.1.2 Gradient velocity (G)

Figure 4.17 displays the velocity gradient in a function of the pressurized water flow rate. From the calculation, G was a summation of gradient from bubble motion and flow of fluid. Therefore, G was increased with Q_{pw} as more bubbles were introduced in the system providing more turbulent condition. However, the total gradients ($5 - 20 \text{ s}^{-1}$) were greatly lower than the value suggested for the coagulation process with a hydrolyzing metal coagulant in the range of $1200 - 2500 \text{ s}^{-1}$ (Bratby, 2006). This indicated the requirement of the static mixer in the case of DAF to facilitate a good mixing between the emulsion and the coagulant. Though, the efficiency was lowered when G was increased even its value was still lower than the recommended range of $50 - 100 \text{ s}^{-1}$ for appropriate contact in the flotation process (Metcalf & Eddy et al., 2004). As aforementioned, too high gradient velocity could provide drawbacks on the contact of bubbles-aggregates. The appropriate G providing the highest separation efficiency was around 10 s^{-1} .

According to these a and G values, the effective separation can occur only in a certain range. The ratio of a to G was proposed and then related with the efficiency.

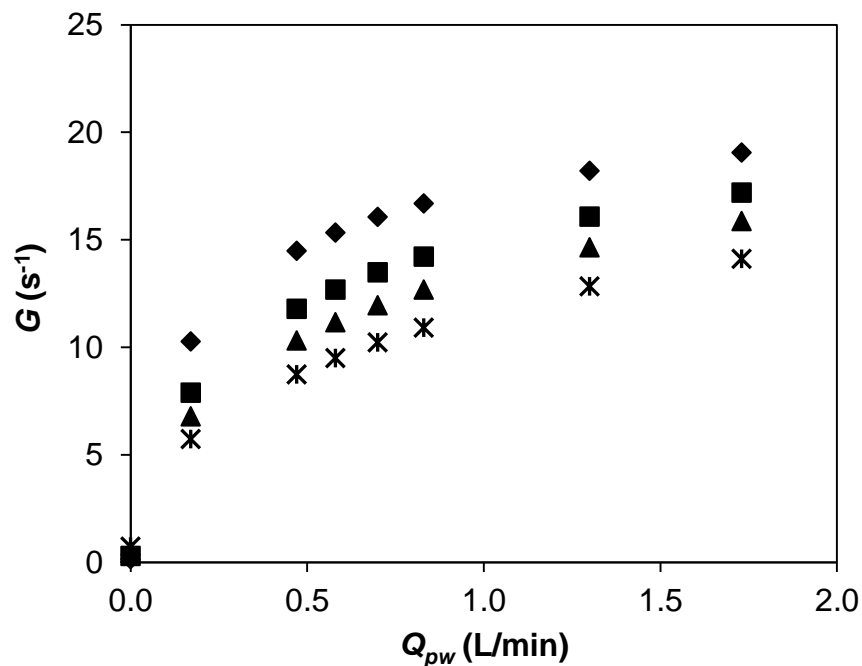


Figure 4.17 Velocity gradients (G) at different Q_{pw} for varied Q_w in DAF (◆) 0.6 L/min, (■) 1.2 L/min (▲) 1.8 L/min, and (✱) 3.0 L/min

4.3.3.1.3 a/G ratio

In this part, the a/G ratio defined as the proportion between the bubble interfacial area and the gradient velocity was proposed. It was expected that a good efficiency can be acquired at a certain range of this a/G ratio. Low a/G ratio implied to the condition of small bubble interfacial area with large mixing. In contrast, larger interfacial area and less turbulence would exist at high a/G .

The a/G ratio in a function of Q_{pw} for the range where the efficiency was increased and quite constant is displayed in Figure 4.18. The a/G was increased with Q_{pw} in this range at which the optimal value giving the highest efficiency was found at 200 – 300 s/m. The relation between the efficiency and the a/G was constructed as shown in Figure 4.19. Parameters from the linear fitting ($Efficiency (\%) = m \cdot (a/G) + c$) are summarized in Table 4.4. A good correspondence can be found with the correlation coefficient (R^2) higher than 0.84, but with different slope (m) and Y-axis interception (c).

However, both m and c were found to have a linear relationship with Q_w as expressed in Equations 4.23 and 4.24, respectively. This could be explain by the fact that both collision and attachment of bubble-particle required a sufficient contact time to occur. The contact time in this system was mainly governed by the flow rate of the emulsion (Q_w). Hence, it should be taken into account as an impacting factor for the flotation efficiency.

$$m = 0.064 \cdot Q_w \quad (4.23)$$

$$c = -13.4 \cdot Q_w + 82.7 \quad (4.24)$$

Finally, the treatment efficiency in the functions of a/G ratio and Q_w can be written as in Equation 4.25.

$$Efficiency (\%) = (0.064 \cdot a/G - 13.4) \cdot Q_w + 82.7 \quad (4.25)$$

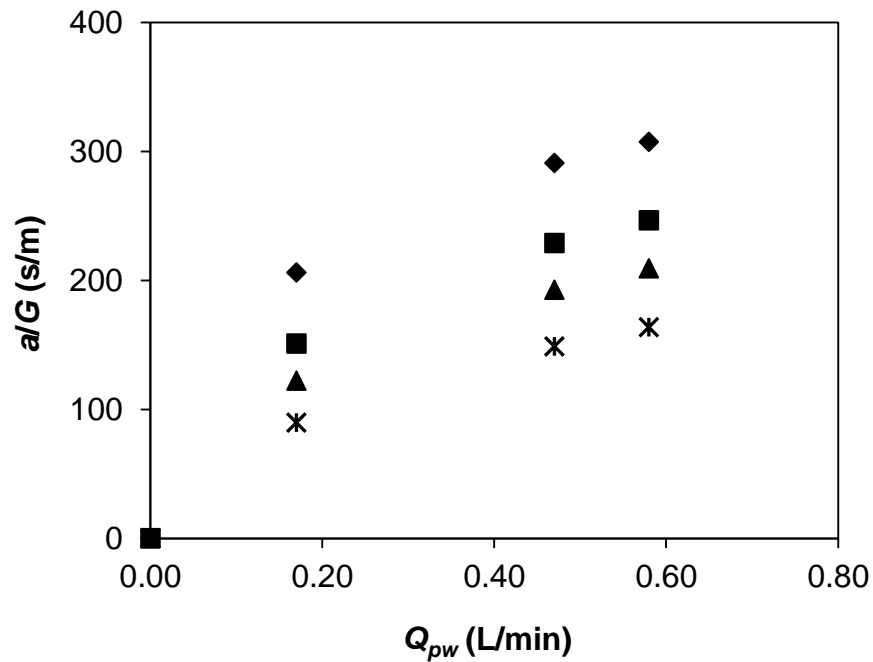


Figure 4.18 a/G ratio vs. pressurized water flow rate at varied Q_w in DAF
 (◆) 0.6 L/min, (■) 1.2 L/min (▲) 1.8 L/min, and (*) 3.0 L/min

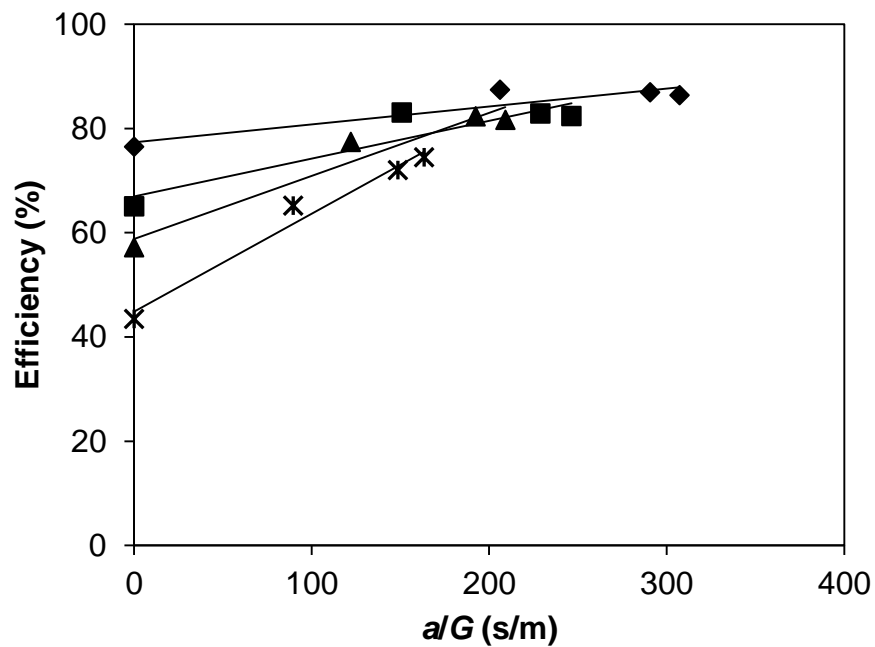
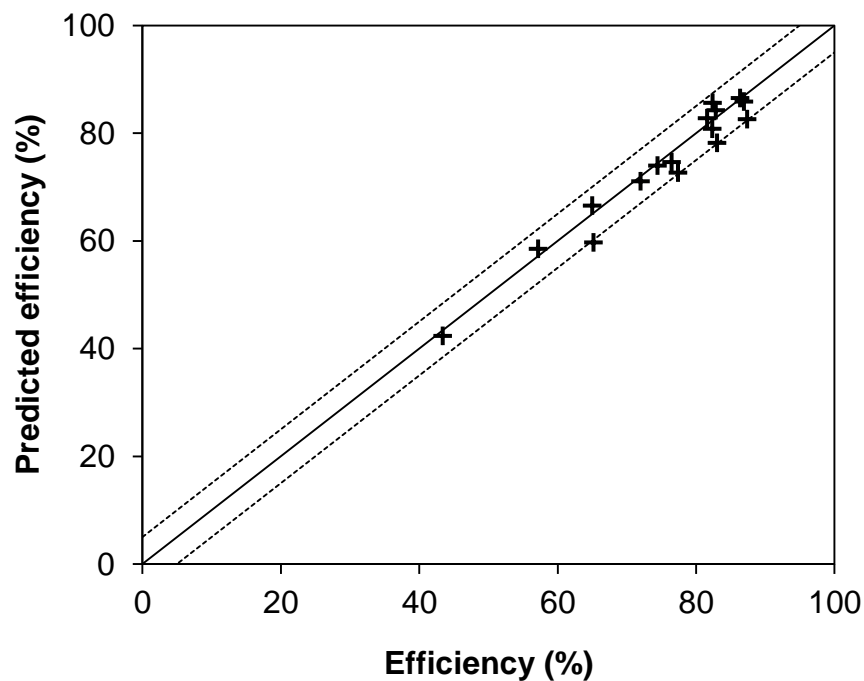


Figure 4.19 Relation between the separation efficiency and the a/G ratio in DAF

Table 4.4 Parameters in linear relation between the efficiency and a/G ratio

Q_w (L/min)	R^2	Slope (m)	Y-axis interception (c)
0.6	0.85	0.03	76.4
1.2	0.84	0.07	65.0
1.8	0.94	0.12	57.2
3.0	0.97	0.19	43.4

Figure 4.20 Comparison of calculated and experimental efficiencies in $\pm 5\%$

The comparison between the experimental and calculated efficiencies from Equation 4.25 is exhibited in Figure 4.20. The calculated results were slightly lower than those obtained from the experiment with the 5% discrepancy range. This emphasized effects of the a/G ratio and Q_w on the treatment efficiency. It should be noted that Q_w play an important role in the flotation due to the fact that it can affect the contact time in the flotation cell. Higher Q_w resulted in shorter contact time. A good separation performance could be promoted by facilitating the bubbles-aggregates contact at optimal a/G and sufficient contact time at appropriate Q_w .

4.3.4.2 Induced air flotation

4.3.4.2.1 Bubble interfacial area (a)

Change of bubble sizes with air flow rates (Q_g) is presented in Figure 4.21. No clear difference of the bubble interfacial area can be observed at varied Q_w ; thus, only the a at Q_w of 0.7 L/min is shown. It can be seen that a was slightly increased when Q_g was raised due to the fact that bubble size were enlarged producing less surface area per bubble. Since n_b was slightly enhanced with Q_g , the overall bubble surface was sparsely increased. Note that the bubble interfacial area in this case was much less than that of DAF as the produced bubbles were larger in sizes.

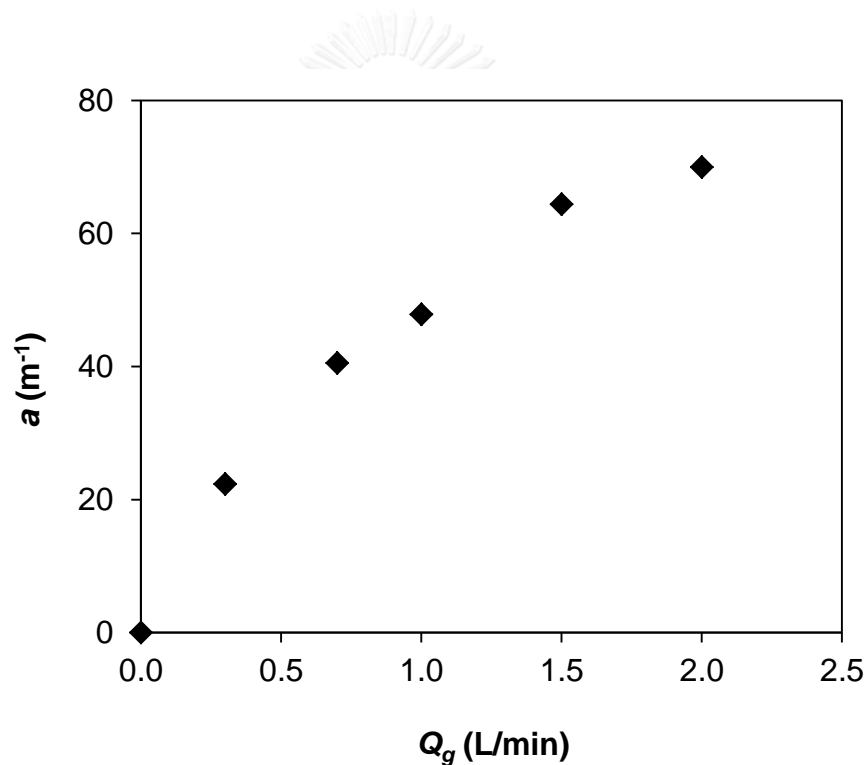


Figure 4.21 Interfacial area of bubbles in IAF at different Q_g .

4.3.4.2.2 Gradient velocity (G)

In contrast with the DAF, the gradient velocity in IAF was solely a result of bubbly flow in the column with higher value since the motion of larger bubbles can cause the turbulence in the flotation cell. Effects of Q_w on the gradient velocity cannot be seen. Consequently, G were increased with the air flow rates as displayed in Figure

4.22. These G were largely higher than in the case of DAF, but they were still lower than the range for the coagulation with metal salts as aforementioned. However, it could still be used for mixing of emulsion and coagulant.

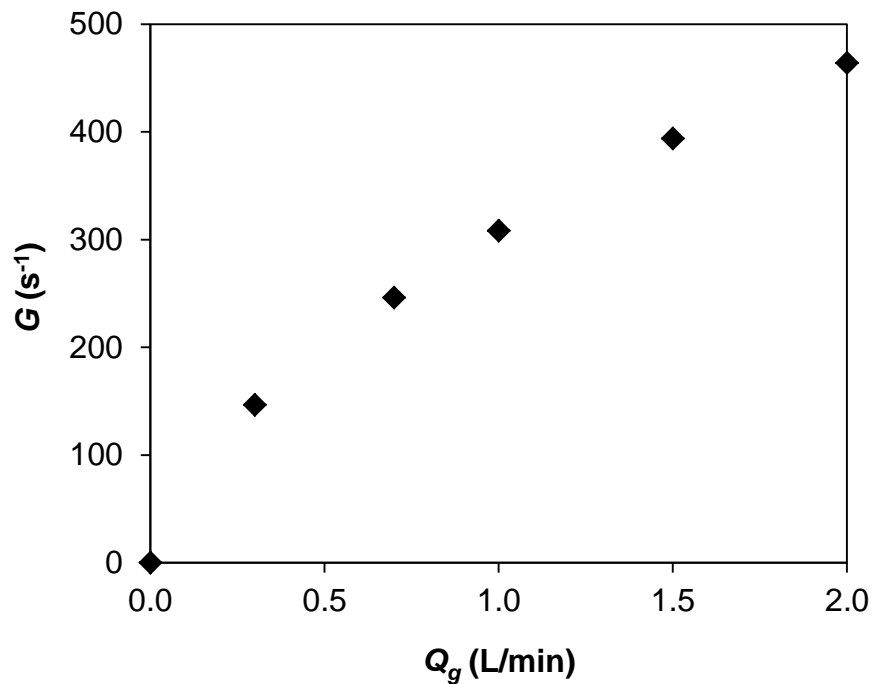


Figure 4.22 Velocity gradients (G) at varied Q_w in IAF

4.3.4.2.3 a/G ratio

Since the variations of a and G with Q_g were similar, the a/G ratio could be unchanged with the increase of Q_g . It can be seen in Figure 4.23 that the ratios were quite constant in this studied Q_g range as expected. Therefore, it would be useless to construct the relation between the a/G ratio and the efficiency. It could be suggested the range of the Q_g applied in this work might be too narrow. This can be proved by the results in Figures 4.13 and 4.14 that the increase of the air flow rate in this range had no impacts on the efficiency. Note that the a/G ratios in this study was much less than those obtained in the work of Painmanakul et al. (2010) for the separation of palm oil emulsion by IAF i.e. $a/G = 3.5 - 9$ s/m.

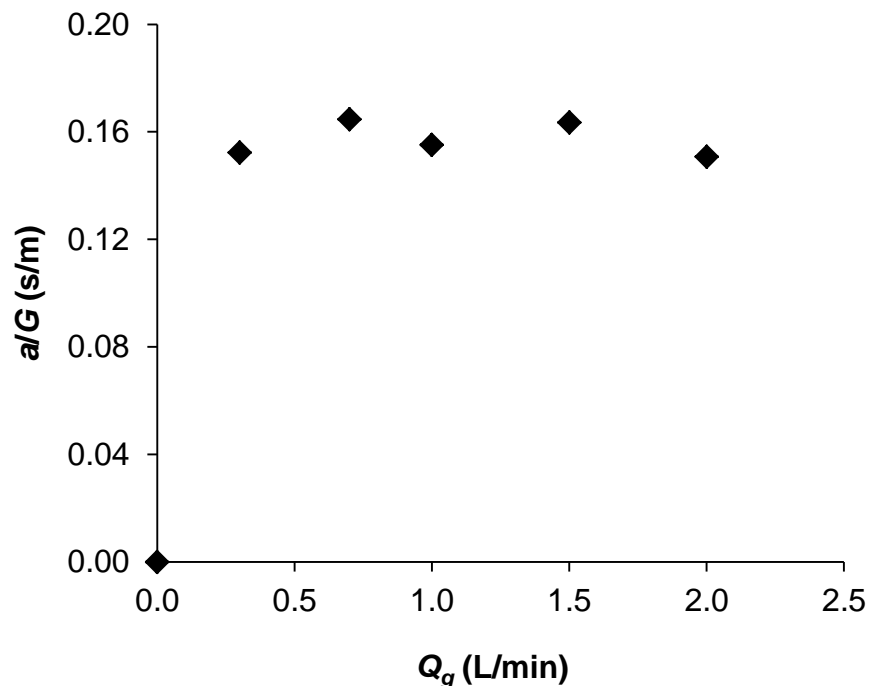


Figure 4.23 a/G ratios at varied air flow rates in IAF

4.3.5 Residence time distribution (RTD)

The study on the residence time distribution (RTD) was conducted in both DAF and IAF to analyze the behavior of flows in the flotation cell. Particular attention was paid on the flow types by the tank-in-series model and the residence time in the contact zone of the flotation tank.

4.3.5.1 Dissolved air flotation

The residence time distribution function ($E(t)$) with time of the flow in the DAF at the optimal flows condition ($Q_{pw} = 0.17$ L/min and $Q_w = 1.2$ L/min) is shown in Figure 4.24. The signal at the inlet is shown to prove that the tracer was introduced as a pulse injection. However, a spread of the signal can be seen as the tracer concentration was depleted after a minute. Using Equation 4.21, the tank number of CSTR in series of this inlet signal was 6 tanks indicating that the flow in the column tended to be a plug flow condition ($N > 6$) (Fogler, 2005). More spreading can be observed for the signal in the contact zone at which $N = 10$. The flow behavior would

be PFR suggesting that the concentration in the column was different at each height. This can be expected since the mixing in the flotation cell was quite low.

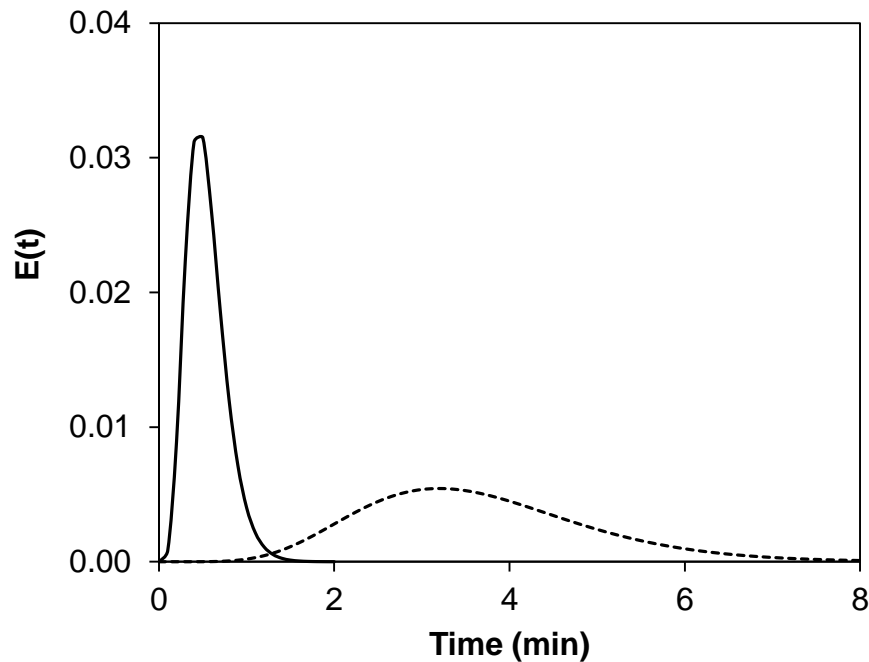


Figure 4.24 Residence time distribution as a function of time in DAF at (—) inlet and (---) contact zone of the flotation tank

Furthermore, the residence time (τ) was calculated from Equation 4.20. The inlet signal contained the residence time of 33 s affirming the spreading of the tracer. In the case of the contact zone, the residence time of 3 minutes 40 seconds was acquired. This τ was in accordance to the contact time recommended for separating particles of 2 – 4 minutes (Metcalf & Eddy, 2004).

4.3.5.2 Induced air flotation

In contrast with the DAF as exhibited in Figure 4.25, the distribution pattern of the inlet signal in IAF can be classified as the CSTR ($N = 1$). This can be explained by the effect of turbulence produced by bubbles resulting in the mixing of fluid in the flotation cell. The flow pattern in the contact zone still possessed the CSTR pattern

with the tank number of 4. This convinced the existence of well-mixed condition in the flotation cell of the IAF.

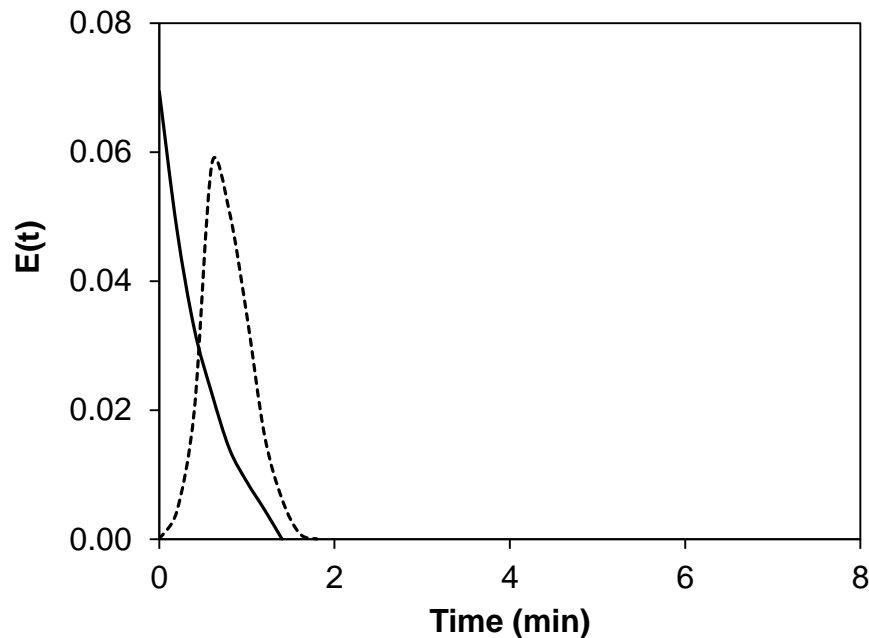


Figure 4.25 Residence time distribution with time of IAF at (—) inlet and (---) contact zone of the flotation tank

The residence time of the tracer at the inlet was also found at 33 s even the flow pattern was difference. However, τ of fluid in the contact zone was 51 s indicating that the emulsion lasted in the cell shorter than in the case of DAF. It can be suggested that the separation of the cutting oil emulsion by IAF only required a short time of aeration. This finding corresponded to the treatment of olive oil emulsion by IAF at which the aeration time of 40 – 50 s can provide the effective reduction of the emulsion's turbidity (Meysami and Kasaieian, 2005).

The results from this RTD study indicated that there was the difference of flow pattern and residence time between these two processes, i.e. DAF and IAF, even similar efficiencies can be achieved. It also reaffirmed effects of bubbles on the mixing condition in the flotation cell.

4.6 Conclusions

It was found from the results in this chapter that the cutting oil emulsion can be effectively separated with the highest efficiency of 85% by the continuous flotation processes, both DAF and IAF, coupling with chemical coagulation. The difference of bubble sizes seemed to have no effects on the separation. Likewise, the operating condition in this work provided a slight difference on the efficiency. The best separation in this work was obtained at the overflow rate (*OFR*) of $0.10 \text{ m}^3/(\text{m}^2 \cdot \text{min})$ in both DAF and IAF but at different air-to-oil ratio (*A/S*). The *A/S* ratio of the DAF ($0.004 - 0.008 \text{ L air/g oil}$) was much lower than that of the IAF one ($2.5 - 4.0 \text{ L air/g oil}$) due to the fact that bubbles in these two processes were differently generated.

The study on effects of hydrodynamic parameters in DAF indicated that the separation performance can be affected by the available bubble surface and mixing in the flotation cell. The sufficient contact time was also required for a good separation. Nevertheless, the relation between the efficiency and the *a/G* ratio cannot be constructed due to the limited operation range.

Finally, the residence time distribution (RTD) study presents the difference between these two processes in terms of the flow pattern and the residence time of the emulsion in the flotation cell. In the case of DAF, the pattern was likely to be a plug flow reactor (PFR) with the residence time of around 4 minutes. On the other hands, the fluid spent time in the flotation cell for only 50 seconds in the IAF with the flow pattern liked a completely stirred tank reactor (CSTR). This emphasized effects of the bubble size on the mixing within the flotation cell.

At this point, it can be suggested that the induced air flotation (IAF) should be selected for separating this cutting oil emulsion due to its effectiveness. Less power consumption, simplicity, and shorter contact time are main advantages of the IAF over the DAF with similar efficiency.

Apart of bubble effects in the separation, the destabilization of emulsion by coagulation also played a key role in the separation since it was found that the emulsion was unable to be separated without the formation of flocs. The

destabilization of this cutting oil emulsion by aluminium sulfate was therefore conducted to analyze effects of various parameters on the separation as well as the characteristics of formed flocs. The results were presented in the next chapter.



CHAPTER 5

DESTABILIZATION AND AGGREGATION OF CUTTING OIL

5.1 Introduction

Due to the high stability of the emulsion, the natural separation of oil droplets would be difficult. Although the flotation was applied, the surface charge of droplets could contribute to hinder the adhesion between droplets and bubbles resulting in inferior separation performance. The destabilization of oil droplets before flotation was necessary.

Destabilization is the process used for separating colloidal particles by allowing particles to form aggregates or flocs, which are large enough to be separated by settling or flotation. Coagulation and aggregation may for instance result from the decrease of the repulsive force between droplets or particles by screening the electrostatic interaction with the addition of salts. For oil droplets, the destabilization occurs due to coagulation and flocculation, but it can also involve a coalescence process. To perform destabilization of oily emulsion, three chemical groups are used, for instance, metal salts, acids, and synthetic polyelectrolytes (Bensadok et al., 2007). Among them, metal salts, e.g. Al(III) or Fe(III) salts, are often employed in the coagulation for water and wastewater treatment processes. Numerous factors were recognized to affect the coagulant performance, such as coagulant concentration, pH, and initial particle concentration as well as presence of some ions in water. Moreover, temperature can also play a role in the destabilization when flocs can be observed (Rios et al., 1998; Hempoonsert et al., 2010). Floc morphology can be changed with varied temperatures. For aluminium salts such as AlCl_3 or $\text{Al}_2(\text{SO}_4)_3$, it is well known that pH and coagulant concentration play a major role since they relate to speciation of aluminium and also destabilization mechanisms (Duan and Gregory, 2003). Numerous researches have been conducted by using aluminium ions, which were applied in forms of chemical coagulation with aluminium salts and electrocoagulation with aluminium electrodes, for destabilizing oily emulsion. Different mechanisms were used to describe the occurred destabilization depending on several factors that

governed the coagulant species. It was suggested that the formed species of coagulants is impacted by coagulant amount, pH and ionic strength of the solution, and concentration of organic compounds (Stephenson and Duff, 1996). The effective destabilization were obtained with the formation of insoluble Al^{3+} species, i.e. $\text{Al}(\text{OH})_3$. The proposed mechanisms acted by this species were adsorption of $\text{Al}(\text{OH})_3$ precipitates on droplets' surface (Bensadok et al., 2008), bridging flocculation (Cañizares et al., 2008), and charge neutralization (Al-Shamrani et al., 2002; Un et al., 2009).

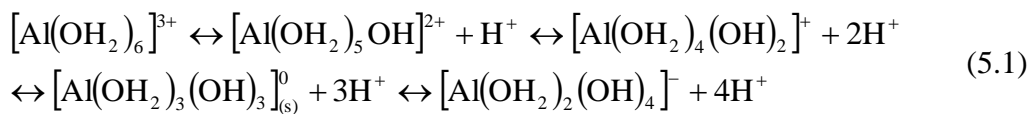
The chemical destabilization has been combined with other processes in order to improve the separation efficiency of oily emulsion. Since oil aggregates normally rise to the water surface due to its density, flotation have been coupled with the destabilization (Bensadok et al., 2007; Zouboulis and Avranas, 2000; Meysami and Kasaeian, 2005; Painmanakul et al., 2010) to improve and fasten the separation. In this case, the understanding on the destabilization mechanism is necessary since it can affect the separation performance by flotation. The difference in the mechanism could provide dissimilar properties of aggregates, which can affect the interaction between bubbles and aggregates (Al-Shamrani et al., 2002).

The following part deals with the investigation on the destabilization mechanisms of cutting oil emulsion by aluminium salt. The same coagulant, i.e. $\text{Al}_2(\text{SO}_4)_3$, as in the flotation experiment was applied. Particular attention was paid on effects of pH and coagulant concentration on the destabilization mechanisms, which can affect the aggregation properties. Floccs formed in the emulsion were also characterized for their chemical composition and crystalline structure.

5.2 Hydrolysis of $\text{Al}_2(\text{SO}_4)_3$

When compounds of aluminium (e.g. $\text{Al}_2(\text{SO}_4)_3$ or AlCl_3) is introduced to water, they can hydrolyze to give trivalent Al^{3+} ions that can react with water molecules. Since the aluminium ion has six coordination (Fratello et al., 1968), it can form the aluminium hexahydrate complex $[\text{Al}(\text{OH}_2)_6]^{3+}$ by bonding with water molecules (Gillberg et al., 2003). Indeed, the speciation of Al^{3+} in aqueous solution is

vastly diverse (Saukkoriipi, 2010). The consecutive proton transfers of aluminium hexahydrate was stated as in Equation 5.1 with the assumptions of (1) the dimeric, trimeric, and polynuclear hydrolysis products are presented in the system and (2) the hydrolysis of a free aluminium ion (Al^{3+}) is neglected (Ikeda et al., 2006). The reaction in Equation 5.1 can explain the decrease of pH when aluminium salts are added into water since protons (H^+) are obtained.



The important factor affecting the speciation of aluminium complexes in water is pH as illustrated in Figure 5.1.

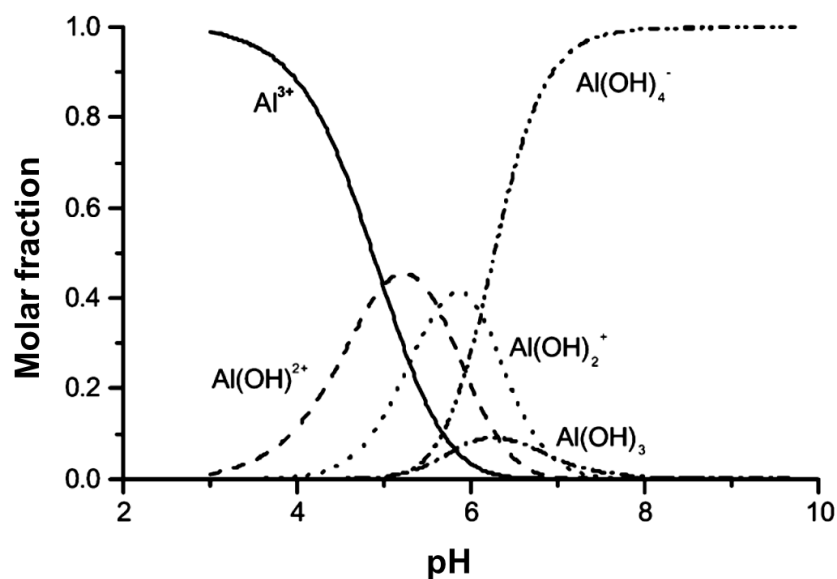


Figure 5.1 Speciation of hydrolyzed monomeric aluminium in water at equilibrium (Duan and Gregory, 2003)

Consider the monomeric Al^{3+} in different pH range, the dominant speciation in acidic pH range ($\text{pH} \leq 4$) is the cationic aluminium hexahydrate ($[\text{Al}(\text{OH}_2)_6]^{3+}$), in other words, a complex of aluminium ion (Al^{3+}) and water molecules. Cationic species also dominates at pH 5 and 6 in the forms of $[\text{Al}(\text{OH})]^{2+}$ and $[\text{Al}(\text{OH})_2]^+$,

respectively (Duan and Gregory, 2003). At the neutral pH range between 5 and 8, the solid aluminium trihydroxide ($\text{Al}(\text{OH})_{3(s)}$) can precipitate, which is also known as gibbsite and bayerite (Duan and Gregory, 2003). Moreover, this solid can lose a water molecule in some conditions resulting in the formation of a solid Boehmite ($\text{AlO}(\text{OH})$) (Brosset, 1952). Besides, the dominant aluminium species at basic pH range ($\text{pH} \geq 8$) is the anionic aluminium hydroxide or aluminate ($[\text{Al}(\text{OH})_4^-]$). Furthermore, it should be well aware that pH plays a role in the hydrolysis of polynuclear aluminium complexes as well (Thomas et al., 1991).

5.3 Destabilization experiments

As indicated in section 2.5.2, only pH adjustment was unable to separate the emulsion. The destabilization experiment the destabilization experiment was therefore conducted with the chemical coagulant, i.e. aluminium sulfate ($\text{Al}_2(\text{SO}_4)_3 \cdot 14\text{H}_2\text{O}$; Carl Roth GmbH + Co. KG, France). The pH of the emulsion was adjusted by hydrochloric acid (HCl) and sodium hydroxide (NaOH) solutions.

Destabilization experiments were carried out by a standard six paddle jar test apparatus (Floculateur 11196, Bioblock Scientific) with 1 L glass beakers. Rapid mixing (120 rpm) for 1 minutes followed by 30 minutes of slow mixing (30 rpm) were applied after the coagulant was added. According to the observation in the preliminary test, oil aggregates mostly rose to water surface due to the lighter density of oil. The treated emulsion was therefore taken from the bottom of beakers after 60 minutes decantation and then analyzed for turbidity, zeta potential, and aggregate size.

Moreover, aggregates were also observed. Small volume of coagulated emulsion (0.2 – 0.4 mL) was sampled for the microscopic observation with 40 times magnification (40X) on a glass slide. A bore-holed dropper was used to avoid the breakage of aggregates during the sampling. Aggregate were investigated under an optical microscope (Nikon Eclipse LV100 POL) installed with a camera (Nikon Digital Sight DS-2MBW) for capturing images.

5.3.1 Critical coagulation concentration (CCC) and aggregation kinetic

The optimal coagulant dosage was firstly determined by mean of the critical coagulation concentration (CCC) obtained from a kinetic study of the aggregation at the early stage of the destabilization. From the DLVO theory, colloidal particles begin to aggregate when the attractive and repulsive energies between particles were balanced by effects of electrolyte concentration. This concentration is called the critical coagulation concentration (CCC). In the optimal Al^{3+} concentration range, the stability ratio (W) of particle aggregation can be acquired as $W = \beta_{fast} / \beta'$. β' is the rate of the reaction-limited aggregation (RLA) regime, which could be slow due the fact that particles attachment rate is slower than the collision rate (Lin et al., 1990). In this regime, higher electrolyte concentration reduces the energy barrier between particles until the faster aggregation rate (β_{fast}) is achieved. Two particles can immediately aggregate after collision in this β_{fast} regime, which is called the diffusion-limited aggregation (DLA) regime. The rate in this case is controlled by the collision between particles by the Brownian diffusion (Elaissari and Pefferkorn, 1990) so it cannot be faster. The CCC can then be determined by the intersection between the extrapolations of the RLA and the DLA regimes, i.e. where W equals unity (Hsu and Liu, 1999). However, the measurement of droplet size changes is unable to provide the aggregation rate (β) directly, but it can indicate the initial rate (k). Therefore, the measurement can exhibit the W in term of ratio between the DLA and the RLA initial rates, in other words, k_{fast}/k' .

In this part, the kinetic in the early stage of the destabilization was investigated. The W values were determined by plotting the change of aggregate size with duration after coagulant adding. The fastest growth rate, i.e. steepest slope, was denoted as k_{fast} at which the aggregation is limited by diffusion. Whilst, growth rates at other Al^{3+} concentrations were classified in the reaction limited regime and stated as k' . Consequently, the W ratio was obtained from the k_{fast}/k' as mentioned above.

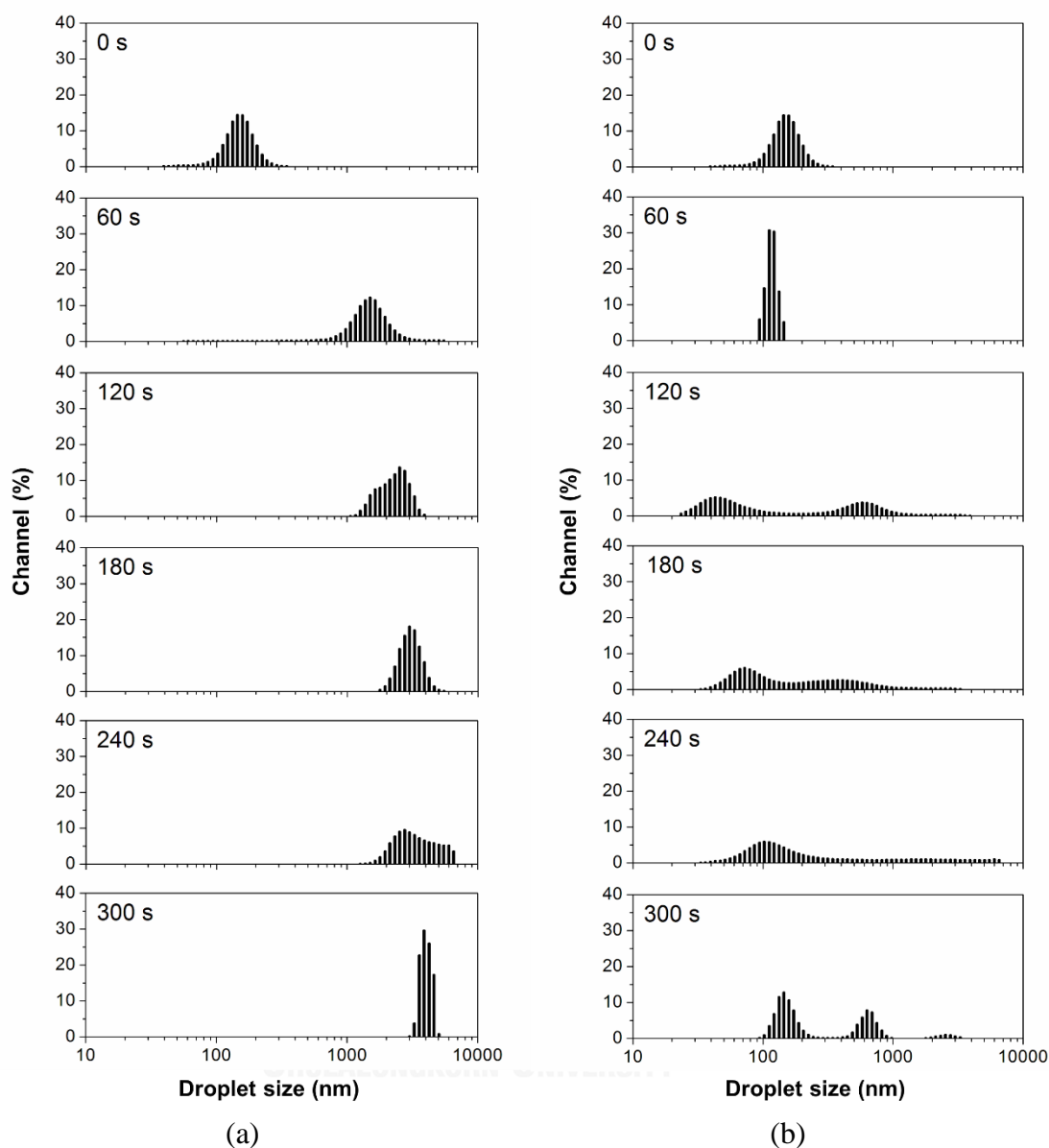


Figure 5.2 Droplet size distributions with time of the emulsion prepared from DI water for Al^{3+} concentrations of (a) 0.75 mM and (b) 1.0 mM

The kinetic of oil droplet aggregation was firstly determined for 1 g/L emulsion in deionized water with varied Al^{3+} concentrations at the pH of 7 as the largest droplet size and lowest zeta potential can be achieved without the coagulant addition in the previous study. The change of droplet size at every 30 seconds after adding the coagulant was measured by Dynamic Light Scattering (DLS) with the Nanotracs NPA250 (Microtrac Inc.) to consider the aggregation at the early stage of the destabilization. Note that the addition of Al^{3+} in the emulsion resulted in the

decrease of pH values to the range of 4.0 – 4.5 at every dosage due to the reactions of Al^{3+} as mentioned in section 5.1. The pH adjustment was needed. The Al^{3+} concentrations of 0.1 – 1.25 mM (30 – 371 mg/L aluminium sulfate) was applied. The growth of aggregate sizes was investigated as shown in Figure 5.2 for Al^{3+} concentrations of 0.75 and 1.0 mM as an example. The sizes were enlarged and the size distributions were shifted to larger range until reaching the upper limit of the measured apparatus. The examination under the optical microscope also affirmed the increase of aggregate sizes.

According to Figure 5.2, the faster growth of aggregations at the early stage of the destabilization can be observed from 0.75 mM (223 mg/L alum). It is worth noting that two peaks of distribution can be noticed at 1.0 mM (297 mg/L alum) indicating the presence of different population groups as flocs were observed. From the blank experiment to form aluminium hydroxide ($\text{Al}(\text{OH})_3$) precipitate at pH 7 in DI water, the size was measured to be 56 nm in average. This value was very close to the 50 nm in pH 9 reported by Du et al. (2009). Hence, the left peak at 120 s (in Figure 5.2b) could represent the precipitated aluminium species, while the right one exhibited the aggregates formed in the system.

Similar changes of droplet size distribution can be found from the emulsion in tap water as displayed in Figure 5.3 for the Al^{3+} concentrations of 0.5 mM and 0.75 mM. The growth rate of aggregation at the 0.50 mM (149 mg/L alum) was faster than at 0.75 mM (223 mg/L alum), which flocs can be seen. At 0.50 mM Al^{3+} , the bimodal distribution of droplet sizes in tap water shifted to the right until presenting only one peak suggesting the possibility of droplets' coalescence. On the contrary, the distribution with two peaks were also noticed at 0.75 mM with the left one at around 50 nm. This insisted the formation of solid $\text{Al}(\text{OH})_3$ when flocs appeared.

Considering the change of aggregate mean diameter with time as presented in Figure 5.4. The growth profiles at 0.75 mM and 0.50 mM for emulsion with DI water and tap water were linear with the slopes (k_{fast}) values of 12.2 and 12.9, respectively. These slopes indicated a similar growth rate of aggregation. Note that the linear

tendencies were also acquired from lower Al^{3+} concentrations in both emulsions with milder slope.

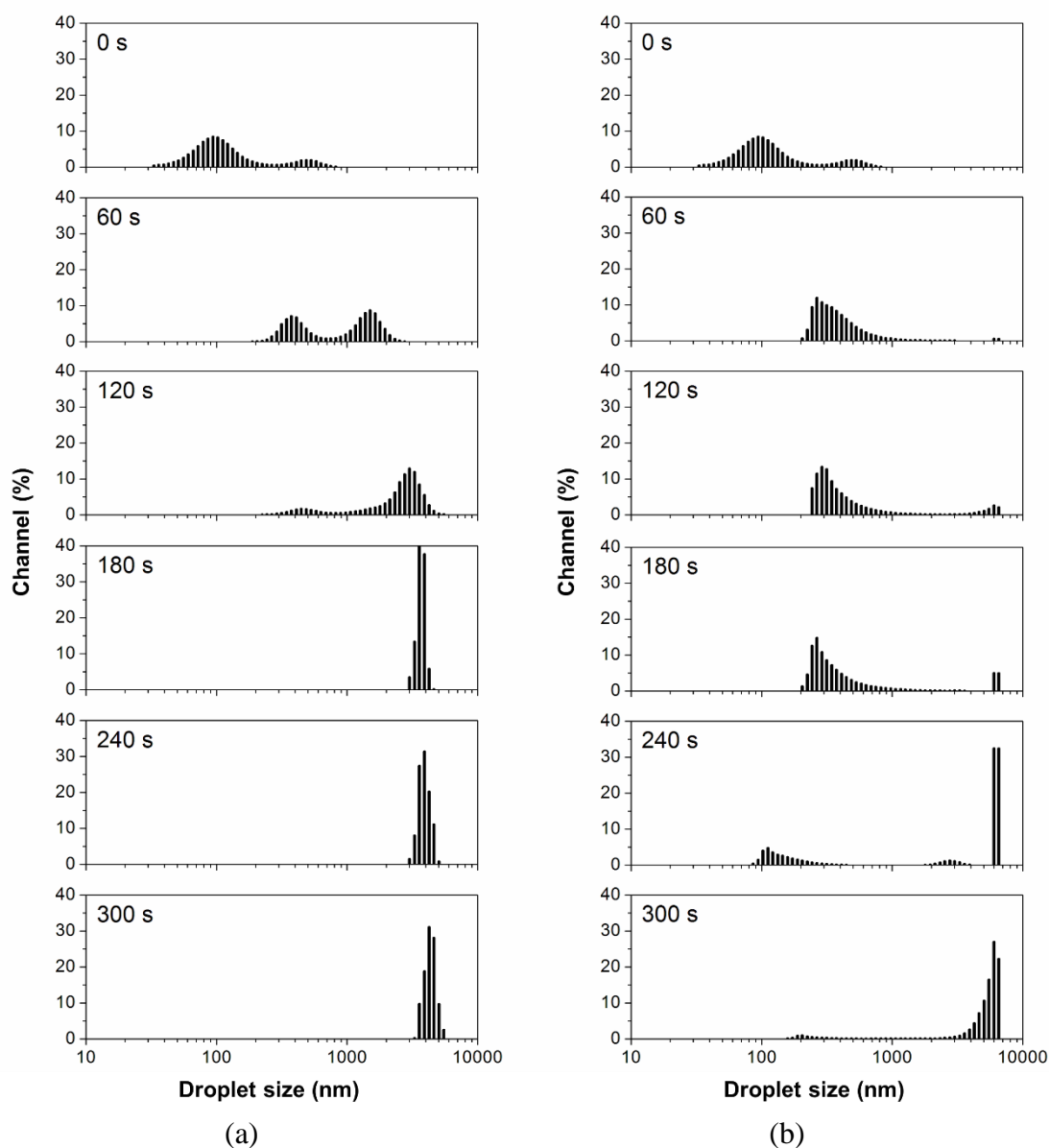


Figure 5.3 Droplet size distributions with time of the emulsion prepared from tap water for Al^{3+} concentrations of (a) 0.75 mM and (b) 1.0 mM

On the other hand, the changes of size at the concentration where flocs can be observed, i.e. 1.0 mM for DI emulsion and 0.75 mM for tap water emulsion, were fitted with polynomial growth. Flocs would require times for aggregation before increasing their sizes. This change was similar to the growth of kaolin flocs at the Al^{3+}

concentration of 0.24 and 0.48 mM (80 mg/l and 160 mg/l of $\text{Al}_2(\text{SO}_4)_3 \cdot 18\text{H}_2\text{O}$), which had the polynomial trend in the work of Harif et al. (2012).

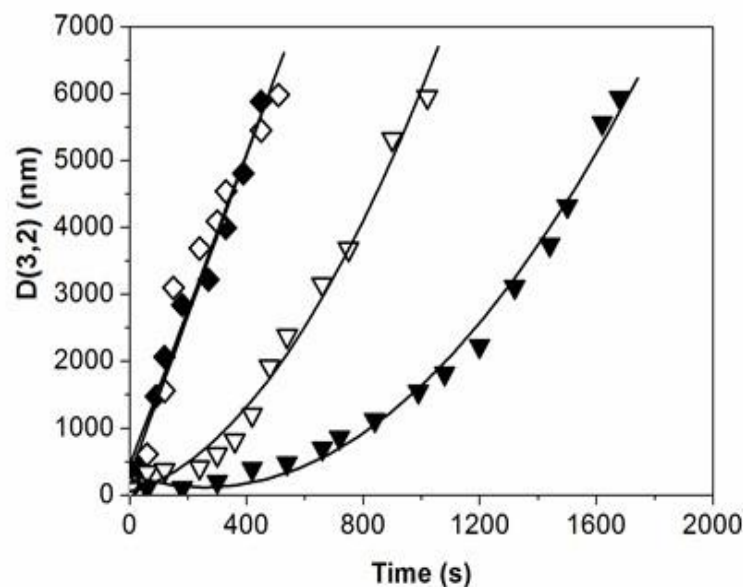
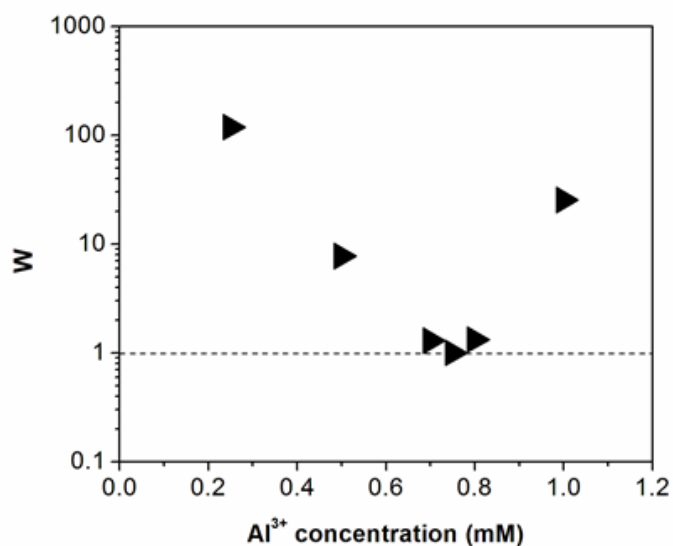


Figure 5.4 Aggregate growths with fitted curves (coefficients of determination, $R^2 > 0.97$) for Al^{3+} of 0.75 mM (◆) and 1.0 mM (▼) in DI water and 0.5 mM (◇) and 0.75 mM (▽) in tap water

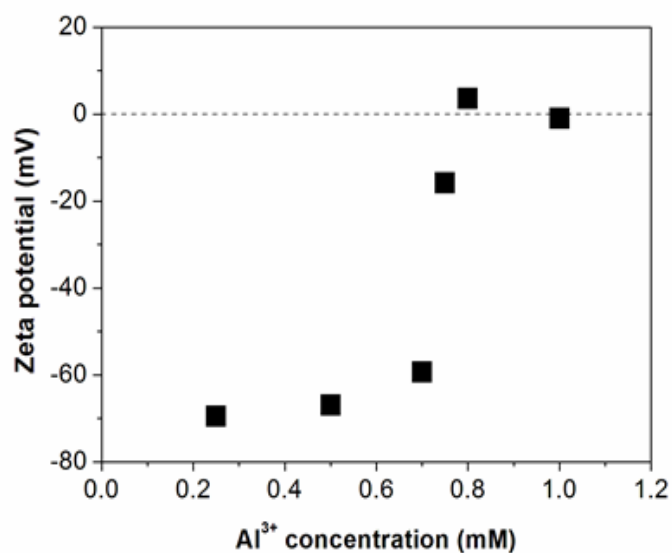
Furthermore, presence of anions could result in the faster growth rate of flocs in tap water since some ions (e.g. SO_4^{2-} , Cl^- , HCO_3^-) can promote the precipitation of aluminium hydroxide in its precipitated pH range (Hayden and Rubin, 1974; Letterman et al., 1979; Xiao et al. 2010). This difference in aggregate growths suggested the dissimilar mechanisms could occur. The destabilization by droplets' coalescence was expected from the Al^{3+} concentrations with linear aggregation growth and lower; on the contrary, the sweep flocculation by precipitated aluminium hydroxide should be responsible for the concentrations which solid flocs can be noticed with polynomial growth tendencies.

In addition, the obtained sizes in the first 2000 s were smaller than the mean value measured after 120 minutes (i.e. $> 10 \mu\text{m}$) corresponding to the experiment

definition for determining the kinetic at the early stage of aggregation where complex aluminium species could express slight effects on the aggregation.



(a)



(b)

Figure 5.5 (a) stability ratio and (b) zeta potential at varied Al³⁺ concentrations for emulsion in DI water

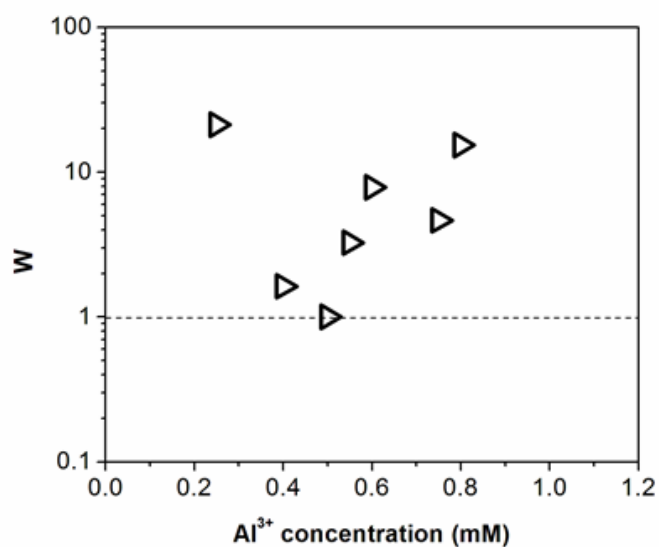
The stability ratio (W) at each Al³⁺ concentration was investigated from the change of aggregate size with time (i.e. slope from Figure 5.4). The fastest growth

rate, i.e. steepest slope, was denoted as k_{fast} at which the aggregation is limited by Brownian diffusion. Whereas, growth rates at other Al^{3+} concentrations were classified in the reaction limited regime and stated as k' . Consequently, the W ratio was obtained from the k_{fast}/k' .

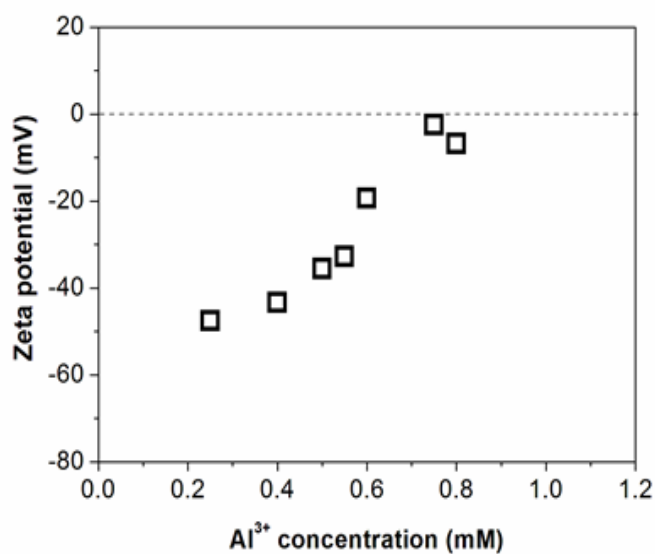
For DI water emulsion as illustrated in Figure 5.5, W values were firstly decreased and then increased at higher Al^{3+} concentrations. The CCC was found at Al^{3+} concentration of 0.75 mM rather than at 1.0 mM where flocs can be observed and the zeta potential was near zero (Figure 5.5b). The increase of W values at higher Al^{3+} concentrations instead of a flat line indicated the precipitation of the solid aluminium hydroxide. The precipitates can eventually form flocs, which can be visually observed, instead of promoting droplets' coalescence. Different destabilization mechanisms were expected as a result.

Although the CCC was obtained at the Al^{3+} concentration of 0.75 mM, the best separation in this work can be observed at 1.0 mM. The layer of floated flocs on the water surface and clear water at the bottom can be clearly seen after 60 minutes. Different mechanisms could be responsible for this result. The coalescence of droplets at the early stage of destabilization, which provided the CCC, might not be the effective separation mechanism in this case.

It was worth noting that the same trend of the stability ratio with the Al^{3+} concentration can be noticed from the emulsion prepared from tap water but with a different CCC as exhibited in Figure 5.6. The lowest W for this case was obtained at the Al^{3+} concentration of 0.5 mM. However, the separation also tended to be more effective at higher Al^{3+} dosage of 0.75 mM at which $\zeta \approx 0$ with the existence of flocs. Effects of Al^{3+} concentration and pH on the separation were further investigated as in the following section.



(a)



(b)

Figure 5.6 (a) stability ratio and (b) zeta potential at varied Al³⁺ concentrations for emulsion in tap water

5.3.2 Effects of coagulant dose, pH, and oil concentration

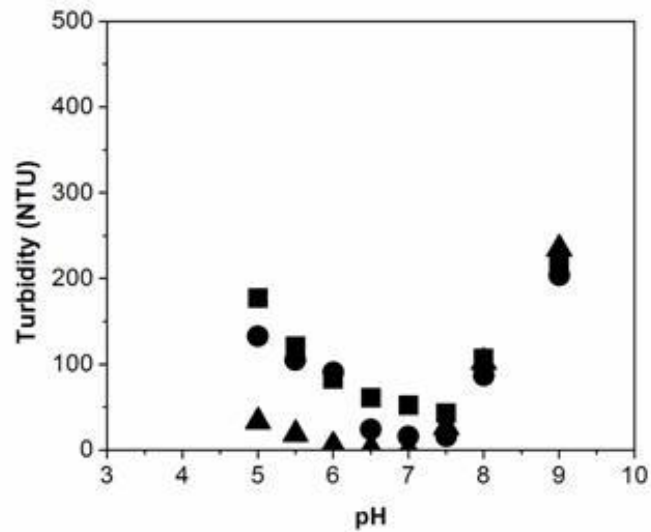
Effects of coagulant dosage and pH were investigated to ensure the optimal concentration acquired from the CCC. Varied concentrations of the coagulant (0.25 – 2.5 mM Al³⁺) were added to the cutting oil emulsion at the pH range of 4 – 9 to

examine impacts of coagulation concentration and pH on the destabilization performance. Influences of oil concentration on the required coagulant dose were also investigated by altering the initial oil concentration in the range of 0.5 – 4.0 g/l (COD \approx 1700 – 15000 mg/l) at the suitable pH condition.

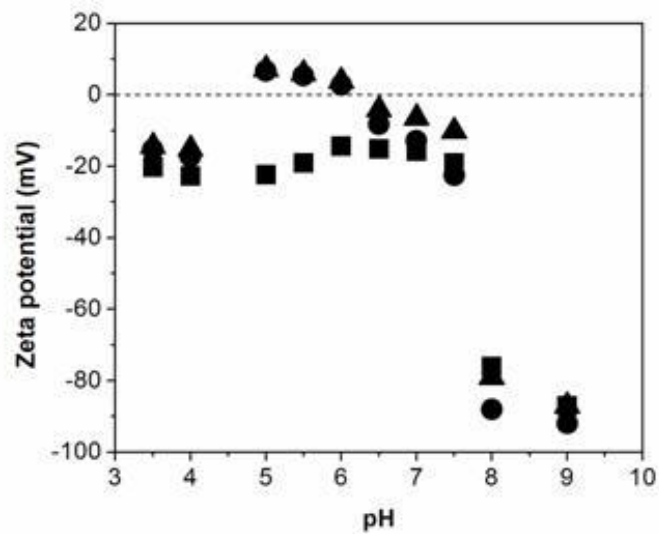
5.3.2.1 Effects of coagulant dose and pH

The optimal dosage of Al^{3+} concentration and pH for the destabilization were determined in this part. From the experiments with DI water emulsion, the turbidity reduction can be observed at Al^{3+} concentrations higher than 0.75 mM as shown in Figure 5.7a. Moreover, turbidity began to decrease at pH of 5 and reached the minimum value at pH around 6.5 – 7.0. The turbidity was increased again at higher pH.

The change of turbidity can be explained by the zeta potential (ζ) as in Figure 5.7b. In the pH range of 6.0 – 7.5, the zeta potentials for all three concentrations were near zero (i.e. isoelectric point); therefore, the repulsive force between droplets could be reduced allowing droplets to form aggregates. Aggregate sizes were larger than 10 μm , which exceeded the applicable range of the measured apparatus. Besides, turbidities at pH apart from 5 – 9 went beyond the turbidimeter limitation of 1000 NTU. This value, which was higher than the initial emulsion, suggested the presence of aggregates. However, their sizes might not be enlarged enough to rise to the water surface themselves. The destabilization of oily emulsion that only occurred in the pH range of 5 – 9 was similar to other works regarding the destabilization of cutting oil by metal salts (Cañizares et al., 2008; Al-Shamrani et al., 2002)



(a)



(b)

Figure 5.7 Figure 5.7 (a) turbidity and (b) zeta potential of the emulsion from DI water at different pH for varied Al^{3+} concentration:

■ 0.75 mM, ● 1.0 mM, ▲ and 2.5 mM

The ζ variation was due to the aluminium speciation in each pH range. The dominant species of aluminium at $pH < 5$, $pH = 5 - 9$, and $pH > 9$, are free aluminium ion (Al^{3+}), solid aluminium hydroxide ($Al(OH)_{3(s)}$), and anionic aluminium hydroxide

($\text{Al}(\text{OH})_4^-$) as mentioned in section 5.1. Therefore, the destabilization mechanism would be different. At pH below 5, the adsorption of the positively charged ion (Al^{3+}) on the droplet surface could be the main destabilization mechanism as in the work of Pinotti and Zaritzky (2001); thus, the zeta potential was then reduced. The destabilization mechanism was different in the neutral pH range (pH = 5 – 9) since the solid precipitated $\text{Al}(\text{OH})_3$ was formed. Note that the minimum solubility of this precipitate can be found at pH of 6 - 7 (Khemis et al., 2006). The applied dose in this work was higher than the water solubilities of $\text{Al}(\text{OH})_3$ in the neutral pH range, which are less than 0.1 mM (Holt et al., 2005). The precipitated $\text{Al}(\text{OH})_3$ can destabilize the emulsion by different mechanisms depending upon the applied dose of aluminium salts.

Effects of Al^{3+} concentrations on droplet sizes at the optimal pH are displayed in Figure 5.8. The 0 mM represents droplet sizes of the initial emulsion in the range of 30 - 300 nm, which cannot be seen under the 40X microscope. Droplet sizes were enlarged with the Al^{3+} concentrations as can be seen from the photos, in accordance with the size distribution. The distribution curves moved to the right along with the growth of droplet sizes. Interestingly, there were two distinguished curves in the case of 1.0 mM where flocs appeared. The formed aluminium hydroxide precipitate could be responsible for this result, which corresponded to the discussion for the aggregation kinetic in Figure 5.2b. Moreover, some coalescence could occur at 0.50 mM and 0.75 mM since larger droplets can be seen.

This could be explained by the Precipitation Charge Neutralization (PCN) model (Dentel, 1991) that the destabilization is a result of the charge neutralization by the deposition of solid aluminium hydroxide on colloidal particle's surfaces. The coalescence could be provoked in these cases as a result.

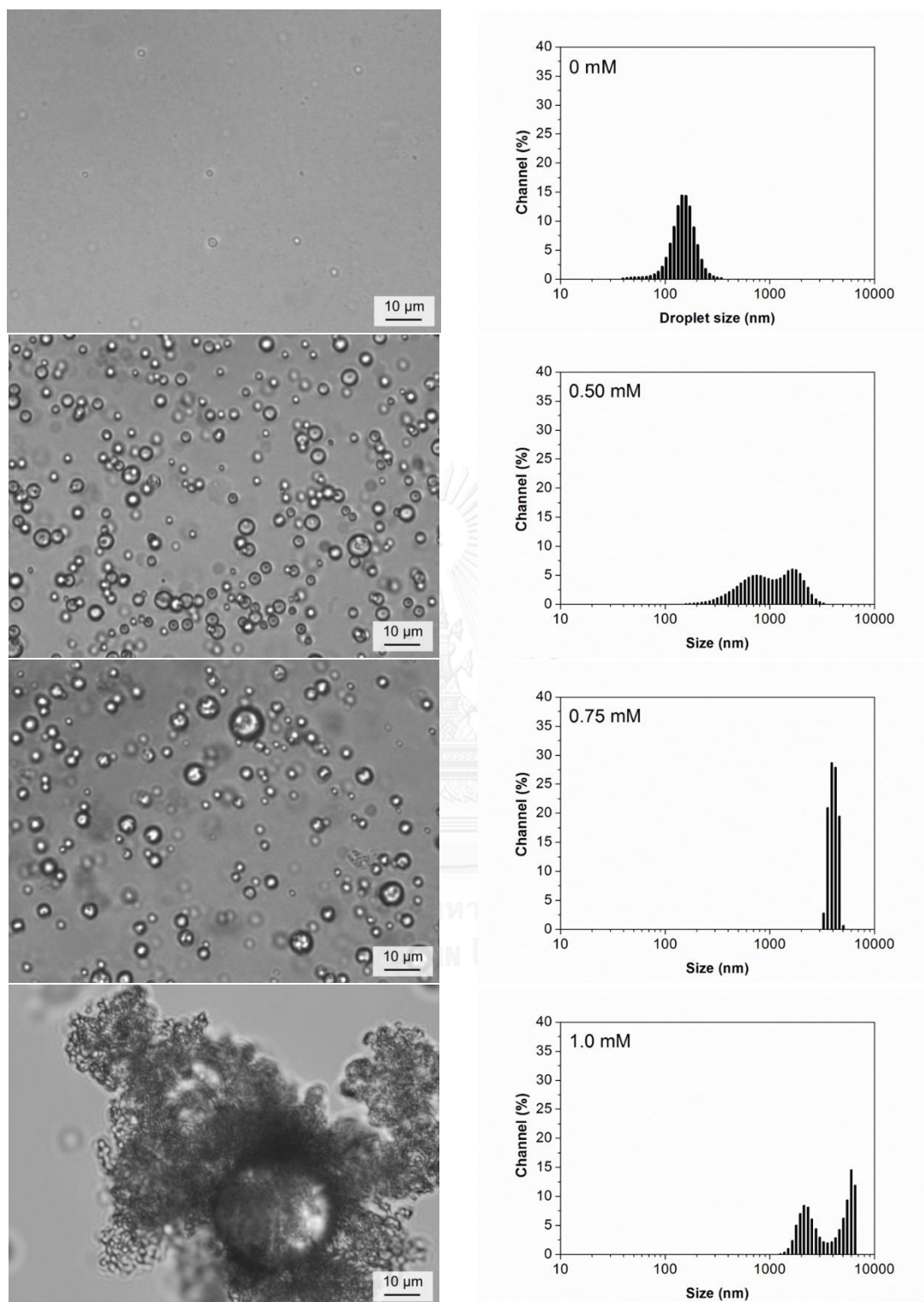


Figure 5.8 Evolution of aggregate and droplet size distribution in emulsion with DI water at the optimal pH for different Al^{3+} concentrations

On the contrary, flocs with enmeshed droplets were noticed at the 1.0 mM Al^{3+} concentration. The sweep flocculation might take place forming agglomerates

since the aluminium precipitates continue to attach on droplets' surface suggested from the kinetic study. Formed flocs can capture oil droplet in their structure producing agglomerates with much larger size compared to the droplets in the emulsion. Note that the size distribution and photo of aggregates for the 1.0 mM and 2.5 mM were very similar, the results are therefore not shown. Furthermore, presence of flocs can also explain the positive zeta potential obtained at the pH of 5 – 6 for Al^{3+} concentrations of 1.0 mM and 2.5 mM as precipitates could be positively or negatively charged due to the adsorbed ions from the solution on their surfaces (Cañizares et al., 2006). The adsorption of anions on the surface of precipitate might be responsible for the high negatively zeta potential obtained at pH 8 – 9 as well (Figure 5.7b). In addition, no destabilization was noticed due to the formation of the negative dissolved aluminium hydroxide ($\text{Al}(\text{OH})_4^-$) at pH higher than 9 (Ahmad et al., 2006).

For the emulsion with tap water, the effective destabilization occurred at the same pH range as shown in Figure 5.9. Though, the minimum Al^{3+} concentrations at which the destabilization and floc forming can be observed were respectively 0.5 mM and 0.75 mM, which were lower than in the case of the emulsion with DI water. Presence of ions in tap water might be the reason for the less dosage required as the initial zeta potential (-48.4 mV) of this emulsion was lower than the emulsion from DI water (-65.8 mV). Moreover, larger droplets than those existing in the initial emulsion could be another reason. These ions could also combine with aluminium resulting in less hydroxyl ion consumption. The pH values were then slightly decreased to the range of 6.2 – 7.0 for the applied Al^{3+} concentrations. Microscopic photos and size distributions of aggregate are depicted in Figure 5.10. It was ensured that droplet sizes were enlarged along with the Al^{3+} concentration, and flocs can be observed at the 0.75 mM Al^{3+} .

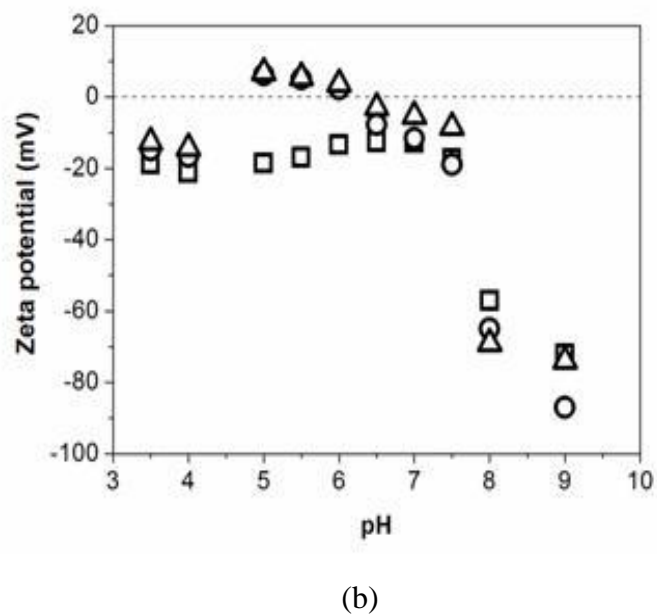
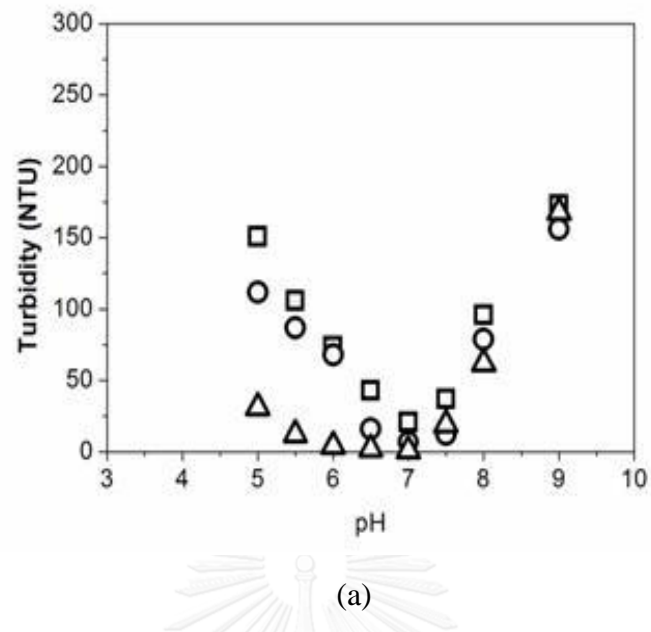


Figure 5.9 (a) turbidity and (b) zeta potential of the emulsion from tap water at different pH for varied Al³⁺ concentration: □ 0.50 mM, ○ 0.75 mM, and △ 1.0 mM

Finally, it was found that the destabilization was governed by the speciation of Al³⁺ formed at different pH. The adjustment to optimal pH was required to facilitate the effective destabilization. In addition, the dosage of Al³⁺ also affect the destabilization mechanism.

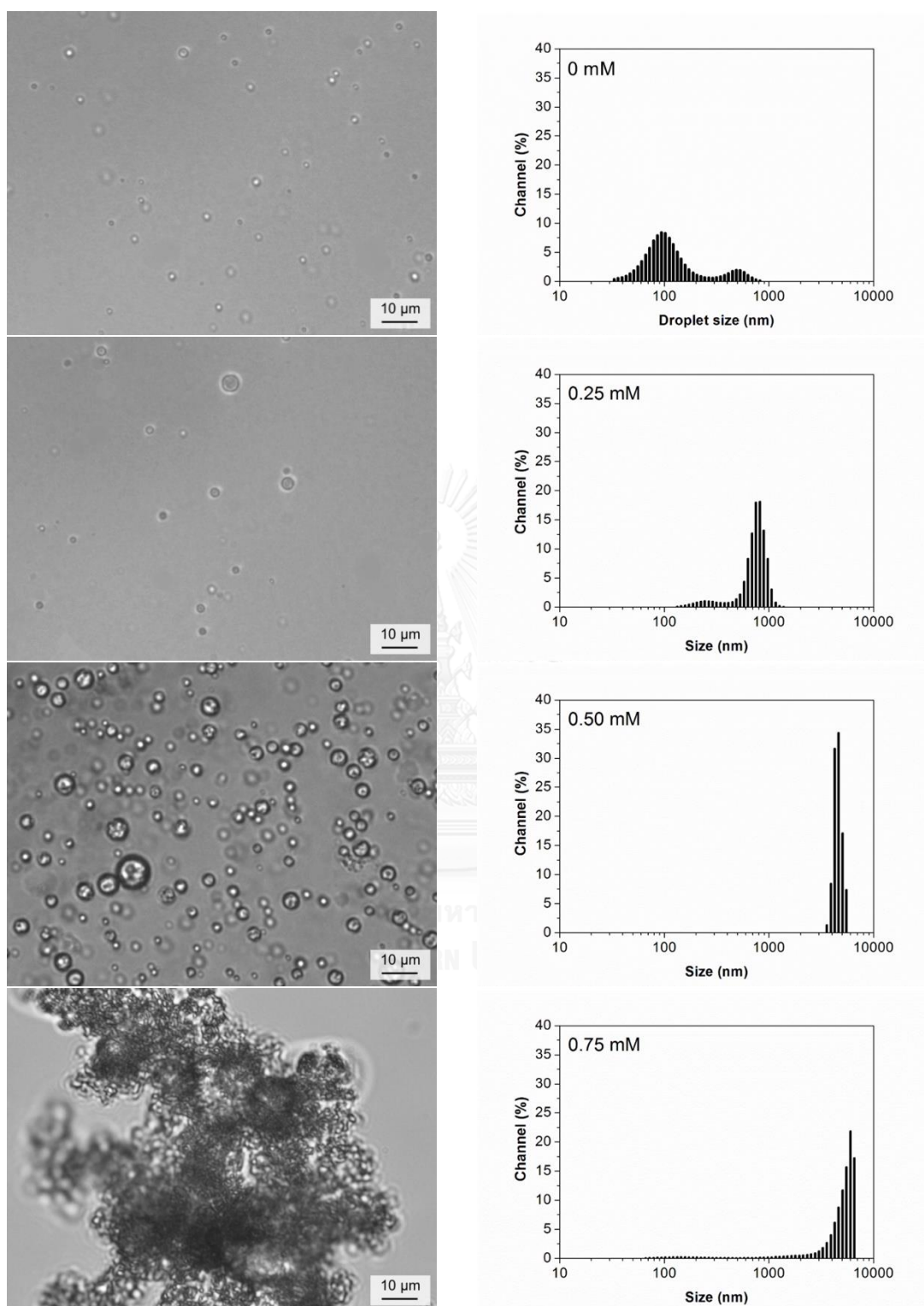


Figure 5.10 Change of aggregate and droplet size distribution in emulsion with tap water at pH 7 for different Al^{3+} concentrations

A certain dosage of Al^{3+} (i.e. 0.75 mM and 0.50 mM in this work for emulsions with DI and tap water, respectively) can form $\text{Al}(\text{OH})_3$ precipitates that can

neutralize surface charges of droplets and promote the coalescence. By raising the dosage, the destabilization mechanism changes to the sweep flocculation. Droplets are captured in the flocs structure forming oil-floc agglomerates with larger size than that of droplets alone, but the coalescence is then limited or slower because the contact between droplets is far less possible. This difference in the destabilization mechanism can have crucial effect on the following separation process e.g. flotation or settling. The study to ensure the formation of aluminium hydroxide precipitate in the destabilization was therefore conducted in the following section in order to prove the discussion on the formed speciation.

5.3.2.2 Effects of oil concentration

The experiment to determine effects of initial oil concentration was conducted at the neutral pH range (i.e. 6.5 - 7.0). It was found that the required Al^{3+} concentrations for the destabilization were increased at higher oil concentrations for emulsions prepared from both water types.

The relationship between the minimum Al^{3+} dose and the oil concentration is exhibited in Figure 5.11. At these Al^{3+} concentrations, flocs cannot be observed by direct visualization and under the microscope. The deposition of $\text{Al}(\text{OH})_3$ on droplets' surface could play a role in the destabilization. The minimum Al^{3+} linearly varied with oil concentration. This was in accordance with the linear variation of the drop number and surface area with oil concentration since the drop sizes were similar in this concentration range.

The minimum Al^{3+} doses were also increased with oil concentrations for the emulsion with tap water, however, with milder slope. This could be explained by the fact that initial droplets in tap water were larger than in the DI water. Droplets' surface area was then less increased when more oil was added. From that reason, the raised minimum Al^{3+} required with oil concentration in tap water was lower than that of the deionized one.

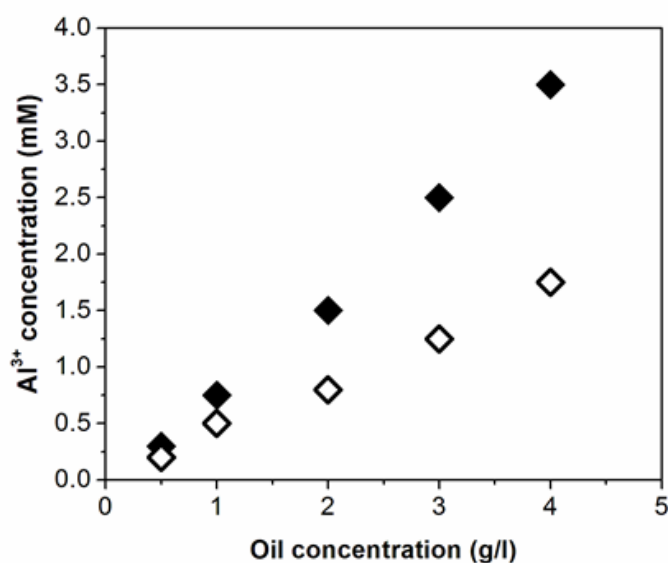


Figure 5.11 Effects of oil concentration on the minimum Al³⁺ concentration required (emulsions prepared from ◆ DI water and ◇ tap water)

5.3.3 Observation of floc

In this part, the obtained flocs were investigated to confirm the presence of Al(OH)₃ precipitates. The morphology and chemical composition of flocs were determined. Moreover, the crystalline structure of the solid formed due to the destabilization of the emulsion by aluminium sulfate was examined. The results are displayed as follows.

5.3.3.1 Floc size

Oil flocs formed in the emulsion were characterized for their sizes by the laser diffraction scattering (LDS) using the Malvern Mastersizer 2000. The size distributions for flocs in DI water and tap water emulsion are shown in Figure 5.12. It can be seen in both cases that floc sizes were in the microscale range with the average diameter of 428 μm, which was much larger than those of the initial emulsion and the destabilized emulsion without flocs. No obvious difference can be noticed from these two waters.

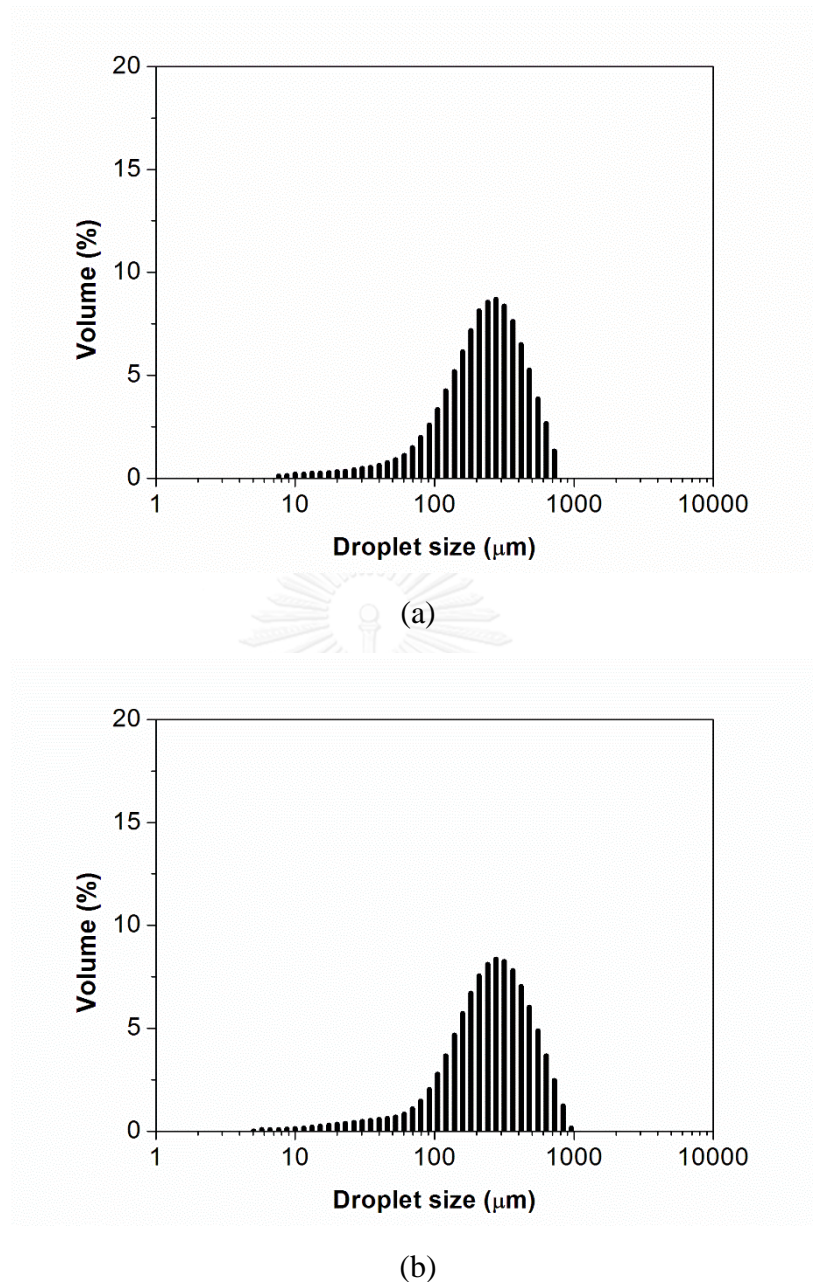


Figure 5.12 Size distribution of flocs in cutting oil emulsion with (a) DI water and (b) tap water

From these size distributions, the fractal dimension of flocs was analyzed from the fractal plots obtained from the Mastersizer 2000. The light intensity I is measured at varied scatter vector Q . This vector is described as the difference between the vectors of incident beam and the scattered beam in the medium, which can be acquired from Equation 5.2 where n , θ , and λ are the refractive index of the medium,

the scattered angle, and the wavelength of the incident beam in vacuum, respectively (Bushell et al., 2002).

$$Q = \frac{4\pi n \sin(\theta/2)}{\lambda} \quad (5.2)$$

The relation between I and Q can be written as in Equation 5.3 for freely scattering aggregates.

$$I \propto Q^{-D_f} \quad (5.3)$$

The fractal dimension (D_f) therefore can be obtained from the slope of the plot between I and Q in the log-log scale if the relation is linear. The values of D_f varied from 1 to 3. Low D_f suggested loose and striated flocs. On the other hands, more compact flocs can be expected at higher D_f (Jarvis et al., 2008)

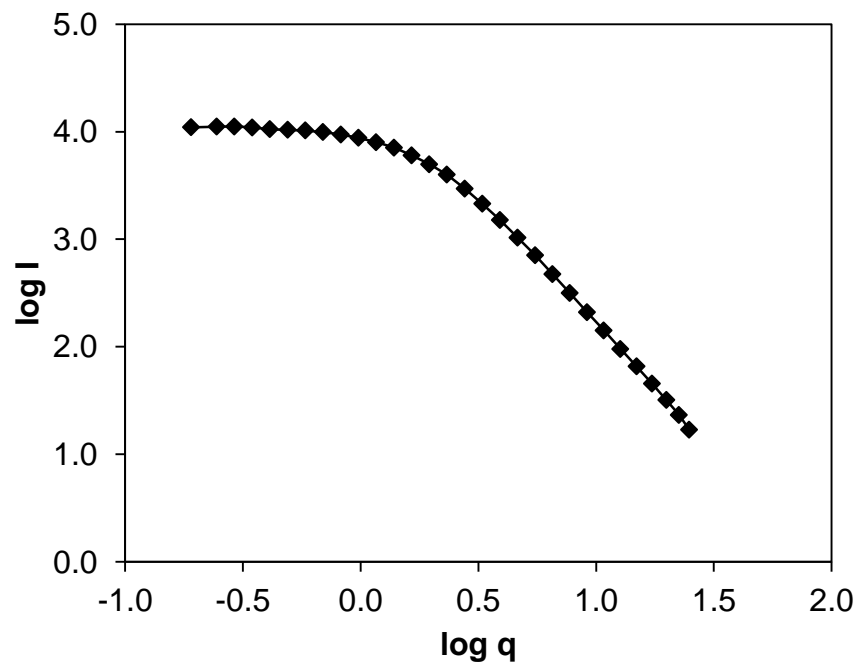


Figure 5.13 Fractal plots of oil flocs in emulsion with DI water from Mastersizer 2000

The log-intensity vs. log-angle of flocs in this study were plotted as displayed in Figure 5.13. From the slope of the linear region in Figure 5.13, the fractal dimension can be deduced. The obtained fractal dimensions for flocs in the emulsion prepared from DI water was 2.24 suggesting a quite compact structure of the formed flocs. This acquired value corresponded to common metal hydroxide flocs, which contains the fractal dimension about 2 (Gregory, 2009). No effects of Al^{3+} concentration in the range of 1.0 – 2.5 mM on the fractal dimension can be noticed.

5.3.3.2 Floc morphology and chemical composition

Flocs were firstly examined for their morphology and composition by the scanning electron microscope (SEM) with energy dispersive X-ray analysis (EDX) (JEOL JSM 5310LV, JEOL, Ltd.). The sampling flocs were filtered through a cellulose acetate membrane with a pore size of 0.45 μm (Whatman GmbH) and dried in an atmospheric condition before a carbon coating. SEM image and EDX results are displayed in Figure 5.14 and Table 5.1, respectively. It was worth noting that no difference can be noticed for flocs formed in different water types in the morphology and element analysis, therefore, only the results for flocs in DI water are shown. Presence of solid was confirmed in the SEM image. From the EDX element analysis, the high percentage of carbon could be contributed by oil in the emulsion and the filter membrane. This solid could be aluminium hydroxide ($\text{Al}(\text{OH})_3$) judging from the atomic ratio of 1:3 between aluminium and oxygen. Furthermore, trace of aluminium sulfate ($\text{Al}_2(\text{SO}_4)_3$) can be observed from Point 20 where the atomic percentage of oxygen was much higher than that of aluminium. However, after subtracting $\text{Al}_2(\text{SO}_4)_3$ ($\text{Al}:\text{S}:\text{O} = 1:1.5:6$), the ratio of approximately 1:3 between Al and O can be obtained. Presence of $\text{Al}_2(\text{SO}_4)_3$, which was supposed to dissolve completely, was a result of drying process. Some $\text{Al}_2(\text{SO}_4)_3$ could be re-precipitated when water was removed.

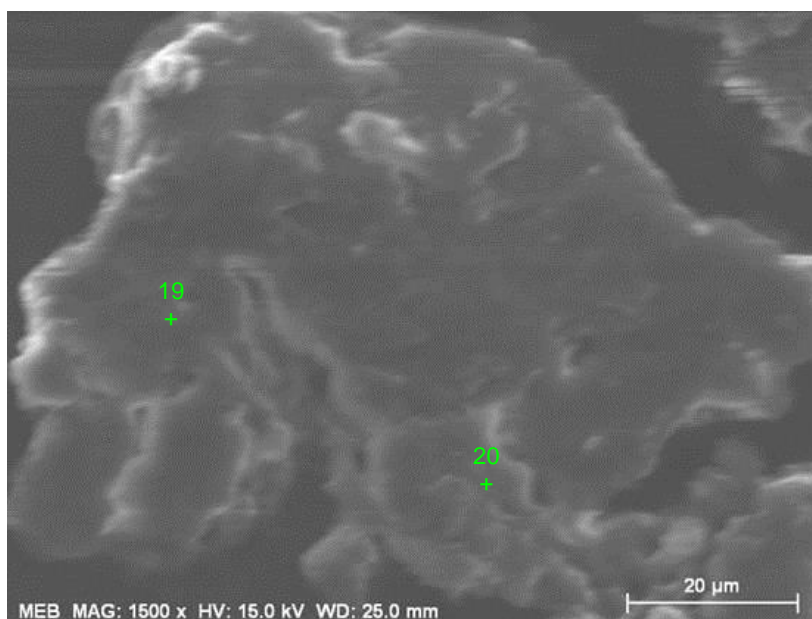


Figure 5.14 SEM image of aluminium floc in cutting oil emulsion with DI water

Table 5.1 EDX results of aluminium floc in the cutting oil emulsion with DI water at pH 7

Atomic percentage	Carbon	Oxygen	Aluminium	Sulfur	Silica	Possible compounds
Point 19	58.17	29.19	9.99	2.20	0.45	Al(OH) ₃
Point 20	43.50	40.33	4.18	4.85	6.05	Al ₂ (SO ₄) ₃ Al(OH) ₃

5.3.3.3 Crystalline structure of floc

The occurrence of Al(OH)₃ in flocs formed in the emulsion was also ensured by the Fourier Transform Infrared Spectroscopy or FTIR (THERMO Nicolet iS50 FT-IR, Thermo Fisher Scientific Inc.). The FTIR spectra and the analysis results are displayed respectively in Figure 5.15 and Table 5.2. From Du et al. (2009), the absorption bands at 400 - 900 cm⁻¹ and 3200 - 3700 cm⁻¹, which respectively related to the Al-O and O-H stretching vibration, expressed the formation of ultrafine particles or amorphous structure of Al(OH)₃. The absorption band at 523 cm⁻¹ associated with the stretching of Al-O in the octahedral structure (octahedral AlO₆) (Meher et al., 2005). Bands at 984 and 1075 cm⁻¹ also related to Al-O bond. The band

at 3345 cm^{-1} expressed the stretch mode of hydroxide (OH) to aluminium (Riesgraf and May, 1978). These obtained bands corresponded to the structure of bayerite (Du et al., 2009), which the structure has close-packed layer of oxygen with aluminium in an octahedral coordinate (Levin and Brandon, 1998). This bayerite is one form of solid $\text{Al}(\text{OH})_3$ precipitate (Duan and Gregory, 2003). The presence of solid aluminium hydroxide in the emulsion is then proved. In addition, bonds of organic compounds were obtained at the bands of 1375, 1458, 2857, and 2922 cm^{-1} suggesting the presence of oil in the sample. Note that these bands were unable to be detected from the floc forming in DI water without cutting oil in the same condition.

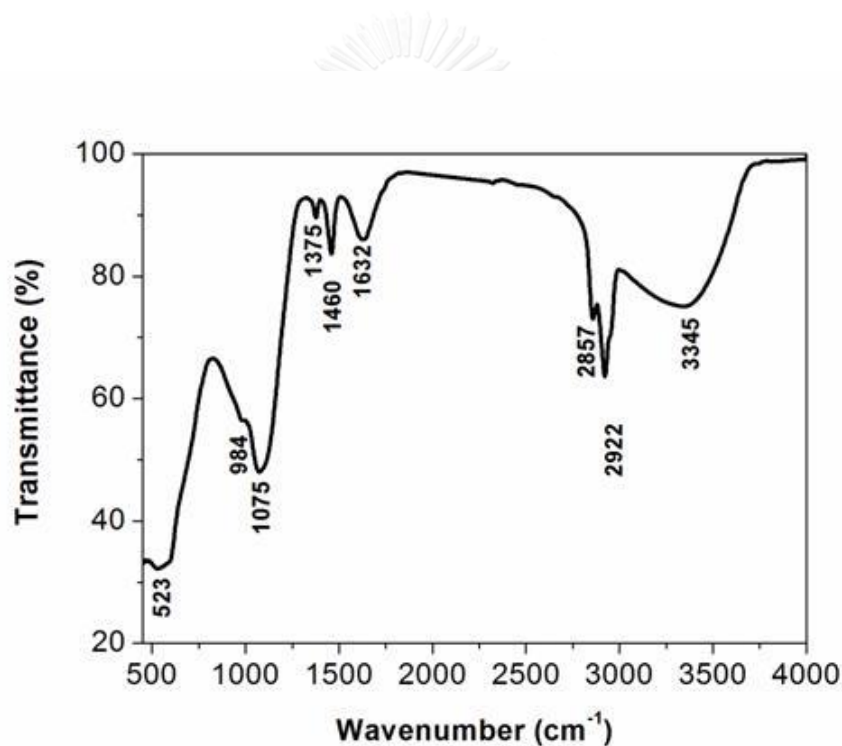


Figure 5.15 FTIR spectra of flocs formed in the DI water emulsion at pH 7

Therefore, according to the result of SEM with EDX and FTIR, it can be stated that the solid $\text{Al}(\text{OH})_3$ was formed as flocs in the emulsion, and can remove oil droplets by the sweep flocculation mechanism.

Table 5.2 Assignment of IR bands in FTIR results

Band position (from FTIR curve)	Band positions (from references*)	Band assignment
523	523	Al-O stretch (AlO_6)
984	1023	Al-O bond
1075	1072	Al-O bond
1375	1375	CH_3 bending
1458	1450 – 1470	C-H bend of alkanes
1632	1639	Bending moments of H_2O
2857 and 2922	2800 - 3000	H-C-H asymmetric and symmetric stretch
3345	3400	Stretch of OH bound to aluminium

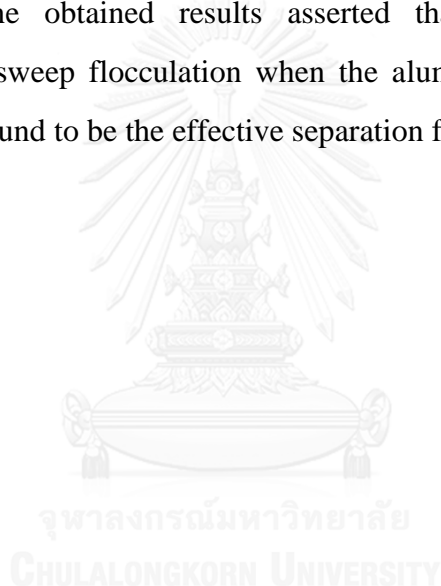
*Source: Du et al., 2009; Meher et al., 2005; Riesgraf and May, 1978; Coates, 2000

5.4 Conclusions

This chapter displays the results from the study of the destabilization of the stabilized cutting oil emulsion by a chemical coagulation using aluminium sulfate or alum as the coagulant. The experiment results showed that both pH and coagulant dosage played a key role in the destabilization. The oil separation can be noticed in the pH range of 5 – 9 where the precipitated aluminium hydroxide is dominant. The critical coagulation concentration (CCC) from the aggregation kinetic study were 0.75 mM (223 mg/L alum) and 0.50 mM (149 mg/L alum) for emulsion with deionized and tap water, respectively. However, zeta potentials of these points were not near the isoelectric point ($\zeta \approx 0$). The $\zeta \approx 0$ was found at the concentration where solid flocs can be observed i.e. 1.0 mM (297 mg/L alum) and 0.75 mM (223 mg/L alum) for emulsion in DI and tap water. Water characteristics can impact the growth rate of flocs since ions in tap water can encourage the precipitation of aluminium hydroxide. Two mechanisms were involved in the destabilization such as adsorption of solid $\text{Al}(\text{OH})_3$ on droplets' surface and sweep flocculation depending on the Al^{3+} concentration. The observation of aggregates under the optical microscope also found

the coalescence of oil droplets and the trapping of droplets in the floc structure as discussed. In addition, the required Al^{3+} concentration was in accordance to the oil concentration.

Flocs formed in the emulsion were analyzed. The morphology and element analysis from the scanning electron microscope (SEM) with energy dispersive X-ray (EDX) suggested the formation of solid aluminium hydroxide. This result can be affirmed by the crystalline structure obtained from the Fourier transform infrared spectroscopy (FTIR) analysis of flocs formed in the emulsion as the $\text{Al}(\text{OH})_3$ in form of bayerite was found. Though, no difference was found for characteristics of flocs in different waters. The obtained results asserted that the main destabilization mechanism was the sweep flocculation when the aluminium hydroxide flocs were formed, which was found to be the effective separation for this oily emulsion.



CHAPTER 6

FLOTATION TEST

From the previous results in the destabilization study, the addition of coagulant can effectively separate the cutting oil emulsion, especially when flocs can form. However, the separation took long time to accomplish. The separation of the emulsion by flotation was then tested for two purposes including (1) improve the efficiency and (2) lessen time required for the separation. In addition, the results from this bench scale flotation can affirm the finding from the pilot-scale experiments in more controlled conditions.

6.1 Flotation experiment device and procedure

The experiments were conducted in a Multiplace Orchidis™ Flottatest as depicted in Figure 6.1.



Figure 6.1 Flottatest device

The deionized water was subjected to high pressure causing air to dissolve at the over-saturated condition. The pressurized water was tangentially fed at the bottom of beakers. Once it was released, the over-saturated air was precipitated from the water forming microbubbles. Three flotation tests can be simultaneously operated in three beakers filled with 500 mL of the 1 g/L cutting oil emulsion prepared with deionized water. Varied volumes pressurized water at 4 bar from 100, 300, and 500 mL was introduced to each beaker. The recycle ratio, which defined as the ratio of the pressurized water to the sample volume, of 0.2, 0.6, and 1 was respectively acquired. These pressure level and recycle ratio range were similar to that was operated in the pilot-scaled flotation experiments.

The average sizes of bubbles in the Orchidis Flottatest obtained from Nanosizer were found to be an inversely proportion to the saturation pressure as reported by Bensadok et al. (2007) as expressed in Equation 6.1 where d_b is the bubble diameter in micrometers. PS is the saturation pressure in the unit of bar. From the correlation, the saturation pressure of 4 bars can provide the bubble diameter of 84 μm . This size corresponds to bubble sizes in DAF, which normally smaller than 100 μm , as suggested by Edzwald (2010). The bubble size in this experiment was therefore supposed to be approximately 80 μm .

$$d_b = 382.52 PS^{-1.09} \quad (6.1)$$

The results of the flotation experiment in this work were exhibited in term of turbidity as previously shown that it can represent oil concentration in the emulsion. However, turbidity can be affected by the change of droplet sizes if aggregation occur. Therefore, the size distribution of droplets had to be considered. The turbidities shown below were obtained from the samples with relatively similar droplet sizes. Besides, the emulsion volume in the beaker was increased when the pressurized water was introduced. The emulsion concentration was decreased due to the dilution effect, which can be calculated from:

$$C_c = \frac{C_0 \times V_0}{V_c} \quad (6.2)$$

where C_c is the emulsion concentration subjected to the dilution effect. C_0 is the initial concentration. V_0 and V_c are the emulsion volume before and after the dilution, respectively. Effects of bubbles can be recognized if the final emulsion concentration (C_f) was less than the C_c . On the other hand, droplets were not captured by bubbles if $C_f \geq C_c$.

The experiment can be divided into 2 parts. The first one dealt with the flotation of cutting oil emulsion without the addition of coagulant, which was conducted to affirm that the coagulation was required for the effective separation. Another part is the flotation test with coagulants at which effects of coagulant dosages and pressurized water volumes were considered.

6.2 Flotation of cutting oil emulsion without coagulant

The flotation was tested without the addition of the coagulant to confirm that the chemical coagulation was necessary. The flotation was operated under two conditions to verify effects of bubbles; for example,

- (1) pressurized water with saturation pressure less than 2 bar in which bubbles were rarely created. The pressure was only required for injecting water to the flotation cell,
- (2) pressurized water with 4 bar saturation pressure.

Samples were collected at the bottom of the flotation cell at 300 seconds (5 minutes) after introducing the pressurized water since bubbles were unable to be observed after this time. Firstly, turbidities at different heights in the column were measured. The pressurized water volume of 300 mL was applied providing the recycle ratio of 0.6 in this experiment. Photographs for the emulsions in this experiments are shown in Figure 6.2.

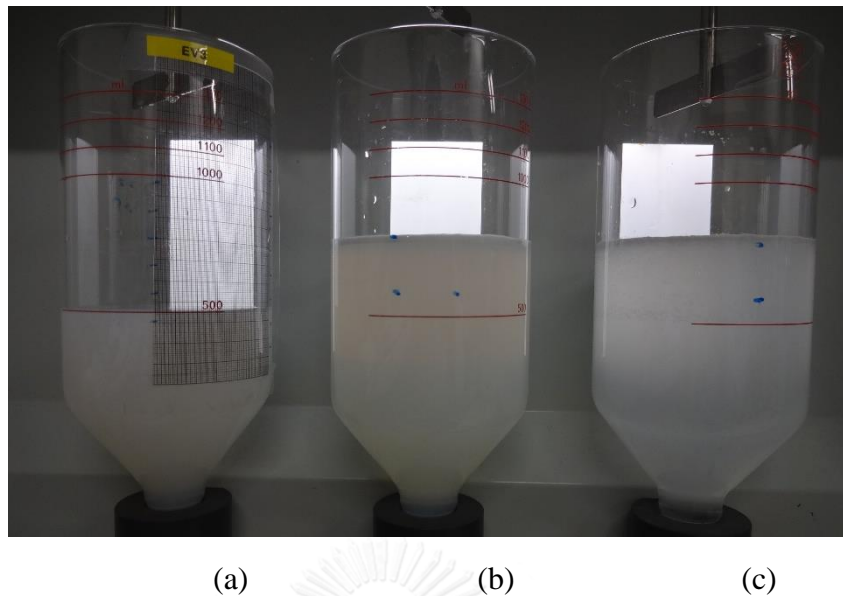


Figure 6.2 Photographs of the initial emulsion (a) and emulsion at 5 minutes after flotation with 300 mL of pressurized water under (b) 2 bars and (c) 4 bars without coagulation.

Turbidities of samples at different heights of the cell were analyzed and estimated for oil concentrations as presented in Table 6.1. It can be seen that concentrations at different heights were almost similar suggesting a well-mixed condition between the emulsion and the pressurized water in the flotation cell. The obtained concentrations from both 2 bars and 6 bars (approximated 0.62 – 0.63 g/L) corresponded to the diluted concentration (C_c) of 0.625 g/L at this recycle ratio. The slight difference of values could be the result of personal and systematic errors in the experiment, for example, water volume measurement and turbidity analysis. Furthermore, the approximation of the oil concentration from the turbidity could also offer a discrepancy. The results indicated that only flotation was ineffective for separating oil from the cutting oil emulsion. This can be affirmed by the results in Table 6.2 where effects of the pressurized water volume were considered. The decrease of turbidity was only due to the dilution by the injected water as indicated by the C_c values. This finding also confirm the result from the pilot-scale flotation as in section 4.3.3 that the flotation alone cannot separate the stable cutting oil emulsion.

Table 6.1 Turbidities and concentrations at different heights for flotation without destabilization

Samples	Turbidity (NTU)		Concentration (g/L)	
	2 bars	4 bars	2 bars	4 bars
Initial	726	738	1.0	1.0
0 - 100 mL	457	464	0.62	0.63
100 - 200 mL	458	467	0.62	0.63
200 - 300 mL	457	465	0.62	0.63
300 - 400 mL	457	465	0.62	0.63
400 - 500 mL	460	465	0.63	0.63
500 - 600 mL	458	466	0.62	0.63
600 - 700 mL	457	464	0.62	0.63
700 - 800 mL	456	464	0.62	0.63

Table 6.2 Turbidities and concentrations of the emulsion at the bottom of the cells after flotation without coagulant addition

Pressurized water volume (mL)	100	300	500
Turbidity (NTU)	579	455	361
Concentration (g/L)	0.79	0.62	0.49
C_c (g/L)	0.77	0.63	0.50

Considering this operating condition, the A/S ratio defined as the proportion between the volume of air and the mass of solids, which is an important factor governing the DAF performance (Metcalf & Eddy, 2004). This ratio was found to have more influence on the separation effectiveness of oil than the saturation pressure (Al-Shamrani et al., 2002). The calculated ratio were obtained as 0.011 – 0.056 mL air/mg oil, which are in the range suggested for solids and biosolids separation of 0.005 – 0.060 mL air/mg solid (Metcalf & Eddy, 2004). Though, the separation rarely

occurred. One explanation could be that the suggested A/S ratio values are valid for solid particles, which might not be compatible with oil droplets.

Furthermore, the very tiny droplet size means that oil can form a large number of droplets. The amount of bubbles produced by a small volume of pressurized water in a batch condition of Flottatest might be insufficient for capturing oil droplets. In order to prove this discussion, the minimum bubble volume (V_{min}) needed for capturing all oil droplets was calculated. Several assumptions were stated for the calculation such as (1) volumes and surface areas of spherical oil droplets and bubbles were calculated from the mean diameters, (2) the attachment of oil droplets was a single layer throughout bubble's surface, and (3) air can dissolve in water at a given saturation pressure according to Henry's law. The calculation can be achieved from Equations 6.3 – 6.6.

$$n_{p/b} = \frac{S_b}{S'_p} \quad (6.3)$$

$$n_p = \frac{6C_0V_0}{\pi d_p^3 \rho_o} \quad (6.4)$$

$$n_b = \frac{n_p}{n_{p/b}} \quad (6.5)$$

$$V_{min} = n_b \times \frac{\pi d_b^3}{6} \quad (6.6)$$

$N_{p/b}$ is the number of captured particles by one bubble. S_b and S'_p are the surface area of a bubble (πd_b^2 , $d_b = 80 \mu\text{m}$) and the cross-sectional area of a droplet ($\pi d_p^2/4$, $d_p = 174 \text{ nm}$), respectively. N_p and N_b are respectively numbers of oil droplet and bubble. The initial concentration and volume of the emulsion before the introduction of the pressurized water are represented by C_0 and V_0 , which are 1 g/L and 500 mL, respectively. The cutting oil density (ρ_o) is 930 kg/m³. The V_{min} of 61.80 mL was therefore obtained. The volume of the pressurized water (V_{PW}) required for

this bubble volume can be estimated from Henry's law as in Equation 6.7 where V_{air} is the volume of the dissolved air in water. The Henry constant (K_h) at the temperature of 20 °C is 18 mL/L·atm (Blazy and Jdid, 2000). The saturation pressure is represented by p , and V_{PW} is the required volume of the pressurized water.

$$V_{air} = K_H \cdot PS \cdot V_{PW} \quad (6.7)$$

From the calculation, the volume of the pressurized water needed for capturing all droplets was 1165 mL, which was much larger than the volume applied in the experiment. The injection of 150, 300, and 500 mL pressurized water at the pressure of 3.95 atm (4 bars) to the atmospheric pressure (1 atm) can respectively produce bubble volumes of 8.0, 15.9, and 26.5 mL. The required pressurized water volume for such volume of emulsion was unreasonable since it will consume large amounts of water and energy to produce bubbles.

Another reason for the ineffective separation could be the electrostatic interaction. As aforementioned, bubbles generally contain negative charges on their surface (Yang et al., 2001; Li and Somasundaran, 1992) as well as droplets. The repulsion can be expected when they approached each other. Therefore, the droplet-bubble attachment would rarely occur resulting in poor separation performance. The reduction of negative charge on droplets' surface before flotation could enhance the separation efficiency. The flotation of the emulsion with the addition of coagulant to destabilize oil droplets before separation was studied as in the following section.

6.3 Flotation of cutting oil emulsion with coagulant addition

Aluminium sulfate (or alum) was applied as coagulant similar to the destabilization study. Firstly, turbidities at different heights of the flotation cell were analyzed. The procedure was similar to the previous section with 300 mL of 2 bars and 4 bars pressurized water. The Al^{3+} concentration of 1 mM, which was the minimum dosage for effective destabilization, was employed at pH of 6.5 - 7.0. The emulsions at 5 minutes after flotation are shown in Figure 6.3. Although the

emulsions seemed to be similar, the turbidity results provided a difference as displayed in Table 6.3. Only turbidity was shown in this case since changes of droplets' size due to the fact that aggregation can influence the turbidity measurement. Even the size distributions of droplets for these emulsions were quite similar, the estimation for oil concentration would provide some errors. Turbidities were solely used for comparing the separation performance.

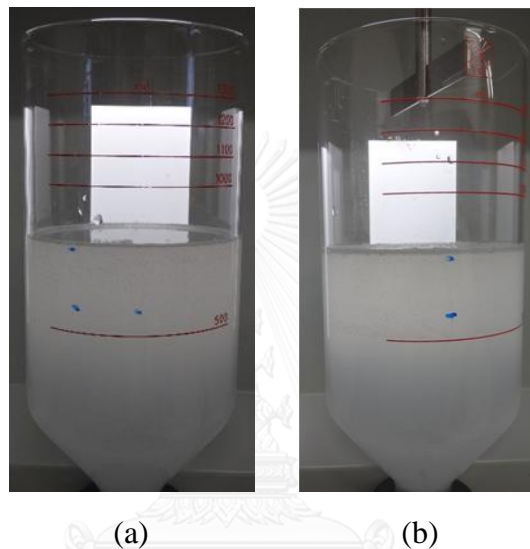


Figure 6.3 Emulsions at 5 minutes after flotation for the pressurized water under (a) 2 bars and (b) 4 bars

From Table 6.3, it can be seen that turbidities were quite similar at different height in both cases suggesting a good mixing condition as in the previous section even with the presence of flocs. Moreover, the difference between two pressure levels can be observed. This suggested the role of bubbles in the separation as the turbidities of emulsion with the presence of bubbles (4 bars) were less than the case without bubbles (2 bars). As indicated in the destabilization study (section 5.3.2.1), zeta potentials of flocs at 1 mM Al^{3+} concentration were close to zero, which could provoke the attachment of flocs on bubbles' surface. The separation performance was enhanced.

Table 6.3 Turbidities (NTU) at different heights after flotation with coagulant addition with the control experiment

Samples	Saturation pressure	
	2 bar	4 bar
initial	733	725
0 - 100 mL	151	112
100 - 200 mL	151	115
200 - 300 mL	150	114
300 - 400 mL	152	114
400 - 500 mL	148	114
500 - 600 mL	147	116
600 - 700 mL	150	113
700 - 800 mL	152	113

Effects of bubbles' number in term of pressurized water volume on the emulsion separation (i.e. 100, 300, and 500 mL) were then determined. In this experiment, the samples were collected from the bottom of the flotation cells at different operation time. The resultant photographs of this experiment are depicted in Figure 6.4 at 5 minutes after the injection of bubbles.

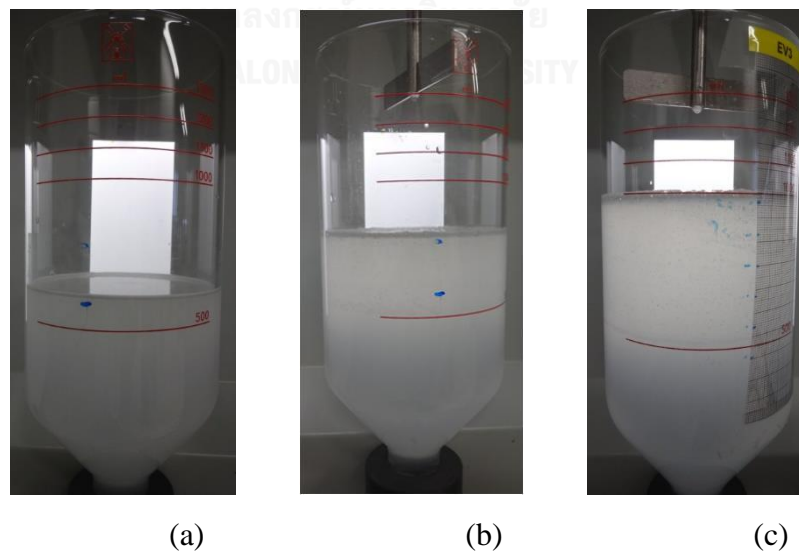


Figure 6.4 Emulsions after flotation with coagulation for 5 minutes with the pressurized water volumes of (a) 100 mL, (b) 300 mL, and (c) 500 mL

Turbidity results are presented in Table 6.4. The results of only destabilization in the flotation cell and destabilization with dilution (by 300 mL of deionized water) are also expressed. The comparison was made at 5 minutes in which bubbles no longer appeared in the flotation cell, and 60 minutes after settling. The decrease of emulsion turbidity can be noticed from every case in Table 6.4. The separation by flotation provided lower turbidities comparing to those obtained from the destabilization with and without dilution. This verified effects of bubbles on the separation. However, the variation in turbidities for different pressurized water volume was merely the influence of the dilution since the distinction was proportional to volume of water injected to the cells. The difference of bubbles' number in this case might be too less to express any influence on the separation.

Table 6.4 Turbidities of the emulsion (NTU) at different time for various volume of pressurized water

Samples	Destabilization	Destabilization with dilution	Pressurized water volume (mL)		
			100	300	500
Initial	736	742	731	724	729
5 minutes	489	310	136	111	89.1
60 minutes	42.3	34.3	36.2	32.7	29.4

Furthermore, the results indicated that the cutting oil emulsion can be separated by the flotation with addition of coagulant. This could be the result from the reduction of charge on droplets' surface by the coagulant, which can be affirmed by the zeta potential. The ξ values of oil flocs in this experiment were in the range of 2 – 5 mV suggesting the decrease of surface charge. Therefore, flocs could attach with bubbles and then separated resulted in a better separation efficiency. Nevertheless, the difference of turbidities among these cases can be obviously noticed after bubbles disappeared and decreased with time. Turbidities were almost similar after 60 minutes in all cases. The separation still took place after the flotation due to the rising velocities of flocs themselves since number of bubbles might be deficient. Flocs were

partly separated by bubbles. This was one limitation of the Flottatest since only small amount of bubbles can be introduced. It is still possible to enhance the flotation efficiency by increasing bubbles in the system with the well awareness on the consumption of water and energy for producing such amount of bubbles. Hence, it can be suggested from the results in this experiment that flotation can only accelerate the separation without improving the efficiency of the destabilization.

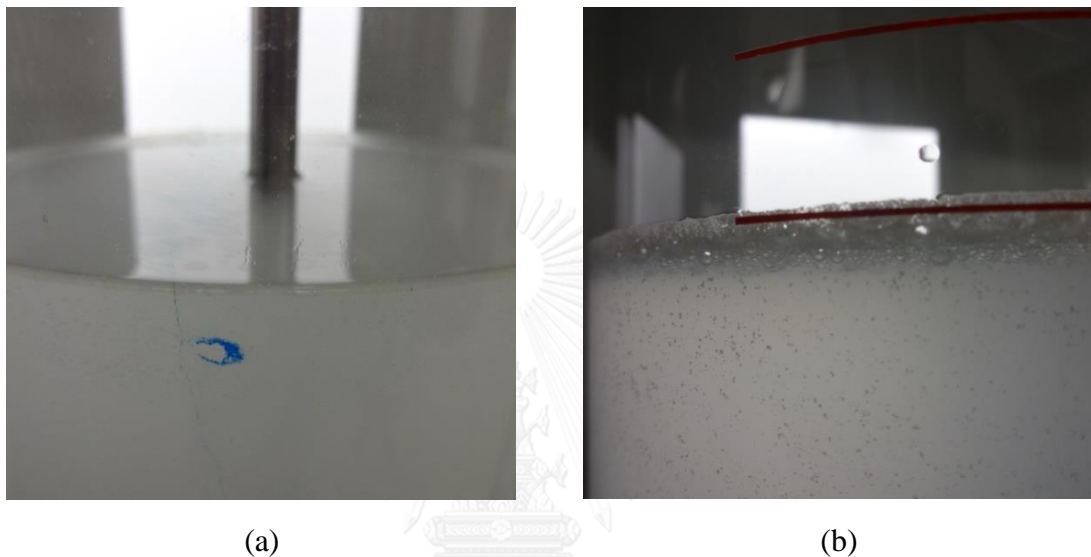


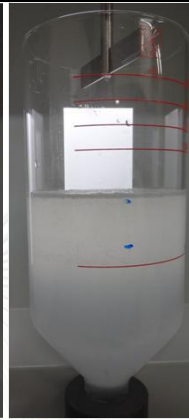

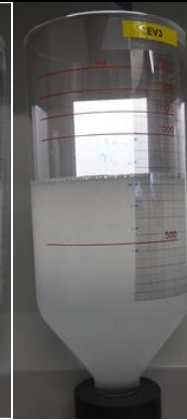


Figure 6.5 Observation of water surface from the flotation with coagulation at (a) 0.75 mM and (b) 1.0 mM Al^{3+} concentrations

Effects of Al^{3+} concentration on the separation performance by flotation after 5 minutes were also investigated as presented in Table 6.5. Without the coagulant, the turbidity was decreased due to dilution as aforementioned. For the 0.75 mM of Al^{3+} , the turbidity was slightly reduced even flocs were unable to be observed. This indicated the separation of larger droplet size with less negative charge due to the addition of the coagulant by bubbles. However, the turbidity was still greater than the cases of higher Al^{3+} concentration above 1.0 mM where flocs appeared. The separation of flocs by bubbles was more effective. It could be suggested that the interaction between bubbles-droplets and bubbles-flocs would be different resulting in dissimilar separation efficiency. A difference at the water surface for the flotation with and without flocs is depicted in Figure 6.5. A layer of oil flocs with attached bubbles can be clearly seen at 1.0 mM Al^{3+} . On the other hands, no distinct layer can

be noticed. The discussion on these different interactions was further investigated in the following experiments.

Table 6.5 Photographs and turbidities of emulsion after 5 minutes for the flotation with addition of coagulant at different concentration (300 mL of pressurized water)

Al^{3+}	0 mM	0.75 mM	1.00 mM	1.25 mM	1.50 mM
Photos					
Turbidity	453 NTU	297 NTU	111 NTU	113 NTU	107U

6.4 Conclusions

The results from flotation test are exhibited in this chapter. The finding from this experiment can affirm the results from the pilot-scale flotation. The flotation alone was unable to separate the cutting oil emulsion. The efficient separation can be obtained when the coagulant was added. No effects of bubble amount by mean of pressurized water volume on the separation can be observed. However, this could be the limitation of Flottatest since it can be only operated as a batch system with small volume of pressurized water.

Moreover, it was found that the application of flotation can only accelerate the separation rate compared to the destabilization without affecting the overall efficiency at 60 minutes. The difference in the separation with and without flocs can be seen. Nevertheless, the separation with flotation at Al^{3+} concentration higher than 1.0 mM was similar. It can be suggested that the difference in the interaction of bubbles-droplets and bubbles-flocs could be responsible for this result. The interaction was therefore investigated in the following section.

CHAPTER 7

OBSERVATION OF BUBBLE-AGGREGATE INTERACTION

7.1 Experimental methods

It is well known that the flotation mainly governed by the particle capture by a bubble. The capture efficiency (E_{capt}) is a product of sub-process efficiencies including collision (E_{coll}), attachment (E_{att}) and stability (E_{sta}), which can be written as $E_{capt} = E_{coll} \cdot E_{att} \cdot E_{sta}$. The interaction between bubbles and particles was therefore important and can affect the flotation performance. As suggested in the previous part, the interaction of bubbles-droplets and bubbles-flocs could be dissimilar resulting in the difference of the flotation performance. This chapter, hence, aimed to prove this presumption by a direct observation on the scenario of a bubble rises through the emulsion with and without flocs.

7.2 Experimental methods

7.2.1 Materials

The water used in this experiment was produced by the Aquasource where particles larger than 1 μm and ions were removed from water respectively by filtration and ion exchange resin. The conductivity of this deionized water was in the range of 0.7 – 1.1 $\mu\text{S}/\text{cm}$ measured by the LF 538 conductivity meter (WTW GmbH). The surface tension of 72.4 mN/m at 20°C was obtained from the du Nuoy ring method.

Glass beads were used for testing the observation device. In this work, spherical glass micro-beads with sizes in the range of 100 – 200 μm were applied. These glass beads were washed by the deionized water twice before using in all the experiments.

The oily emulsion prepared for the observation can be divided into 3 types. Firstly, the cutting oil emulsion at 1 g/L concentration with 0.75 mM Al^{3+} was applied. This emulsion had the zeta potential of -17.4 mV and the average droplet size

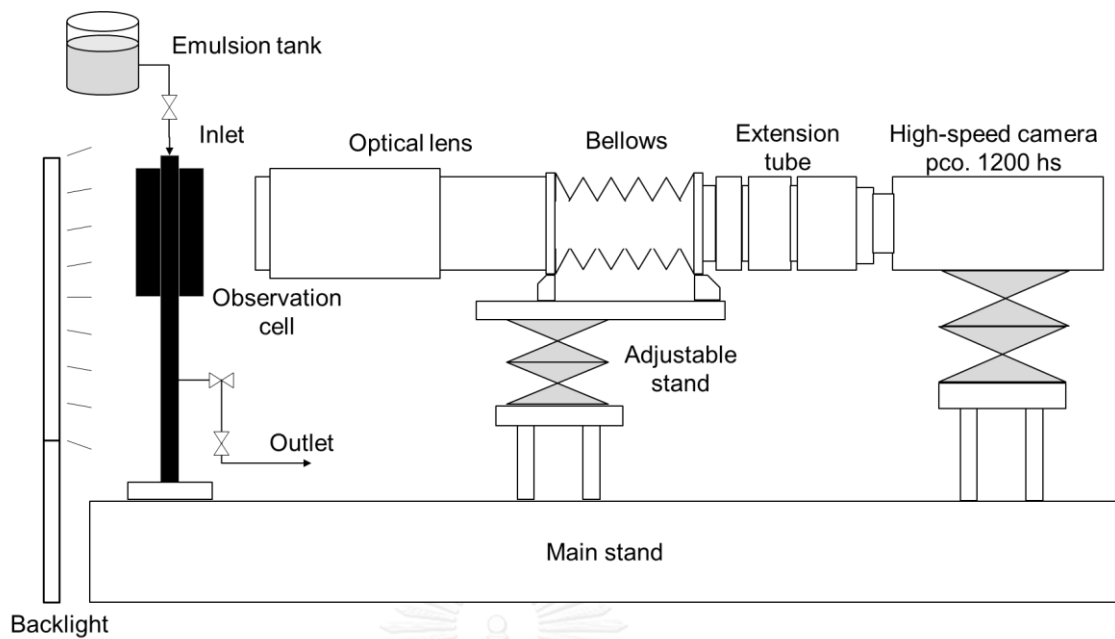
in term of d_{32} as 5.2 μm . Another type of emulsion was the destabilized emulsion with oil flocs containing 2.4 mV zeta potential were then tested.

7.2.2 Observation device

The observation device consisted of 2 parts such as the observation cell and the recording system as illustrated in Figure 7.1. The cell was made of stainless steel in a circular shape with the diameter and thickness of 13 cm and 2 cm, respectively. Two special glasses with low refraction were installed on both sizes as the observed windows with the diameter of 9 cm. The schematic diagram of this observation cell is presented in Figure 7.2. Samples can be introduced and drained out via channels of 0.2 cm in diameter at the top and the bottom of the cell. A screw was placed on each side of the cell to set up the bubble capture system consisting of four thin nylon threads with the diameter of 80 μm to form a diamond grid at the center. This method for capturing bubble can block the rising movement without interfering the interface mobility or occupying the rear part of the bubble where particles can be captured (Huang et al., 2011).

The glass beads suspension and oily emulsion were retained in the beaker placed above the cell by a valve and can be introduced to the cell at the top by gravity flow. The flow rate was regulated by two globe valves at the drainage.

The observation was recorded by high speed camera (10 bit CMOS camera, pco.1200 hs) with high magnification system composed of a Nikon 200 mm lens, Nikon PB-6 Bellows, and Kenko DG Auto extension tube. A backlight with adjustable brightness was placed behind the observation cell to provide sufficient light for the recording.



(a)



(b)

Figure 7.1 (a) schematic diagram and (b) photograph of the observation device set up

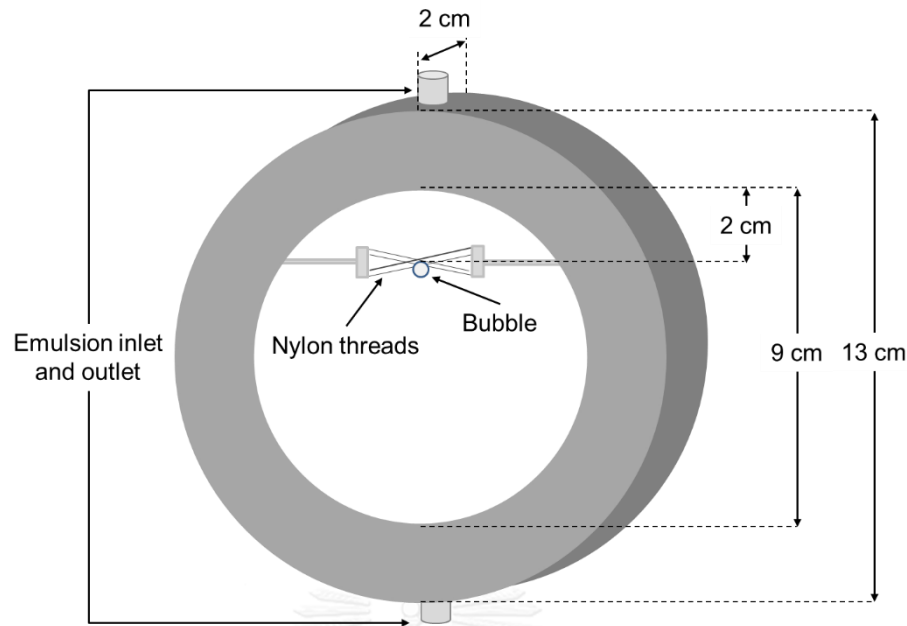


Figure 7.2 Schematic diagram of the observation cell

7.2.3 Experimental procedure

Small bubbles with sizes between 1 – 2.5 mm were released by a needle just beneath the blocking threads. The flow rates of the suspension were controlled to be equal the terminal rising velocity (U_b) of a 1 mm bubble in order to simulate the scenario of a 1 mm bubble rises through the suspension. U_b can be evaluated from Equation 7.1 with the drag coefficient from Equation 1.41 as a function of bubble's Reynolds number ($Re_b = \rho_f U_b d_b / \mu_f$) (Mei et al., 1994). By a trial and error calculation, the rising velocity of 0.31 m/s can be obtained. Note that the bubble Reynolds number in this condition varied in the range 300 – 775. These intermediate Reynolds numbers indicated the existence of a recirculation zone (vortex) or wake close to the rear stagnant point of a bubble (Brennen, 1995). Furthermore, the flow is unstable and the ring vortex starts to oscillate at $Re_b \approx 130$ (Taneda, 1956). The vortices are still close to the bubble surface until $Re_b \approx 500$ (Torobin and Gauvin 1959) before the vortex shedding to the downstream occurs at higher Re_b . It is interesting to note that the flow becomes moderately steady near the wake when vortices are shed forming turbulence at the downstream far from a bubble. The flow around a bubble is quite steady again when Re_b exceeds 1000 (Brennen, 1995).

Moreover, Weber number (We_b) was obtained in the range of 1.3 – 3.3 suggesting that the bubble could be deformed ($We_b > 1$). Bubbles with these sizes could contain ellipsoidal shape, which was affirmed by Bond number (Bo_b) between 0.14 and 0.84. A bubble can be categorized in the ellipsoidal regime when its size is 1.3 – 6 mm and Bo_b of 0.25 – 40 (Clift et al., 1978). An example of captive bubble is depicted in Figure 7.3

$$C_d = \frac{4}{3} \frac{(\rho_b - \rho_f)}{\rho_f} g \frac{d_b}{U_b^2} \quad (7.1)$$

$$C_d = \frac{16}{Re_b} \left(1 + \frac{Re_b}{8 + 0.5(Re_b + 3.315 Re_b^{0.5})} \right) \quad (1.41)$$

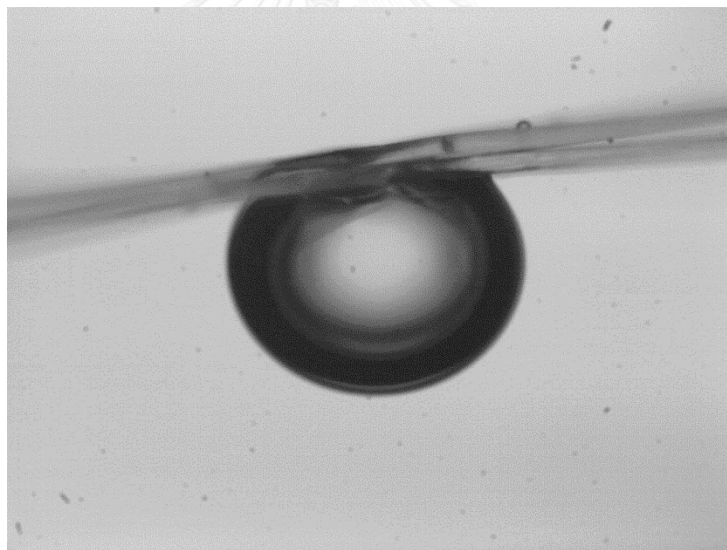


Figure 7.3 Bubble blocked by the capture system ($d_b \approx 1.3$ mm)

Moreover, a velocity profile of the suspension from the entrance to the capture bubble was also taken into account since the entrance is similar to a source embedded in a wall as presented in Figure 7.4.

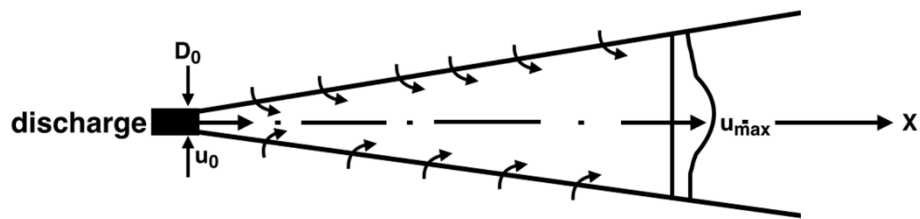


Figure 7.4 Diagram of circular turbulent jet profile

Assuming that the suspension forms the circular jet from the entrance towards the bubble, the jet velocity at the source (u_0) can be estimated from Equation 7.2 where u_{\max} is the centerline velocity at the bubble surface ($u_{\max} = U_b$). D_0 is the diameter of the source equals to 2 mm. The distance from the entrance to the bubble surface (x) is 20 mm.

$$\frac{u_{\max}}{u_0} = 6.2 \frac{D_0}{x} \quad (7.2)$$

The velocity of the suspension at the entrance (u_0) was calculated as 0.50 m/s. Therefore, the flow rate of 95 ml/min measured at the entrance channel was applied for feeding the suspension and the emulsion to the observation cell.

Examples of the emulsion flow in the observation cell recorded by a digital camera Sony Cyber-shot DSC-WX100 are presented in Figure 7.5.

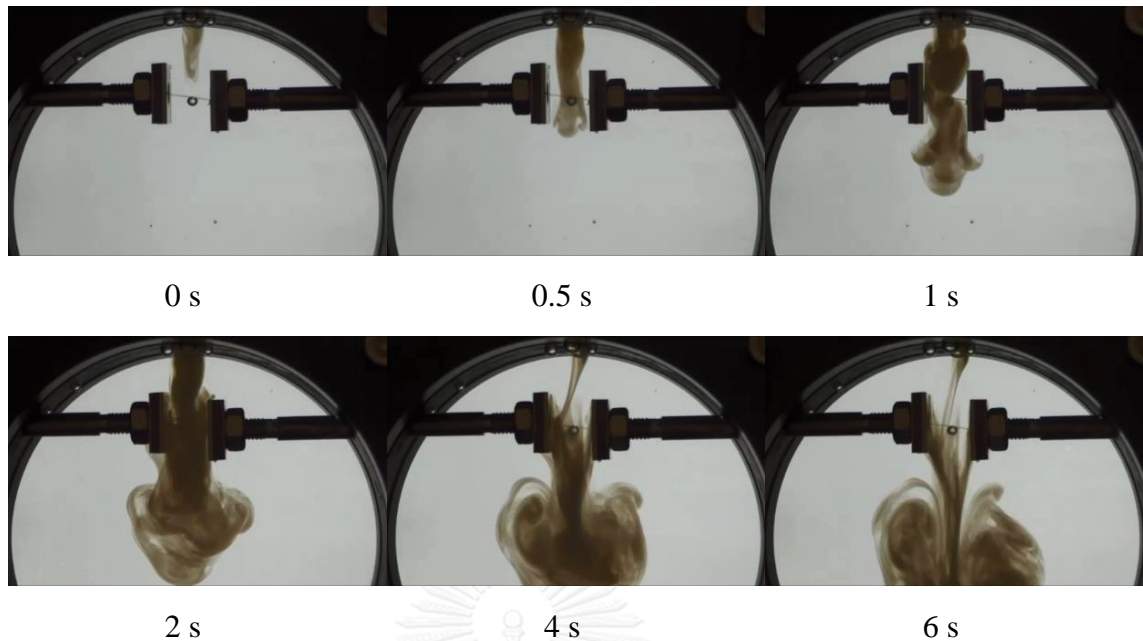


Figure 7.5 Flow of the cutting-oil emulsion in the observation cell at the flow rate of 95 mL/min

7.3 Results and discussions

7.3.1 Observation of bubble and glass beads interaction

Figure 7.6 presents images of a glass bead moving around a bubble ($d_b = 2.4$ mm, $Re_b \approx 744$) recorded at 448.2 frames/s. The time interval of each frame was 22 milliseconds. The cluster of particles captured at the rear part of the bubble can be clearly notice. The multilayer adhesion of glass beads on bubble surface occurred in this case.

Furthermore, it can be seen that a glass bead moving towards the bubble at the front part before approaching the bubble surface as in Frame 2. The bead slipped on the interface but not adhere to the bubble. Eventually, the glass bead left the bubble after passed the bubble equator (Frame 5). According to Nguyen (2011), the flow streamlines around a bubble with intermediate Reynolds number deviate from the cases of Stokes flow ($Re_b \rightarrow 0$) and potential flow ($Re_b \rightarrow \infty$) as shown in Figure 7.7. Typically, the flow fields around a bubble in both Stokes flow and potential flow regimes are considered to be symmetric with respect to the equatorial plane of a bubble, i.e. fore-and-aft symmetric. However, the streamlines are compressed at the

front part of a bubble before changing their direction away from a bubble before reaching the equator (Nguyen, 1999). This asymmetric flow field is related to the formation of vortex as aforementioned. The colliding area is therefore limited from the entire hemisphere to only the front part of a bubble as presents in Figure 7.8. However, the collision area could be expanded if the colliding particle is subjected to the inertia effect. The particle could graze the surface at the bubble equator.

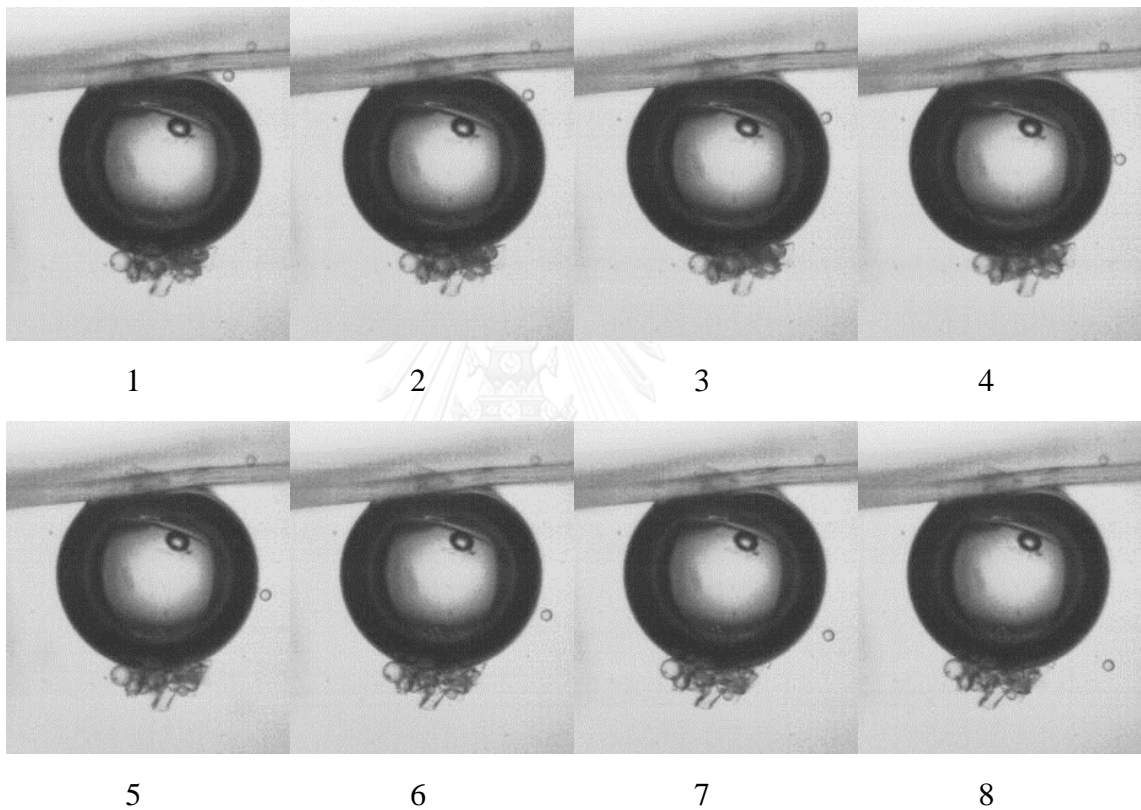


Figure 7.6 Images of a glass bead moving around a captured bubble ($d_b = 2.4$ mm, $Re_b \approx 744$) at every 22 milliseconds

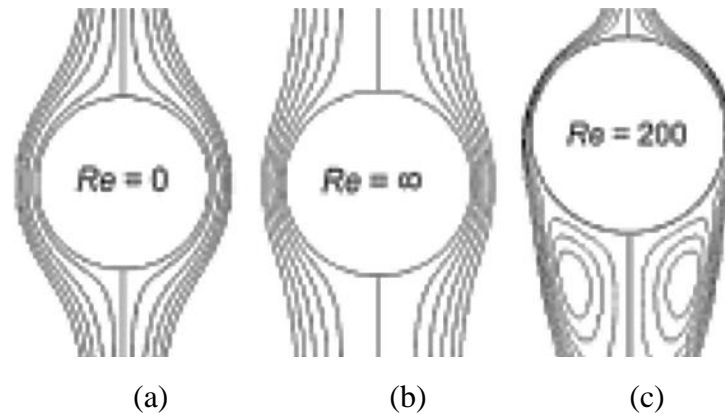


Figure 7.7 Flow streamlines around a bubble different Re_b regime (a) $Re_b \rightarrow 0$ (Stokes flow), (b) $Re_b \rightarrow \infty$ (potential flow), and (c) intermediate Re_b (Nguyen, 2011)

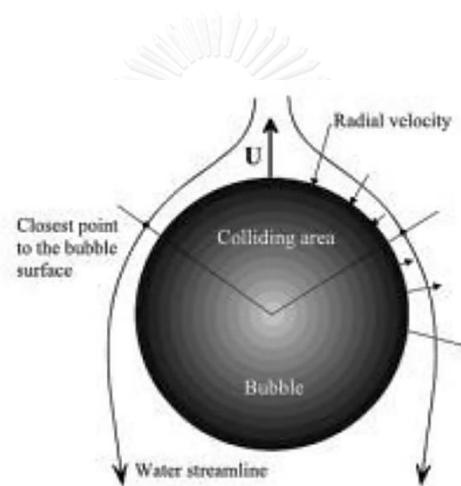


Figure 7.8 Colliding area of a bubble at intermediate Reynolds number with asymmetric flow streamline (Nguyen, 2011)

Apart of the change of streamline that affect the collision, glass beads were also subjected to the gravitational and inertia effects as indicated by the dimensionless settling velocity ($u_s = 0.44$) and Stokes number ($St_p = 0.81$). Particles are unlikely to follow the streamline and could deviate from the bubble surface.

In addition, the oscillation of the adhered agglomerate of glass beads along the bubble surface can be observed. This could be an effect of a vortex formed at the rear part of the bubble due to the liquid flow at intermediate Reynolds number.

7.3.2 Observation of bubble and oil droplet interaction

The interaction between bubble and droplet was observed when the emulsion was introduced into the cell. The record was carried out at 293.7 frames/s. Images at every second are exhibited in Figure 7.9. It can be seen that the emulsion flowed through a bubble with $d_b = 2.06$ mm and $Re_b \approx 639$. However, no layer of emulsion adhered on bubble surface can be seen. It can be suggested that oil droplets cannot be captured by a bubble. From the calculation, oil droplets with this size contained St_p of 6.5×10^{-10} and u_s of 6×10^{-4} indicating no effects of inertia and gravitational settling can be expected. Droplets tended to follow the streamline around a bubble. No contact would occur if the streamline is not close to the bubble enough for droplets to graze the surface.

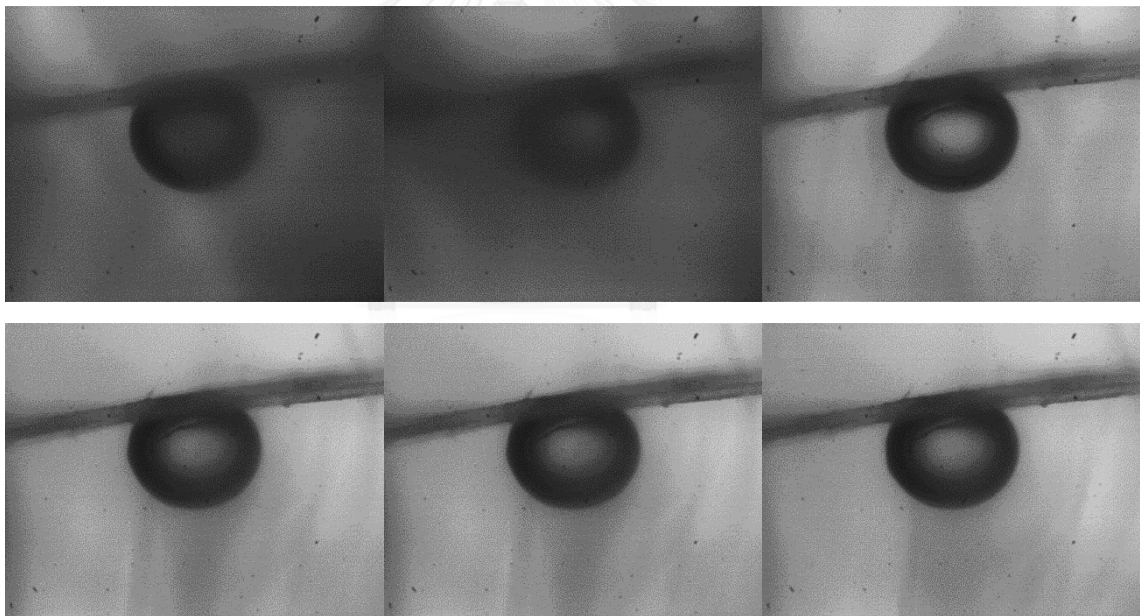


Figure 7.9 Images of the emulsion flow around a bubble ($d_b = 2.1$ mm, $Re_b \approx 651$) every second

The electrostatic interaction between droplets and a bubble would be another reason. Generally, air bubbles contain negative surface charges at this pH range (Yang et al., 2001; Li and Somasundaran, 1992). The repulsion could occur since droplets still contained negative charges suggesting by its zeta potential. Therefore, droplets and a bubble was unable to get close enough for the capture to exist.

7.3.3 Observation of bubble and oil floc interaction

In contrast with the oily emulsion, the capture of oil flocs on the bubble surface can be observed. Images of this observation were captured at 293.7 frames/s as shown in Figure 7.10. Flocs could approach the bubble surface as the zeta potential of oil flocs was near the iso-electric point. The repulsion could be decreased resulting in the higher possibility of the attachment of oil droplets on a bubble. Furthermore, the adhered flocs can move along the bubble surface without detaching due to the impact of liquid flow around the bubble. It indicated the stability of the agglomerate between a bubble and flocs. From these results, it can be suggested that the capture of oil flocs by a bubble can occur.

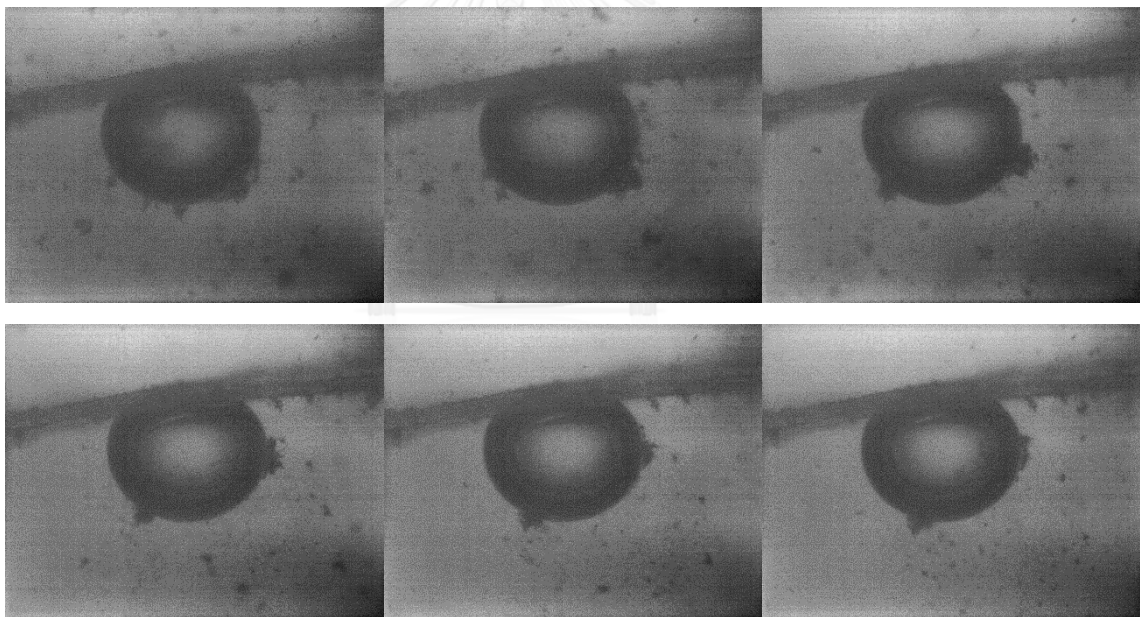


Figure 7.10 Images of oil flocs flow around a bubble ($d_b = 2.1$ mm, $Re_b \approx 651$) every second

7.4 Conclusions

The results from this chapter affirmed that the interactions of bubbles to droplets and bubbles to oil flocs were dissimilar. Oil droplets can be rarely captured by a bubble. On the other hands, the adhered flocs on the bubble surface can be

observed. This results in the difference of flotation performance for the destabilized cutting-oil emulsion with and without floc. To achieve the effective separation by flotation, the addition of coagulant to destabilize the emulsion is necessary. Furthermore, the results also emphasized effects of the characteristics of the targeted particle on the flotation. In this work, the characteristics of oil droplets and oil flocs were very distinct as well as the separation efficiency.



CONCLUSIONS AND PERSPECTIVES

Conclusions

The objective of this work was to study the separation of the cutting oil emulsion by coalescer and flotation processes. The results can be concluded as:

- The synthesized cutting oil emulsion in deionized water contained droplet sizes in nanoscale range (174 nm). Combining with its high negative zeta potential (-65.8 mV), it can be suggested that this emulsion had high stability. The characteristics of the emulsion prepared from tap water were quite similar but with larger oil droplets (444 nm) and lower zeta potential (-48.4 mV) due to effects of ions present in tap water. However, this emulsion was still stable. Oil droplets in these emulsions were unlikely to separate themselves. A separation process was required.
- The highest efficiency of coalescer in this work was 44% obtained from the 10 cm bed of tubular PP media with the emulsion flow velocity of 2 cm/s. Media shape and bed porosity can affect the separation mechanisms occurred in the media bed.
- The dissimilar in bubble sizes between the two flotation processes IAF and DAF resulted in different hydrodynamic conditions and flow behaviors in the flotation cell. However, these difference did not affect the separation performance as the efficiencies of 85% can be achieved from both continuous IAF and DAF only with the addition of 220 mg/L aluminium sulfate ($\text{Al}_2(\text{SO}_4)_3$) as the coagulant. Without the coagulation, the separation cannot be observed. Destabilization of the emulsion was an important factor for the effective separation.
- The optimal operating condition from this work can be found as concluded.

Parameter	DAF	IAF
Overflow rate ($\text{m}^3/(\text{m}^2 \cdot \text{min})$)	0.10	0.10
Air to oil ratio (L air/g oil)	0.004 – 0.008	2.5 – 4.0
Contact time (min)	3.6	0.9

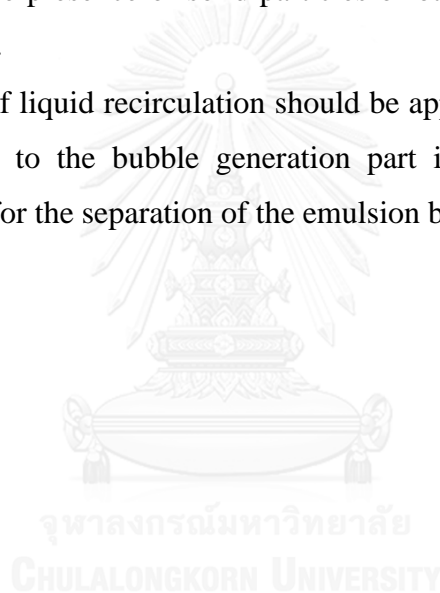
Due to the fact that similar efficiency can be achieved, IAF should be preferred since it requires less energy consumption, shorter contact time, and more simplicity for the bubble generation than the DAF.

- From the destabilization study, it was found that pH and coagulant dosage can affect the destabilization mechanism. The optimal condition was obtained at the Al^{3+} concentration of 1.0 mM in the pH range of 6.5 – 7.5 where the formation of flocs can be noticed. The effective destabilization was a result of the sweep flocculation rather than the coalescence of droplets. Flocs were analyzed to affirm the formation of aluminium hydroxide ($\text{Al}(\text{OH})_3$), which plays an important role in the destabilization by sweep flocculation.
- The results from the bench scale flotation test confirmed those findings from the pilot scale experiments. It convinced the importance of the destabilization of the emulsion before flotation for the efficient separation. Nevertheless, no influences of the coagulant addition beyond 1.0 mM on the separation efficiency can be noticed.
- The observation on the interaction between bubbles and oil droplets suggested that no attachment occurred on the bubble surface. On the contrary, the capture of oil floc at the rear part of the bubble can be observed. This emphasized the difference on the interactions, which played a major role in the separation of oily emulsion by flotation.

Perspectives

The results presented in this work suggests that flotation, both DAF and IAF, can efficiently separate the cutting oil emulsion despite the generation of bubbles with different sizes.

- Further study on the flotation mechanisms, particularly the collision of droplets or flocs with a bubble, should be carried out for investigating effects of numerous parameters on the mechanism in the local scale. A simulation of the aggregates' movement could be conducted.
- The separation of the cutting oil emulsion from the real discharge should be tested since the presence of solid particles or other contaminants could affect the separation.
- The concept of liquid recirculation should be applied. The treated water could be introduced to the bubble generation part in order to reduce the water consumption for the separation of the emulsion by DAF.



REFERENCES

- Ahmad, A.L., Sumathi, S., and Hameed, B.H. 2006. Coagulation of residue oil and suspended solid in palm oil mill effluent by chitosan, alum, and PAC. Chemical Engineering Journal. 118: p. 99–105.
- Akers, R.J. and Ward, A.S. 1977. Liquid filtration theory and filtration pretreatment, in Filtration Principles and Practices, Part I. Dekker, New York, US.
- Al-Shamrani, A.A., James, A., and Xiao, X. 2002. Separation of oil from water by dissolved air flotation. Colloids and Surfaces A: Physicochemical and Engineering Aspects. 209: p. 15–26.
- Allen, T. 1997. Particle size measurement Volume 1. 5th ed. ed. Chapman & Hall, London, U.K.
- American-Public-Health-Association and American-Water-Works-Association-and-Water-Pollution-Control-Federation. 1998. Standard methods for the examination of water and wastewater. 20th ed. ed. U.S.
- Aurelle, Y. 1985. Treatments of oil-containing wastewater. Department of Sanitary Engineering, Chulalongkorn University, Bangkok, Thailand.
- Bansal, S., Von Arnim, V., Stegmaier, T., and Planck, H. 2011. Effect of fibrous filter properties on the oil-in-water-emulsion separation and filtration performance. Journal of Hazardous Materials. 190: p. 45-50.
- Benitez, J. 2009. Principles and modern applications of mass transfer operations. 1st ed ed. Wiley-Interscience, U.S.
- Bensadok, K., Belkacem, M., and Nezzal, G. 2007. Treatment of cutting oil /water emulsion by coupling coagulation and dissolved air flotation. Desalination. 206: p. 440-448.
- Bensadok, K., Benammar, S., Lapique, F., and Nezzal, G. 2008. Electrocoagulation of cutting oil emulsions using aluminium plate electrodes. Journal of hazardous materials. 152: p. 423-430.
- Blazy, P. and Jdid, E.A. 2000. Flottation: Aspects pratiques. Techniques de l'ingénieur. Génie des proceeds. J3(J3360): p. J3360.1-J3360.22.
- Boothroyd, G. and Knight, W.A. 2006. Fundamentals of machining and machine tools. CRC Press., Boca Raton, US.
- Bratby, J. 2006. Coagulation and flocculation in water and wastewater treatment. 2nd ed ed. IWA Publishing, London, UK.
- Brennen, C.E. 1995. Cavitation and bubble dynamics. Oxford University Press, U.S.
- Brosset, C. 1952. On the reactions of the aluminium ion with water. Acta Chemica Scandinavica. 6: p. 910-940.
- Bushell, G.C., Yan, Y.D., Woodfield, D., Raper, J., and Amal, R. 2002. On techniques for the measurement of the mass fractal dimension of aggregates. Advances in Colloid and Interface Science. 95: p. 1-50.
- Byers, J.P. 2006. Laboratory evaluation of metalworking fluids, in: J.P. Byers (Ed.), Metalworking fluids. 2nd ed. ed. Taylor & Francis group, U.S.
- Cañizares, P., Martínez, F. Jiménez, C., Sáez, C., and Rodrigo, M.A. 2008. Coagulation and electrocoagulation of oil-in-water emulsions. Journal of Hazardous Materials. 151: p. 44-51.
- Cañizares, P., Martínez, F., Jiménez, C., Lobato, J., and Rodrigo, M.A. 2006. Comparison of the aluminium speciation in chemical and electrochemical

- dosing processes. Industrial & Engineering Chemistry Research. 45: p. 8749-8756.
- Carman, P.C. 1956. Flow of gases through porous media. Academic Press, New York, US.
- Cheng, C., Phipps, D., and Alkhaddar, R.M. 2005. Review treatment of spent metalworking fluids. . Water research. 39: p. 4051-4063.
- Cheremisinoff, N.P. 1998. Liquid filtration. 2nd ed. ed. Butterworth-Heinemann, Oxford, UK.
- Chieu, J.N., Schechter, R.S., Humenick, M.J., and Gloyna, E.F. 1975. Coalescence of emulsified wastes by fibrous bed. Technical Report EHE-75-05, CRWR-126. Department of Civil Engineering, University of Texas, Texas, U.S.
- Clift, R., Grace, J.R., and Weber, M.E. 1978. Bubbles, Drops and Particles. New York : Dover Publications, U.S.
- Coates, J. 2000. Encyclopedia of Analytical Chemistry. John Wiley & Sons Ltd, U.K.
- Coulson, J.M., Richardson, J.F., J.R., B., and Harker, J.H. 2002. Chemical Engineering Volume 2. 5th ed. ed. Butterworth-Heinemann, Oxford, U.K. .
- Cuenot, B., Magnaudet, J., and Spennato, B. 1997. The effects of slightly soluble surfactants on the flow around a spherical bubble. Journal of Fluid Mechanics. 339: p. 25-53.
- da Rosa, J.J. and Rubio, J. 2005. The FF (flocculation–flotation) process. Minerals Engineering. 18: p. 701-707.
- Dani, A., *Transfert de masse entre une bulle et un liquide : simulations numeriques directes et fluorescence induite par nappe laser*. 2007, Institut National des Sciences Appliquees de Toulouse: French.
- de Sena, R.F., Moreira, R.F.P.M., and Jose, H.J. 2008. Comparison of coagulants and coagulation aids for treatment of meat processing wastewater by column flotation. Bioresource Technology 99: p. 8221-8225.
- Dentel, S.K. 1991. Coagulant control in water treatment. Critical Reviews in Environmental Control 21: p. 41-135.
- Derjaguin, B.B. and Dukhin, S.S. 1961. Theory of flotation of small and medium size particles. Transactions of The Institution of Mining and Metallurgy. 70(221-246).
- Du, X., Wang, Y., Su, X., and Li, J. 2009. Influences of pH value on the microstructure and phase transformation of aluminium hydroxide. Powder Technology. 192: p. 40-46.
- Duan, J. and Gregory, J. 2003. Coagulation by hydrolysing metal salts. Advances in Colloid and Interface Science. 100-102: p. 475-502.
- Edzwald, J.K. 2010. Dissolved air flotation and me. Water Research. 44: p. 2077-2106.
- El Baradie, M.A. 1996. Cutting fluids: part I. Characterization. Journal of Material Processing Technology 56: p. 786-797.
- El Baradie, M.A. 1996. Cutting fluids: part II. Recycling and clean machining. Journal of Material Processing Technology. 56: p. 798-806.
- Elaissari, A. and Pefferkorn, E. 1991. Aggregation modes of colloids in the presence of block copolymer micelles. Journal of Colloid and Interface Science. 143: p. 343-355.

- Essadki, A.H., Gourich, B., Vial, C., and Delmas, H. 2011. Residence time distribution measurements in an external-loop airlift reactor: Study of the hydrodynamics on the liquid circulation induced by the hydrogen bubbles. Chemical Engineering Science. 66: p. 3125-3132.
- Fogler, H.S. 2005. Elements of chemical reaction engineering. 4th ed. ed. Pearson Education, Inc., U.S.
- Foust, A.S., Wenzel, L.A., Clump, C.W., Maus, L., and Andersen, L.B. 1980. Principles of unit operations. 2nd ed. ed. John Wiley & Sons, Inc., Canada.
- Fratiello, A., Lee, R.E., Nishida, V.M., and Schuster, R.E. 1968. Proton magnetic resonance coordination number study of Al(III), Be(II), Ga(III), In(III), and Mg(II) in water and aqueous solvent mixtures. Journal of Chemical Physics 48: p. 3705-3711.
- Gillberg, L., Hansen, B., Karlsson, I., Nordströmm, E.A., and Pålsson, A. 2003. Water treatment. Kemira Kemwater, Sweden.
- Gleabey, C.A., Horgan, G.W., and Darbyshire, J.F. 1991. Image analysis and three-dimensional modeling of pores in soil aggregates. Journal of Soils. 42(3): p. 479-486.
- Graff, M. 2012. Disposal of metalworking fluids. Woodhead Publishing Limited, UK.
- Greely, M. and Rajagopalan, N. 2004. Impact of environmental contaminants on machining properties of metal working fluids. Tribology International. 37: p. 327-332.
- Gregory, J. 2009. Optical monitoring of particle aggregates. Journal of Environmental Sciences. 21: p. 2-7.
- Grzesik, W. 2008. Cutting fluids. Advanced machining processes of metallic materials: Theory, modeling, and application. Elsevier, U.S.
- Hadamard, J.S. 1911. Mouvement permanent lent d'une sphère liquide et visqueuse dans un liquide visqueux. Comptes Rendus de l'Académie des Sciences Paris 152: p. 1735-1738.
- Harif, T., Khai, M., and Adin, A. 2012. Electrocoagulation versus chemical coagulation: Coagulation/flocculation mechanisms and resulting floc characteristics. Water Research. 46: p. 3177-3188.
- Hayden, P.L. and Rubin, A.J. 1974. Aqueous-Environmental chemistry of metals. Ann Arbor Science Publishers, U.S.
- Hazlett, R.N. 1969. Fibrous bed coalescence of water: Steps in the coalescence process. Industrial & Engineering Chemistry Fundamentals. 8: p. 625-632.
- Hendricks, D.W. 2006. Water treatment unit processes: Physical and chemical. CRC/Taylor & Francis, U.S.
- Hilal, N., Busca, G., Hankins, N., and Mohammad, A.W. 2004. The use of ultrafiltration and nanofiltration membranes in the treatment of metal-working fluids. Desalination. 167: p. 227-238.
- Holt, P.K., Barton, G.W., and Mitchell, C.A. 2005. The future for electrocoagulation as a localised water treatment technology. Chemosphere 59: p. 355-367.
- Hsu, J.P. and Liu, B.T. 1999. Stability of colloidal dispersions: charge regulation/adsorption model. Langmuir. 15: p. 5219-5226.
- Huang, Z., *Efficacité de capture dans les procédés de flottation*. 2009, INSA Toulouse: France.

- Ikeda, T., Hirata, M., and Kimura, T. 2006. Hydrolysis of Al^{3+} from constrained molecular dynamics. Journal of Chemical Physics 124: p. 074503-1-074503-7.
- Jarvis, P., Parsons, S.A., Henderson, R., Nixson, N., and Jefferson, B. 2008. The practical application of fractal dimension in water treatment practice-the impact of polymer dosing. Separation Science and Technology. 43: p. 1785-1797.
- Ji, F., Li, C., Dong, X., Li, Y., and Wang, D. 2009. Separation of oil from oily wastewater by sorption and coalescence technique using ethanol grafted polyacrylonitrile. Journal of Hazardous Materials. 164: p. 1346-1351.
- Juneja, B.L., Sekhon, G.S., and Seth, N. 2003. Fundamentals of metal cutting and machine tools. 2nd ed. ed. New Age International (P) Ltd., Delhi.
- Khemis, M., Leclerc, J.P., Tanguay, G., Valentin, G., and Lapique, F. 2006. Treatment of industrial liquid wastes by electrocoagulation: experimental investigations and an overall interpretation model. Chemical Engineering Science. 61: p. 3602-3609.
- Khiewpuckdee, P., *Treatment of oily wastewater by ultrafiltration process*. 2012, Chulalongkorn University.
- Kim, B.R., Matz, M.J., and Lipari, F. 1989. Treatment of a metal-cutting-fluids wastewater using an anaerobic GAC fluidized-bed reactor. Journal of the Water Pollution Control Federation 1989: p. 1430-1439.
- Kim, B.R., Zemel, J.F., Anderson, S.G., Stroup, D.P., and Rai, D.N. 1992. Anaerobic removal of COD in metal-cutting-fluid wastewater. Water Environment Research. 61: p. 216-222.
- Kitchener, J.A. 1985. The froth flotation process: Past, present, and future-in brief. In: The Scientific Basis of Flotation, Part 1. NATO Advances Study Institute: p. 1-26.
- Kobyas, M., Ciftci, C., Bayramoglu, M., and Sensoy, M.T. 2008. Study on the treatment of waste metal cutting fluids using electrocoagulation. Separation and Purification Technology. 60: p. 285-291.
- Kulkarni, P.S., Patel, S.U., and Chase, G.G. 2012. Layered hydrophilic/hydrophobic fiber media for water-in-oil coalescence. Separation and Purification Technology. 85: p. 157-164.
- Letterman, R.D., Tabatabaie, R.S., and Ames Jr., R.S. 1979. Effects of the bicarbonate ion concentration on flocculation with aluminium sulfate. Journal of the American Water Works Association. 7-8: p. 467-473.
- Levenspiel, O. 1999. Chemical reaction engineering. 3rd ed. ed. John Wiley & Sons, Inc., U.S.
- Levich, L.G. 1962. Physicochemical Hydrodynamics. Englewood Cliffs, NJ: Prentice-Hall, U.S.
- Levin, I. and Brandon, D.G. 1998. Metastable alumina polymorphs: crystal structures and transition sequences. Journal of American Ceramics Society. 81: p. 1995-2012.
- Li, C., Somasundaran, P. 1992. Reversal of bubble charge in multivalent inorganic salt solutions – effect of aluminum. Journal of Colloid and Interface Science. 148(2): p. 587-591.
- Li, J. and Gu, Y. 2003. Coalescence of oil-in-water emulsions in fibrous and granular beds. Separation and Purification technology. 42(1): p. 1-13.

- Lin, M.Y., Lindsay, H.M., Weitz, D.A., Klein, R., Ball, R.C., and Meakin, P. 1990. Universal diffusion-limited colloid aggregation. Journal of Physics: Condensed Matter. 2: p. 2090-3113.
- Loubière, K. and Hébrard, G. 2003. Bubble formation from a flexible hole submerged in an inviscid liquid. Chemical Engineering Science. 58: p. 135-148.
- Magiera, R. and Blass, E. 1997. Separation of liquid-liquid dispersions by flow through fibre beds. Filtration & Separation. 34: p. 369-376.
- Maiti, S., Mishra, I.M., Bhattacharya, S.D., and Joshi, J.K. 2011. Removal of oil from oil-in-water emulsion using a packed bed of commercial resin. Colloids and Surfaces A: Physicochemical and Engineering Aspects. 389: p. 291-298.
- Mathavan, G.N. and Viraraghavan, T. 1992. Coalescence/filtration of an oil-in-water emulsion in a peat bed. Water Research. 26: p. 91-98.
- Matis, K.A. 1995. Flotation science and engineering. Marcel Dekker, U.S.
- Mavros, P. and Matis, K.A. 1992. Innovations in flotation technology. Kluwer academic publishers, The Netherlands.
- McCabe, L.W., Smith, J.C., and Harriott, P. 2000. Unit operations of chemical engineering. 6th ed. ed. Mcgraw-Hill Publ. Comp, New York, US.
- Meher, T., Basu, A.K., and Ghatak, S. 2005. Physicochemical characteristics of alumina gel in hydroxyhydrogel and normal form. Ceramic International. 31: p. 831-838.
- Mei, R., Klausner, J.F., and Lawrence, C.J. 1994. A note on the history force on a spherical bubble at finite Reynolds number. Physics Fluids. 6: p. 418-420.
- Meysami, B. and Kasaeian, A.B. 2005. Use of coagulants in treatment of olive oil wastewater model solutions by induced air flotation. Bioresource Technology 96: p. 303-307.
- Mittal, K.L. 2009. Contact angle, wettability and adhesion. 6th ed. ed. VSP: Leiden, The Netherlands.
- Moore, D.W. 1963. The boundary layer on a spherical gas bubble. Journal of Fluid Mechanics. 16: p. 161-176.
- Moosai, R. and Dawe, R.A. 2003. Gas attachment of oil droplets for gas flotation for oily wastewater cleanup. Journal of Separation and Purification Technology. 33: p. 303-314.
- Nguyen, A.V. 1999. Hydrodynamics of liquid flows around air bubbles in flotation: a review. International Journal of Mineral Processing. 56: p. 161-205.
- Nguyen, A.V. 2011. Particle-Bubble interaction in flotation, in Bubble and drop interfaces. VSP, The Netherlands.
- Nguyen, A.V., Schulze, H.J., and Ralston, J. 1997. Elementary steps in particle-bubble attachment. International Journal of Mineral Processing. 51: p. 183-195.
- Occupational-safety-and-health-administration and Metalworking-fluids-standard-advisory-committee. 1999. Metalworking fluids: safety and health best practices manual. [Online]. Available from: <http://www.osha.gov> 2009, July 20th]
- Oliveira, R.C.G., Gonzalez, G., and Oliveira, J.F. 1999. Interfacial studies on dissolved gas flotation of oil droplets for water purification. Colloids and Surfaces A: Physicochemical and Engineering Aspects. 154: p. 127-135.

- Oseen, C.W. 1910. Ueber die Stokessche Formel und uber eine verwandte A b e in der Hydrodynamikb. Arkiv för Matematik, Astronomi och Fysik. 6(29): p. 154-160.
- Painmanakul, P., Loubiere, K., Hebrard, G., and Buffiere, P. 2004. tudy of different membrane spargers used in wastewater treatment: characterization and performance. Chemical Engineering and Processing. 43: p. 1347-1359.
- Painmanakul, P., Loubière, K., Hébrard, G., Peuchot, M., and Roustan, M. 2005. Effect of surfactants on liquid-side mass transfer coefficients. Chemical Engineering Science. 60: p. 6480-6491.
- Painmanakul, P., Sastaravet, P., Lersjintanakarn, S., and Khaodhiar, S. Effect of bubble hydrodynamic and chemical dosage on treatment of oily wastewater by induced air flotation (IAF) process. Chemical Engineering Research and Design. 88 (693-702).
- Perez, M., Rodriguez-Cano, R., Romero, J.I., and Sales, D. 2006. Anaerobic thermophilic digestion of cutting oil wastewater: effect of co-substrate. Biochemical Engineering Journal. 29: p. 250-257.
- Pinotti, A. and Zaritzky, N. 2001. Effect of aluminium sulfate and cationic polyelectrolytes on the destabilization of emulsified wastes. Waste Management 21: p. 535-542.
- Prommajun, C., *Treatment of cutting oily-wastewater by electro-coagulation/flotation process in external-loop airlift reactor*. 2012, Chulalongkorn University.
- Pyke, B., Fornasiero, D., and Ralston, J. 2003. Bubble particle heterocoagulation under turbulent conditions. Journal of Colloid and Interface Science. 265: p. 141-151.
- Rabenstein, A., Thomas, K.T., Markko, R., Ekkard, B., and Jan, K. 2009. Microbial degradation of water miscible metal working fluids. International Biodeterioration & Biodegradation. 63: p. 1023-1029.
- Rachu, S., *Computer program development for oily wastewater treatment process selection, design and simulation*. 2005, INSA-Toulouse: French.
- Ralston, J. and Dukhin, S.S. 1999. The interaction between particles and bubbles. Colloids and Surfaces A: Physicochemical and Engineering Aspects. 151: p. 3-14.
- Ralston, J., Dukhin, S.S., and Mishchuk, N.A. 1999. Inertial hydrodynamic particle-bubble interaction in flotation. International Journal of Mineral Processing. 56(a): p. 207-256.
- Ralston, J., Dukhin, S.S., and Mishchuk, N.A. 2002. Wetting film stability and flotation kinetics. Advances in Colloid and Interface Science 95: p. 145-256.
- Rawle, A. 2003. Basic principles of particle size and analysis. Surface Coatings International. Part A, Coatings Journal. 86(2): p. 58-65.
- Rhodes, M. 2008. Introduction to particle technology. 2nd ed. ed. John Wiley & Sons, Ltd., U.K.
- Riesgraf, D.A. and May, M.L. 1978. Infrared spectra of aluminium hydroxide chlorides. Applied Spectroscopy. 32: p. 362-366.
- Rios, G., Pazos, C., and Coca, J. 1998. Destabilization of cutting oil emulsions using inorganic salts as coagulants. Physicochemical and Engineering Aspects. 138: p. 383-389.

- Rojvilavan, N., *Treatment of cutting oil wastewater by electro-coagulation and photo electro Fenton process*. 2012, Chulalongkorn University.
- Rubio, J., Souza, M.L., and Smith, R.W. 2002. Overview of flotation as a wastewater treatment technique. Mineral Engineering. 15: p. 139-155.
- Rybczynski, W. 1911. On the translatory motion of a fluid sphere in a viscous medium. Bultein of the Academy of Sciences, Cracow, series A: p. 40.
- Sabreen, S.R. 1991. Surface wetting & pretreatment methods. The Sabreen group, Inc., U.S.
- Sadhil, S.S. and Johnson, R.E. 1983. Stokes flow past bubbles and drops partially coated with thin films. Journal of Fluid Mechanics. 126: p. 237-247.
- Sam, A., Gomez, C.O., and J., F. 1996. Axial velocity profiles of single bubbles in water/frother solution. Journal of Mineral Processing. 47: p. 177-196.
- Sarrot, V., *Capture de fines particules par des inclusions fluides*. 2006, Institut National des Sciences Appliquees de Toulouse: France.
- Sarrot, V., Huang, Z., Legendre, D., and Guiraud, P. 2007. Experimental determination of particles capture efficiency in flotation. Chemical Engineering Science. 62: p. 7359-7369.
- Saukkoriipi, J., *Theoretical study of the hydrolysis of aluminium complexes*. 2010, University of Oulu: Finland.
- Savic, P. 1953. Circulation and distortion of liquid drops falling through a viscous medium. Technical Report MT-22. National Research Council Canada, Division of Mechanical Engineering,
- Schiller, L. and Nauman, A. 1935. A drag coefficient correlation. V.D.I. Zeitung. 77: p. 318.
- Schreyer, H.B. and Coughlin, R.W. 1999. Effects of stratification in a fluidized bed bioreactor during treatment of metal-working wastewater. Biotechnology and Bioengineering. 63: p. 129-140.
- Schulze, H.J. 1989. Hydrodynamics of bubble-mineral particle collisions. Mineral Processing and Extractive Metallurgy Review 5: p. 34-76.
- Seo, D.C., Lee, H.J., Hwang, H.N., Park, M.R., Kwak, N.W., Cho, I.J., Cho, J.S., Seo, J.Y., Joo, W.H., Park, K.H., and Heo, J.S. 2007. Treatment of non-biodegradable cutting oil emulsion by ultrasonication-Fenton oxidation process. Water Science and Technology. 55: p. 251-259.
- Sherony, D.F. and Kintner, R.C. 1971. Coalescence of an emulsion in a fibrous bed: Part I, theory. The Canadian Journal of Chemical Engineering. 49: p. 321-325.
- Sokolović, R.M.Š., Govedarica, D.D., and Sokolović, D.S. 2010. Separation of oil-in-water emulsion using two coalescers of different geometry. Journal of Hazardous Materials. 175: p. 1001-1006.
- Sokolović, R.M.Š., Vulić, T.J., and Sokolović, S.M. 2007. Effect of bed length on steady-state coalescence of oil-in-water emulsion. Separation and Purification Technology. 56: p. 79-84.
- Sokolović, R.Š., Sokolović, S., and Sević, S. 2009. Oily water treatment using a new steady-state fiber-bed coalescer. Journal of Hazardous Materials 162: p. 410-415.
- Sokovic, M. and Mijanovic, K. 2001. Ecological aspects of cutting fluids and to their quantifiable influence one parameters of the cutting processes. Journal of Material Processing Technology 109: p. 181-189.

- Solisio, C., Lodi, A., Converti, A., and Del Borghi, M. 2002. Removal of exhausted oils by adsorption on mixed Ca and Mg oxides. Water Research. 36: p. 899-904.
- Speth, H., Pfennig, A., Chatterjee, M., and Franken, H. 2002. Coalescence of secondary dispersions in fiber beds. Separation and Purification Technology 29: p. 113-119.
- Stephenson, R.J. and Duff, S.J.B. 1996. Coagulation and precipitation of a mechanical pulping effluent-I. Removal of carbon, colour and turbidity. Water Research. 30: p. 781-792.
- Stokes, G.G. 1851. For creeping flow around an object of arbitrary shape. Transactions of the Cambridge Philosophical Society. 9(2): p. 8.
- Svarovsky, L. 2000. Solid-liquid separation. 4th ed. ed. Butterworth-Heinemann, Oxford, U.K.
- Taneda, S. 1956. Studies on wake vortices (III). Experimental investigation of the wake behind a sphere at low Reynolds number. Report of Research Institute for Applied Mechanics, Kyushu University. 4: p. 99-105.
- Tansel, B. and Pascual, B. 2011. Removal of emulsified fuel oils from brackish and pond water by dissolved air flotation with and without polyelectrolyte use: Pilot-scale investigation for estuarine and near shore applications. Chemosphere. 85: p. 1182-1186.
- Taylor, T.D. and Acrivos, A. 1964. On the deformation and drag of a falling viscous drop at low Reynolds number. Journal of Fluid Mechanics. 18(3): p. 466-476.
- Thomas, F., Masion, A., Bottero, J.Y., Rouiller, J., Génévrier, F., and Boudot, D. 1991. Aluminum (III) speciation with acetate and oxalate. A potentiometric and ²⁷Al NMR study. Environmental Science and Technology 25(9): p. 1553-1559.
- Tir, M. and Moulai-Mostefa, N. 2008. Optimization of oil removal from oily wastewater by electrocoagulation using response surface method. Journal of Hazardous Materials. 158: p. 107-115.
- Torobin, L.B. and Gauvin, W.H. 1959. Fundamental aspects of solids-gas flow. Part II. The sphere wake in steady laminar fluids. Canadian Journal of Chemical Engineering. 37(167-176).
- Tri, P.T. 2002. Oily wastewater treatment by membrane bioreactor process coupled with biological activated carbon process. Asian Institute of Technology School of Environment, Resources and Development, Bangkok, Thailand.
- Un, U.T., Koparal, A.S., and Ogutveren, U.B. 2009. Electrocoagulation of vegetable oil refinery wastewater using aluminium electrodes. Journal of Environmental Management 90: p. 428-433.
- Vaidyanathan, V., *Different methods for particle diameter determination of low density and high density lipoproteins – comparison and evaluation*. 2006, Texas A&M University: U.S.
- van der Gast, C.J. and Thompson, I.P. 2005. Effects of pH amendment on metal working fluid wastewater biological treatment using a defined bacterial consortium. Biotechnology and Bioengineering 89: p. 357-366.
- Vasudevan, G. and Chase, G.G. 2004. Performance of B-E-glass fiber media in coalescence filtration. Aerosol Science 35: p. 83-91.

- Wang, W., Zhou, Z., Nandakumar, K., Masliyah, J.H., and Xu, Z. 2006. An induction time model for the attachment of an air bubble to a hydrophobic sphere in aqueous solutions. International Journal of Mineral Processing 75: p. 69-82.
- Wanichkul, B., *Etude des potentialities de nouveaux procedes de traitement d'emulsions hydrocabure-eau; ultrafiltration, distillation et couplage coalesceur-hydrocyclone*. 2000, INSA-Toulouse: France.
- Xiao, F., Yi, P., Pan, X., Zhang, B., and Lee, C. 2010. Comparative study of the effects of experimental variables on growth rates of aluminium and iron hydroxide flocs during coagulation and their structural characteristics. Desalination. 250: p. 902-907.
- Xu, R. 2001. Particle characterization: Light scattering methods. Kluwer Academic Publishers, The Netherlands.
- Zheng, Y.Y. and Zhao, C.C. 1993. A study of kinetics on induced-air flotation for oil-water separation. Separation Science and Technology. 28: p. 1233-1240.
- Zhou, Y.B., Chen, L., Hu, X.M., and Lu, J. 2009. Modified resin coalescer for oil-in-water emulsion treatment: Effect of operating conditions on oil removal performance. Industrial & Engineering Chemistry Research. 48: p. 1660-1664.
- Zisman, W.A. 1964. Relation of the equilibrium contact angle to liquid and solid constitution. Advances in Chemistry. 43: p. 1-151.
- Zouboulis, A.I. and Avranas, A. 2000. Treatment of oil-in-water emulsions by coagulation and dissolved-air flotation. Colloids and Surfaces A: Physicochemical and Engineering Aspects 172: p. 153-161.



APPENDIX



จุฬาลงกรณ์มหาวิทยาลัย
CHULALONGKORN UNIVERSITY

This article was downloaded by: [Chulalongkorn University]
 On: 06 January 2015, At: 00:37
 Publisher: Taylor & Francis
 Informa Ltd Registered in England and Wales Registered Number: 1072954 Registered office: Mortimer House,
 37-41 Mortimer Street, London W1T 3JH, UK



Separation Science and Technology

Publication details, including instructions for authors and subscription information:
<http://www.tandfonline.com/loi/lst20>

Study of Cutting-Oil Emulsion Separation by Coalescer Process in Terms of Medium Characteristics and Bed Packing

Nattawin Chawaloephonsiya^{ab} & Pisut Painmanakul^{bc}

^a International Postgraduate Program in Environmental Management, Graduate School, Chulalongkorn University, Bangkok, Thailand

^b Center of Excellence on Hazardous Substance Management (HSM), Bangkok, Thailand

^c Department of Environmental Engineering, Faculty of Engineering, Chulalongkorn University, Bangkok, Thailand

Accepted author version posted online: 26 Aug 2014. Published online: 01 Dec 2014.



[Click for updates](#)

To cite this article: Nattawin Chawaloephonsiya & Pisut Painmanakul (2014) Study of Cutting-Oil Emulsion Separation by Coalescer Process in Terms of Medium Characteristics and Bed Packing, *Separation Science and Technology*, 49:18, 2960-2967, DOI: [10.1080/01496395.2014.943768](https://doi.org/10.1080/01496395.2014.943768)

To link to this article: <http://dx.doi.org/10.1080/01496395.2014.943768>

PLEASE SCROLL DOWN FOR ARTICLE

Taylor & Francis makes every effort to ensure the accuracy of all the information (the "Content") contained in the publications on our platform. However, Taylor & Francis, our agents, and our licensors make no representations or warranties whatsoever as to the accuracy, completeness, or suitability for any purpose of the Content. Any opinions and views expressed in this publication are the opinions and views of the authors, and are not the views of or endorsed by Taylor & Francis. The accuracy of the Content should not be relied upon and should be independently verified with primary sources of information. Taylor and Francis shall not be liable for any losses, actions, claims, proceedings, demands, costs, expenses, damages, and other liabilities whatsoever or howsoever caused arising directly or indirectly in connection with, in relation to or arising out of the use of the Content.

This article may be used for research, teaching, and private study purposes. Any substantial or systematic reproduction, redistribution, reselling, loan, sub-licensing, systematic supply, or distribution in any form to anyone is expressly forbidden. Terms & Conditions of access and use can be found at <http://www.tandfonline.com/page/terms-and-conditions>

Study of Cutting-Oil Emulsion Separation by Coalescer Process in Terms of Medium Characteristics and Bed Packing

Nattawin Chawaloephonsiya^{1,2} and Pisut Painmanakul^{2,3}

¹International Postgraduate Program in Environmental Management, Graduate School, Chulalongkorn University, Bangkok, Thailand

²Center of Excellence on Hazardous Substance Management (HSM), Bangkok, Thailand

³Department of Environmental Engineering, Faculty of Engineering, Chulalongkorn University, Bangkok, Thailand

This work aimed to consider the effects of media shape, size, and packing on the coalescer efficiency. Different shaped polypropylene was applied as media for separating the cutting-oil emulsion. The results exhibited that polypropylene media can separate the emulsion with the highest efficiency of 43% at the optimal condition. The dissimilar shape provided the difference in the equivalent size and the packing by means of porosity, permeability, and pore uniformity. Furthermore, the approach for determining application possibility of materials as coalescer media was proposed. Wetting properties and bed permeability were suggested as key factors for media selection and coalescer process design.

Keywords cutting-oil emulsion; coalescer; media shape; media size; packing behavior

INTRODUCTION

Oil is a prevalent contaminant in wastewater and normally forms a stabilized emulsion with surfactants, which is difficult to separate. Coalescer is a physical process that aims to enlarge oil-droplets sizes in order to increase the oil separation from water. The important mechanisms governing its efficiency are collision and attachment between droplets and media or droplets and droplets (1). There has been a lot of research on the effects of several parameters on the coalescer performance. For example, the impacts of operating conditions (e.g., flow velocity, bed length, and oil concentration) on the separation efficiency were investigated in several works (2–6). It was found that the efficiency was affected by media characteristics, for instance, material type, size, and wettability (7–11). Packing of a coalescer bed by means of porosity and permeability was also proved for its influences on the process (8,

10, 12–13). In addition, several studies mentioned the effects of the dispersed phase characteristics, which were justified as another important factor (6, 8, 14). According to these studies, a coalescer process has been analyzed in 3 perspectives, including characteristics of oil phase, surface properties of media (e.g. wettability, surface energy, etc.), and the geometry of media. Indeed, the effects of the first two aspects on the efficiency have been considerably understood by numerous researchers. The impacts of media geometry, however, were still unobvious.

The complexity of this perspective resulted in the lack of the process design criteria. In addition, a better understanding in the relation between media shape and size was required since both of them can affect the bed packing (e.g., bed porosity and permeability), separation mechanisms, and operating conditions (e.g., flow velocity and bed length) of the coalescer. Hence, the objective of this study was to acquire a better understanding in the relation among media shape, size, and bed packing. Polypropylene (PP) media with dissimilar shapes were applied as a coalescer medium. Cutting-oil was selected to represent the stabilized emulsion due to its high stability. The bed height and the emulsion flow rate were varied. Afterwards, the effects of these media characteristics were investigated.

MATERIALS AND METHODS

Experimental Set-Up

The process configuration is schematically displayed in Fig. 1. The process can be divided into 3 parts including

1. the emulsion generation,
2. the coalescer unit, and
3. the decantation tank.

Cutting-oil and water in the storage tank (1) were vigorously mixed by the turbine to generate the emulsion. This cutting-oil emulsion was then introduced by the centrifugal pump (2) to the coalescer column (5) with the coalescer medium (6) and the salting-out device (7). The emulsion flow rate controlled by the flow meter (4) was adjusted by the globe valve (3). The

Received 26 May 2013; accepted 8 July 2014.

Address correspondence to Pisut Painmanakul, Department of Environmental Engineering, Faculty of Engineering, Chulalongkorn University, Bangkok 10330, Thailand. E-mail: Pisut.P@chula.ac.th

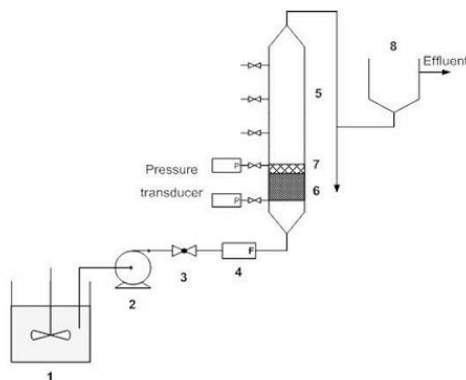


FIG. 1. Schematic diagram of the coalescer process.

effluent from the coalescer was separated and then entered to the decantation tank (8). Note that the pressure transducers were installed before and after the coalescer bed for measuring the pressure loss of the emulsion that passes through the bed.

The coalescer column was a clear cylindrical acrylic with a diameter and a height of 8 cm and 80 cm, respectively. The coalescer media were polypropylene with different shapes including granule, fiber, and tube, were used as the coalescer media (Fig. 2). A stainless steel mesh was applied as a salting out device. The decantation tank was a clear cylinder made of acrylic with 8-cm in diameter and 40-cm in height.

Analytical Parameters

Oil concentrations in this study were analyzed by mean of turbidity in the unit of NTU (Nephelometric Turbidity Unit) by Lovibond PCcheckit turbidimeter. As reported by several researchers, turbidity can represent an oil concentration in an emulsion (15–18). In addition, COD was also determined by the close-reflux method (19) to represent the oil concentration as suggested in several studies (20–23). The treatment efficiency was evaluated by the ratio of the difference between the inlet and the outlet concentrations to the initial oil concentration.

In addition, the oil-droplet size distribution of the emulsion was examined by the microscopic technique for investigating the change of droplet sizes. The optical microscope Nikon YS2-H with an ocular scale and a stage microscope were applied. The sizes of the approximated 300 oil-droplets were measured and exhibited in terms of mean diameter. The number-length mean diameter (d_{NL}) and the surface-volume mean diameter (d_{SV}) were applied as expressed in Eqs. (1) and (2), respectively (24). Note that the d_{SV} is commonly used in calculation where the active surface area of particles is important (25).

$$d_{NL} = \frac{\sum d_e dN}{\sum dN} \quad (1)$$

$$d_{SV} = \frac{\sum d_e^3 dN}{\sum d_e^2 dN} \quad (2)$$

Preparation of the Synthetic Cutting-Oil Emulsion

The 1 g/L emulsion was prepared by diluting 1 g of cutting-oil in 1 L of tap water at $20 \pm 2^\circ\text{C}$. This water contained $204\text{--}221 \mu\text{S}/\text{cm}$ conductivity with pH and turbidity of 7.2 ± 0.2 and $0.94\text{--}3.3$ NTU, respectively. The mixture was vigorously mixed until the homogeneous milky emulsion was formed. This synthetic emulsion contained the droplet sizes of $1.52 \mu\text{m}$ and $4.12 \mu\text{m}$ for d_{NL} and d_{SV} , respectively, which can be categorized as a secondary stabilized emulsion (26). The average COD and turbidity of the initial emulsion were $3900 \text{ mg}/\text{L}$ and 1600 NTU, respectively. Moreover, the zeta potential of -52 mV indicated negatively charged surface of droplets and the stability of the emulsion since it was higher than the stability threshold in colloidal system, i.e. $\pm 30 \text{ mV}$ (27).

Experimental Procedure

The experiment was divided into 3 parts. First, the coalescer media were analyzed for their characteristics including surface energy (γ_c), contact angle (θ_c), and porosity (ϵ). However, the contact angle of the cutting-oil droplet on the media in water cannot be directly measured due to the very low interfacial tension of oil in water. The oil cannot form a droplet that the measurement for contact angle can be conducted. The indirect

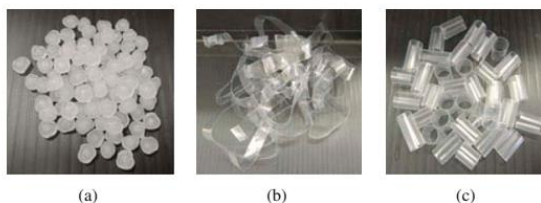


FIG. 2. Coalescer media: (a) granule, (b) fiber, and (c) tube.

method was applied by using Young's equation as expressed in Eq. (3) (28) to determine the θ_C .

$$\gamma_{WC} = \gamma_{OC} + \gamma_{OW} \cos \theta_C \quad (3)$$

The interfacial tensions γ_{WC} and γ_{OC} can be obtained from Eqs. (4) and (5) for droplets of water and oil on the media in air, respectively. The contact angles were evaluated by the sessile-drop method (28). The Wilhelmy plate was used for measuring the surface tensions of water (γ_W) and oil (γ_O). Moreover, the γ_C of the media was analyzed by the Zisman method (29). The contact angles on the media of liquid with varied surface tension in the range of 38–72 mN/m adjusting by sodium dodecyl sulfate (SDS) were measured. In addition, the bed porosities were determined by water saturation method defining as a replacement of void volume in the bed with water (30).

$$\gamma_C = \gamma_{OC} + \gamma_O \cos \theta_O \quad (4)$$

$$\gamma_C = \gamma_{WC} + \gamma_W \cos \theta_W \quad (5)$$

Afterwards, the effects of operating conditions on the treatment efficiency were evaluated. The experiments were conducted with varied bed length of 2–10 cm and flow velocity of 2.0–6.8 cm/s. The emulsion was passed through the bed and retained in the decantation tank for 120 minutes. Note that all experiments were operated at the saturated bed condition achieved by the recirculation of emulsion through the bed until the constant pressure loss can be observed. The emulsion was sampled after being passed through the bed and from the decantation tank and then analyzed for the oil concentration and droplet size distribution. Finally, the mathematical models were applied with the experimental results for describing the separation mechanisms in the process.

RESULTS AND DISCUSSION

Characteristics of Coalescing Media

Characteristics of coalescer media are presented in Table 1. The surface energy (γ_C) of 35 mN/m was obtained for the polypropylene media. This γ_C was slightly greater than those

reported in the range of 29–31 mN/m by (31) and 31 mN/m (32). However, the surface energy of PP was lower than other polymer, for example, polyester (41–44 mN/m) and nylon (33–46 mN/m) (31), but higher than that of the polyurethane fiber (23 mN/m) in the work of Sokolović et al. (13). Due to this γ_C , the PP can be implied as a low surface energy material indicating its hydrophobicity (29). This surface energy result corresponded to the contact angle of oil-droplets on the media of approximately 68°. Since the contact angle was between 0° to 90°, the media can be categorized as a hydrophobic material and was suitable for applying as a coalescer medium (1).

It can be seen from Table 1 that the PP media with different shapes were hydrophobic with similar contact angle. However, the porosities of the media when packing were obviously different due to their sizes and shapes as well as their arrangement in the bed. The highest porosity was found from the fibrous medium following by the tubular and granular media, respectively. The granular medium contained the porosity of 0.55, which was slightly higher than those of a sand filter (0.40–0.45) (33) and the expanded polystyrene bed (0.45) in Sokolović et al. (14). This porosity could result in filtration in the bed. On the contrary, porosities of tubular and fibrous media (0.82 and 0.90, respectively) were in the same range with other research (8, 34). Influences of different bed porosities on the separation performance of the oily emulsion will be further discussed.

Effects of Operating Conditions on Treatment Efficiencies

Figure 3 displays treatment efficiencies of coalescer process under different operating conditions. As can be seen, the highest efficiency of each medium was achieved at the bed length of 10 cm with flow velocity of 2 cm/s, which was denoted as the optimal condition in this work. The highest treatment efficiency of approximated 40% was obtained from the tubular medium (Fig. 3c). It can be noticed that the separation efficiency was influenced by the flow velocity. This optimal flow velocity of 2 cm/s corresponded to the works of Wanichkul (35) and Rachu (26). On the contrary, the efficiency was slightly affected by the bed length, which was similar to the work of Li and Gu (3). The highest efficiencies of nearly 25% were observed in the cases of granular and fibrous media with no obvious impacts

TABLE 1
Coalescer media characteristics

Characteristics	Polypropylene		
	Granule	Fiber	Tube
Porosity	0.55	0.90	0.82
Dimension (mm)	4.5 – 5.5 (Diameter)	10 × 280 × 0.5 (Width × Length × Thickness)	5 × 8 (Diameter × Length) 4 mm of inner diameter
θ_C (°)		68.3	

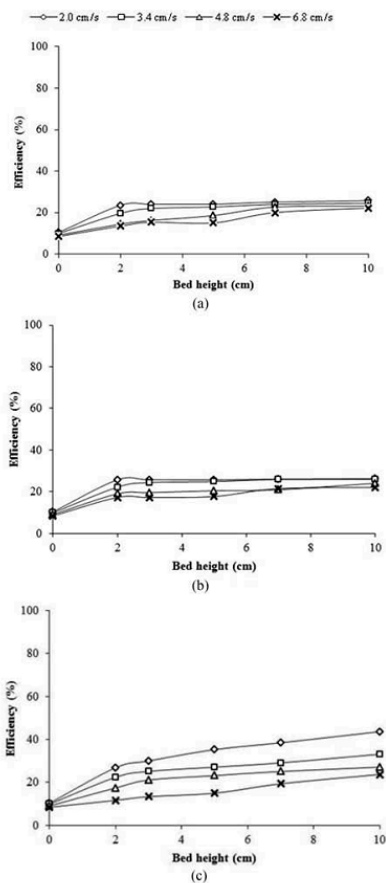


FIG. 3. Treatment efficiencies in different operating conditions for (a) granular, (b) fibrous, and (c) tubular media.

from different operating conditions (Figs. 3a and 3b). However, the occurred mechanisms might be distinct due to the difference in porosities between granular (0.55) and fibrous (0.90) media.

Table 2 displays the oil-droplet sizes and the treatment efficiencies of decantation and coalescer processes under the optimal condition. The emulsion cannot be separated by the conventional decantation process, and the droplet size did not clearly change. In the case of granular medium, the oil-droplet

TABLE 2
Oil-droplet sizes (μm) at 2.0 cm/s flow velocity and 10 cm bed height (Inlet emulsion: $d_{\text{NL}} = 1.52 \mu\text{m}$ and $d_{\text{SV}} = 4.12 \mu\text{m}$)

Coalescer	After bed		After decantation		Efficiency (%)
	d_{NL}	d_{SV}	d_{NL}	d_{SV}	
Decantation	—	—	3.60	5.99	0.0
Granule	3.84	7.91	4.12	7.27	25.8
Fiber	4.83	17.41	3.39	5.76	26.3
Tube	5.64	21.86	4.67	8.54	43.6

*Droplet sizes are in the unit of μm .

size after the bed and after decantation did not varied from the inlet one. These sizes indicated that the oil-droplets coalescence was rarely occurred. Filtration of droplet by the media might be the dominated mechanism. On the contrary, the droplet sizes were enlarged after being passed through the fibrous and tubular bed, implying the occurrence of oil-droplets coalescence. Besides, the highest efficiency of 43% from tubular medium would be the result of differential settling. Large droplets with higher rising velocity would collide with the smaller ones resulting in the aggregation. The separation was then faster due to their larger size and higher possibility for further collision and aggregation (36). At this point, it can be stated that the media shape and the bed porosity could be the key factors affecting the performance of the coalescer process. Moreover, it can be suggested that larger coalesced droplets can be separated by the decantation, which conformed to the results of discrete settling test. The remaining droplet sizes after decantation of these coalescer processes were relatively close to that of the decantation process only.

Regarding the media shape, the efficiency difference could be a result of distinctive specific surface area of media (a), which can be defined as a surface area per unit mass of material (37). The tubular medium contained the specific surface area of 6708 m^{-1} , which was much higher than those of the granular and fibrous ones (1200 and 2007 m^{-1} , respectively). This difference could impact the collision probability of oil-droplets on the media, which is the relevant phenomenon in the coalescence and the filtration processes (1). Besides, the process performance was also influenced by the bed porosity. The denser granular bed ($\epsilon = 0.55$) might filter oil-droplets out from the emulsion as discussed above. In contrast, the more porous beds (i.e., fiber and tube) could result in higher probability of oil-droplets coalescence as corroborated by the droplet sizes in Table 2.

Effects of Coalescer Media Characteristics

Size of Coalescer Media

The media sizes were determined by 2 different approaches. First, Ergun's equation (Eq. 6), which defined as correlation

between the friction factor and Reynolds number of a packed column with granule collector (38), was applied for determining the media diameter (d_p).

$$\frac{\Delta P}{L} = \frac{150v_0\mu(1-\varepsilon)^2}{\phi^2 d_p^2 \varepsilon^3} + \frac{1.75\rho v_0^2(1-\varepsilon)}{\phi d_p \varepsilon^3} \quad (6)$$

The ϕ is the sphericity, which can be defined as the ratio of the surface area of a sphere (with the same volume as the given particle) to the surface area of the particle as expressed in Eq. (7) (37).

$$\phi = \frac{A_0}{A_p} = \frac{\pi D_0^2}{A_p} = \frac{\pi(6V_p/\pi)}{A_p} \quad (7)$$

The media size can be calculated from the measured pressure loss of emulsion passing through the bed (ΔP). The sizes of 4.8, 7.5, and 8.3 mm were obtained for granular, fibrous, and tubular media, respectively. This calculated diameter of the granular medium was close to its actual size (4.5–5.5 mm). Therefore, it can be stated that the media size determination by Ergun's equation can be applied for a sphere-like media. Though, the calculated sizes of the fibrous and tubular media were larger, which did not correspond to their specific surface area (a). This approach might be restricted to apply with a non-sphere media.

As a result, another approach for determining the media size was proposed by applying the filtration efficiency equation as expressed in Eq. (8) (i.e., for sphere collectors) (1).

$$\ln \frac{C_1}{C_0} = -\frac{3}{2d_p} \alpha \eta_T (1-\varepsilon) L \quad (8)$$

The α and η_T were the attachment and the collision efficiencies between oil-droplets and collectors, respectively. The collision mechanism of droplets by collectors features 3 main transport phenomena such as gravitational settling, interception, and diffusion. The η_T is a summation of the sub-efficiencies of these phenomena. The acquired η_T for each medium was then employed for determining the relative sphere-like diameters of fibrous and tubular media to the diameter of the sphere one. However, the geometric dimension of the media had to be considered since the filtration efficiency equation relied on the projection area of a collector. The areas of these two media were varied due to their shapes and orientations in the packed bed. The filtration efficiency equations were then modified as displayed in Eqs. (9) and (10), respectively, for the fibrous and the tubular media. The θ is an inclined angle of medium related to a horizontal plain varying from 0° to 90° as illustrated in Fig. 4.

$$\ln \frac{C_1}{C_0} = -\left(\frac{\cos \theta}{t} + \frac{\sin \theta}{L}\right) (1-\varepsilon) \alpha \eta_T H \quad (9)$$



FIG. 4. Inclined angles (θ) of (a) fibrous and (b) tubular media.

$$\ln \frac{C_1}{C_0} = -\frac{1}{(d_o^2 - d_i^2)} \left(\frac{A d_o \cos \theta}{\pi} + d_o^2 \sin \theta \right) (1-\varepsilon) \alpha \eta_T H \quad (10)$$

where t and L are the thickness and length of the fibrous medium. The d_o is the outer diameter, and d_i is the inner diameter of the tubular medium. The sphere-like diameters can be therefore determined from the inlet and the outlet concentrations by dividing Eqs. (9) and (10) by Eq. (8). The attachment efficiency (α) was assumed to be constant for all media as the attachment occurred between the cutting-oil and PP surface. The calculated diameters are summarized in Table 3 as the sizes of fibrous and tubular media from the filtration efficiency equation were smaller than those of Ergun's equation. The diameters from the second approach tended to correspond with the specific surface area as previously discussed.

In addition, it was found from the calculation that the inclined angle of 90° provided the highest collection efficiency under every operating condition. This 90° orientation of the tubular medium was similar to the stacked raschig ring, which provided the advantages on low pressure drop and good liquid distribution in the bed (39). Higher contact and attachment probability of oil-droplets to media would be achieved.

At this point, the size determination approach by the filtration efficiency equation provided a more reasonable result. This approach could be applied for a media selection. The efficiency from the small column test could be used for suggesting a media selection in a practical coalescer or filtration process.

TABLE 3
Calculated diameters obtained from Ergun's and filtration efficiency equations

Media types	Calculated diameter (mm)	
	Ergun's equation	Filtration efficiency equation
Granule	4.8	—
Fiber	7.5	2.2
Tube	8.3	1.2

Packing Behavior of Coalescer Bed

The behavior of a packed bed was a relevant factor affecting the treatment efficiency since it could influence the mechanisms occurred while the emulsion flowed through. First, Ergun's equation (Eq. 6) and the measured pressure loss was applied to evaluate the bed porosity at the saturated bed condition, denoted as ε_t . Note that the media sizes used for this calculation were obtained from Ergun's equation for granular medium, and the filtration efficiency equation for fibrous and tubular media as aforementioned. This ε_t value was consequently used for estimating the average saturation factor (\bar{S}_d) or the fraction of oil amount in the bed at the saturated condition as expressed in Eq. (11) (40).

$$\bar{S}_d = 1 - \frac{\varepsilon_t}{\varepsilon} \quad (11)$$

The ε_t and \bar{S}_d of media are exhibited in Table 4. The granular medium contained the lowest saturated porosity in this study following by the tubular and the fibrous media, respectively. This result verified the discussion regarding the dominated filtration mechanism in granular bed. Furthermore, this value can indicate the coalescence possibility in packed bed according to Chieu et al. (41). It was stated that the complete coalescence can occur with at least 10–15% of the oil volume saturation. Therefore, the obtained values in this study exhibited the coalescence probability of oil in every case.

This accumulated oil indicated by the \bar{S}_d and the ε_t could change the pore structure and affected the emulsion flow in the bed as it could alter the single-phase flow (i.e. water) to the two-phase flow (i.e., water and oil) (12). To investigate this effect, the Carman-Kozeny equation was employed as expressed in Eqs. (12) and (13), respectively, for the single-phase and the two-phase flows (40).

$$\Delta p_1 = \frac{16Hv_0\mu k_1(1-\varepsilon)^2}{d_p^2 g \varepsilon^3} \quad (12)$$

$$\Delta p_2 = \frac{16Hv_0\mu k_2(1-\varepsilon_t)^2}{d_p^2 g \varepsilon_t^3} \quad (13)$$

The Carman-Kozeny constants (k_1 and k_2) indicate the uniformity of pore structure within the bed. According to Akers and Ward (42), the Carman-Kozeny constants depend on particle

TABLE 4
Calculated saturated porosity (ε_t) and average saturation factor (\bar{S}_d) of packed beds

Media Types	Saturated porosity (ε_t)	Saturation factor (\bar{S}_d)
Granule	0.12	0.79
Fiber	0.28	0.68
Tube	0.26	0.68

size and shape as well as the packing. Small Carman-Kozeny constant implies to low uniformity of media pore (43). Additionally, the specific permeability coefficient (B_{01}) of single-phase flow in the bed can be calculated from Eq. (14) (43). Likewise, the coefficient for two-phase flow (B_{02}) can be evaluated by substituting the ε and k_1 with ε_t and k_2 , respectively. The specific permeability of bed is a function of pore structure only (44), which could impact the flow of the emulsion through the bed.

$$B_0 = \frac{d_p^2 \varepsilon^3}{16k_1(1-\varepsilon)^2} \quad (14)$$

Carman-Kozeny constants and specific permeability coefficients are displayed in Table 5. The distinction of k_1 and k_2 values demonstrated the dissimilar pore uniformity between these two scenarios.

For single-phase flow, the granule contained the highest uniform pore amongst the applied media due to its rigid configuration. The emulsion could flow through the pore structure of the bed as depicted in Fig. 5(a1). The lower pore uniformity

TABLE 5
Carman-Kozeny constants for single- and two-phase flow with bed permeability

Media Types	k_1	k_2	$B_{0,1}$ (m ²)	$B_{0,2}$ (m ²)
Granule	30.3	19.8	6.8×10^{-9}	5.2×10^{-11}
Fiber	19.3	10.7	1.3×10^{-8}	3.8×10^{-11}
Tube	13.6	10.4	3.5×10^{-9}	2.1×10^{-11}

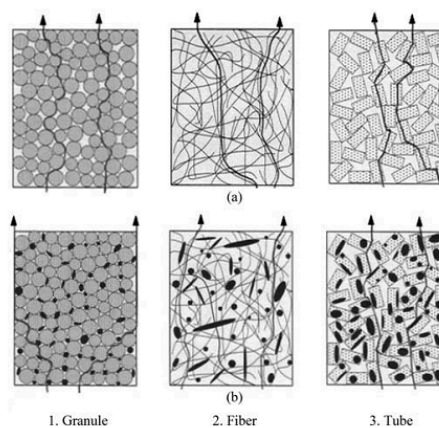


FIG. 5. Flow pathways of the emulsion for three medium types in (a) single-phase flow and (b) two-phase flow.

was found in the case of fiber as the emulsion can randomly pass through the porous ($\varepsilon = 0.90$) and disorganized bed as displayed in Fig. 5(a2). In contrast, the tubular medium possessed the lowest uniformity even with its rigid shape as the emulsion can flow through the gap between as well as the hollow of media as shown in Fig. 5(a3).

In the case of saturated bed, the porosities as well as the pore uniformity were changed since oil-droplets attached in the bed. The two-phase flow could occur. The oil phase in the emulsion would flow along the attached droplets while the water phase passed through the center of pores. The flow streamline of the emulsion was therefore affected as exhibited in Fig. 5(b). The attached oil-droplets in the granular bed could link the media together resulting in bed clogging. The emulsion flow was obstructed and the pore uniformity was then decreased (Fig. 5b1). This same reason can describe the decrease of pore uniformity for fibrous bed (i.e., 19.3 \rightarrow 10.7) as shown in Fig. 5(b2). Nevertheless, the coefficient of the tubular bed was slightly decreased (i.e., 13.6 \rightarrow 10.4). The emulsion can still pass through the gap between media even with attached oil-droplets in the bed as in Fig. 5(b3).

The change of bed porosity and pore structure between the single-phase and the two-phase flow conditions also resulted in the decrease of the specific permeability coefficient (B_0) as in Table 5. The coefficient for the single-phase flow ($B_{0,1}$) was in the range of 10^{-9} – 10^{-8} m², which were slightly higher than those reported in several studies for fibrous bed (10^{-13} – 10^{-9} m²) (12–13). The higher permeability might be a result of the porous and disorganized bed. The lowest permeability in this work was found in the case of the tubular bed due to its low pore uniformity and high surface area. The permeability suggested that the emulsion was able to flow through the bed more than that of the filtration process. On the other hand, the coefficient diminished in the two-phase flow condition ($B_{0,2}$). This result was compatible with the decreased porosity, which expressed that the pore structure was changed as aforementioned. Therefore, the bed permeability could be suggested as a key factor influencing the process performance since it relates to other parameters such as media size, media shape, and bed porosity.

From the results, it can be concluded that the separation efficiency of oily emulsion by a coalescer was affected by both operating conditions (e.g., flow velocity) and media characteristics (e.g., shape, size, and packing). Characteristics of media, in particular, can influence the occurred mechanisms in the bed. The wetting property and the permeability of media should be well considered for selecting an effective coalescer media.

CONCLUSIONS

The objective of this work was to study the relation among the media shape, size, and packing behavior and their effects on the coalescer. For this purpose, experiments with different media shapes (granule, fiber, and tuber) and operating

conditions (bed height and flow velocity) were performed. According to the result, the conclusion was as follows:

- Polypropylene was hydrophobic and can be applied as a coalescer medium. The dissimilar media shape resulted in the difference of bed porosity
- The highest separation efficiency of 43% was obtained from the optimal operating condition of 2 cm/s flow velocity and 10 cm the tubular medium bed.
- Ergun's equation can only be used for examining the size of a sphere-like media. However, the proposed determination approach by filtration efficiency equation provided more reasonable sizes for non-sphere media
- The difference of media shape affected their equivalent sizes as well as the porosity (ε) and the saturation factor (\bar{S}_d). These latter two parameters can be used for identifying the dominant mechanism. Besides, the ε and can be applied to determine the bed permeability
- The size and shape of media can impact the permeability and the pore structure of the bed, which affect the flow pathway of the emulsion
- The wetting properties of media and the bed permeability were two important factors that should be considered for selecting a coalescer medium.

Further study should be conducted in a larger scale process or with other media (in terms of material, size, and shape) to validate the applicability of this media consideration approach.

NOMENCLATURE

γ_{wc}	water-media interfacial energy (mN/m)
γ_{oc}	oil-media interfacial energy (mN/m)
γ_{ow}	oil-water interfacial energy (mN/m)
Δp	pressure loss due to flow through media bed (Pa)
L	media bed length (m)
v_0	superficial velocity of liquid (m/s)
μ	dynamic viscosity of liquid (Pa-s)
ε	initial media bed porosity (–)
d_p	diameter of media (m)
ρ	density of liquid phase (kg/m ³)
C_f	final emulsion concentration (g/L)
C_0	initial emulsion concentration (g/L)
ε_f	saturated media bed porosity (–)
\bar{S}_d	saturation factor (–)
B_0	permeability of media bed (–)

FUNDING

This work was financed by the 90th Anniversary of Chulalongkorn University Fund (Ratchadaphiseksomphot Endowment Fund), the Center of Excellence on Hazardous Substance Management (HSM), and Department of Environmental Engineering, Faculty of Engineering,

Chulalongkorn University. This research is also supported by the Rachadaphiseksomphot Endowment Fund Part of the "Strengthen Chulalongkorn University Researcher's Project" and the Rachadaphiseksomphot Endowment Fund 2013 of Chulalongkorn University (CU-56-509-CC).

REFERENCES

- Aurelle, Y. (1985) *Treatments of Oil-Containing Wastewater*; Department of Sanitary Engineering, Chulalongkorn University; Bangkok, Thailand.
- Hazlett, R. N. (1969) Fibrous bed coalescence of water: Steps in the coalescence process. *Industrial & Engineering Chemistry Fundamentals*, 8: 625-632.
- Li, J.; Gu, Y. (2003) Coalescence of oil-in-water emulsions in fibrous and granular beds. *Separation and Purification Technology*, 42(1): 1-13.
- Sokolović, R. M. Š.; Vulić, T. J.; Sokolović, S. M. (2006) Effect of fluid flow orientation on the coalescence of oil droplets in steady-state bed coalescers. *Industrial & Engineering Chemistry Research*, 45: 3891-3895.
- Zhou, Y. B.; Chen, L.; Hu, X. M.; Lu, J. (2009) Modified resin coalescer for oil-in-water emulsion treatment: Effect of operating conditions on oil removal performance. *Industrial & Engineering Chemistry Research*, 48: 1660-1664.
- Maiti, S.; Mishra, I. M.; Bhattacharya, S. D.; Joshi, J. K. (2011) Removal of oil from oil-in-water emulsion using a packed bed of commercial resin. *Colloids and Surfaces A: Physicochemical and Engineering Aspects*, 389: 291-198.
- Magiera, R.; Blass, E. (1997) Separation of liquid-liquid dispersions by flow through fibre beds. *Filtration & Separation*, 34: 369-376.
- Speth, H.; Pfennig, A.; Chatterjee, M.; Franken, H. (2002) Coalescence of secondary dispersions in fiber beds. *Separation and Purification Technology*, 29: 113-119.
- Ji, F.; Li, C.; Dong, X.; Li, Y.; Wang, D. (2009) Separation of oil from oily wastewater by sorption and coalescence technique using ethanol grafted polyacrylonitrile. *Journal of Hazardous Materials*, 164(2-3): 1346-1351.
- Bansal, S.; von Arnim, V.; Stegmaier, T.; Planck, H. (2011) Effect of fibrous filter properties on the oil-in-water-emulsion separation and filtration performance. *Journal of Hazardous Materials*, 190: 45-50.
- Kulkarni, P. S.; Patel, S. U.; Chase, G. G. (2012) Layered hydrophilic/hydrophobic fiber media for water-in-oil coalescence. *Separation and Purification Technology*, 85: 157-164.
- Mathavan, G. N.; Viraraghavan, T. (1992) Coalescence/filtration of an oil-in-water emulsion in a peat bed. *Water Research*, 26: 91-98.
- Sokolović, R. M. Š.; Vulić, T. J.; Sokolović, S. M. (2007) Effect of bed length on steady-state coalescence of oil-in-water emulsion. *Separation and Purification Technology*, 56: 79-84.
- Sokolović, R. M. Š.; Govedarić, D. D.; Sokolović, D. S. (2010) Separation of oil-in-water emulsion using two coalescers of different geometry. *Journal of Hazardous Materials*, 175: 1001-1006.
- Gray, S. R.; Harbour, P. J.; Dixon, D. R. (1997) Effect of polyelectrolyte charge density and molecular weight on the flotation of oil in water emulsions. *Colloids and Surfaces A: Physicochemical and Engineering Aspects*, 126: 85-95.
- Rios, G.; Pazos, C.; Coca, J. (1998) Destabilization of cutting oil emulsions using inorganic salts as coagulants. *Colloids and Surfaces A: Physicochemical and Engineering Aspects*, 138: 383-389.
- Bensadok, K.; Belkacem, M.; Nezzal, G. (2007) Treatment of cutting oil/water emulsion by coupling coagulation and dissolved air flotation. *Desalination*, 206: 440-448.
- Al-Shamrani, A. A.; James, A.; Xiao, X. (2002) Separation of oil from water by dissolved air flotation. *Colloids and Surfaces A: Physicochemical and Engineering Aspects*, 209: 15-26.
- APHA; AWWA; WEF (1998) *Standard method for the examination of water and wastewater*, 20thEd; United Book Press: Baltimore, U.S.
- Meysami, B.; Kasaean, B. (2005) Use of coagulants in treatment of olive oil wastewater model solutions by induced air flotation. *Bioresource Technology*, 96: 303-307.
- de Sena, R. F.; Moreira, R. F. P. M.; Jose, H. J. (2008). Comparison of coagulants and coagulation aids for treatment of meat processing wastewater by column flotation. *Bioresource Technology*, 99: 8221-8225.
- Tir, M.; Moulai-Mostefa, N. (2008) Optimization of oil removal from oily wastewater by electrocoagulation using response surface method. *Journal of Hazardous Materials*, 158: 107-115.
- Painmanakul, P.; Sastaravet, P.; Lersjintanakarn, S.; Khaodhiar, S. (2010) Effect of bubble hydrodynamic and chemical dosage on treatment of oily wastewater by induced air flotation (IAF) process. *Chemical Engineering Research and Design*, 88: 693-702.
- Allen, T. (1997) *Particle Size Measurement*, Vol. 1, 5th ed.; Chapman & Hall: London.
- Coulson, J. M.; Richardson, J. F.; Backhurst, J. R.; Harker, J. H. (2002) *Chemical Engineering*, Vol. 2, 5th ed.; Butterworth-Heinemann: Oxford, U.K.
- Rachu, S. (2005) *Computer Program Development for Oily Wastewater Treatment Process Selection, Design and Simulation*; Doctoral dissertation. INSA Toulouse, France.
- Xu, R. (2001) *Particle Characterization: Light Scattering Methods*; Kluwer Academic Publishers: Dordrecht, The Netherlands.
- Mittal, K.L. (2009) *Contact Angle, Wettability and Adhesion*, 6th ed.; VSP: Leiden, The Netherlands.
- Zisman, W. A. (1964) Relation of the equilibrium contact angle to liquid and solid constitution. *Advances in Chemistry*, 43: 1-151.
- Gleabey, C. A.; Horgan, G. W.; Darbyshire, J. F. (1991) Image analysis and three-dimensional modeling of pores in soil aggregates. *Journal of Soils*, 42(3): 479-486.
- Sabreen, S. R. (1991) *Surface Wetting and Pretreatment Methods*; The Sabreen Group, Inc., US.
- Zhao, H.; Li, G. (2011) Application of fibrous coalescer in the treatment of oily wastewater. *Procedia Environmental Sciences*, 10: 158-162.
- American Water Works Association and American Society of Civil Engineers (AWWA) (1990) *Water Treatment Plant Design*, 3rd ed.; McGraw-Hill: NY.
- Vasudevan, G.; Chase, G. G. (2004) Performance of B-E-glass fiber media in coalescence filtration. *Aerosol Science*, 35: 83-91.
- Wanichkul, B. (2000) Etude des potentialities de nouveaux procedes de traitement d'emulsions hydrocarbure-eau; ultrafiltration, distillation et couplage coalesceur-hydrocyclone. Ph.D. dissertation, INSA Toulouse, France.
- Svarovsky, L., 2000. *Solid-Liquid Separation*, 4th ed.; Butterworth-Heinemann: Oxford.
- Foust, A. S.; Wenzel, L. A.; Clump, C. W.; Maus, L.; Andersen, L. B. (1980) *Principles of Unit Operations*, 2nd ed.; Wiley: Canada.
- McCabe, L. W.; Smith, J. C.; Harriott, P. (2000) *Unit Operations of Chemical engineering*, 6th ed.; McGraw-Hill: New York.
- Benitez, J. (2009) *Principles and Modern Applications of Mass Transfer Operations*, 1st ed.; Wiley: NJ.
- Sherony, D. F.; Kintner, R. C. (1971) Coalescence of an emulsion in a fibrous bed: Part I, theory. *The Canadian Journal of Chemical Engineering*, 49: 321-325.
- Chieu, J. N.; Schechter, R. S.; Humenick, M. J.; Gloyna, E. F. (1975) *Coalescence of emulsified wastes by fibrous bed*. Technical Report EHE-75-05, CRWR-126, Department of Civil Engineering, University of Texas: Texas, US.
- Akers, R. J.; Ward, A. S. (1977) *Liquid Filtration Theory And Filtration Pretreatment, in Filtration Principles and Practices*, Part I; Dekker: New York.
- Carman, P. C. (1956) *Flow of Gases Through Porous Media*; Academic Press: New York.
- Cheremisinoff, N. P. (1998) *Liquid Filtration*, 2nd ed.; Butterworth-Heinemann: Oxford.

VITA

Mr. Nattawin Chawaloespornsia was born on March 25th, 1986 in Bangkok. After graduated from Srinakharinwirot University Prasarnmit Demonstration School (Secondary), he went to study in Faculty of Engineering at Chulalongkorn University. He graduated the Bachelor degree of Environmental Engineering in 2008. Afterwards, he continued his study and obtained a Master Degree of Science in Environmental Management (International program) at Chulalongkorn University in 2010. He pursued his study in Doctoral of Philosophy in Environmental Management at Chulalongkorn University in November 2010. Furthermore, he was granted by Erasmus Mundus program TECHNO project I under the European Union to study in Environmental Engineering at University Paul Sabatier – Toulouse III, France in September 2012.

